



Cytoskeletal reorganization in human blood platelets during spreading

Aishwarya Kishore Paknikar

Göttingen, 2016

Cytoskeletal reorganization in human blood platelets during spreading

Dissertation
for the award of the degree

"Doctor of Philosophy" Ph.D.
Division of Mathematics and Natural Sciences
of the Georg-August-Universität Göttingen

within the doctoral program Biology
of the Georg-August University School of Science (GAUSS)

Submitted by
Aishwarya Kishore Paknikar
From Pune, India

Göttingen, 2016

Thesis committee and members of the examination board

Reviewer: **Prof. Dr. Sarah Köster**

Institute for X-Ray Physics, "Nanoscale Imaging of Cellular Dynamics"
Georg-August-University, Göttingen

Second reviewer: **Prof. Dr. Erwin Neher**

Emeritus group "Membrane Biophysics"
Max Planck Institute for Biophysical Chemistry, Göttingen

Further members of the examination board

Prof. Dr. Jörg Großhans

Universitätsmedizin
Department for Developmental Biochemistry
Georg-August-University, Göttingen

Prof. Dr. Kai Tittmann

Schwann-Schleiden Forschungszentrum
Department of Molecular Enzymology
Georg-August-University, Göttingen

Prof. Dr. Stefan Jakobs

Department of NanoBiophotonics, "Mitochondrial Structure and Dynamics group"
Max Planck Institute for Dynamics and Self-Organization, Göttingen

Prof. Dr. Ivo Feußner

Department for Plant Biochemistry
Albrecht-von-Haller-Institute for Plant Sciences
Georg-August-University, Göttingen

Date of the oral examination

19.01.2017

Affidavit

I hereby confirm that this thesis has been written independently, with no other sources and aids than quoted. It is based on my own work and has not been submitted for any other degree.

Aishwarya Kishore Paknikar

Göttingen, 15.12.2016

Contents

1.	Introduction	1
2.	State of the Art.....	5
2.1	Overview of platelet functions	5
2.2	The history and origin of platelets	6
2.3	General aspects of platelet structure at rest	9
2.4	Molecular mechanisms of actin and MT dynamics.....	12
2.4.1	Actin	12
2.4.2	Microtubules (MTs).....	14
2.5	Cytoskeleton of platelets in resting state	17
2.5.1	Glycoprotein receptors	17
2.5.2	The spectrin cortex	18
2.5.3	The acto-myosin cortex and the cytoplasmic actin network	18
2.5.4	The MT coil.....	19
2.6	Platelet activation, their cytoskeleton and its role	21
2.6.1	Initiation of platelet activation and their adhesion	21
2.6.2	General structural features of activated platelets.....	22
2.6.3	Actin cytoskeletal reorganization	26
2.6.4	MT reorganization and actomyosin contraction.....	32
2.6.5	Platelet secretion, aggregation and clot compaction	37
2.7	Real-time monitoring of the platelet cytoskeleton	38
2.7.1	Novel advances in monitoring actin cytoskeleton.....	39
2.7.2	Novel advances in monitoring MT cytoskeleton.....	40
2.8	SiR-actin and SiR-tubulin for live F-actin, MT imaging.....	40

2.9	Open questions	43
3.	Materials and Methods	45
3.1	Fibrinogen coating of coverslips	45
3.2	Platelet purification	46
3.3	Platelet cytoskeleton and plasma membrane staining	49
3.3.1	Fixed staining for actin, myosin and vinculin	49
3.3.2	Labeling with SiR-actin and SiR-tubulin, probe characterization	51
3.3.3	Platelet plasma membrane staining	51
3.4	Platelet treatment with pharmacological agents	52
3.5	Microscopy and image acquisition	52
3.5.1	Sample preparation during live platelet imaging	52
3.5.2	Bright-field imaging and epifluorescence imaging	53
3.5.3	Bright-field and epifluorescence image processing	57
3.6	Analysis of F-actin fluorescence intensity	57
3.6.1	F-actin normalized intensity plots	57
3.6.2	Histogram analysis of F-actin normalized intensities	58
3.7	Platelet spread area determination	59
3.8	Determination of time point of zero (adhesion)	60
3.9	F-actin filament detection	63
3.9.1	Pre-processing	63
3.9.2	Binarization	64
3.9.3	Width map generation	64
3.9.4	Line (filament) detection and total line length plots	65
3.10	Piecewise linear model fit	67
3.11	Spreading status counts and statistics	67
4.	Results and Discussion	71
4.1	The cytoskeleton post-fixation	71

4.1.1	Distribution of F-actin only	71
4.1.2	Distribution of F-actin-vinculin or F-actin-myosin	74
4.1.3	Discussion of the results	78
4.2	Real-time F-actin dynamics	81
4.2.1	Direct visualization of platelet F-actin reorganization	81
4.2.2	Temporal evolution of F-actin fluorescence intensities	84
4.2.2.1	Quantification of F-actin fluorescence intensity increase	84
4.2.2.2	Characterization of the SiR-actin probe	86
4.2.3	Multiple timescales of F-actin formation and reorganization	89
4.2.3.1	Platelets spread within minutes but reorganize F-actin for hours.....	89
4.2.3.2	Temporal evolution of F-actin filaments	92
4.2.4	Effects of pharmacological agents on F-actin dynamics	94
4.2.5	Discussion of the results	99
4.2.5.1	SiR-actin labeling is a promising tool for real-time imaging	99
4.2.5.2	The existence of multiple time-scales of F-actin reorganization.....	101
4.2.5.3	The effects of the pharmacological agents in real-time.....	102
4.3	Real-time MT dynamics	106
4.3.1	Imaging of MT over time	106
4.3.2	The role of MTs and myosin in complete platelet spreading	108
4.3.3	Discussion of results	111
5.	Summary & Conclusions	115
	References.....	119
	Appendix.....	133
A.	Recipes of buffers (sample preparation and platelet purification)	133
B.	Normalized F-actin intensity analysis MATLAB script.....	134
C.	Platelet contour detection and spread area calculation MATLAB scripts.....	136
D.	Parameters used for Filament Sensor program.....	140

E. Relative numbers of spread/unspread platelets and statistical analysis by <i>t</i> -test.	141
F. Representative images of fixed-platelet cytoskeleton time series.....	143
G. SiR-actin probe characterization and spreading tests.....	146
H. Normalized F-actin intensity profiles of platelets treated with pharmacological agents are similar to those of control conditions	147
I. F-actin morphologies of CMGreen and SiR-actin double labeled are different than only single SiR-actin labeled platelets	148
List of Abbreviations and Symbols.....	149
Acknowledgements.....	153
Curriculum Vitae	157

1. Introduction

Blood clotting is an essential, life-sustaining process in mammals and involves many soluble blood clotting factors and the blood platelets [13]. Platelets are anucleate cells, and are one of the smallest cells in the human body with a discoid shape and with diameters between 2-5 μm . However, they play a huge role in preventing excessive blood loss from a damaged blood vessel. These discoid platelets circulate in the bloodstream and are quiescent in a healthy blood vessel. However, upon vessel damage, they immediately respond to activation signals by transforming themselves dramatically. They change their shape from discoid to spherical, adhere to the underlying, exposed extracellular matrix (ECM), form filopodial and lamellipodial extensions, flatten by spreading and eventually contract in a hemostatic plug, to pull the wound edges together (Figure 1.1). This rapid and dramatic morphological transformation of platelets occurs due to dynamic and ordered rearrangements of their cytoskeletal components, which mainly include their actin and microtubules (MTs).

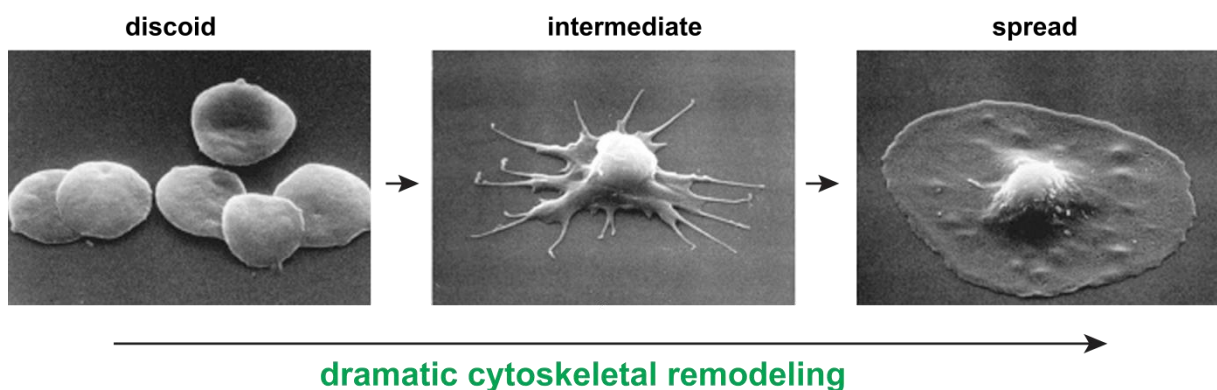


Figure 1.1: Platelets remodel their cytoskeleton when activated²

At a damaged wound site, in response to activation signals, platelets adhere to the ECM and undergo dramatic morphological shape changes, from discoid to spherical along with the formation of extensions (intermediate), to fully flat, spread stage, to enable wound closure. These dramatic changes are a result of the rapid and extensive remodeling of mainly their actin and MT cytoskeleton. Images are adapted from [151].

Upon response to stimuli, the MTs of discoid platelets dismantle and constrict, and their actin cytoskeleton severs from the membrane due to which the platelets become spherical. After this, there is extensive actin polymerization, during which the platelets form filopodia and lamellipodia, spread and continue to strengthen their adhesion to the ECM [139]. The platelets also secrete their granules which contain activation factors that recruit more platelets at the

²activation refers to morphological changes occurring in platelets exposed to glass/ foreign surfaces/agonists in suspension

INTRODUCTION

site of injury and also make platelets stick to each other. These platelets aggregate together, forming a platelet plug (a thrombus) and via their actin-myosin contraction, they pull on the plug to make it contact.

The platelet thrombus formation process is very complex and involves the concerted actions of many signaling proteins that activate numerous signaling cascades, which together bring about blood clotting and prevent excessive bleeding. During this thrombus formation, the metamorphosis of the platelets from discoid to spherical, their subsequent adherence and spreading, due to the actions of their actin, myosin and MT cytoskeleton, is of utmost importance. Any genetic defects or dysfunctions in any of the proteins that regulate these processes, affects the cytoskeletal structure and arrangement and lead to bleeding disorders which show effects like prolonged bleeding time, thrombocytopenia and formation of defective blood clots [23, 114, 140]. The study of platelets and their cytoskeleton is thus of extreme medical importance.

Since mammalian platelets lack a nucleus, most of the knowledge about their cytoskeletal components has been gathered from studying their cytoskeleton, after their chemical fixation, by performing electron microscopy and immunofluorescence studies. This lack of a nucleus has both its merits and demerits. On the one hand, even though they lack a nucleus, these tiny, miraculous cells are enriched in all the proteins that are involved in complex signaling pathways that govern the important processes of cell adhesion, spreading and contraction. Hence, platelets make an excellent example of a model for a simple biological cell [140], where various cellular aspects such as cytoskeletal remodeling can be studied, without the interference of a nucleus, and the knowledge gained, can be extrapolated to other cells. On the other hand, this lack of a nucleus makes it impossible to transfect, microinject, or in any way manipulate the human platelets. Thus it is not easy to visualize and study the cytoskeletal dynamics of human platelets in real-time. It is, of course possible to study platelets from transgenic mice, and indeed real-time studies on such platelets have added valuable information to the existing knowledge about the platelet cytoskeleton and the genetic alterations that lead to various bleeding disorders [20, 23, 78, 108, 112, 113, 114, 120, 140]. However, owing to their importance in medicine, and because of the role of the cytoskeleton in bleeding disorders, it is desirable to study human blood platelets. It is especially desirable to have a quick diagnostic tool that can directly visualize the cytoskeletal changes taking place in human platelets in real-time.

The introduction of the novel, fluorogenic, SiR-actin and SiR-tubulin probes, that bind only to filamentous actin (F-actin) and MTs, and which can be used for cells that are difficult to

transfect [86], are a step forward in achieving this goal. These fluorogenic cytoskeletal probes are highly cell permeable and have excellent properties, such as brightness, photostability, far-red excitation and emission, low cytotoxicity, that make them ideal for live-cell imaging [86].

In this dissertation, these SiR-actin and SiR-tubulin probes are used to directly visualize the F-actin and MT changes occurring during platelet spreading in real-time, and the temporal dynamics of these two cytoskeletal components during platelet spreading are explored. In that context, the dissertation is structured as below.

Chapter 2 introduces the biology and importance of human blood platelets and their cytoskeleton in aiding in the platelet functions. Particular emphasis is given on their actin and MT cytoskeleton. Also, the current approaches available for visualizing the actin and MT platelet cytoskeleton are briefly summarized and the SiR-actin and SiR-tubulin cytoskeletal probes are introduced [86] followed by a brief mention of the open questions that these studies have raised.

Chapter 3 describes the experimental techniques used in this dissertation which includes purification of the platelets, their post-fixation cytoskeletal stainings, their labeling with the SiR-actin and SiR-tubulin probes, the methodology of the time-lapse experiments with these probes and the data analysis steps carried out to analyze the results.

Chapter 4 describes the platelet actin, myosin and vinculin cytoskeleton after their chemical fixation. This chapter gives a broad overview of the development of the platelet cytoskeleton especially the F-actin cytoskeleton, as the platelets spread.

Chapter 5 demonstrates the real-time F-actin dynamics in platelets as they spread and points towards the existence of multiple time-scales of F-actin reorganization during their spreading. The results are discussed in context with the existing literature.

Chapter 6 demonstrates the real-time MT dynamics in platelets as they spread and points towards their role in platelet exocytosis and shows that myosin plays a major role in this process. The results are discussed in context with the existing literature.

Chapter 7 summarizes the findings and discusses the relevance of the results in the context of the *in vivo* platelet function. The new possibilities in understanding the platelet cytoskeleton, that may open up, with the use of these live-cytoskeletal imaging probes are also briefly mentioned.

2. State of the Art

In this chapter the important functions of platelets and their biological background is briefly introduced with particular emphasis on the structure of their cytoskeleton and how it aids in the platelet functions. The current approaches available for visualizing this platelet cytoskeleton are also briefly summarized. Lastly, the recently developed cytoskeletal probes SiR-actin and SiR-tubulin are introduced [86]. Most of the basic biological introduction of platelets given here is taken from the information available in [94].

2.1 Overview of platelet functions

The primary role of platelets is in haemostasis. By the coordinated efforts of platelets and many clotting factors, the damage to a blood vessel is sealed by the formation of a thrombus i.e. a blood clot. A sketch of an overview of the various steps that occur during thrombus formation is shown in Figure 2.1. In a healthy blood vessel (resting state in Figure 2.1) the platelets traverse close to the walls of the blood vessels and are quiescent (resting). Their quiescent state is maintained by the release of agents like nitric oxide (NO) and prostaglandin I₂ (PGI₂). When there is damage to the blood vessel, the endothelial layer lining the vessel is lost and the underlying ECM is exposed. The ECM contains collagen which is a major agonist of platelets. Other than collagen other agonists like von Willebrand factor (vWF), adenosine diphosphate (ADP), thrombin and thromboxane A₂ (TXA₂) are also released. All these agonists stimulate the platelets and cause their shape change from a discoid to a sphere. The platelets adhere to the ECM and spread (adhesion, spreading in Figure 2.1), by extending their filopodia and lamellipodia and quickly cover the damaged surface. Furthermore, the platelets secrete more stimulation signals and recruit other platelets to the damaged area which eventually form a platelet thrombus. All of these events are collectively referred to as platelet activation. The platelets then aggregate and pull on fibrin strands that are formed during thrombus formation and close the damaged wound edges together [94]. The cytoskeleton of platelets brings about all these dramatic changes in the platelets and it plays a major role in these adhesion, spreading, secretion and aggregation processes. The molecular details of these cytoskeletal-mediated processes are discussed in the later sections.

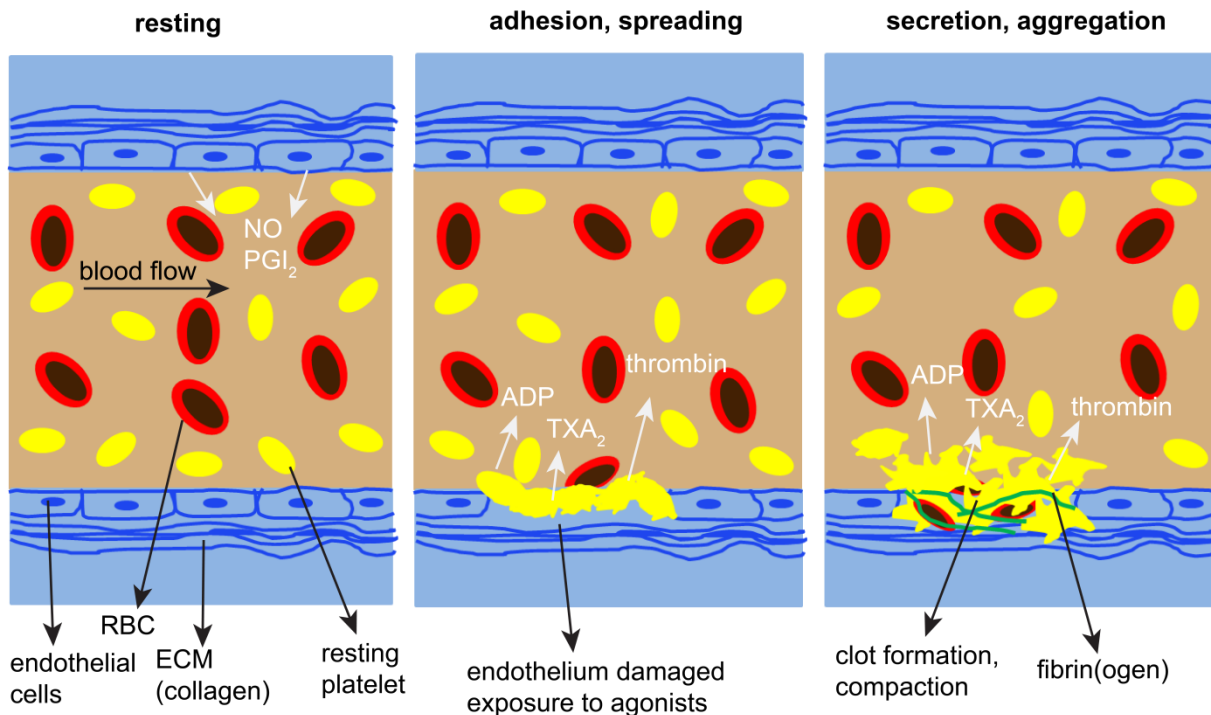


Figure 2.1: Overview of platelet function in haemostasis

In a healthy blood vessel, the platelets that traverse the blood vessels are in a resting state which is maintained by agents like NO and PGI₂, secreted by the endothelial cells. Upon damage to the blood vessel, the underlying ECM is exposed which contains platelet agonists like collagen. The platelets start to adhere and spread at the site of damage and quickly cover the damaged area. More platelets are recruited to the damaged site by secretion of soluble agonists like ADP, TXA₂ and thrombin and a clot forms. The platelets aggregate in this clot and pull on it to compact it and stop the blood flow.

2.2 The history and origin of platelets

The discovery of platelets in the early 19th century can be credited to many scientists who all described the existence of the 'blood plates/plaques' in some way or the other. Notable amongst them were, Max Schultze who was one of the first anatomists to accurately describe these cells after looking at them under a microscope in the year 1865. At that time he referred to them as 'granules' which he saw in his own as well as other people's blood and described them as a normal constituent of the blood which tended to form irregular clumps of various sizes. He further 'enthusiastically recommended' the study of these objects 'to those who are concerned with the in-depth study of the blood of humans' [16]. In the later years, Giulio Bizzozero (1882) identified these cells when he used 'intravital microscopy of mesenteric venules of guinea pigs' [94] and observed them to be 'disk-shaped and circulating in isolation' in blood [94]. He also quoted that what he was studying were the same 'granules' that Schultze

had previously described. He called them *blutplättchen* in German and 'blood plates' in English which is most likely the source of the current use of the word 'platelets' [16, 33]. Bizzozero's contemporary William Osler (1881-1186), built on his observations and established a clear role for these cells in thrombosis and termed these cells as blood 'plaques' [94]. He noted that these blood plaques "are the elements which first settle on the edges of a wounded vessel and form the basis for thrombosis" [33]. At this time, the origin of blood platelet production was unknown. Although Bizzozero had also identified bone marrow megakaryocytes (MKs), he was unaware that they were the precursors of blood platelets [94]. Then in 1906, Homer Wright using his self-made polychrome staining solution (Wright's stain) noted that the red to violet granules present in both platelets and MKs were similar in shape and color and thus clarified that platelets originated from the MKs in the bone marrow [33, 94].

There are several models proposed in the literature to suggest how platelets form from their progenitor MKs [94]. The most promising model is that of the production of platelets via proplatelets that extend from MKs because proplatelets have been found in blood [153] and their extension from MKs into blood vessels has been shown [94]. The production of platelets based on this model is briefly summarized here and a schematic is shown in Figure 2.2 [88]. In response to the hormone thrombopoietin (TPO), hematopoietic stem cells (HSCs) which in adults are present mainly in the bone marrow, differentiate into immature MKs (Figure 2.2-step 1). The nucleated MKs then undergo maturation and become polyploid by endomitosis i.e. several cycles of DNA replication which takes place without cell division. During this time the mature MKs migrate to the vascular niche and both the endomitosis and migration are regulated by the acto-myosin cytoskeleton [88, 115]. During maturation, the MKs increase in size (50-100 μm diameter) thus allowing them to accumulate protein, mRNA, organelles, platelet-specific granules and internal membrane pools that are later distributed in the platelets [115]. They also develop an invaginated membrane system (IMS) that serves as a reservoir for the next step of proplatelet formation (Figure 2.2-steps 2 and 3). At the vascular niche, the MKs extend protrusions called proplatelets which appear as barbell-shaped structures (Figure 2.2- step 4) that are released in the vascular sinusoids. The MTs have a major role during this process when they slide past each other and provide the driving force to the proplatelet extension via the MT motor protein dynein. Bipolar MTs line the length of these proplatelets and serve as a cargo route on which the organelles and granules that the MKs have accumulated during maturation are transported towards the proplatelet tips driven by the MT motor protein kinesin [88, 115]. Once the proplatelets are formed, the terminal formation of

platelets from them can occur in the blood stream [88]. Recent studies have speculated that MKs release a heterogeneous mixture of nascent platelets in the blood stream which then finally mature into platelets in circulation. These speculations come from the identification of proplatelets in blood [88, 153]. A recent *in vitro* study has shown that proplatelets are capable of generating progeny [133] and another study has identified intermediate forms between proplatelets and platelets, termed as preplatelets [154]. These preplatelets (discoid, 2-10 μm diameter) can twist their MT cytoskeleton in the center [154] and reversibly convert into the barbell-shaped proplatelets (Figure 2.2-step 5). The nuclei from the MKs, which are converted to the pre/proplatelets, are extruded and eventually phagocytosed [88]. In the final step, the barbell-shaped undergo a fission event to divide into two individual anucleate platelets that are released into circulation [88, 115]. These proplatelets have MT coils ($\sim 2 \mu\text{m}$ diameter) at each end and these MT coils are further retained in the individual platelets. The conversion of preplatelets to proplatelets is driven by MT forces as discussed above and formation of these proplatelets is determined by the marginal MT coil diameter and thickness [88, 153]. These cortical forces thus regulate the final sizes of platelets [153]. The actin and MT cytoskeleton hence play a major role in the production and final sizes of the platelets.

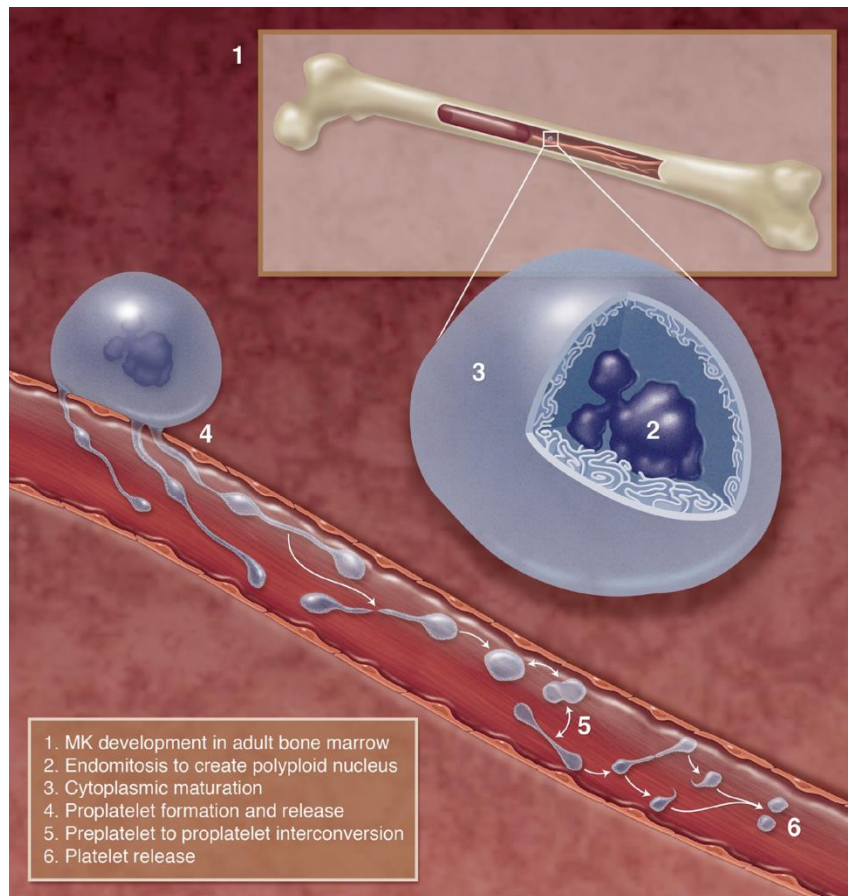


Figure 2.2: Scheme of platelet production in the bone marrow

1) In the bone marrow, HSCs differentiate into immature MKs in response to the hormone TPO. 2 & 3) Then these MKs mature during which they become polyploid by undergoing endomitosis, increase in size, accumulate mRNA, protein, organelles etc. and develop an IMS. 4) The MKs then migrate to the vascular niche and extend proplatelets which can also interconvert to 5) preplatelets. The nuclei from these pre/proplatelets are extruded and phagocytosed and in the final step 6) in an MT-dependent process, the proplatelets undergo a fission event and form two individual platelets. The figure caption information is adapted and the figure is reproduced with permission from Machlus KR and Italiano JE., 2013 originally published in *The Journal of Cell Biology* <http://dx.doi.org/10.1083/jcb.201304054> [88]. © 1979 Rockefeller University Press, License number-4003210614697, Licensed content publisher- Rockefeller University Press.

2.3 General aspects of platelet structure at rest

Before discussing the specific structural features of the platelet cytoskeleton (given in the following sections) the general structure of the whole platelet is briefly summarized first. As discussed above platelets are produced from mature MKs and are released into the bloodstream. The entire process of platelet production from MKs takes ~5 days in humans. In a healthy adult, approximately 10^{11} platelets are produced each day. The released platelets then remain in circulation for 7-10 days and are then destroyed in the spleen [40, 41].

In their inactive (resting/quiescent) state, platelets are discoid in shape with a diameter of 2-5 μm and a thickness of 0.5 μm . As mentioned before, when circulating in a healthy blood vessel, the platelets are maintained in their quiescent state by agents like NO, heparin, and PGI₂ which are secreted mainly by the endothelial cells. The resting platelets are anatomically divided into four zones, from the outer to the innermost areas, as described below.

1) Peripheral zone:

This zone is responsible for the adhesion and aggregation of platelets. Low-voltage, high-resolution scanning electron microscopy (LVHR-SEM) suggests that the outer surface of the platelets i.e. the plasma membrane resembles the gyri and sulci like those on the brain surface making it appear wrinkled [166]. There are also small openings of the open canalicular system (OCS) randomly dispersed on the outer surface. The OCS traverses the entire platelet and is also surface-connected. It is composed of invaginations of the plasma membrane and serves as a pathway for the transport of substances into the platelets and also the release of granular contents to the extracellular environment.

Besides this, the peripheral zone consists of a glycoprotein-rich exterior coat called the glycocalyx. The glycocalyx is covered with many glycoprotein receptors which bind to adhesive agents, aggregating agents and procoagulant factors to facilitate the adhesion of platelets to damaged surfaces, transmit extracellular signals to the platelet interior and trigger their activation followed by aggregation and in general speed up the clot retraction process. The major glycoprotein surface receptors involved belong to two different categories, the G-protein-coupled receptors (GPCRs), and the tyrosine kinase-linked receptors. The GPCRs induce platelet activation through G proteins and include mainly the protease activated receptors (PAR) for thrombin- PAR1 and PAR4, receptors for TXA₂, PGI₂, ADP etc. The tyrosine kinase-linked receptors induce platelet activation by signaling through tyrosine kinases like Src (proto-oncogene tyrosine protein kinase) and Syk (spleen tyrosine kinase). Receptors in this category include the GP-VI and GP-Ib-IX-V complex which bind to collagen and von Willebrand factor (vWF), and the integrins like GPIIb-IIIa complex (also known as the integrin $\alpha\text{IIb}\beta\text{3}$) and $\alpha\text{2}\beta\text{1}$. There are many $\alpha\text{IIb}\beta\text{3}$ copies on the surface of the platelets and they mediate the binding between fibrinogen and vWF during platelet activation whereas $\alpha\text{2}\beta\text{1}$ is a platelet collagen receptor [32, 111]. Other receptors present on platelet surfaces include P-selectin, immunoglobulins and receptors for ADP, epinephrine etc. [69].

The peripheral zone also consists of a lipid bilayer (also called unit membrane) which comprises of asymmetrically distributed phospholipids and provides a surface for the

interaction of coagulant proteins. Just below the lipid bilayer and closely associated with is a distinct layer called the submembrane area which contains submembrane filaments comprising of short actin filaments. This submembrane area serves as a barrier for the internal organelles and also serves as a platform for the interaction of the cytoplasmic domains of transmembrane receptors e.g. the cytoplasmic tails of GPIIb-IIIa with various proteins that regulate signaling processes during platelet activation e.g. myosin [94].

2) Sol-gel zone:

This zone is responsible for cytoskeletal support and contraction and is continuous with the submembrane area of the peripheral zone. It consists mainly of a circumferential coil of MTs which maintains the discoid shape of the platelets and an acto-myosin filament system which is involved in various processes that eventually lead to the contraction of platelets and retraction of blood clots. These MT and acto-myosin cytoskeleton are described in details in section 2.5.

3) Organelle zone:

This zone consists of several types of membrane-enclosed bodies which are randomly dispersed in the cytoplasm. These include the three major secretory granules- the α granules, dense bodies and lysosomes. There are nearly 40-80 α granules per platelet that store the adhesion molecule P-selectin and the receptor complexes α IIb β 3 and GP-Ib-IX-V. Other than those, α granules contain more than 300 secretory proteins which include chemokines, cytokines, growth factors, coagulant factors etc. There are about 4-8 dense bodies present per platelet. These mainly store the adenosine and guanosine nucleotides- adenosine diphosphate (ADP), adenosine triphosphate (ATP), guanosine-5'-diphosphate (GDP) and guanosine-5'-triphosphate (GTP). Besides that the dense bodies also have stores of calcium which is crucial required the platelet activation process. This zone also consists of some mitochondria which are involved in energy metabolism. Other organelles present in this zone include peroxisomes, glycosomes, tubular inclusions and electron dense chains and clusters [94].

4) Membrane zone:

This comprises of the OCS which is also surface-connected as discussed above and a dense tubular system (DTS) which refers to a number of channels distributed randomly in the cytoplasm and are just a remnant of the rough and smooth endoplasmic reticulum of MKs. The DTS channels act as calcium binding sites and are also speculated to be involved in incorporating enzymes involved in prostaglandin synthesis. The OCS and DTS are not

completely isolated from each other. Apparently, platelets cannot seem to synthesize proteins as they do not retain any rough endoplasmic reticulum and ribosome complexes, nor do they have Golgi complexes. However, this notion is disputable as platelets contain tiny amounts of mRNA and some studies have demonstrated that platelets are capable of *de novo* protein synthesis [131].

2.4 Molecular mechanisms of actin and MT dynamics

Before describing the platelet cytoskeleton in detail, the basic concepts of actin and MT and their polymerization dynamics are briefly summarized here since the actin and MT cytoskeleton of platelets is most relevant in the context of this dissertation. The cytoskeleton of a cell is an important part of it that gives the cell its shape and also prevents the cell from deforming by providing a mechanical resistance. When necessary, the cytoskeleton can actively contract, which enables the cells to perform vital functions like migration or contraction. Besides that the cytoskeleton plays major roles in cellular functions like cell signaling pathways, cytokinesis, endocytosis and intracellular transport. All these dynamic processes of the cytoskeleton are possible due to the presence of proteins in it that can rapidly polymerize to form filaments or depolymerize, depending on the particular cellular requirements. Eukaryotic cells have three main cytoskeletal filaments- microfilaments (actin filaments), microtubules (MTs) and intermediate filaments. All these filaments along with additional proteins bring about the dynamics changes of the cytoskeleton. The general aspects of actin and MTs and some details of their occurrence in platelets are discussed below-

2.4.1 Actin

Actin is a 42 kDa protein and actin filaments are ~7 nm in diameter. The monomeric globular form of actin called as G-actin, polymerizes to form the actin filaments also called as F-actin (filamentous actin) which are composed of two strands of actin. F-actin filaments further assemble to form bundles and networks. The actin filaments along with these bundles and networks play important roles in cell spreading, cytokinesis, muscle contraction and other cellular processes. In a cell, actin filaments are constantly growing (polymerizing) and shrinking (depolymerizing) to bring about dynamic changes in the cell. This actin polymerization and depolymerization can be easily visualized *in vitro* by, adding salts to a solution of G-actin, which induces polymerization and creates F-actin filaments. These F-actin

filaments are not distinguishable from those isolated from cells [84]. Actin polymerization *in vitro* proceeds in three sequential steps as shown in Figure 2.3.

In the first step, the ATP-G-actin (indicated in gray in Figure 2.3) aggregates into unstable, short oligomers. In the next step called as the nucleation phase, the oligomers reach a certain length of three to four subunits and form a stable nucleus (indicated in blue in Figure 2.3) which then acts as a 'seed' and rapidly elongates into F-actin filaments by adding ATP-G-actin monomers to both its ends known as plus/barbed and minus/pointed ends with a rate constant k_{on} (elongation phase in Figure 2.3). After ATP-G-actin gets incorporated into F-actin filaments, the bound ATP slowly hydrolyses to ADP thus ADP-F-actin filaments are formed (red F-actin filament in Figure 2.3). Along with this addition of ATP-G-actin, there is a simultaneous depolymerization caused by the loss of ADP-G-actin with a rate constant k_{off} . In the last step, the entire system reaches a steady state when the rate of ATP-G-actin addition equals the rate of ADP-G-actin loss (steady state in Figure 2.3). In the steady state the concentration of ATP-G-actin monomers decreases until it is in equilibrium with F-actin and is called the critical concentration, C_c where $k_{off} = C_c k_{on}$. The rate of addition of G-actin monomers differs at the two ends of the actin filaments. It is faster at the plus end/barbed end (k_{on}^+) and slower (ten times slower) at the minus end/pointed end (k_{on}^-), hence there also exist two different C_c for the two ends where $C_c^- > C_c^+$. When the G-actin monomer concentration is in between the C_c^+ and C_c^- , G-actin monomers are added at the (+) end and simultaneously dissociate from the (-) end. This phenomenon of addition of G-actin monomers at the (+) ends their subsequent travel along the F-actin filament and removal at the (-) ends resembles the action of a 'treadmill'. Thus this process is known as 'actin treadmilling'. At physiological salt concentration and RT conditions, the critical concentrations of actin at respective ends are $C_c^- \geq 0.5 \mu\text{M}$ and $C_c^+ = 0.12 \mu\text{M}$ [161]. In platelets, the $C_c^- = 1.0 \mu\text{M}$ and $C_c^+ = 0.2 \mu\text{M}$ respectively [13].

The assembly and disassembly of actin filaments are regulated additionally by accessory proteins. Some proteins like the actin-related-protein ARP2 and ARP3 complex (Arp2/3 complex) stabilize the actin nucleus and thus promote actin filament nucleation. Other proteins like profilin catalyze the ADP to ATP exchange and proteins like actin depolymerizing factor (ADF)/cofilin, mediate filament disassembly. All of these proteins are present in platelets [13].

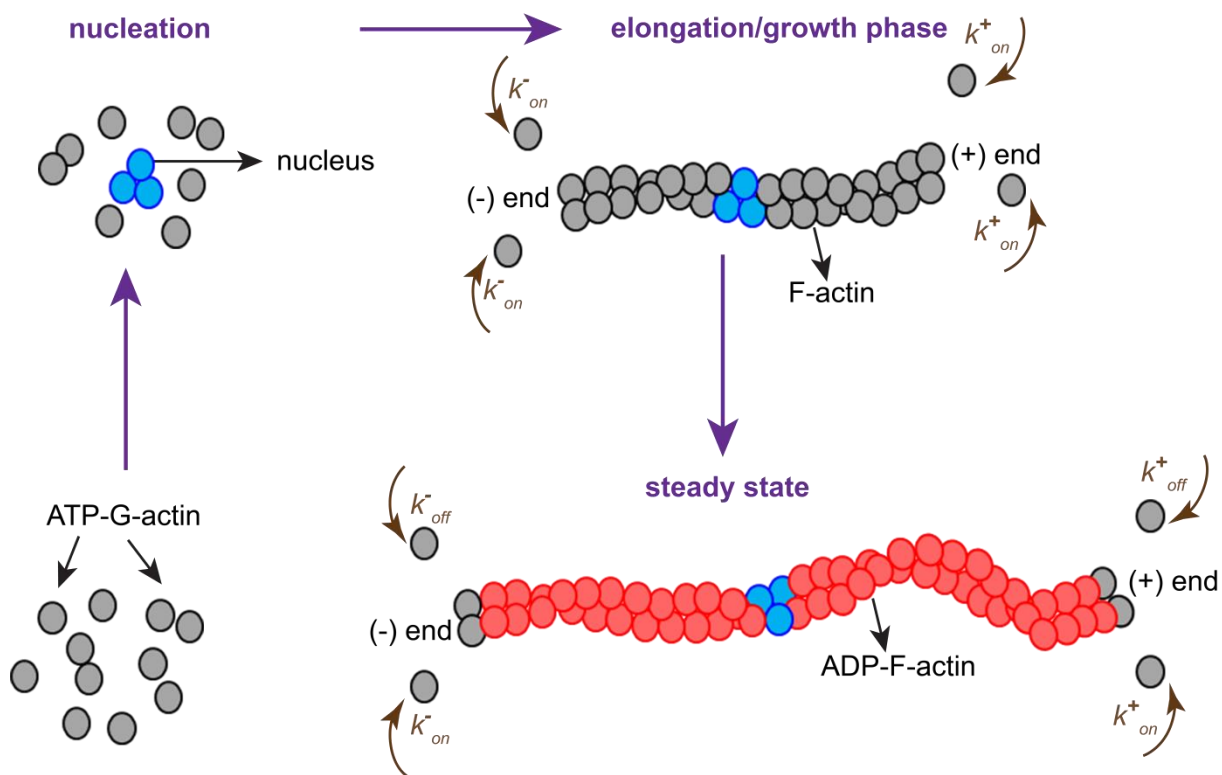


Figure 2.3: Actin polymerization and depolymerization

Actin polymerization *in vitro* proceeds in three sequential steps. ATP-G-actin monomers initially form unstable oligomers that in the nucleation phase form stable nuclei (blue; 3-4 oligomers). These then rapidly elongate by the addition of more ATP-G-actin monomers at both ends forming F-actin filaments (gray). Stable ADP-F-actin filaments (red) form due to ATP hydrolysis. In the last step, there is a steady state where the rate of addition of ATP-G-actin monomers equals the rate of loss of ADP-G-actin monomers.

2.4.2 Microtubules (MTs)

Microtubules are the largest of the cytoskeletal filaments and have a diameter of ~25 nm. They are rigid, hollow tubes composed of heterodimers that are made from the polymerization of α and β -tubulin subunits which are both ~50 kDa. MTs play important roles in mitosis, cell polarization, cell motility, secretion, intracellular transport and other cellular processes. Like actin filaments, MTs also continuously undergo dynamic changes within a cell to bring about its functions. A sketch of the MT dynamics is shown in Figure 2.4. The α and β -tubulin subunits polymerize in a head to tail manner forming a 'protofilament' (Figure 2.4A and B). In most mammalian cells, 13 of these protofilaments then associate laterally to form a hollow MT cylinder wall which is 25 nm in diameter (Figure 2.4C and cross-section). More $\alpha\beta$ heterodimers can then add to this existing MT and elongate it. Because of the head-to-tail

association of $\alpha\beta$ heterodimers, MTs are polar structures and also have different polymerization rates at the two ends. In every protofilament, the β -tubulin monomer is exposed at the faster-growing (+) end and the α -tubulin monomer is at the slower-growing (-) end (Figure 2.4C). The major MT nucleator is γ -tubulin and some other proteins which mimic the (+) end of MT and thus allow faster growth. The γ -tubulin is found in the centrosome of mammalian cells and the site is called microtubule organizing center (MTOC). MT polymerization is initiated at the centrosome and $\alpha\beta$ heterodimers are added mainly at the (+) end.

A phenomenon called 'dynamic instability' occurs during MT dynamics *in vitro* as well as *in vivo* where the tubulin subunits both, associate and disassociate from the (+) end, resulting in MTs alternately growing and shrinking rapidly (Figure 2.4D and E). This process uses the energy of GTP hydrolysis [35]. During MT polymerization, $\alpha\beta$ heterodimers are bound to two GTP molecules and are incorporated (preferentially) at the (+) end of the existing MT (Figure 2.4D). After incorporation, the GTP bound to the β -tubulin hydrolyzes to GDP but the GTP bound to the α -tubulin does not hydrolyze. There is a difference in the assembly properties of GTP- β -tubulin and GDP- β -tubulin with GDP- β -tubulin being more prone to depolymerization. Hence if the (+) end of the existing MT becomes capped with such a GDP- β -tubulin cap, then the MT becomes unstable and rapidly starts to depolymerize. This event is called 'catastrophe' (Figure 2.4E). Such events can occur when a MT grows so slowly that the GTP- β -tubulin hydrolyzes to GDP- β -tubulin, even before $\alpha\beta$ heterodimers can be added to the (+) end, or a catastrophe event can also occur when a MT shrinks rapidly, thus exposing the GDP- β -tubulin. Before the shrinking MT can vanish completely, a 'rescue' event (Figure 2.4D) can occur where a GTP- β -tubulin cap is added to the (+) end, before hydrolysis can start. This GTP- β -tubulin cap then acts as a template for further addition and growth of the MT. Just like the treadmilling of actin filaments, this dynamic instability of MTs also occurs at monomer concentrations that are near the C_c .

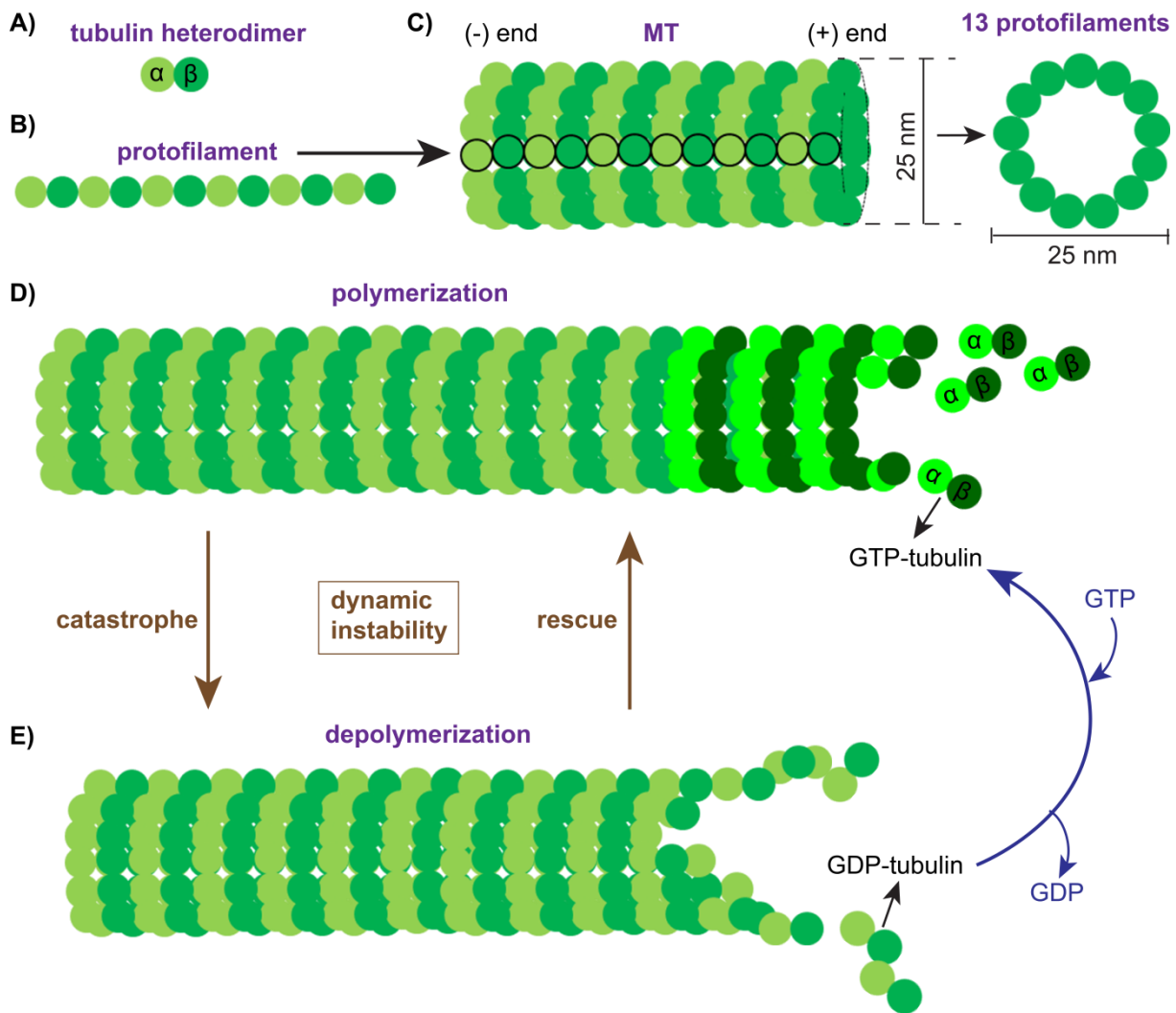


Figure 2.4: Microtubule polymerization and depolymerization

A) MT polymerization starts with $\alpha\beta$ -tubulin heterodimers associating in a head-to-tail fashion to form B) a protofilament. C) Typically, 13 of these protofilaments (one protofilament outlined in black) then associate laterally to form a hollow MT that has a diameter of 25 nm. D) During polymerization GTP-tubulin is added to the (+) end and existing MTs are elongated. The GTP- β -tubulin hydrolyses to GDP- β -tubulin which results in the destabilization of the MT and E) its subsequent depolymerization which is called as a 'catastrophe'. The catastrophe event is prevented by a 'rescue' event where GTP- β -tubulin forms a cap on the (+) end of the MT and starts to elongate it again. This rapid switching between growth and shrinkage phases is known as the dynamic instability of MTs.

Just like for actin, there exist many accessory proteins that regulate MT dynamics. These are called microtubule associated proteins (MAPs) and they include mainly the motor proteins like dynein and kinesin that help to transport cargo along MTs. These motor proteins have two motor domains that act like two 'feet' which walk along the MTs and transport the cargos [150]. Besides these, MAPs also include proteins that bind only (+) ends like EB1, EB2, EB3, proteins that sever or destabilize existing MTs like catastrophein and katanin, crosslinking proteins that stabilize MT structures, proteins that regulate nucleation, and proteins that

regulate parameters of dynamic instability such as frequencies of catastrophe and rescue events and rates of tubulin assembly [145]. Apart from these, post-translational modifications (PTMs) which are dynamic, reversible processes also occur on MTs on the $\alpha\beta$ heterodimers, post polymerization. These refer to alteration of proteins by the addition of some chemical groups or proteins to their amino acid residues. The PTMs occurring on MTs include tyrosination/detyrosination and acetylation/deacetylation and serve to stabilize the MTs [67]. The tubulin tyrosine ligase (TTL) adds a tyrosine residue to the α -subunit of MTs but the enzyme responsible for removal of tyrosine is not yet identified. Tubulin acetyltransferase (α -TAT1), adds an acetyl group to the α -subunit of MTs and the tubulin histone deacetylase 6 (HDAC6) removes the acetyl group. These PTMs are associated with the stability of MTs, where newly polymerizing, dynamic MTs are tyrosinated/deacetylated and stable, long-lived MTs are detyrosinated/acetylated [67, 122].

Platelets dominantly express the β 1-tubulin isoform of β -tubulin. Besides that platelets also express the plus-end MT assembly proteins EB-1 and EB-3 and the MT motors dynein and kinesin, as well as the enzymes like HDAC6 that are responsible for MT PTMs [10, 36, 94, 123].

2.5 Cytoskeleton of platelets in resting state

As has been discussed before, disc-shaped platelets that are released into the bloodstream from the ends of proplatelets circulate in humans for 7-10 days. The platelets can vary in size and in their granular contents. However, the structure of their internal cytoskeleton is very much consistent. This cytoskeleton helps to maintain the discoid shape of the platelets and also maintains their integrity, especially since they encounter high shear forces generated by blood flow [94]. The internal cytoskeleton of platelets in their resting state, in order of their occurrence from the plasma membrane towards to the inner side, is described in this section and a sketch of the cytoskeleton is shown in Figure 2.5.

2.5.1 Glycoprotein receptors

As has been discussed in 2.3, the plasma membrane of platelets has many glycoprotein-rich transmembrane receptors which mainly include the α IIB β 3 integrins (indicated in Figure 2.5 by magenta color) which are the most abundant glycoproteins on the platelet surface and the GP-Ib-IX-V complex. Resting platelets contain about 80,000 copies of the α IIB β 3 integrins on

their surfaces [135, 160]. In response to a stimulus for e.g. a vascular injury, these receptors help the platelets to adhere to the ECM at the site of injury. In resting platelets, the integrins are in a low-affinity state and have a bent conformation which prevents them from binding to extracellular ligands. However, once the platelets are activated by a stimulus, the integrins switch to the high-affinity state by unbending and change their conformation making it easier to bind to the ligands [94].

2.5.2 The spectrin cortex

The first structure beneath the platelet plasma membrane is a spectrin-based cytoskeleton (indicated in Figure 2.5 by amber color). The spectrin strands assemble in two-dimension and interconnect to each other at their ends by binding to actin filaments. There is an actin-binding site at each molecular end of the spectrin molecule. The RBCs also have a spectrin cytoskeleton which has been studied in great details. Under an electron microscope, the spectrin strands in RBCs are seen to be heterotetramers which are composed of head-to-head aggregates of $\alpha\beta$ chains [94]. The $\alpha\beta$ subunit chains associate laterally to form heterodimers which in turn associate to form the heterotetramers. There is an actin-binding site at the amino terminus of the β subunit of each heterodimer. Ankyrin helps to anchor the spectrin strands to the plasma membrane. In platelets, spectrin is highly expressed in MKs just before they start to make the proplatelets and it has been recently shown that the assembly of spectrin tetramers are essential for MK maturation, proplatelet extension and also in the maintenance of the 'barbell-shapes' of proplatelets [109].

2.5.3 The acto-myosin cortex and the cytoplasmic actin network

Underlying the spectrin is an actin cortex that too supports the platelet membrane skeleton and is both, directly and indirectly, connected to the spectrin cortex. Actin is the most abundant protein in platelets with a concentration of 0.55 mM, which approximately equals to 2×10^6 copies per platelet. In the resting platelet, ~ 40% of the actin is in the form of filaments i.e. F-actin. About 800,000 actin molecules assemble into 2000-5000 actin filaments that span the cytoskeleton of the resting platelet [13, 94]. The rest of the actin (~ 60%) is in the form of monomeric globular actin i.e. G-actin [47]. Also, platelets express high concentrations of actin cross-linking proteins such as filamin and α -actinin. Electron microscopy studies have described that the actin cytoskeleton of resting platelets resembles the structure of a spoked wheel [56]. At the rim of this wheel, is a two-dimensional spectrin-actin network where the

two spectrin strands interconnect with each other via long actin filaments. These filaments originate from a highly crosslinked three-dimensional actin filament core in the cytoplasm that forms the hub of this wheel (indicated in Figure 2.5 by red color). Filamin connections from the sides of actin filaments connect with the cytoplasmic tails of the GP-Ib-IX-V receptors and hold the membrane skeleton in compression in between the cytoplasmic actin and the plasma membrane. Apart from actin, platelets also have non-muscle myosin IIA. The actin filaments are polarized structures and are decorated with myosin heads whose stereospecific binding defines this polarity thus allowing the actin barbed ends and pointed ends to be distinguished [94]. It is believed that the presence of myosin at the membrane skeleton keeps it in a taut state by maintaining contractile tension on the actin filaments which are connected to the GP-Ib-IX-V receptors [56].

Apart from the physical constraints provided by the internal cytoskeleton to maintain the platelet discoid shape, there are also some biochemical constraints that prevent the platelets from polymerizing the G-actin and changing their shape. These include proteins like profilin and thymosin β 4 that sequester G-actin and lower free monomer concentrations. Furthermore monomer addition to the barbed ends of actin filaments is prevented by proteins like gelsolin and capZ which cap these ends. Additionally, the stable actin filaments are continuously undergoing treadmilling (as explained in section 2.4.1) which keeps the lengths of the filaments constant. The protein profilin, apart from sequestering monomers, helps in maintaining this treadmilling, as it catalyzes the exchange of ADP-G-actin to the ATP-G-actin, the form that can polymerize. However, to ensure that not all ADP-G-actin is exchanged, thymosin β 4 binds to ADP-G-actin and prevents the nucleotide exchange [25]. The F/actin filaments are further stabilized along their lengths by proteins like vasoactive-stimulated phosphoprotein (VASP), which prevents actin depolymerization from the (-) end.

2.5.4 The MT coil

As has been discussed before (see section 2.2), the platelets released from MKs contain MT. In platelets, there exist several MTs which are organized in a circumferential ring structure called the marginal band (MB) which is located just beneath the actin cortex (indicated in Figure 2.5 by shades of blue). This 'MB' has also been referred to as circumferential MT coil [169] or microtubule (MT) coil [108] or even microtubular (MT) ring structure [36]. It has been recently shown that this MB is a bipolar array and consists of multiple MTs that coil several times and form a single long-lived, detyrosinated/acetylated (stable) MT and is

associated with 8-12 tyrosinated/deacetylated (dynamic) MTs which polymerize in both directions around the MB of the resting platelet. The dynamic MTs are required to efficiently and quickly change the MB size because platelets reduce in size as they age which in turn requires the shrinkage of the MT coil. Platelets do not have a MTOC but instead γ -tubulin within the MB nucleates the MTs [108]. Furthermore, an equilibrium between the MT (+) end directed motor protein kinesin and (-) end directed motor protein dynein keeps the platelet MBs in their resting state and the dynein motors anchor the MB to the actomyosin cortex [122]. The MB of the platelets is important for maintaining their discoid shape (Figure 2.6A) as it has been observed that, mice that have $\beta 1$ -tubulin deficient MKs, are affected by platelet spherocytosis [64]. In this dissertation, the terms MT coil/ring refer to the MB structure described above.

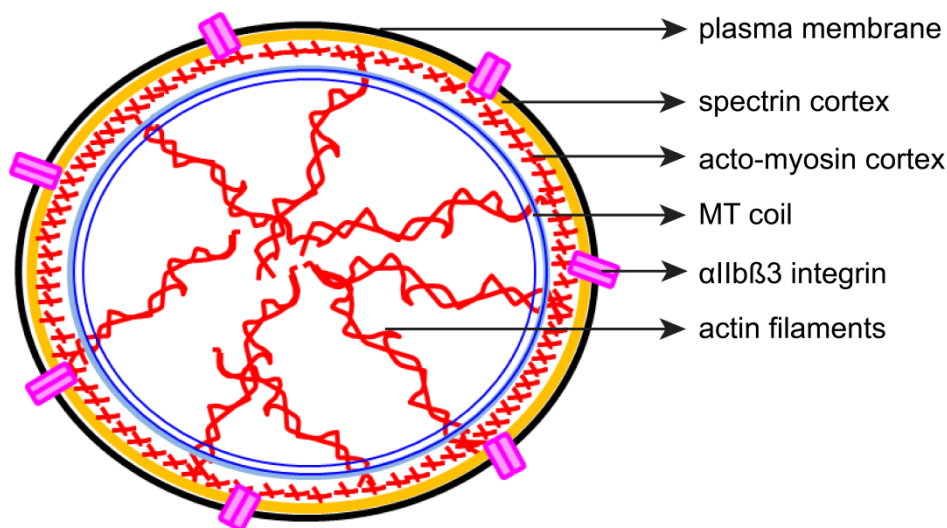


Figure 2.5: Sketch of platelet cytoskeleton at rest

A simplified sketch of the structure of the platelet cytoskeleton at rest is shown. Platelets in the resting, quiescent state circulate in the bloodstream and have a discoid shape which is maintained due to their internal cytoskeleton. The discoid platelets have a plasma membrane (black) which has transmembrane receptors like α IIb β 3 integrins (magenta). Below this is a spectrin cortex (orange) that forms the backbone of the cytoskeleton and which is connected to an actomyosin cortex (short red filaments). Together actin and myosin provide tension and hence maintain the shape. Below this lies the circumferential MB (blue) that comprises stable and dynamic MTs. The cytoplasm is filled with a rigid network of F-actin filaments (long red filaments) that resemble the spokes of a wheel and maintain the platelet shape.

2.6 Platelet activation, their cytoskeleton and its role

In the previous sections, the general structure of the platelets circulating in the bloodstream in their quiescent state, and also the structure of their cytoskeleton which helps keep them in this quiescent state, has been discussed. This section describes briefly the events that occur after the platelets encounter a vascular breach and the activation signals that are involved in their stimulation, with particular emphasis on the accompanying cytoskeletal changes that happen in these stimulated platelets and how these changes aid in the platelets to form a clot and seal the vascular breach.

2.6.1 Initiation of platelet activation and their adhesion

The platelets circulating in the bloodstream are quiescent but as soon as there is a vascular breach and the endothelium is damaged, the underlying basement membrane is exposed which contains the platelet agonist proteins collagen and laminin. This is a trigger for the platelets to rapidly arrive and adhere and gradually take several actions to seal the breach. Once there is a vascular breach, the flowing platelets are captured and instantaneously tethered to the underlying collagen via their surface receptors. Additionally, the vWF gets immobilized on the collagen surface. The platelets bind directly to collagen through their integrin receptor $\alpha 2\beta 1$ or through the binding of the GPIb-IX-V complex to the immobilized vWF [94]. In blood vessels where the shear rates are high, these tethering interactions between the receptors and platelets are not stable due to which the platelets tend to roll on the collagen or immobilized vWF until stable adhesion occurs. So the GPIb-IX-V complex helps in recruiting platelets to the site of vascular injury and reduces their velocity so that other receptors can aid in adhesion [158]. The binding of GPIb-IX-V complex to vWF further enables the binding of the low affinity collagen receptor GPVI to collagen. This in turn activates the integrins $\alpha 2\beta 1$ and the $\alpha \text{Ib}\beta 3$ and they switch from their low affinity to high affinity for their ligands. The integrin $\alpha 2\beta 1$ reinforces its binding to collagen and the integrin $\alpha \text{Ib}\beta 3$ binds to fibrinogen and vWF respectively. These integrins which have a high affinity for their ligands also have slow dissociation rates. So the integrin activation stabilizes the adhesion of platelets and also contributes to further internal signaling which is termed as 'inside-out signaling'. Subsequently, these bound ligands promote and accelerate the clustering of these $\alpha \text{Ib}\beta 3$ integrins which further triggers more intracellular signaling. This event is termed as 'outside-in signaling' [62]. It has been recently shown that the head domain of the major cytoskeletal

ABP talin, binds to the $\beta 3$ cytoplasmic domain with high affinity and activates the $\alpha \text{IIb}\beta 3$ integrin [21], thus indicating that the integrin activation is linked to the further activation of the actin cytoskeleton.

Apart from these receptors, the signaling events that occur downstream of the PAR receptors for thrombin, the P2Y₁ and P2Y₁₂ receptors for ADP and the TP receptor for TXA₂, are also the major drivers of platelet activation [94]. The binding of all these receptors to their respective ligands triggers a cascade of internal signals in the platelets. Although these cascades are slightly different for each of the receptors, all of them eventually instigate the activation of the phospholipase C₂ (PLC₂). The PLC₂ hydrolyzes the phosphatidylinositol-4,5-bisphosphate (PIP₂) which is present in the membrane, which then produces diacylglycerol (DAG) and the second messenger inositol-1,4,5-triphosphate (IP₃) [94]. The DAG activates several forms of protein kinase C (PKC) and the IP₃ is needed to raise the cytoplasmic Ca²⁺ concentrations which eventually trigger a lot of intracellular signals and pathways [94]. The IP₃ mediates the release of Ca²⁺ from the DTS. In resting platelets, the cytoplasmic Ca²⁺ concentration is about 0.1 μM but once the platelets are activated, the Ca²⁺ levels increase by 10-fold to greater than 1 μM . Thrombin is one of the most potent agonists that drives this increase in Ca²⁺ levels. [94]. This increase in Ca²⁺ levels has various effects on platelets which include the reorganization of the platelet actin cytoskeleton, platelet secretion and actomyosin mediated platelet contraction.

2.6.2 General structural features of activated platelets

The above described regulatory signals synergistically stimulate the platelets and in turn activate many complex internal signaling cascades in platelets. All of these together contribute to bringing about morphological and biochemical changes in the platelets whereby they dramatically change their shape from discoid to spherical, remodel their internal cytoskeleton, spread and release their granules. All these changes are collectively referred to as 'platelet activation'.

Most of these morphological changes can also occur in platelets when they come in contact with foreign surfaces like glass [79, 102, 123] and these changes also occur in platelets that are activated in suspension [94]. Such changes in the platelets have been visualized by electron microscopy studies (Figure 2.6A and B). In general, when platelets are activated, their peripheral MT coil which maintains their discoid shape contracts in the platelet center. This contraction is brought about by the actomyosin cytoskeleton. The constriction of both the

acto-myosin cytoskeleton and the MT coil drive the platelet granules (like α granules and dense bodies) towards the platelet centers in a structure termed as the granulomere [79, 94, 102]. In the initial stages of activation, the platelets extend numerous filopodia and thin hyalomeres (Figure 2.6B). These lamellipodia and the granulomere are separated from the ring of cytoskeletal filaments that contracts into the platelet centers [94, 102]. Such morphological changes occur in the platelets when their stimulus is weak. If it is strong, the granules that have moved into the center are secreted to the platelet exterior surface through the channels of the OCS [94]. Furthermore, the MT coil may fragment and get distributed in the newly formed filopodia [102].

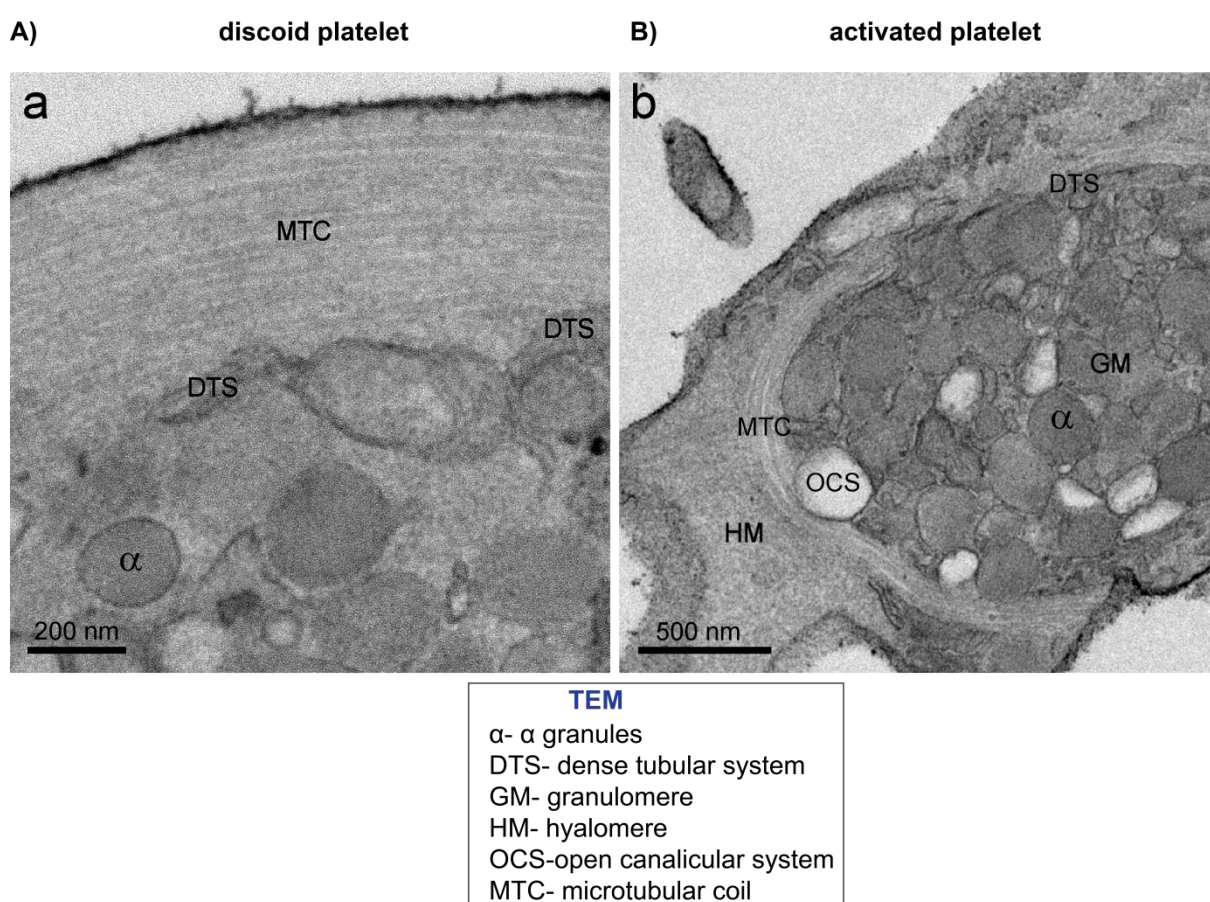


Figure 2.6: Transmission electron microscopy images of glass-adhered platelets

The TEM images of platelets adhered to glass are shown. A) Discoid platelet, incubated for 5 minutes before fixation shows peripheral MTC that stabilizes the discoid shape. Parts of the DTS line the margin and the α granules are randomly distributed. B) Activated platelet, incubated for 15 minutes before fixation has extended hyalomere. The MTC has contracted into the center and the α granules have also moved into the center in the granulomere. The granulomere and hyalomere distinctly appear to be separated by this MTC. The openings to the surface-connected OCS are also seen.

The figure caption information is adapted and the figure is reproduced from Neumüller J, Ellinger A, and Wagner T., 2015 originally published in Maaz K (ed) *The Transmission Electron Microscope - Theory and Applications*. InTech <http://dx.doi.org/10.5772/60673> [102]. © 2015 (Neumüller et al). This chapter is open-access under the Creative Commons Attribution License.

The transformation of platelets when they get activated by surfaces has also been imaged by differential interference contrast (DIC) microscopy (Figure 2.7). On adherence to glass the platelets change their shape from disc to sphere and undergo dramatic morphological transformation, spread completely and release their granules [7]. The platelets accomplish spreading within 10-12 minutes by first forming pseudopodia which extend and retract and then form hyalomeres that extend in between these pseudopodia and also laterally form from them. Furthermore, these platelets show granulomere hillocks in their center, during the early stages of spreading when pseudopodia form and which are described as being 'dome-shaped' [7]. The granules contained within these granulomeres are the dense bodies which can be seen with DIC. As these platelets begin to spread, the granulomeres slowly flatten and the dense bodies that are clustered inside are released from the granulomere and they leave 'craters' [7] at the places in the granulomeres, from where they are released (Figure 2.7-4). The craters are suggested to be part of the OCS [7]. After full spreading, the hyalomeres show membrane ruffling (Figure 2.7-5) which is reminiscent of the lamellipodia in tissue cells [7]. The releasing of granules is referred to as 'exocytosis' or 'degranulation event' and occurs mostly after formation of hyalomeres (Figure 2.7-6, 7) when the spreading has advanced but can also occur during the entire transformation process. In fully spread platelets, the craters eventually disappear, and the granulomeres flatten, sometimes completely, and within 30 minutes (Figure 2.7-8, 9), most platelets have exocytosed as much as they can [7]. It has also been suggested that platelets activated by contact with glass may show only one exocytosis event that will go on during their entire morphological transformation, unlike several events shown by chemically activated platelets [7]. The terms pseudopodia and hyalomere are synonymous with the terms *filopodia* and *lamellipodia* [7, 127]. This platelet shape change and their transformation to a flat form, with the extension of filopodia, flattening via the lamellipodia and the squeezing of their granules into the center gives them the appearance of a *fried-egg* and these morphological changes are a result of the remodeling of their cytoskeleton [94]. In fact, ultrastructural studies have shown that these platelet protrusions contain F-actin [7, 173]. The platelet shape change is important for their ability to firmly attach to the ECM, and to each other in a platelet plug and also efficiently secrete their granular contents [106]. The platelets can spread rapidly and increase their surface area up to 420% [94]. This newly expanded membrane material is obtained by pulling out membrane material from within the invaginations of the OCS. The wrinkled surface (of the discoid platelet, described in section 2.3) too serves as an additional reservoir that contribute to the overall, 4-fold platelet plasma membrane expansion during their spreading [94, 166].

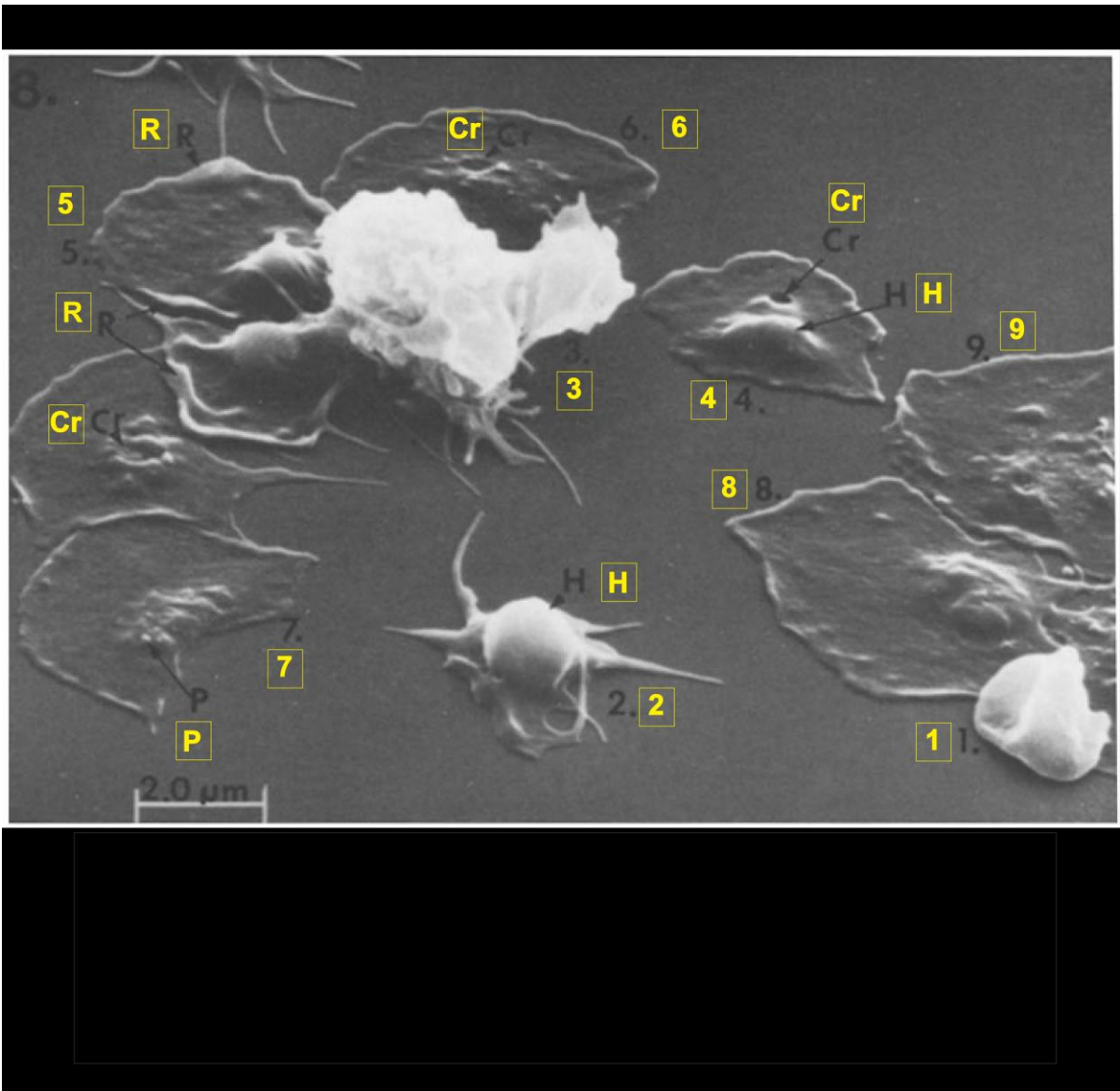


Figure 2.7: Differential interference contrast (DIC) microscopy of glass-adhered platelets

The DIC image of platelets in different spreading stages during their morphological transformation is shown. The numbering is in order of the spreading sequence seen in these platelets. 1) Platelet is not properly attached. 2) This platelet is in the late pseudopodial stage and is beginning to spread. It shows the granulomere hillock (H). 3) Aggregate of platelets which are poorly attached. 4) This platelet is in the intermediate spreading stage and shows the hillock (H) granulomere which also shows a crater (Cr) formed presumably due to the release of dense bodies. 5) Another platelet showing the hillock with its hyalomere showing ruffles (R). 6 and 7) These platelets have flattened and so have their granulomeres, which have exocytosed particles (P) i.e. dense bodies (according to [7]), and the spaces where these particles were before show craters (Cr). 8 and 9) These are fully flattened platelets that have finished spreading.

The figure is adapted and the information in the caption is reproduced with permission from Allen RD, Zacharski LR, Widirstky ST, et al., 1979 originally published in *The Journal of Cell Biology* <http://dx.doi.org/10.1083/jcb.83.1.126> [7]. © 1979 Rockefeller University Press, License number-4003211252475, Licensed content publisher- Rockefeller University Press.

The platelet activation and the subsequent events of shape change, spreading and granule release described above, can occur in response to a number of activation stimuli like adhesion to the ECM, release of soluble agonists or even by shear stress when passing through a blood vessel that is stenosed [61, 122]. The platelets only spread when they adhere to a surface. However, the platelet shape change and granule release can also occur when platelets are activated in suspension [122]. Furthermore, the platelets can be transiently activated (where they only undergo transition from discoid shape to spherical shape) or can be irreversibly activated (where they release their granular contents) and this depends on the strength of the activation stimulus [122].

2.6.3 Actin cytoskeletal reorganization

As has been discussed in the previous sections, the concerted activation of the receptors via the binding of their agonists activate intracellular signaling pathways in platelets, which bring about various changes in their structure, and allow the platelets to perform all those functions that are required to form and compact platelet plugs. Particularly the agonists thrombin, ADP and TXA₂, activate the GPCRs which couple to many heterotrimeric G-proteins that mediate signaling pathways and bring about complete platelet activation. These G-proteins include G_q/G₁₁ family, G₁₂/G₁₃ family and the G_i family. Through their respective receptors, the platelet agonists like ADP activate the G_q and G_i, whereas the TXA₂ and thrombin mainly activate the G_q and G₁₂/G₁₃. These G-proteins are involved in activating signal transduction pathways. The G_q/G₁₁ family of G-proteins activates PLC₂ that, as explained above, forms IP₃ and DAG that eventually leads to increase in cytoplasmic levels of Ca²⁺ and the activation of PKC. The G₁₂/G₁₃ family activates the Rho family of GTPases which are known to regulate many aspects of actin dynamics in cells [18]. These primarily include the subfamilies Cdc42, Rac1 and RhoA which affect the formation of filopodia, lamellipodia and stress fibers respectively. Platelets mainly express the G-proteins G_q and G₁₂/G₁₃ [106] so when the GPCRs are activated, there is activation of PLC₂ with an increase in Ca²⁺ levels and also the activation of the Rho family of GTPases, which in turn leads to remodeling of the platelet actin cytoskeleton.

The first set of changes that occur rapidly in activated platelets is morphological changes as described in the previous section. The circumferential MT coil of platelets starts to depolymerize, due to which the platelets change their discoid shape and become spherical and eventually start to extend the F-actin-rich filopodia and spread (if adhered to a surface) and

flatten by extending F-actin-rich lamellipodia. Besides these structures, spread platelets also show F-actin-rich stress fiber-like structures which are associated with myosin [148]. The MT coil of spread platelets appears compressed in their center [94]. The formation of all these actin-rich structures occurs by actin polymerization, during the reorganization of the actin cytoskeleton in platelets. The molecular aspects of these changes taking place in the actin cytoskeleton are discussed first followed by the changes in the MT cytoskeleton in the next section 2.6.4.

The reorganization of the platelet actin cytoskeleton is mediated by the proteins that regulate actin dynamics [94]. Before the platelets rapidly burst out their F-actin rich protrusions, they first undergo 'rounding' where they change their shape from discoid to spherical. This rounding depends on the depolymerization (disassembly) of the existing F-actin filaments that have hitherto kept the platelets in the resting state (see section 2.5.3). This depolymerization is brought about by the protein gelsolin which is present in abundance (5 μM) in platelets [13]. Gelsolin severs the existing F-actin filaments in the presence of Ca^{2+} and then binds to the (+) ends of the filaments to prevent elongation. Another protein, cofilin/ADF synergistically acts together with gelsolin to aid in the depolymerization [13]. Thus the connections between these F/actin filaments present in the core and the membrane are disassembled. Additionally, myosin II is also activated and it is speculated that the now severed F/actin filaments in the core, by the contractile action of myosin II, form a microfilamentous shell/ring in the central region of the platelet which also centralizes the platelet granules, as they start to spread [13, 141]. The disassembly of the F-actin filaments during the rounding step, thus breaks down the rigid cytoskeleton, and is now more open to allowing new F-actin protrusions and structures to be formed by distortion of the platelet membrane. The disassembly also results in the release of G-actin monomers from (-) ends of filaments. Furthermore, the affinity of the monomer sequestering proteins like thymosin β_4 is lost. All of this synergistically leads to an increase in the concentration of G-actin monomers.

The abundant G-actin monomers generated during the rounding step, then start to polymerize into new F-actin filaments which are extruded in the form of the platelet actin-rich structures—the filopodia and lamellipodia. This actin filament polymerization (assembly) process, which provides the protrusive force for spreading the platelets, is driven by the generation of (+) ends. These (+) ends are generated by the uncapping of F-actin filaments that were previously severed by gelsolin. Also, the gelsolin that is bound to the (+) ends is removed by phosphoinositide binding [58]. These (+) ends can also be synthesized *de novo* by the activation of the Arp2/3 complex. It has been recently suggested that the Arp2/3 complex is

responsible for forming new nucleation sites that function just like the (+) ends [13, 82]. In platelets, the Arp2/3 complex is expressed abundantly, with concentrations ranging between 2-10 μM . In the resting platelets, about 25-30% of this complex is bound to the cytoskeleton. When platelets are activated, these levels increase to 70-80% and the complex is mainly concentrated at the plasma membrane of platelets, where new F-actin assembly occurs [58, 94]. There exist upstream proteins that regulate this presence of the Arp2/3 complex at the periphery and also activate its nucleation activity. These include the proteins cortactin and the family members of the Wiskott-Aldrich syndrome protein (WASp) [58].

So actin polymerization and assembly of the F-actin filaments proceeds from these (+) ends (as explained in section 2.4.1) and there is a doubling of the F-actin content in platelets. The different F-actin rich structures formed during platelet spreading and actin reorganization are explained below and a sketch is shown in Figure 2.8.

1) Filopodia:

Filopodia are thin (0.1-0.3 μm), long, finger-like membrane protrusions that contain tightly arranged parallel bundles F-actin filaments [89]. The tight F-actin bundles are maintained by the cross-linking ABP, fascin. The F-actin filaments are in turn linked to the plasma membrane by the ERM (ezrin, radixin, moesin) proteins [100]. It has been shown that the subfamily Cdc42 of the Rho family of GTPases when activated, causes the growth of filopodia in fibroblasts [103] and the neuronal-WASp (N-WASp) further mediates this signaling from Cdc42 to the Arp2/3 complex [26]. Platelets are known to express Cdc42 [112] so it seems that the N-WASp-Cdc42 pathway occurs in platelets. However, WASp $-/-$ platelets still show the formation of filopodia [41] which suggests that there may be alternative mechanisms by which filopodia are formed. Indeed, it has been recently shown in neuronal cells that the smaller GTPase Rif (RhoF), and the formin mDia1, drive filopodia formation independently of Cdc42 and N-WASp [51]. Platelets are known to express both Rif and mDia1 [50, 152] which lead to the belief that these proteins may be involved in filopodia formation which is independent of Cdc42. Formins are localized at the tips of filopodia and may directly form linear F-actin filaments there [93]. Both these pathways ultimately bring about actin polymerization which in turn leads to filopodia formation (Figure 2.8A). Platelet filopodia are formed during the early activation stages of the platelets and extend from within the platelet interior and are additionally associated with the $\alpha\text{IIb}\beta\text{3}$ integrins [57, 60]. Also, platelets are known to express only the moesin ERM protein which links filopodia to the membrane [136]. Filopodia play important roles in mechanosensing which include roles in

wound healing, adhesion to ECM, roles as pathfinders for neuronal cone growth and as guiding sources for chemoattractants [89]. Naturally, in platelets, filopodia too are essential for mechanosensing as well as adherence to the ECM. They also capture and recruit more platelets to the platelet plug.

2) Lamellipodia:

Lamellipodia are broad but thin (0.1-0.2 μm), F-actin sheet-like structures that protrude from the membrane. They are filled with a branched network of F-actin filaments [89] which helps in cell spreading and locomotion. Like other motile cells, such as leucocytes, platelets do not move and once they adhere to a surface, they start to spread very rapidly by forming circumferential lamellipodia [58]. The subfamily Rac of the Rho family of GTPases is responsible for lamellipodia formation and it targets Arp2/3 complex whose activity is responsible for the F-actin branching [91]. Since the Arp2/3 complex can associate at both the (+) and (-) ends of F-actin filaments, it can promote actin polymerization in various new directions and thus enables the formation of a branched network [94]. It has been shown in platelets that formation of both lamellipodia and filopodia require (+) end actin assembly, as the addition of the actin polymerization inhibitor cytochalasin B (that binds to (+) ends of actin), inhibits the formation of both lamellipodia and filopodia and that Ca^{2+} is required for the formation of lamellipodia but not for the formation of filopodia [57]. Platelets express Rac1 which is essential to form lamellipodia and to also maintain the integrity of thrombi under flow. Furthermore, platelets express Arp2/3 and it is seen to localize in the rim of spread platelets indicating that it is present at the edge of newly formed lamellipodia [92]. In platelets, apart from the Arp2/3 complex, the p21-activated kinases (PAKs) are also the effectors of Rac1 [9] that bring about actin polymerization which in turn leads to lamellipodia formation (Figure 2.8B). The major function of actin-force driven lamellipodia in platelets is to allow them to spread rapidly at the site of injury to quickly cover as much damaged area as possible.

3) Stress fiber-like structures:

Stress fibers are bundles of F-actin filaments that also contain myosin II and crosslinking proteins like α -actinin which together form higher order structures in non-muscle cells. They play a major role in mediating cellular contraction and their structures are compare to those of the highly ordered actomyosin arrays typically seen in muscle cells [110]. The stress fibers are connected to focal adhesions (FAs) which are integrin-based structures that provide dynamic links between the ECM and the actin cytoskeleton [104] and exert their contractile force through them. These focal adhesions and focal complexes (which are small FAs) which are found at the periphery of migrating and spreading cells, are regulated by the GTPases Rho, Rac and Cdc42 [172]. There are also various proteins that are found at the FAs and interact with them. Such proteins are further linked to other agents that further allow cells to form complex signaling pathways that mediate the various cellular behaviors. Examples of such FA associated proteins include talin, vinculin, paxillin [172]. The subfamily RhoA of the Rho family of GTPases plays a major role in the formation of stress fibers and regulating the actomyosin mediated contractility [18]. The RhoA activation is mediated via the Rho-associated kinase (ROCK)/myosin II pathways and can also mediate stress fiber formation via its formin effectors mDia1 and mDia2 [71, 155], all of which are also found in platelets [49, 113] and (Figure 2.8C). The presence of stress fiber-like structures associated with myosin II and α -actinin, in platelets that have spread, has been confirmed by immunoelectron microscopy and immunofluorescence studies [148]. It has further been shown that these stress fiber-like structures form in platelets after they have completed spreading and focal adhesion proteins like vinculin are found at the tips of the F-actin bundles [99]. This may imply that platelets require stress fiber-like structures to mediate their contractile forces through these FA proteins which may play a role in compacting in the blood clot. It has been shown that the integrity of blood clots is weakened in the absence of stress fiber-like structures [19].

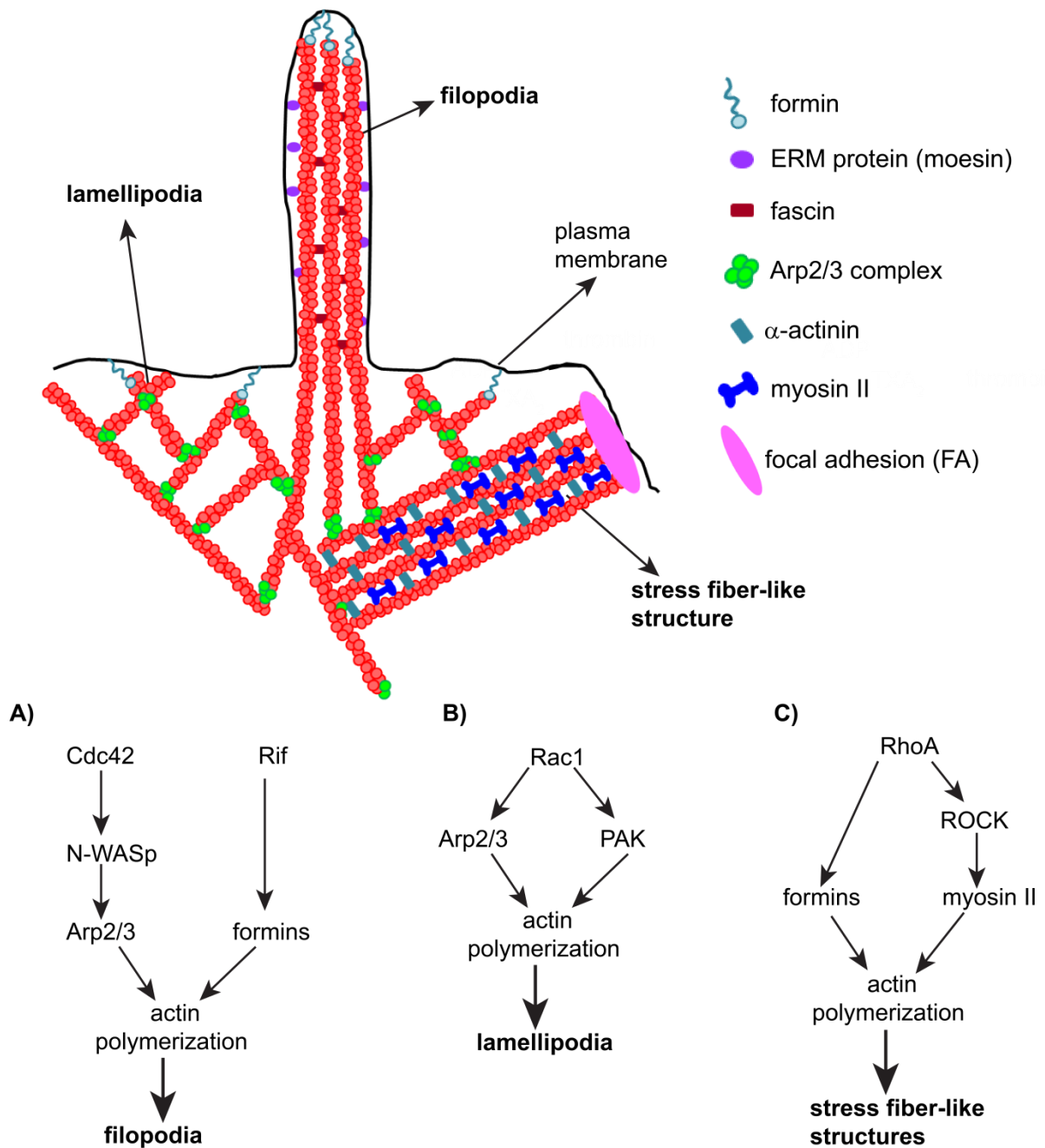


Figure 2.8: Sketch of filopodia, lamellipodia and stress fiber-like structures

Sketch of the F-actin rich structures – the filopodia, lamellipodia and stress fiber-like structures (in platelets) is shown. The signaling pathways that lead to their formation via actin polymerization are also shown. A) The filopodia contain parallel bundles of F-actin filaments that are linked to the plasma membrane by ERM proteins, of which platelets express moesin. Filopodia formation occurs via Cdc42 and Rif (formin) pathways. The formins are present near filopodial tips. B) The lamellipodia contain short networks of F-actin which are branched due to the Arp 2/3 complex. Lamellipodia formation occurs via Rac1 whose effectors include Arp2/3 and PAK. C) The stress fiber-like structures are high order structures of F-actin bundles that are crosslinked by the α -actinin and contain myosin II. Their formation occurs via RhoA whose effectors include formins and ROCK/myosin II. FAs are found at their tips.

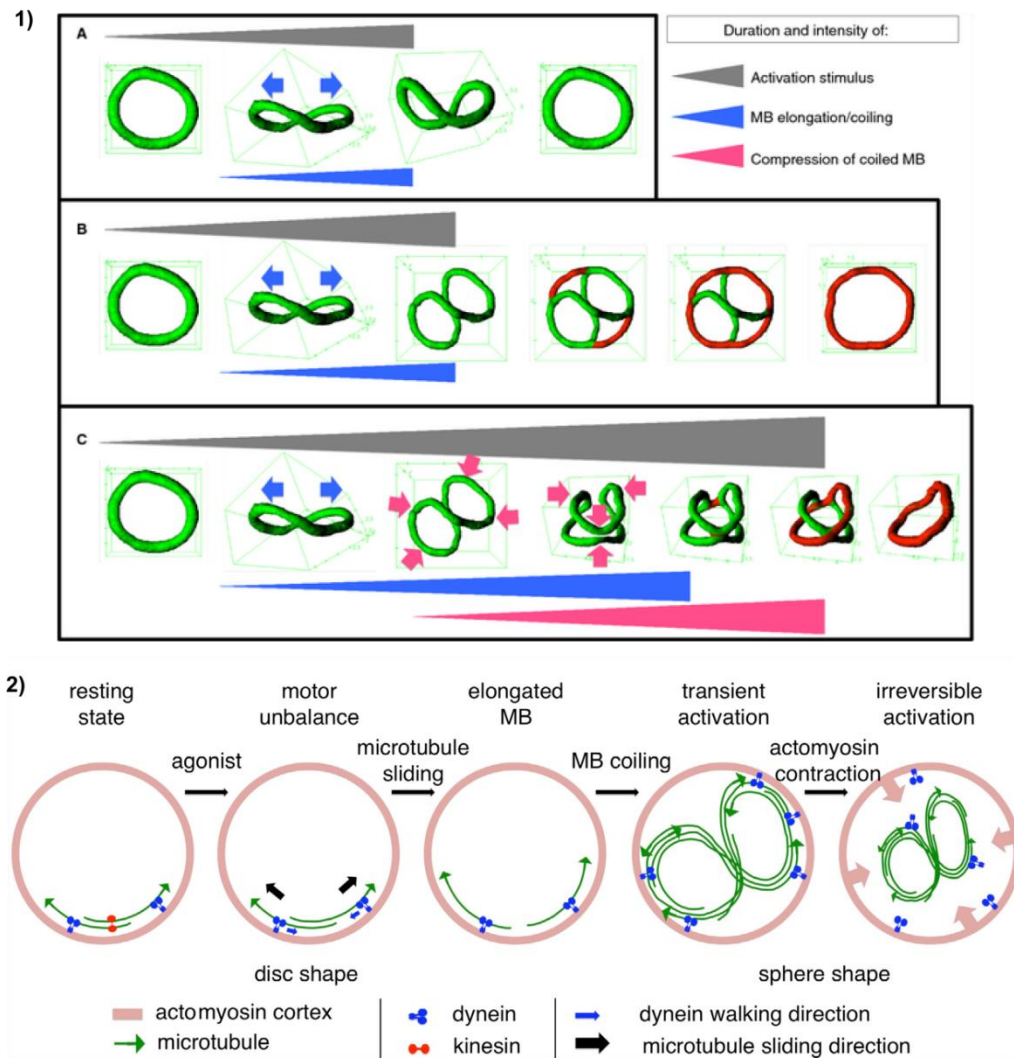
2.6.4 MT reorganization and actomyosin contraction

Along with reorganizing their actin, the platelets also reorganize their MT cytoskeleton. The MT ring¹ that maintains the discoid shape of the platelets has to remodel so that the platelets can change their shape during activation. In activated platelets which are spherical in shape, a smaller MT ring is observed and it is suggested that this ring forms due to the action of actomyosin which bring about the contraction of the platelet MB. This process is referred to as 'internal contraction' [68, 165]. The mechanisms which lead to this smaller MT ring formation have been only recently understood [36].

The MB of platelets consists of multiple MTs that coil several times and form a single stable MT and is associated with 8-12 dynamic MTs that can polymerize in both directions [108]. Based on the work in [108], a recent study has shown that the MTs in the MB of platelets elongate and the MB coils during platelet activation. The crosstalk between MT motors and the actomyosin cortex play major roles in this process [36]. The degree of MB coiling depends on whether the platelets are transiently activated or irreversibly activated [36, 122]. The mechanisms that lead to different degrees of MB coiling and the molecular mechanisms behind it are shown in Figure 2.9 (reproduced with permission from [36, 122]). During transient activation of platelets (i.e. when they change their shape from discoid to spherical and this shape change is reversible), if the activation stimulus is weak (indicated in grey in Figure 2.9-1A), the MB (which is in the resting state) elongates slightly and the MB ring slightly coils by distortion (indicated in blue and green respectively in Figure 2.9-1A). However if there is no further stimulation, the slightly coiled MB relaxes back to its resting state. If the transient activation stimulus is strong (indicated by blue in Figure 2.9-1B), the MB elongates just like before but coils more tightly and the newly polymerizing MTs (i.e. the dynamic MTs) present in the MB switch to the opposite end of this coiled structure which slightly compresses (indicated in red in Figure 2.9-1B) and deviate from the coiled path to form a new flat MB. Thus such platelets simultaneously show an elongated-coiled and flat-resting MB. The contraction of actomyosin is responsible for the compression of this coiled MB structure [36]. When the platelets are irreversibly activated (i.e. granule release occurs), the coiled MB is even more strongly compressed (indicated in pink in Figure 2.9-1C) because of which the two ends of this coiled structure come closer. The dynamic MTs that deviate towards the opposite side thus have to follow a shorter path and they form a smaller MT ring in such irreversibly activated platelets [36, 122]. The molecular mechanisms behind this MB coiling have also been investigated and based on these findings a model for the MB coiling

¹In this dissertation, the MT coil/ring refers to the MB structure described in section 2.5.4

has been proposed (Figure 2.9-2, [36, 122]). The MB is kept in its resting state by the antagonistic actions of kinesin and dynein, and dynein is anchored to the acto-myosin cortex. When the platelets are activated, the kinesin motor counteractions are inhibited and the dynein motors slide the MTs apart, which leads to MB elongation. The dynein motors can move whole MTs by attaching via their two motor domains to a MT and walking towards the (–) end. They can also slide anti-parallel MTs which are adjacent to each other by binding their two motor domains to each of the MTs and walking to the respective (–) ends [122, 150]. This leads to the three-dimensional twist of the MB probably because there is a weakening of the MB bundle and/or because there is limited space available [122] and the platelets undergo the discoid to spherical transition (MB elongation/elongated MB in Figure 2.9). For the sliding of the MB and inducing its coiling, high forces may be required. It is possible for dynein motors alone to exert such high forces due to their ability to establish catch-bonds that strengthen at higher load [117]. These high forces first of all have to be proportional to the strength of the activation stimulus and also have to be sensed by the acto-myosin cortex [122] which, in the event of a strong, irreversible activation of the platelets, will contract and lead to the compression of the coiled MB (compression/irreversible activation in Figure 2.9, [122]). Myosin II plays a role in this process, as its inhibition strongly reduces internal contraction of the MB in activated platelets [36, 68, 134]. Also it has been recently implicated that acto-myosin themselves can act as force mechanosensors and their force is proportional to the substrate rigidity [46, 96]. This may indicate that acto-myosin can sense the forces developed by the action of dynein motors and when these forces are strong enough (e.g. during irreversible platelet activation), the surrounding environment may become rigid (MB elongation and coiling can stiffen the plasma membrane), and this could be the trigger for the acto-myosin cortex to contract (acto-myosin contraction in Figure 2.9) in platelets [122]. It can be advantageous to have both a sensory and a response function in the same molecule (i.e. in myosin IIA in case of platelets), as the actions can be performed a lot faster and can be adapted accordingly to the strength of the activation stimulus. These concerted actions of acto-myosin and MTs may explain the cytoskeletal crosstalk occurring during platelet activation [122].

MB coiling and role of MT motors and actomyosin in response to strength of activation stimulus**Figure 2.9: MB coils during platelet activation by action of MT motors and actomyosin**

Sketch of the MB coiling and compression in response to activation stimulus, and the molecular interactions behind it is shown. The MB elongates, coils and compresses during transient or reversible platelet activation. 1A) When stimulus (grey) is weak during transient activation, MB elongates (blue) and distorts (green) resulting in spherical shape but relaxes to the resting state when stimulus is not sustained. 1B) When stimulus (grey) is strong during transient activation, MB elongates (blue), coils and dynamic MTs form new flat MB (red), which becomes the new resting MB, if stimulus is not sustained. 1C) When stimulus (grey) is strong during irreversible activation, MB elongates (blue), coils and compresses (pink), and dynamic MTs diverge around a shorter path to form smaller MT ring (red). 2) The dynein motor anchored to acto-myosin cortex, slides MB, when kinesin counteractions are reduced, leading to MB elongation. Due to space constraints, MB coils (transient activation) and compresses due to acto-myosin contraction (irreversible activation).

The figure 1) is adapted and the information in the caption is reproduced with permission from Sadoul K., 2015 originally published in *Journal of Thrombosis and Haemostasis* <http://dx.doi.org/10.1111/jth.12819> [122]. © 2014 International Society on Thrombosis and Haemostasis, License number- 4003761272552, Licensed content publisher- John Wiley and Sons. The figure 2) is adapted and the information in the caption is reproduced with permission from Diagouraga B. Grichine A, Fertin A, et al., 2014 originally published in *The Journal of Cell Biology* <http://dx.doi.org/10.1083/jcb.201306085> [36]. © 2014 Rockefeller University Press, License number- 4003730176881, Licensed content publisher- Rockefeller University Press.

Electron microscopy studies have seen that the platelet granules are concentrated in the center and the smaller MT ring surrounds these granules in the center of activating platelets [165]. It is suggested that the granules are packed closely for allowing rapid secretion of their contents into the exterior of the platelets via their fusion with the plasma membrane of the OCS (see section 2.6.2) that spans the entire platelet [143, 157]. The MB coiling and its compression by acto-myosin-mediated contraction are suggested to be responsible for this concentration of the granules in the center of activating platelets [122] and whether the platelets get transiently activated or irreversibly activated is determined by the efficacy of this acto-myosin contraction [122]. It has also been suggested that the acto-myosin contractile force generated during this contraction accelerates fusion of granules not only with the plasma membrane but also with each other, and this force may also help in discharging the granules towards the plasma membrane of platelets [107]. These observations are supported by another observation that RhoA-deficient platelets, which have reduced acto-myosin abilities, also show defect in shape change and α granule release [113].

In most of these electron microscopy studies where smaller MT rings have been observed, the platelets were activated in suspension or were surface-activated only for few seconds to minutes. Some of these studies where they also looked for platelet shape change and internal contraction have also observed MT rings surrounding central organelles, after treatment of MTs with stabilizing agent taxol and have seen no obvious difference in the diameters of these MT rings between control and taxol treated platelets [165, 167] which leads to the speculation that MTs have no apparent role in platelet shape change and internal contraction. These studies also suggest no role of MTs in secretion of platelet granules [167]. However, immunofluorescence studies on adhered, fixed platelets have shown that granular trafficking is strongly regulated by F-actin filaments and MTs during adhesion process of platelets and begins with centralization of the granules in the granulomere by F-actin contractile rings. The MTs then further reorganize from the granulomere to traffic the granules to the plasma membrane of platelets [27, 28].

To summarize, when the platelets are activated and adhere to the ECM, their cytoskeleton is dramatically remodeled (Figure 2.10). The platelets adhere to their ECM via their integrins which are linked to ABPs like talin and vinculin. The platelets change their discoid shape and become spherical due to the sliding of their MT coil by dynein. The MT coil compresses via the contractile action of acto-myosin. The platelets extend filopodia and lamellipodia and start to spread. The MT coil along with platelet granules moves towards the platelet center. How the cytoskeleton reorganizes during sustained spreading has not been looked at in much details.

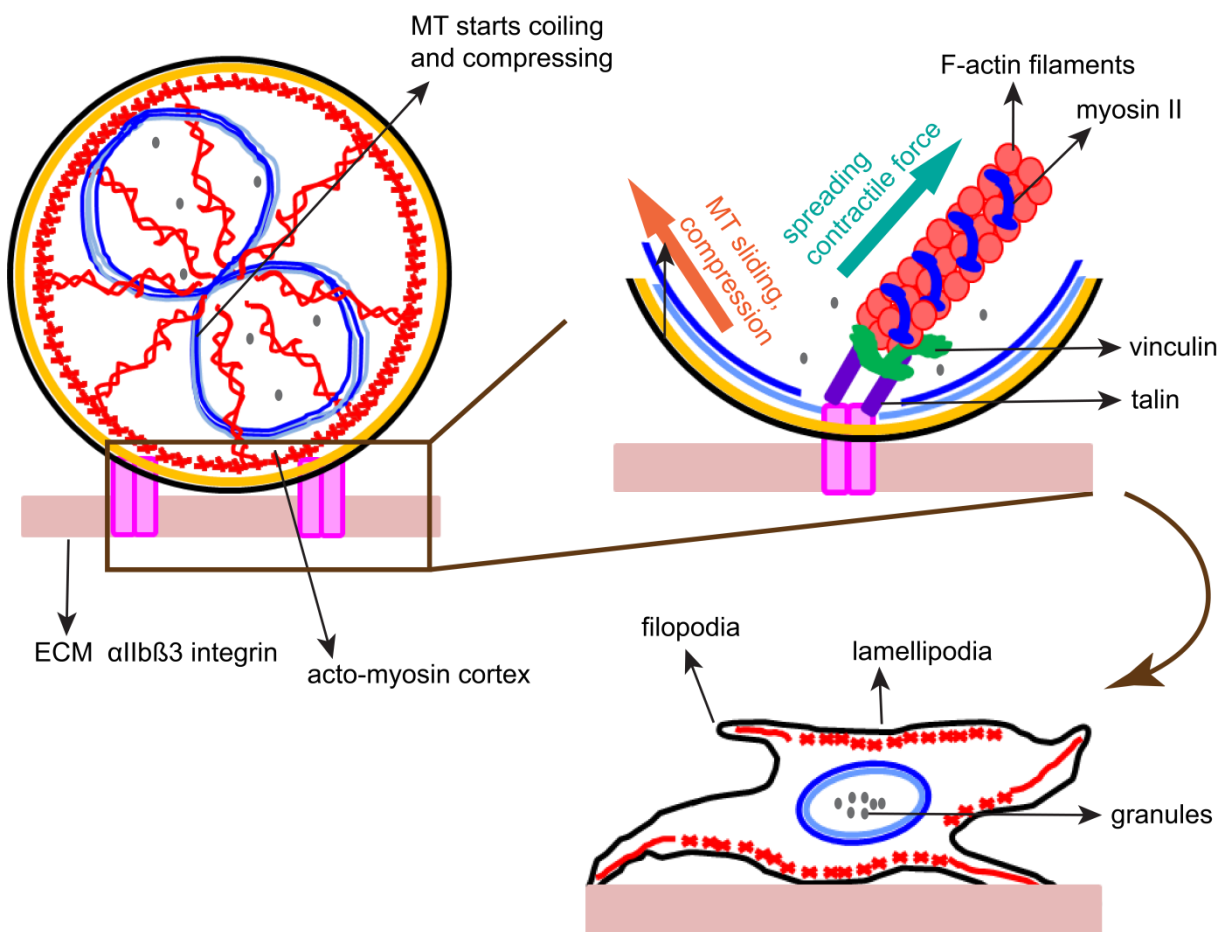


Figure 2.10: Sketch of activated platelet cytoskeleton

A simplified sketch of the structure of the platelet cytoskeleton when it is activated is shown. Platelets change their shape from discoid to spherical which is brought about by remodeling of their cytoskeleton. The platelets attach to the ECM via their integrins like the $\alpha\text{IIb}\beta\text{3}$ (magenta) which are linked to the ABPs talin (violet) and vinculin (green). The circumferential MT¹ coil slides by action of dynein motors and starts to coil, inducing shape change. In irreversibly activated platelets, the actin (red) and myosin (blue) act together to compress the MT coil. The platelets extend filopodia and lamellipodia and start to spread and the MT coil starts to move towards the platelet center enclosing the platelet granules.

¹In this dissertation, the MT coil/ring refers to the MB structure described in section 2.5.4

2.6.5 Platelet secretion, aggregation and clot compaction

During platelet activation, apart from the platelet shape change, spreading and cytoskeletal remodeling, the platelets in a thrombus/clot, recruit more platelets to grow the clot by secreting various molecules that signal more platelets to join this clot. These secretory signals are in turn amplified, thus recruiting more and more platelets to the clot. The platelets then aggregate and eventually compact the clot. These processes are highly complex and dynamic, and *in vivo* all of these processes occur simultaneously.

1) Platelet secretion and role of cytoskeleton:

When the Ca^{2+} levels increase during platelet activation, the platelets secrete their granular contents towards the platelet exterior [94]. The purpose of this is to generate more activation signals in the exterior so as to recruit more platelets to the growing thrombus. As mentioned before, granules fuse with the OCS at the platelet center and their contents travel through the OCS channels towards the extracellular environment. The contents of these granules include adhesive receptors such as P-selectin, $\alpha\text{IIb}\beta 3$ integrins and GPIb-IX-V complexes that increase the efficiency of platelets to adhere to the damaged surface and also allow platelet adherence to each other in the later stages of haemostasis [94]. The released granular contents also include more ATP, ADP, vWF, Ca^{2+} , coagulant proteins such as fibrinogen and factor V, serotonin. Additionally platelets also release TXA_2 and thrombin.

It is suggested that the cytoskeletal contraction that occurs during platelet activation also governs the secretion of granules by promoting their interaction with each other and with the OCS [45]. It has been demonstrated by electron microscopy and by functional studies that platelet α -granules are coated with F-actin. Furthermore, actin polymerization facilitates release of α -granules and the F-actin cytoskeleton differentially regulates the release of α -granules and dense granules [45, 171]. The role of MTs in granule secretion is uncertain. In some studies it has been demonstrated that MTs are involved in granule secretion [14, 138] whereas other studies suggest that MTs play no role in secretion or any platelet activation processes [167]. However, some recent immunofluorescence studies done on platelets adhered and spread on glass have showed that MTs along with actin are involved in granule distribution in platelets [27].

2) Platelet aggregation and clot compaction:

A concerted effect of this granular secretion is the amplification of the platelet activation. The ADP, TXA₂ and thrombin are the major amplifiers of platelet activation [94]. They further activate their GPCRs which bring about the intracellular signaling cascades described in the previous section. Eventually, platelets start to aggregate at the growing thrombus and many of the mechanisms described previously, are important for this process. The platelets attach to each other via their filopodia. Furthermore, they degranulate and their secreted adhesive receptors such as P-selectin help intracellular adhesion. These signals also accelerate the formation of platelet agonists ADP, TXA₂ and thrombin. The platelet aggregation can then proceed in two phases [94]. Initially, vWF bonds are established between platelets via the GPIb-IX-V complex. These bonds are very tight and help to keep the platelets in close proximity to each other which is essential in high shear flow. This in turn allows the α IIB β 3 integrins to form more stable bonds with its ligand, fibrinogen and also fibronectin bonds are formed [94]. As these platelet-fibrinogen aggregates grow, RBCs are incorporated into the growing thrombus. It is implied that RBCs also play an active role in platelet haemostasis [8]. Finally, the platelet clot contracts by the concerted action of actin and myosin and the clots are further stabilized by several mechanisms which include thrombin-mediated conversion of fibrinogen to fibrin strands which are insoluble. Furthermore, the generation of contractile force needs myosin ATPase activity and is also dependent on the ROCK and MLCK mediated regulation of actin and myosin [42, 94].

2.7 Real-time monitoring of the platelet cytoskeleton

The importance of the platelets and the role of their actin and MT cytoskeleton have been highlighted in the previous sections. Because platelets lack a nucleus, they cannot be transfected or microinjected with fluorescent labels. Hence, all the information about their cytoskeleton that is available so far has been majorly done after chemical fixation of the platelets. The traditional approaches used are mainly immunofluorescence studies with phalloidin or anti-actin and anti-tubulin antibodies and electron microscopy studies, which have been discussed in previous sections. Such studies have certainly contributed immensely to the knowledge about the cytoskeletal changes that take place in platelets during their shape change. However, the real-time monitoring of cytoskeletal dynamics, without impairing the cytoskeleton in any way, is always desirable. Since the focus of this dissertation is actin and MT, in this section, some of the recent advances made in the real-time imaging of platelet

actin and MT cytoskeletal dynamics and the novel findings from them that have contributed to the existing knowledge about the platelet cytoskeleton are discussed briefly. All of these real-time studies are done with mouse blood platelets, because, as discussed above, human platelets lack a nucleus and cannot be transfected.

2.7.1 Novel advances in monitoring actin cytoskeleton

Green fluorescent protein (GFP) is one of the most commonly expressed protein in cells. It can be fused to the protein of interest and is expressed in cells to monitor the cellular localization of that protein. GFP-actin fusion protein has been used to study actin dynamics in live cells. Using GFP-actin expressing platelets from mice, a novel actin structure has been identified in platelets and is termed the actin nodule [20]. The mouse platelets were allowed to spread on fibrinogen-coated coverslips for 30 minutes in the absence of any agonist. Mouse platelets, unlike human platelets, do not form broad lamellipodia and stress fibers in absence of agonists such as thrombin. It was observed in these platelets that small nodule-like structures formed during the early stages of spreading that underwent dynamic movement continuously [20]. These actin nodule structures disappeared as soon as thrombin was added and when stress fibers formed [20]. Also, the nodules were associated with low RhoA and ROCK activity but required actin polymerization. Overall, it is suggested that these actin nodules are novel structures that are formed during early platelet spreading stages and drive the formation of the lamellipodia and stress fibers that are formed later in the spreading process [20]. In a recent development, a 17-amino-acid-peptide called Lifeact has been fused with GFP (Lifeact-GFP) and has been shown to be an attractive alternative to GFP-actin. It does not interfere with in vitro and in vivo actin dynamics [119]. Lifeact-GFP expressing mice have been generated and it has also been shown that Lifeact-GFP platelets show rapid modeling of their actin during spreading on fibrinogen and also that their spreading is not affected [120, 129]. Recently, Lifeact-GFP platelets have been used to investigate details about the actin nodules [20] by using structured illumination microscopy (SIM) and direct stochastic optical reconstruction microscopy (dSTORM) super-resolution microscopy, along with live-cell total internal reflection fluorescence (TIRF) microscopy [114]. It was observed that the actin nodules comprise of actin-rich structures linked by actin bundles. The nodules were enriched in the adhesion proteins, talin and vinculin. Furthermore, actin nodule formation was dependent on the WASp protein and the Arp2/3 complex and the nodules were required for interaction of platelets with each other [114].

2.7.2 Novel advances in monitoring MT cytoskeleton

A novel technique of expressing a GFP-linked, MT (+) end marker protein, EB3 (EB3-GFP) in MKs was recently shown. These MKs produced platelets that expressed this EB3-GFP and hence it was possible to monitor the MT dynamics in living platelets [108]. With this novel way, it was shown (as discussed in the previous section 2.5.4) that the platelet MB is a bipolar-array comprising of a stable MT and 8-12 dynamic MTs which have mixed polarities [108]. Besides that, such EB3-GFP expressing platelets were thrombin-activated and the dynamics of EB3-GFP were followed for 2 minutes. The platelets changed shape and extended filopodia and the MT coil was compressed in the center. It was seen that MT polymerization was increased following activation and the coil was fragmented or was totally disassembled as individual MTs radiated outwards in the filopodial extensions and appeared to polymerize away from the platelet. The EB3-GFP was present at the tip of these filopodia [108]. These findings suggest that agonist generated platelet activation controls MT nucleation activity [108].

Recently, the formation of the small MT ring described in section 2.6.4 has been shown in platelets that adhered, changed their shape and started to spread on a glass surface [36, 122]. The platelets were stained with a MT tracker dye, Tubulin tracker (a taxol based compound coupled to a fluorochrome). The discoid platelets showed the resting MB and when they were activated with ADP, the platelets changed their shape from discoid to spherical showing a coiled MB and later spread, forming the smaller MT ring [36]. The sphere shape to spread shape transition as seen from the time-lapse video, was about 6 minutes, after which the imaging was not continued [36].

2.8 SiR-actin and SiR-tubulin for live F-actin, MT imaging

In the previous section, recent advances in the real-time monitoring of platelet actin and MT cytoskeleton in mouse platelets have been discussed. Many platelet-related disorders such as Glanzmann thrombasthenia, Bernard–Soulier syndrome etc. are characterized with impaired cytoskeletal reorganization [140]. Hence it is more desirable to study *human* blood platelets considering their high importance from a medical point of view. However, since these platelets are anucleate, real-time visualization of their cytoskeleton has hitherto been difficult. But now it is possible to visualize the actin and MT cytoskeleton of anucleate cells like human

blood platelets in real-time due to the recently introduced fluorogenic cytoskeletal probes, SiR-actin and SiR-tubulin [86].

An ideal fluorophore for live imaging of the cytoskeleton of cells must possess special properties. These include being highly fluorogenic, nontoxic and having far-red excitation and emission wavelengths, because at such wavelengths there is no phototoxicity to cells and there is also no undesirable autofluorescence. Also such a fluorophore should be cell permeable and also very specific to the molecule of interest [86, 87]. Such an ideal fluorophore, which is cell permeable and has far-red excitation and emission wavelengths has been recently developed [87]. This fluorophore, called the silicon-rhodamine (SiR) fluorophore, can be specifically coupled to proteins in live cells, using various labeling strategies [87]. The SiR is a silicon-containing rhodamine derivative which have been shown to be membrane permeable and having supreme spectroscopic properties [38].

The recently introduced SiR-actin and SiR-tubulin probes (Figure 2.11) are based on these SiR-derivatives and are conjugated with ligands that are specific to the F-actin and MT cytoskeletal proteins [86]. The SiR-actin probe (Figure 2.11A) is conjugated to a desbromo-desmethyl-jasplakinolide which specifically binds to F-actin in cells. The SiR-tubulin probe (Figure 2.11B) is conjugated to docetaxel which specifically binds to MTs. The specialty of the SiR-derivatives is that they exist in an equilibrium state between a non-fluorescent spirolactone (OFF state) and a fluorescent zwitterion (ON state; Figure 2.11C, [86]). If the SiR-derivatives aggregate or unspecifically bind to hydrophobic surfaces, the OFF state is favored. However, if these derivatives interact with polar proteins, they switch into the ON state (Figure 2.11C, [86]). Moreover, these probes are highly fluorogenic, meaning the fluorescence intensity is increased after they bind to their specific proteins (F-actin and MTs). It has been shown that the binding of SiR-actin to F-actin *in vitro*, increased its fluorescence intensity by more than 100-fold as compared to binding to BSA (Figure 2.11D and [86]). The binding of SiR-tubulin to polymerized tubulin, increased its fluorescence intensity by more than 10-fold (Figure 2.11E and [86]). Besides, it has also been shown that these SiR-actin and SiR-tubulin probes did not exhibit any substantial cytotoxicity or any undesirable effects on the actin and tubulin kinetics in the cells, at the concentrations that were used [86]. These probes were also demonstrated to be permeable to cells such as, human primary dermal fibroblasts and RBCs, that are normally difficult to transfect and the probes also showed no detectable phototoxicity [86]. Hence these properties of having far-red far-red excitation and emission wavelengths, being fluorogenic and highly specific, being minimally cytotoxic and

phototoxic and being highly cell permeable, make these SiR-actin and SiR-tubulin probes very suitable for live-cell imaging [86].

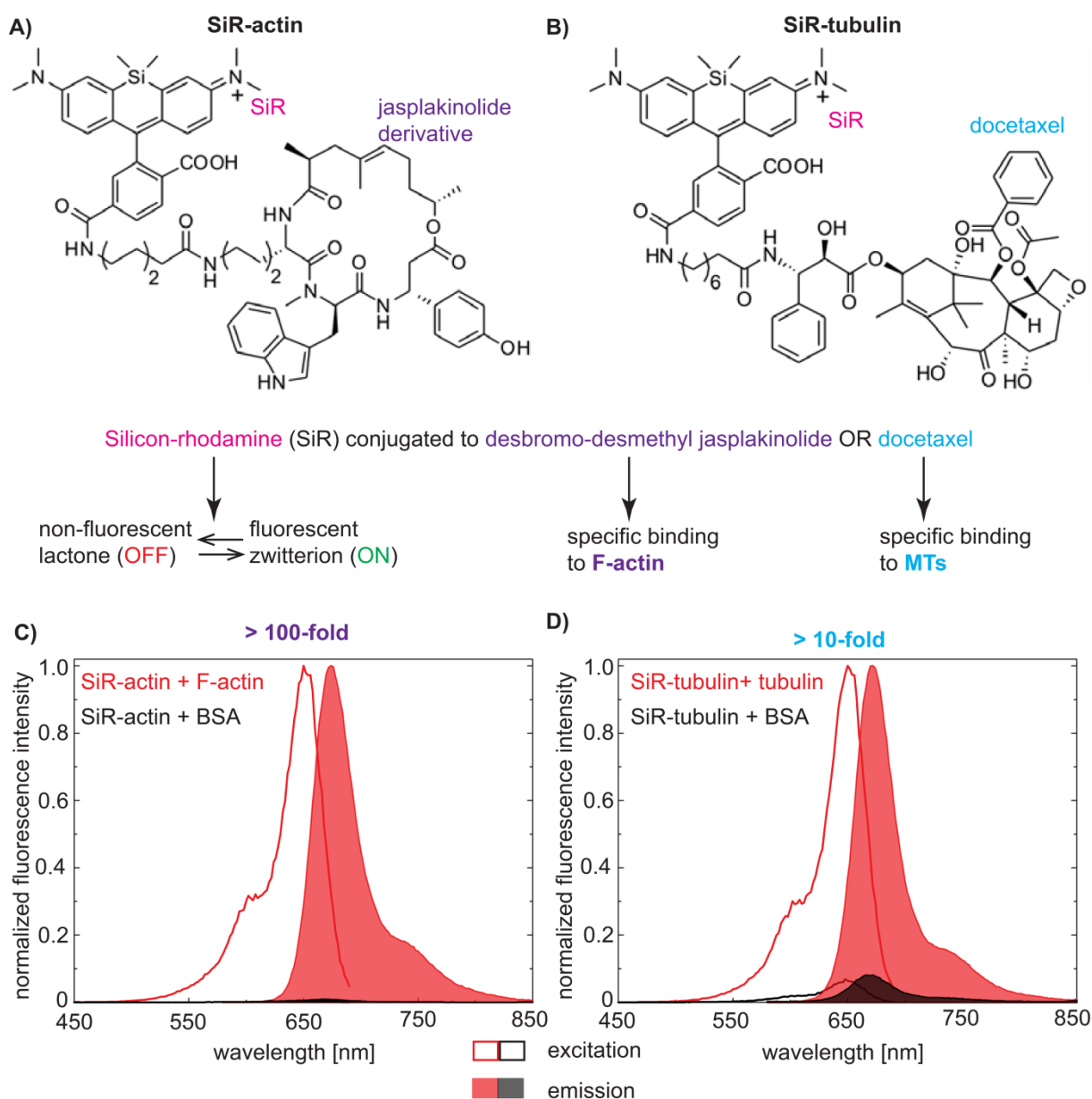


Figure 2.11: Properties of the SiR-actin and SiR-tubulin cytoskeletal probes

The structure of the SiR-actin and SiR-tubulin cytoskeletal probes is shown along with their mechanism. A and B) The SiR-actin and SiR-tubulin probes are conjugated to a jasplakinolide derivative and docetaxel respectively which specifically bind to F-actin and MTs. The SiR exists in an equilibrium state between a non-fluorescent lactone (OFF) and fluorescent zwitterion (ON). When it binds to proteins, in this case F-actin or MTs, the ON state is favored and the probes increase their fluorescence intensity. C and D) The increase in the *in vitro* fluorescence intensity of SiR-actin binding to F-actin, is > 100-fold, and that of SiR-tubulin to polymerized tubulin, is > 10-fold, as compared to binding to BSA.

The structures of the probes (A and B) are reproduced with permission from Lukinavičius G, Reymond L, D'Este E, et al., 2014 originally published in Nature Methods <http://dx.doi.org/10.1038/nmeth.2972> [86]. © 2014, Rights Managed by Nature Publishing Group, License number-4002931300284, Licensed content publisher- Nature Publishing Group. The spectral data has been plotted from the source data available from [86].

Due to these ideal properties, the SiR-actin and SiR-tubulin probes are also suitable for super-resolution microscopy such as stimulated emission depletion (STED) microscopy. In fact, in this same study, using the SiR-tubulin probe, the MT diameters in centrosomes of human fibroblast cells, have been imaged at the highest resolution (39 ± 10 nm) so far known in living cells [86]. Also, it has been shown using the SiR-actin probe in live rat hippocampal neurons that, these neurons have periodic structures along their axons with a periodicity of 181 ± 20 nm [86]. These values agree with values reported from fixed phalloidin-stained neurons, thus highlighting the creditability of these probes for usage in super-resolution imaging [86].

Apart from their use in super-resolution imaging of nucleated cells, these probes have also been recently used to image anucleate blood cells and their usage has revealed novel findings. It has been shown that the F-actin in RBCs, which was previously assumed to be not dynamic, is in fact dynamic, and owing to this dynamic feature, the F-actin of the RBC membrane controls its biomechanical properties [52]. A very recent study has used the SiR-tubulin probe in platelets, and has modeled the MB coiling during their shape change from discoid to sphere, by activating the platelets in suspension, using ADP [37]. It is suggested that, the MB coils and shortens, if the cortical tension increases rapidly, whereas, it only shortens but does not coil, if there is a slow increase of the cortical tension [37].

2.9 Open questions

There are some aspects of the platelet cytoskeleton that are yet to be studied carefully. The first open question, as discussed previously, is the inability to view the cytoskeleton of human blood platelets in real-time, because of their lack of a nucleus. Now that the SiR-actin and SiR-tubulin probes that specifically bind to F-actin and MTs are available, this dissertation has addressed this question. Secondly, until now, most of the studies on the platelet actin and MT cytoskeleton (both post-fixation and real-time) have concentrated on studying the early activation process in platelets and the platelet shape change. In many of these studies, the platelets have been activated in suspension. Only few studies have looked at the platelet cytoskeleton after their adherence and spreading on foreign surfaces. Out of these, most of them are immunofluorescence studies done post-fixation. Also, the real-time monitoring of platelet cytoskeleton, described in the previous section 2.7, has mainly concentrated on the earlier activation processes taking place in platelets either in suspension or in early activation stages. Since it is implied that glass-surface activated platelets seldom

spread longer than 30 minutes, most of the platelet cytoskeletal studies have not been carried out beyond this half hour and details of the later stages of cytoskeletal reorganization in platelets are lacking. The adherence of platelets to the ECM triggers a complex, dynamic intracellular process that consists of multiple signaling events that occur both simultaneously and sequentially and in which the platelet actin and MT cytoskeleton play major roles. The observation that platelet FAs continue to mature at least an hour after initial contact or that platelets mediate their clot contraction process after an hour of their activation [13], point towards the notion that important cytoskeletal-mediated platelet processes continue for a long time. Thus a crucial understanding of these processes is necessary. Hence in this dissertation, the real-time, temporal dynamics of the F-actin and MT cytoskeleton, in platelets spreading on fibrinogen-coated coverslips, for longer than 1 hour, are explored.

3. Materials and Methods

In this chapter, the materials and methods which include the methods of platelet purification and sample preparation, the experimental techniques followed and all materials used for the experimental measurements are described in details. Furthermore, all the data analysis steps and approaches taken to interpret the experimental results are also described here. All graphs were plotted and statistical data analyses were made using the data analysis and graphing software, OriginPro 8.5 (OriginLab, Northampton, MA, USA), if not otherwise stated. The data analysis for detecting the F-actin filaments of SiR-actin labeled platelets by the Filament Sensor program [39], and the linear fitting of platelet spread areas and F-actin total line length plots was performed by Dr. Benjamin Eltzner from the Institute for Mathematical Stochastics, Georg-August-University, Göttingen. Hence, the description of these data analyses (see sections 3.9 and 3.10) were written together with Dr. Eltzner.

3.1 Fibrinogen coating of coverslips

Glass coverslips were completely coated with fibrinogen for allowing platelet adherence. For this purpose, coverslips (24×60 mm or 21×26 mm or \varnothing 20 mm, No.1 thickness, VWR, Radnor, Pennsylvania, USA) were cleaned thoroughly with isopropanol and dried with a stream of nitrogen gas. To facilitate complete and even coating of fibrinogen, the coverslips were rendered hydrophilic by activation in a plasma cleaner (Plasma Cleaning, PDC-32 G, Harrick Plasma, Ithaca, New York, USA) with the radio frequency (RF) power at medium level, for approximately 1.5 minutes. Afterwards, enough labeled fibrinogen solution (Alexa Fluor 488 conjugate, Ex/Em: 495/519 nm, at a final concentration 0.1 mg/mL prepared from a 1.5 mg/ml stock of fibrinogen from human plasma, Invitrogen, Darmstadt, Germany) or unlabeled fibrinogen solution (at a final concentration 0.1 mg/mL prepared from a 20 mg/mL stock of fibrinogen from human plasma, Invitrogen, Darmstadt, Germany) was put on the activated coverslips to completely coat them. The coverslips were then incubated at RT for 1 hour (in the dark in case of labeled fibrinogen coating) and then washed thrice with phosphate buffered saline (PBS; buffer recipe in Appendix A) to remove any unbound fibrinogen. Usually, the coated coverslips were prepared one day prior to the experiments and were stored in PBS at 4°C until further use. For live platelet imaging experiments, labeled

fibrinogen coated coverslips were used. Figure 3.1A shows an epifluorescence image of a typical, completely coated fibrinogen coverslip. Sometimes the fibrinogen coating was uneven at some places or showed bright spots which were presumably fibrinogen clusters (Figure 3.1B and C). Such areas were omitted for live platelet imaging (see section 3.5.2).

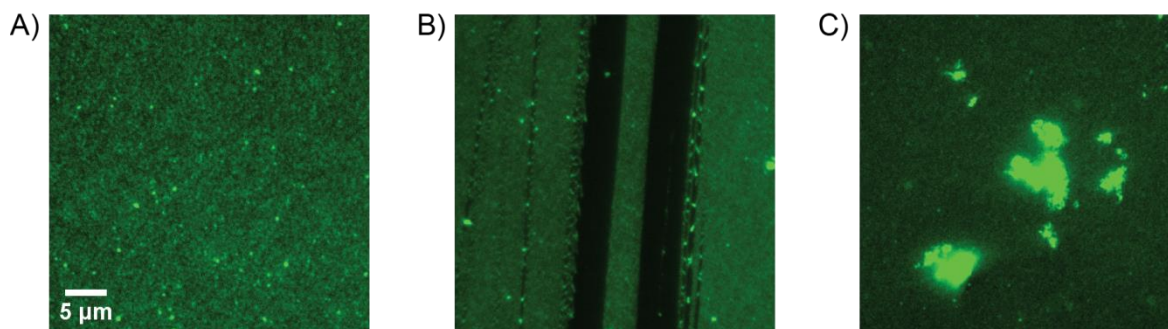


Figure 3.1: Quality of fibrinogen coatings

Typical epifluorescence images of labeled (Alexa Fluor 488 conjugated) fibrinogen coatings on glass coverslips. The areas on the coverslips which were completely coated with fibrinogen like in A) were chosen for platelet imaging. The areas that showed B) scratches or uneven fibrinogen coating or C) fibrinogen clusters were not chosen for subsequent imaging of platelets.

3.2 Platelet purification

Platelet purification from platelet concentrates was performed on the same day of the experiments. All the experiments were conducted in agreement with the ethical vote of the Ethic Committee of the University of Gottingen, votum 11/11/09.

Human blood platelets were purified from platelet concentrates obtained from the Department of Transfusion Medicine of the University Medical Center, Göttingen. These concentrates were prepared from the blood of healthy volunteer donors who had not taken any anti-platelet medication at least 7 days prior to donation. Either the apheresis system or buffy coats pooled from 4 donors with the same ABO blood group was used to prepare the platelet concentrates. For the purpose of experiments, concentrates that were typically 5-6 days old and not valid anymore for transfusion, were used. The concentrates however, still contained many viable platelets as the platelets have a typical lifespan of 7-10 days [94], and hence were suitable for our experimental purposes.

The platelet concentrates consisted of blood plasma, platelets and some red blood cells but no leucocytes. The platelets were purified by separating them from the plasma in order to avoid any uncontrollable influences of the plasma on the experiments. The purified platelet solution

contained red blood cells. However their number was usually very low as compared to that of the platelets and they did not interfere with the experiments.

The platelet purification steps were carried out in the PIPES-saline-glucose buffer (PSG; buffer recipe in Appendix A). After the final purification step, the platelets were re-suspended in HEPES-Tyrode-BSA (HT-BSA; buffer recipe in Appendix A) buffer. The HT buffer was mixed with BSA (10% BSA in PBS, MACS BSA stock solution, Miltenyi Biotech, Bergisch Gladbach, Germany) on the day of the platelet purification. Prior to purification, the PSG and HT buffers were prewarmed to 37°C in a CO₂ incubator (5% CO₂; HeraCell 150, Thermo Scientific, Waltham, Massachusetts, USA).

A sketch of the steps involved is shown in Figure 3.2A. The platelets were extracted from the concentrate bag using 2 and 5 mL sterile syringes (BD Discardit™ II, Becton, Dickinson and Company, Franklin Lakes, New Jersey, USA) and a sterile needle (Nr.1, \varnothing 0.90 × 40 mm, 100 Sterican®, B.Braun, Melsungen, Germany). At first, the seal at the top of the platelet concentrate bag was broken and the bag was pierced with the needle connected to the 2 mL syringe and 2 mL of the platelet concentrate solution was drawn out and discarded. This step ensured that any contamination that may have occurred during the opening of the bag would not be carried forward in the next purification steps. After this, 4 mL of the platelet concentrate solution was gently drawn out from the bag using the same needle and a 5 mL syringe. The needle connected to the syringe was discarded and the concentrate solution was collected in a tube (15 mL Falcon™, Thermo Scientific, Waltham, Massachusetts, USA) by holding the syringe against the wall of the tube and letting the solution run down gently. Then, 100 μ L of prostaglandin E₁ (PGE₁, ~0.106 mg/mL, Cayman Chemical Company, Ann Arbor, Michigan, USA) was added to keep the platelets quiescent and the platelet concentrate solution was centrifuged at 480 × g for 20 minutes at 21-22°C (Eppendorf Centrifuge 5810R, Eppendorf, Hamburg, Germany). Afterwards, the supernatant was discarded and the cell pellet was re-suspended in 4 mL PSG buffer. This addition of PGE₁, followed by centrifugation and re-suspension of platelet pellet in 4 mL PSG buffer was repeated twice. The PSG and HT buffers were always kept warm at 37°C in between the centrifugation steps. After the third centrifugation step, the platelet pellet was gently re-suspended in 1 mL HT-BSA buffer without addition of PGE₁. The tube now containing the purified platelet solution was stored on a rotator (MACSmix™ Tube rotator, Miltenyi Biotech; speed 12 rpm) to keep the platelets quiescent until further experimental use.

The final number of platelets in the purified solution was determined using a hematocrit capillary (Heparinized Micro-Hematocrit Capillary Tubes, FisherBrand, Thermo Fisher

Scientific Inc., Waltham, Massachusetts, USA). The capillary was filled with the purified platelet solution to its capacity (indicated by the red line) and its other end was sealed with clay sealant to avoid leaking. The capillary was then carefully wrapped in a piece of tissue and was put in a tube and this tube was centrifuged at $1000 \times g$ for 10 minutes at 21-22°C. Due to the centrifugation, the platelet pellet was separated from the liquid and the platelet number was determined by comparing the height of the liquid and height of the pellet column (Figure 3.2 B) using a Reader Card (ZIPocrit, Microhematocrit Centrifuge, LW Scientific, Inc., Lawrenceville, Georgia, USA).

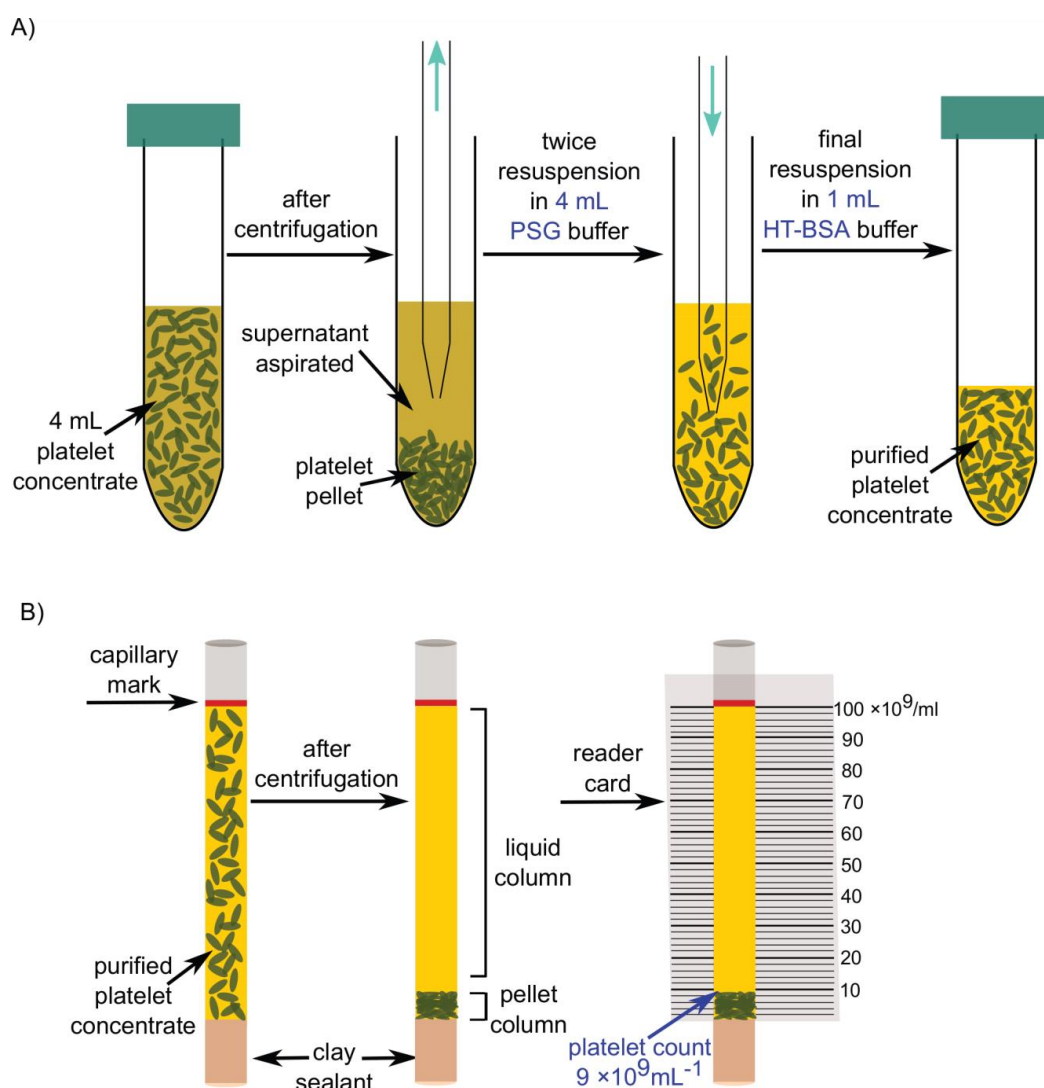


Figure 3.2: Sketch of platelet purification and counting

A) 4 mL of platelet concentrate (platelets in blood plasma) were centrifuged and the platelet pellet was re-suspended in PSG buffer. After the last centrifugation step, the pellet was re-suspended in 1 mL HT-BSA buffer and the number of platelets were counted from this purified platelet concentrate. B) A hematocrit capillary was filled with the purified platelet concentrate up to its mark and centrifuged. The number of platelets was determined by comparing the height of the separated liquid and platelet column. In this example, the platelet count was $9 \times 10^9 \text{ mL}^{-1}$.

3.3 Platelet cytoskeleton and plasma membrane staining

3.3.1 Fixed staining for actin, myosin and vinculin

The platelets were fixed at different time points during their spreading and stained to visualize their F-actin reorganization and their distribution of the focal adhesion protein, vinculin and the force generating motor protein, myosin. Single phalloidin staining time series to visualize only F-actin were performed along with double stainings for either actin-vinculin or actin-myosin. Prior to fixation, platelets were allowed to spread for 5, 10, 15, 30, 60 and 120 minutes for each staining series.

To begin with, glass coverslips were completely coated with unlabeled fibrinogen (\varnothing 20 mm) to allow platelet adherence, as described in the previous section (section 3.1). All the fibrinogen coated coverslips were placed in plastic petri dishes on pieces of parafilm. The parafilm aided in keeping the bottom of the coverslips dry which made it easier to pick them up at the time of mounting. After coating, the coverslips were briefly washed once with 200 μ L PBS and then twice with 200 μ L HT-BSA buffer. All liquid was removed by tilting the petri dishes containing the coverslips and sucking out the liquid that ran out with an Eppendorf pipette. It is important to note here that there were still some traces of liquid on the coverslips after this process but this did not interfere with our experiments. Afterwards, 200 μ L of 10% BSA solution was added to the coverslips to block unspecific binding sites and left to react for 30 minutes. Again, all the liquid was removed and immediately 90 μ L of purified and diluted platelet solution (concentration of 2×10^7 mL⁻¹) was added to the coverslips followed immediately by addition of 10 μ L of thrombin solution (at a final concentration of 4 U/mL, thrombin from human plasma, 1 KU, \geq 2800 NIH units/mg protein, Sigma-Aldrich, Munich, Germany) to trigger platelet spreading. The addition of thrombin was considered as time point zero. All the petri dishes containing the coverslips were quickly transferred to the 37°C CO₂ incubator. At defined time intervals (5, 10, 15, 30, 60 or 120 minutes, counted after addition of thrombin) the coverslips were removed from the incubator and the platelets were fixed and stabilized by adding 100 μ L of 3.7% (diluted in PBS) formaldehyde fixative (37% stock solution, Merck, Darmstadt, Germany,). The formaldehyde was allowed to react for 20 minutes after which the coverslips were washed thrice with 200 μ L, warm PBS. The fixed platelets were then permeabilized by adding 0.5% Triton-X 100 for 10 minutes followed by three washing steps again with PBS. All liquid was removed and then 200 μ L of 10% normal goat serum (GS, Abcam, Cambridge, United Kingdom) was added to the coverslips to block

MATERIALS & METHODS

unspecific binding sites in the platelets and was left to react for 30 minutes. This step was followed by washing the coverslips thrice with 200 μ L of a mixture of PBS-1% GS. In the following steps this PBS-1% GS mixture was always used for washing. The fixed platelets were then incubated for 1 hour at RT with 200 μ L of the primary antibodies to either vinculin (2 μ g/mL, monoclonal antibody from mouse, Abcam, Cambridge, United Kingdom) or non-muscle myosin IIA (0.04 μ g/mL, monoclonal antibody from rabbit, Abcam, Cambridge, United Kingdom). Afterwards, the coverslips were washed thrice with 200 μ L PBS-1% GS. Then 200 μ L of the secondary goat anti-mouse IgG (5 μ g/mL, conjugated to Alexa Fluor 488 Ex/Em: 490/525 nm, Thermo Fisher Scientific Inc., Waltham, Massachusetts, USA) or goat anti-rabbit IgG (5 μ g/mL, conjugated to Alexa Fluor 488 Ex/Em: 490/525 nm, Abcam, Cambridge, United Kingdom) antibodies were immediately added to the coverslips and were incubated for 2 hours at RT. At this time, all the coverslips were covered with aluminum foil and were incubated in the dark. After the incubation, the coverslips were washed six times with 200 μ L of a mixture of PBS-1% GS. Here the washing steps were increased to remove any traces of unspecific binding. Then, 200 μ L of phalloidin solution (0.11 μ M, Abberior STAR 635- $\lambda_{\text{abs}}/\lambda_{\text{fl}}$: 634/654 nm, Abberior GmbH, Göttingen, Germany) was added to the coverslips to stain the F-actin and was incubated for 30 minutes. This was followed by the final washing steps repeated four times with 200 μ L of PBS-1% GS. Appropriate positive (addition of only the primary antibody or only the secondary antibodies) and negative controls (no addition of any antibodies) were also performed along with the double staining series.

For single phalloidin staining time series, the steps performed until platelet fixation were same as described above. Afterwards the platelets were not permeabilized but were directly incubated with the phalloidin solution followed by the usual washing off of the coverslips before mounting.

The coverslips with the fixed and stained platelets were then mounted on microscope slides (cut edges, VWR, Radnor, Pennsylvania, USA) using a mounting solution (ProLong Gold Antifade Mountant, Thermo Fisher Scientific Inc., Waltham, Massachusetts, USA). 1-2 drops of the mounting solution were placed in the center of the slides and the coverslips having the fixed and stained platelets were carefully placed upside down on this mounting medium. The coverslips were gently tapped to remove any air bubbles. The mounting medium was left to harden for 1-2 hours at RT. Afterwards the edges of the coverslips were sealed with nail polish.

3.3.2 Labeling with SiR-actin and SiR-tubulin, probe characterization

For the live imaging of the F-actin or MT reorganization in platelets, they were labeled with the cytoskeletal probes SiR-actin that specifically binds to F-actin or SiR-tubulin that specifically binds to MTs (stock concentration of 1 mM in DMSO, Spirochrome Ltd., Stein am Rhein, Switzerland; $\lambda_{\text{abs}}/\lambda_{\text{fl}}$: 652/674 nm). These probes were diluted in HT-BSA buffer to a final concentration of 6 μM to which the purified platelets were added to a final cell concentration of 1.5×10^7 cells mL^{-1} . The platelets were incubated with the cytoskeletal probes, on the tube rotator for approximately 30 minutes and the excess SiR-actin/SiR-tubulin probe was not washed off prior to the microscope experiments except where indicated.

The final probe concentration, labeling time and the decision for no need of a washing step after the labeling, were determined by carrying out some characterization tests for the probes. These characterization tests were done using the SiR-actin probe by looking at the F-actin intensity distributions of spreading platelets as described in section 4.2.2.2. Probe concentrations of 2 μM and 6 μM and labeling times of 0, 30 and 120 min were tested. During washing off the excess probe, a concentration of 6 μM was used and the platelets were initially labeled for 15 min and then the cell solution was centrifuged at $480 \times g$ for 5 min followed by re-suspension of the cell pellet in 1 mL fresh, probe-free HT-BSA buffer. Thus, in total the platelets were in contact with the SiR-actin probe for approximately 30 min. In experiments where the probe concentration was changed, the platelets were labeled for 30 min, too. In all other characterization experiments, except where indicated, the excess probe was not washed off.

3.3.3 Platelet plasma membrane staining

For some real-time experiments, the platelets were double stained with the SiR-actin probe to analyze the F-actin formation and reorganization, as well as with a plasma membrane dye CellMask (CM) Green (Ex/Em: 522/535 nm, Thermo Fisher Scientific Inc., Waltham, MA, USA), to obtain the platelet areas as they spread. For that purpose, initially, the purified platelets with a final concentration of 1.5×10^7 cells/mL were incubated in 1 mL of HT-BSA buffer containing 6 μM of the SiR-actin probe for 15 minutes. Immediately afterwards, the plasma membrane dye CM Green was added to this platelet solution at a final concentration of 2.5 $\mu\text{g}/\text{mL}$ and incubated with the platelets for 5 minutes at 37 °C in the CO₂ incubator. Then, PGE₁ was added to this double stained platelets solution and the tube containing this solution

was centrifuged at $480 \times g$ for 5 min. The resulting pellet was then gently re-suspended in 1 mL of fresh HT-BSA buffer and immediately brought to the microscope for the live imaging experiments. Thus, in total, the platelets were incubated with the SiR-actin probe for approximately 30 min and with the CM Green stain for approximately 15 min prior to the microscope experiments.

3.4 Platelet treatment with pharmacological agents

In order to image the effects of different pharmacological agents on platelet cytoskeleton in real-time, the platelets were labeled with either the SiR-actin or SiR-tubulin probes and simultaneously treated with these agents. For that purpose, the agents blebbistatin, a non-muscle myosin II inhibitor (Sigma Aldrich, Munich, Germany; final concentrations used-20 and 50 μM), Y-27632, a Rho-kinase inhibitor (Abcam, Cambridge, UK; final concentration used 50 μM), nocodazole, a MT depolymerizer (Sigma Aldrich, Munich, Germany; final concentration 5 μM) and aspirin, a platelet aggregation inhibitor (Bayer, Leverkusen, Germany; final concentration 3.33 mM) were diluted to their indicated final concentrations in HT-BSA buffer along with either SiR-actin/ SiR-tubulin at a final concentration of 6 μM . Platelets were added to this probe-and-agent containing solution at a final concentration of 1.5×10^7 cells mL^{-1} and were incubated with them on the tube rotator for approximately 30 minutes before starting the microscope experiments.

3.5 Microscopy and image acquisition

3.5.1 Sample preparation during live platelet imaging

The SiR-actin or SiR-tubulin labeled or CM Green stained platelet samples were prepared at the microscope (see section 3.5.2) shortly before starting the live imaging. The fibrinogen-coated coverslips were washed thrice with 100 μL warm HT-BSA buffer and were anchored in the coverslip holder that was placed inside a preheated, humid, stage top incubator (see section 3.5.2 for details). Before adding the platelets, traces of liquid on the coverslips were gently blotted out with a piece of tissue. Then 90 μL of the labeled and/or treated platelet solution was pipetted onto the coverslips. This step was followed by the addition of 10 μL of thrombin solution (final concentration of 4 U/mL, thrombin from human plasma, 1 KU, \geq

2800 NIH units/mg protein, Sigma-Aldrich, Munich, Germany) to trigger the platelet spreading. Details of imaging are described in the following sections.

3.5.2 Bright-field imaging and epifluorescence imaging

The imaging of both fixed and live platelets was performed using an inverted microscope (IX 81, Olympus, Hamburg, Germany) with built-in shutters that was equipped for both bright-field and epifluorescence imaging in various ranges of magnifications (10X - 100X) and was also equipped with a digital camera for recording the imaging. The SiR-actin live spreading experiments and the fixed-platelet time series (see section 3.3.1) were recorded with a charge-coupled device (CCD) Retiga 6000 camera (QImaging, Surrey, BC, Canada). Some of the SiR-actin and all the SiR-tubulin live experiments with the pharmacological inhibitors were recorded with a complementary metal-oxide semiconductor (CMOS) ORCA-Flash 4.0 V2 C11440-22CU camera (Hamamatsu Photonics Deutschland GmbH, Herrsching am Ammersee, Germany).

For imaging both, the fixed-platelet time series, and the SiR-actin and SiR-tubulin live, time-lapse movies of platelet spreading and cytoskeletal reorganization, a 60X oil immersion objective (UPLSAPO 60XO, numerical aperture NA = 1.35, working distance WD = 0.15 mm, Olympus, Hamburg, Germany) was used.

During live imaging of platelets, a stage top incubator (INUG2E-ONICS, Tokai Hit, Shizuoka-ken, Japan) was mounted on top of the microscope stage. The incubator and the 60X objective were preheated to 37°C and the atmosphere inside the incubator was saturated with water vapor and 5% CO₂, to maintain physiological conditions for the platelets.

For the SiR-actin/SiR-tubulin time-lapse experiments, the platelet plasma membrane was visualized by either bright-field (BF; in case of singly labeled SiR-actin/SiR-tubulin platelets) or by epifluorescence in the FITC channel (in case of CM Green stained platelets). The F-actin/MT reorganization was subsequently visualized by epifluorescence imaging in the Cy5 channel. In few of the experiments, instead of imaging the platelet plasma membrane, the underlying labeled fibrinogen coating was imaged in the FITC channel together with the F-actin/MT reorganization in the Cy5 channel.

A sketch of our microscope setup is shown in Figure 3.3. A halogen lamp (12 V, 100 W, Olympus, Hamburg, Germany) provided the illumination source for the bright-field imaging. The transmitted light is focused on the platelet samples via a condenser and magnified by the objective. For the epifluorescence imaging, the MT20 illumination system with a 150 W

xenon arc lamp provided the illumination source (Olympus, Hamburg, Germany). During the imaging, a FITC/Cy5- dualband filterset (AHF Analysentechnik, Tübingen, Germany) was used which consisted of an excitation filter (470/622 Dualband Exciter H) that allowed for excitation of the fluorescently labeled platelet samples around 470 nm (FITC) and a second one around 622 nm (Cy5). The excitation light was further filtered by a dichroic mirror/beam splitter (497/655 H Dualband Beamsplitter) which selectively allowed light only above 497 nm and light only above 655 nm to pass through. An emission filter (537/694 Dualband Emitter H) selectively allowed the emission from the samples around 537 nm and around 694 nm. The spectra of the optical filters, the probes, and the dyes used are shown in Figure 3.4.

The imaging parameters for the SiR-actin/SiR-tubulin-labeled platelet time-lapse movies in Cy5, FITC (fibrinogen coating) and BF channels were 50 ms of illumination time, with epifluorescence lamp intensity of 23.1% and BF lamp power of 4 V. The imaging parameters for the CM Green-stained platelet time-lapse movies in Cy5 (SiR-actin) and FITC (CM Green) channels were 36 ms of illumination time, with epifluorescence lamp intensity of 11.49%. Time-lapse images of both the plasma membrane or fibrinogen coating (in BF or FITC channel) and the F-actin/MT (in the Cy5 channel) were simultaneously recorded, with an interval of 10 seconds between each frame and for a total time period of 60-120 minutes.

The imaging parameters for the fixed-platelet time series in Cy5 (F-actin), FITC (vinculin/myosin) and BF channels were 100 ms of illumination time, with epifluorescence lamp intensity of 100 % and BF lamp power of 4 V.

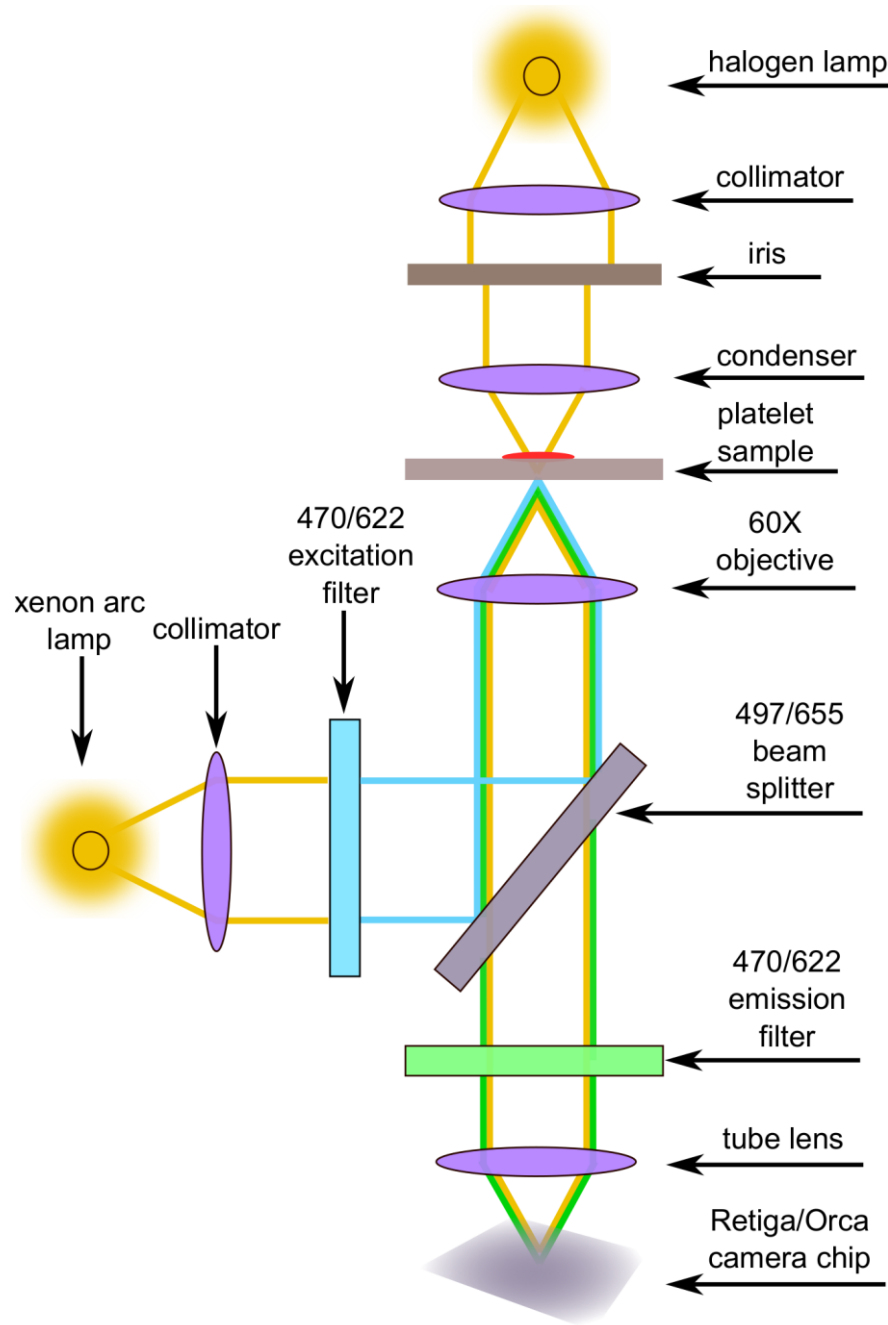


Figure 3.3: Microscope setup with bright-field and epifluorescence imaging

Plasma membrane of platelets was imaged by bright-field microscopy which used a halogen lamp as the light source. The fluorescently labeled cytoskeletal components were imaged by epifluorescence microscopy which used a xenon arc lamp as the light source and highly selective excitation and emission filters. The images were recorded by a digital camera.

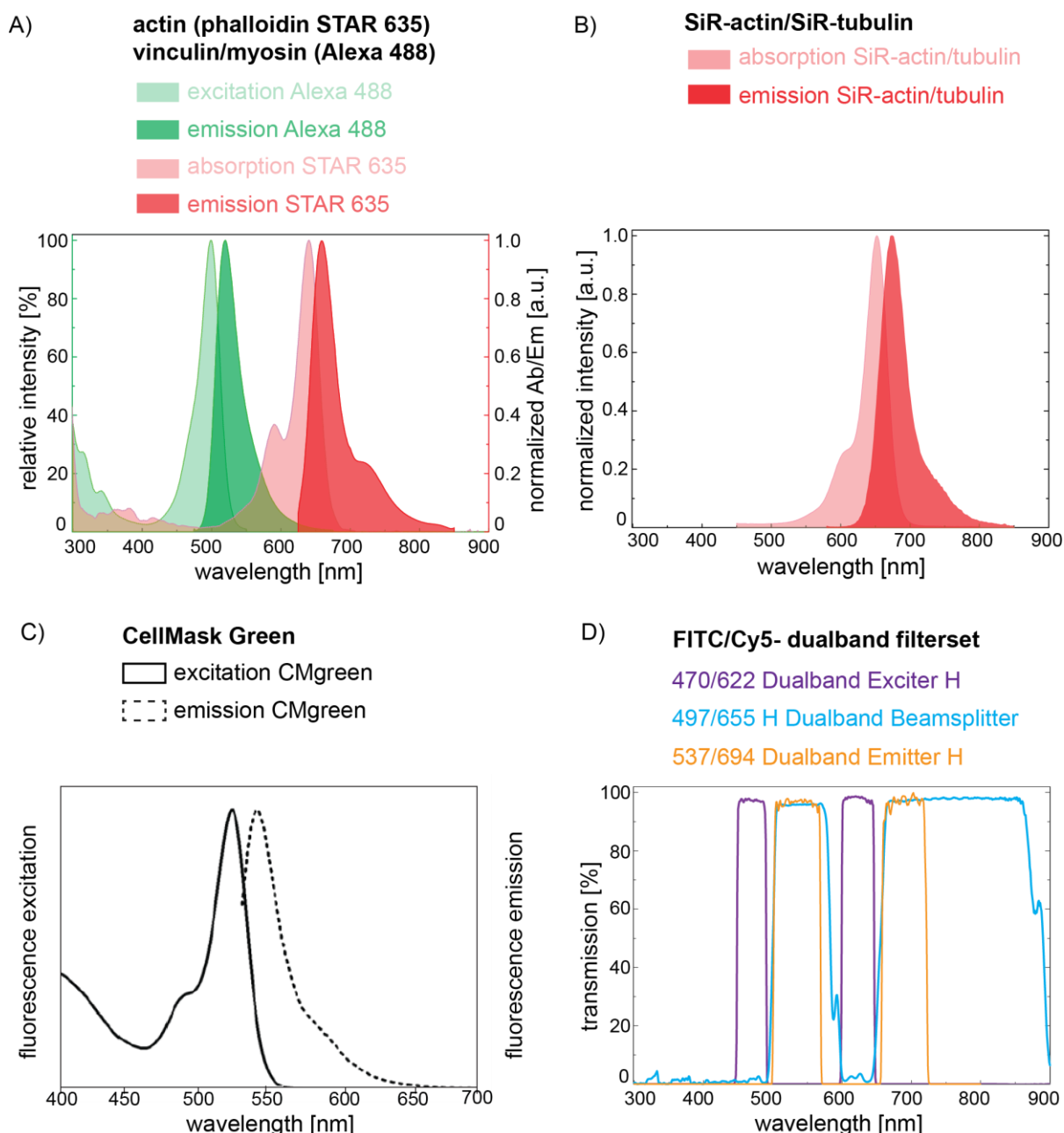


Figure 3.4: Spectra of the filters and fluorophores used for imaging

A) Excitation and emission spectra of STAR 635 phalloidin and vinculin/myosin secondary antibodies conjugated to Alexa Fluor 488 used for the fixed platelet time series. The spectral raw data values were obtained from Abberior and ThermoFisher [2, 2, 6]. B) Excitation and emission spectra of SiR-actin/SiR-tubulin used to visualize the F-actin/MT during live imaging. The spectral raw data values were obtained from Spirochrome [4]. C) Excitation and emission spectra of CM Green used to visualize platelet plasma membrane during live imaging. The graph was taken from [5] as the spectral raw data values were not available. D) The spectra of the dualband FITC/Cy5 filterset used for the platelet experiments to match the excitation and emission wavelengths of all the fluorophores used for imaging. The spectral raw data values were obtained from AHF Analysentechnik [3].

3.5.3 Bright-field and epifluorescence image processing

All time-lapse images and fixed-platelet images recorded with the microscope (see section 3.5.2) were processed to adjust their brightness and contrast, using ImageJ [130]. The fluorescence intensity of the SiR-actin and SiR-tubulin probes increases with increasing F-actin or MT content. During the initial spreading stages, the platelets had less F-actin/MT content which increased as they spread over time. Hence the time-lapse fluorescence images were not of equal brightness. Thus, each of the epifluorescence images was individually adjusted for their brightness and contrast whereas the brightness and contrast values for all BF images (belonging to one single dataset) were adjusted to the same values. For the fixed-platelet double staining series (see section 3.3.1), the fluorescence images in different channels (F-actin in Cy5 and vinculin/myosin in FITC) were overlaid in ImageJ to reveal the overlapping regions.

3.6 Analysis of F-actin fluorescence intensity

3.6.1 F-actin normalized intensity plots

The fluorescence time-lapse spreading movies of SiR-actin labeled platelets were obtained as described in section 3.5.2. As they spread, these platelets formed and reorganized their F-actin higher-order structures. Since the fluorescence intensity of the SiR-actin probe is proportional to the amount of F-actin, increasing fluorescence intensities were seen in the epifluorescence (Cy5) channel, as the platelets spread. These intensity increases were analyzed by plotting profiles of normalized fluorescence intensities (I) of SiR-actin labeled platelets as they spread over time.

For this purpose, only those platelets from the time-lapse movies were chosen, that were isolated, and had shown full spreading with stress fiber-like structure formation, at the end of the time-lapse movies. The normalized fluorescence intensities in each image of the fluorescence stack were obtained by using an in-house MATLAB script (MATLAB R2009b, The MathWorks, Inc., Natick, MA, USA; see Appendix B). Firstly, the script summed up all the individual images in the fluorescence stack giving an average image. This average image was then used to manually draw a region of interest (ROI) as close as possible to the average fluorescent platelet. The intensity values were then calculated for all the individual images within this single ROI and these values were normalized by the pixel number in the ROI

(Figure 3.5) and the normalized F-actin intensity curves were plotted. Sometimes, these F-actin intensity curves showed spikes in the normalized intensity values. These spikes came from SiR-actin labeled platelets that floated over or nearby the platelet of interest, during the time-lapse movie. Hence, such time-lapse movies were carefully looked at, and the normalized intensity data in the frames where SiR-actin labeled platelets interfered and increased the normalized intensity values, was not taken into consideration (e.g. gap in the curve in Figure 3.5C refers to such missing data points).

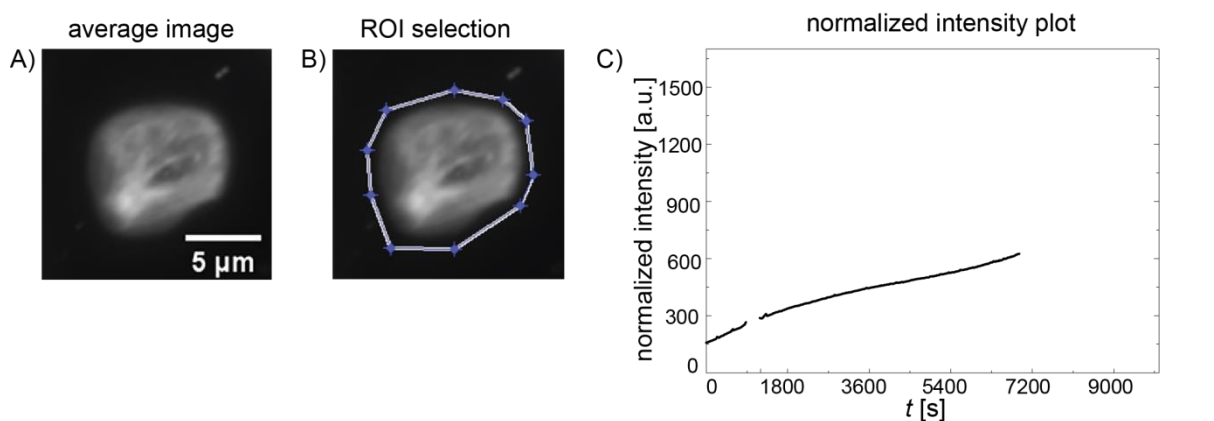


Figure 3.5: Plotting normalized F-actin intensities of SiR-actin labeled platelets

A) Individual images in the fluorescence images stack of SiR-actin labeled platelets were summed up to give an average image. B) This image was used to manually draw a ROI and C) normalized intensities were calculated and plotted. The gap seen in the curve comes from missing data points (as explained above).

3.6.2 Histogram analysis of F-actin normalized intensities

The normalized F-actin intensity profiles were plotted for both untreated and SiR-actin labeled platelets treated with pharmacological agents (see section 3.4). To better compare the the intensity profiles of untreated and treated platelets, a histogram distribution of the normalized F-actin intensity values (I) was plotted at three different time points of platelet spreading. The time points chosen were 5, 20 and 60 minutes. The bin width h , of the histograms was adjusted individually for each experimental dataset and was determined as $h = \frac{I_{max} - I_{min}}{\sqrt{n}}$ [95] where, n is the total number of values and I_{max} and I_{min} are the maximum and minimum intensity values in the data series. The relative frequencies were calculated using OriginPro 8.5.

3.7 Platelet spread area determination

The plasma membrane of platelets was stained with CM Green dye (see section 3.3.3) to determine their spread areas over time. Fluorescence time-lapse spreading images were obtained as described in section 3.5.2. Only single, isolated platelets were chosen for analysis. The parameters mentioned below are given in pixels, where 1 pixel equals 0.109 μm .

In the first step, the plasma membrane contour of the platelet in each image of the fluorescence stack was detected by an in-house MATLAB script [22, 125]. The script first applied a Wiener filter (*wiener2* function using neighborhoods of size 8×8 pixels) which reduced the background noise in the images. Then, the script used a *canny* edge detection algorithm to detect the cell edges. The algorithm computes a gradient of an image and then finds the edges by looking for local maxima in the magnitude of the gradients. It also employs two thresholds to detect both strong and weak edges including those weak edges that are connected to the strong ones [22]. This feature of the algorithm is useful for the purpose of our experiments, as the staining of the plasma membrane may differ between individual platelets or may not necessarily be uniform over an entire platelet. For our experiments, these low and high thresholds were set to 0.08 and 0.18 pixels, respectively. In the second step, the automatically detected contours of the platelet by the canny algorithm, were overlaid with the original fluorescence image stack in ImageJ [130] in order to ensure that the detected contours were consistent with the platelet contours. In a few instances, some parts of the platelet were not detected by the algorithm. Such parts were normally the filopodia or certain thin areas of the platelet that showed low fluorescence intensities and thus shallower gradients which were difficult to detect. Such non-detected contours were traced manually, by using the pencil tool in ImageJ, based on the corresponding fluorescence images. After detecting the contours, they were filled manually in ImageJ, using the fill tool, in order to create masks of the platelet. A second in-house MATLAB script was then employed to this filled platelet images stack, to remove all detected objects other than the platelet itself. The script used a threshold of 1 pixel and removed all objects below this size. In the last step, this binarized and filled platelet images stack was used to compute the spread area for each time point using another in-house MATLAB script that employed the *regionprops* function. A sketch of the steps involved in platelet spread area determination is shown in Figure 3.6. The MATLAB scripts used are given in Appendix C.

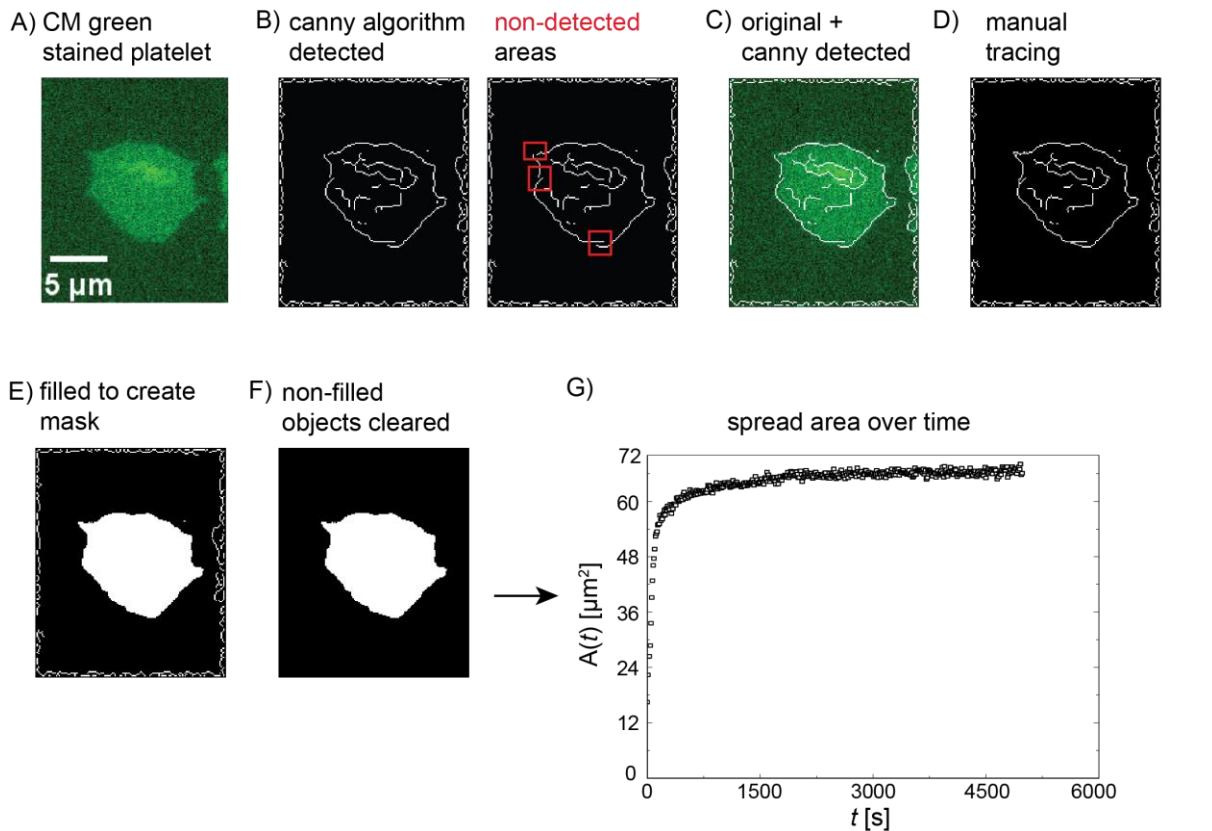


Figure 3.6: Determination of platelet spread area

A single frame from the fluorescence stack of a CM green stained platelet is shown in this example. A) Contours of the platelet were automatically detected by B) a *canny* edge detection algorithm. To trace the non-detected areas (marked in this example in red), C) the original fluorescence images and the contour detected images were overlaid and D) the contours were manually traced. E) These masks were filled in ImageJ and F) non-filled objects were removed. G) These masks were used to calculate the spread areas using the *regionprops* function.

3.8 Determination of time point of zero (adhesion)

Defining the time point 'zero' i.e the time point of platelet adhesion to the fibrinogen-coated coverslips was an important consideration in our time-lapse spreading experiments of SiR-actin labeled and CM Green stained platelets. The time point 'zero' (t_{zero}) was manually determined by careful observation of the time-lapse movies. As described in section 3.5.2, the SiR-actin labeled platelets were imaged in the Cy5 channel simultaneously with their plasma membrane in the BF channel or with the underlying labeled fibrinogen coating in the FITC channel. In the experiments where both the Cy5 and BF time-lapse images were taken, the ' t_{zero} ' was determined by looking at the BF image frames after the platelet came into the field of view (FOV), and the frame in which the platelet extended out a filopodium and anchored itself to the underlying fibrinogen coating, was considered as the ' t_{zero} ' of adhesion (see Figure

3.7A). This time point zero determination approach was prone to less error as it was quite easy to see the platelets extending their first filopodium, in the BF channel. A noteworthy observation that must be taken into account here is that sometimes the platelets, after anchoring themselves via a filopodium, did not immediately spread, but instead moved up and down for a few seconds forming more filopodia and then continued to spread in a fried-egg-like manner.

In the experiments where only the Cy5 time-lapse images were taken, the time point 'zero' determination of the platelets was slightly tricky as in the initial frames the platelets extended only a single filopodium, or few, thin filopodia, which contained less SiR-actin labeled material and hence showed lower fluorescence intensities, making it difficult to see these filopodia. In these cases, the Cy5 image frames after the platelet came into the FOV, were individually adjusted for their brightness and contrast and carefully observed, and the ' t_{zero} ' was determined as that 'frame' where the platelet movement slowed down and its fluorescence intensity appeared 'brighter' than that in the previous frame indicating that it had adhered (see Figure 3.7B). This 'frame zero' was generally a few seconds before the platelet had extended lamellipodia and had started to spread. This approach was however prone to some error (± 10 -30 seconds) in the 'real' t_{zero} determination because sometimes, although the platelet appeared 'bright' in that ' t_{zero} ' frame, it did not look bright in the next frame. This phenomenon could be attributed to the up and down movement of platelets we saw in the BF channel, where they first anchored via one filopodium and then moved up and down until they formed enough filopodia to adhere firmly and start spreading. It may be possible that when the platelets moved upward, they appeared less 'bright'.

In the experiments where the SiR-actin labeled platelets were double stained with the CM Green dye (FITC channel; see section 3.3.3), the ' t_{zero} ' was determined by looking at the FITC image frames. It was relatively easy to decide the ' t_{zero} frame' because the plasma membrane stained platelet, that initially hovered, appeared as a 'bright spot' the moment it adhered to the underlying fibrinogen, and initiated spreading in the next frames as seen by its expanding plasma membrane (see Figure 3.7C).

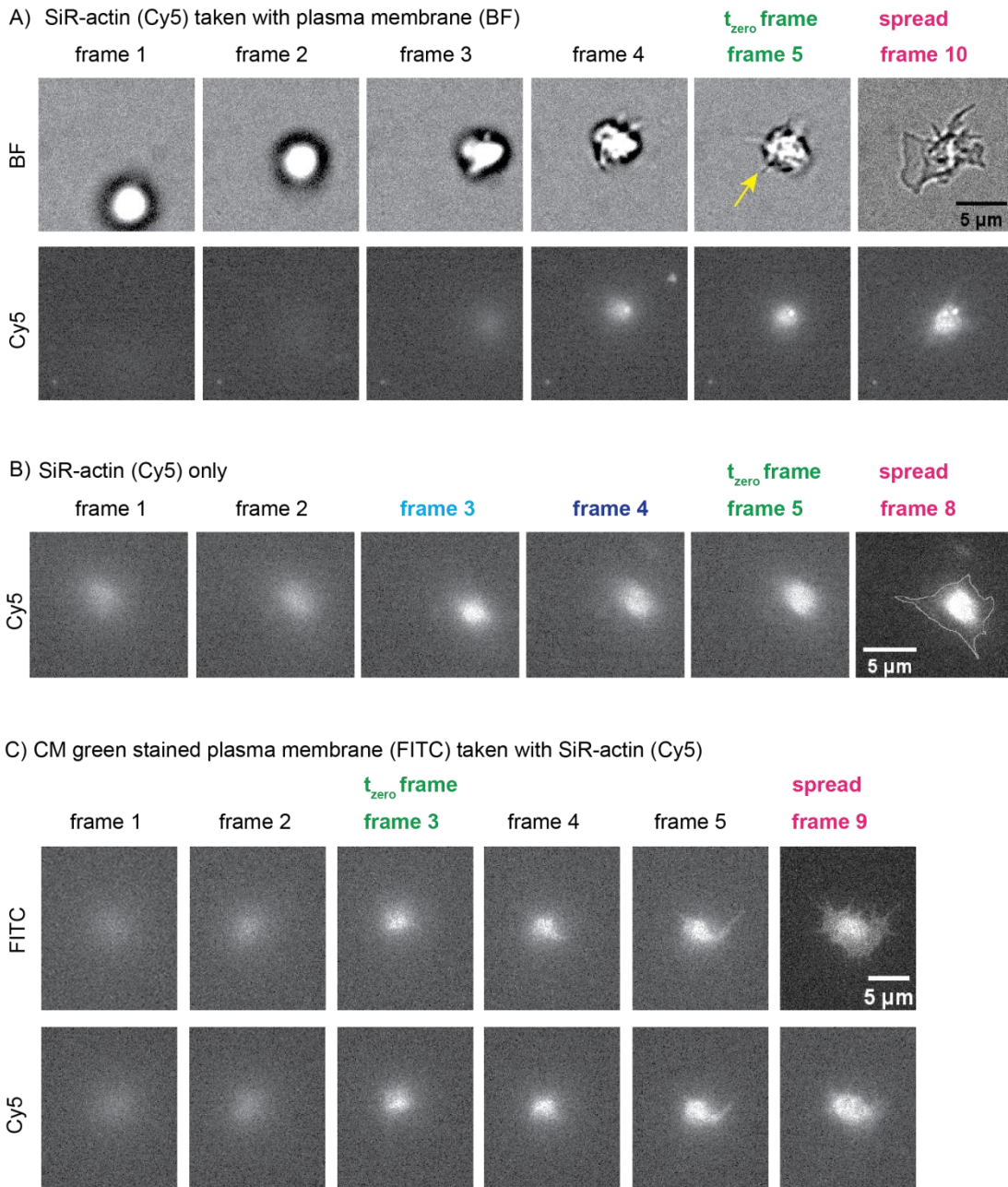


Figure 3.7: Determination of t_{zero} of SiR-actin labeled platelet adhesion

The t_{zero} i.e. the time point of adhesion of platelets to the underlying fibrinogen coating was determined by observing the BF or epifluorescence time-lapse movies. A) In experiments taken together with BF images, the t_{zero} was the frame in which the platelet extended a filopodium (indicated by yellow arrow). B) In experiments where only SiR-actin images were taken, determining the t_{zero} was prone to error due to the low fluorescence intensity of the images and the bobbing movement of platelets. In this example, frames 3 and 4 could have been possible candidates as the platelet appeared brighter in these images. But frame 5 was selected as the t_{zero} , because in the next frame the platelet had already started to spread (traced outline). C) In experiments taken together with CM Green stained dye in FITC channel, the t_{zero} was the frame in which the platelet appeared brighter when it adhered.

3.9 F-actin filament detection

The F-actin filaments formed and assembled by SiR-actin labeled platelets over time were detected with a modified version of the Filament Sensor (FS) program [39]. The total line (filament) lengths formed over the entire spreading time of these SiR-actin labeled platelets were then plotted. The FS is a program developed to detect filaments from fluorescence images and is based on a finger print analysis algorithm. It was developed in the research group of Professor Stephan Huckemann's from the Institute for Mathematical Stochastics in the University of Göttingen. Most of the FS program features have been established by Dr. Benjamin Eltzner, a postdoctoral researcher from Prof. Huckemann's group. The complete details of the working of the FS program have been recently published [39]. Dr. Eltzner carried out the analysis for the detection of the F-actin filaments from our experimental data. The fluorescence image stacks of SiR-actin labeled, completely spread platelets were obtained as described in section 3.5.2 and only single, isolated platelets were chosen for the analysis. A brief description of how the FS program detects the F-actin filaments is given below. The FS program was recently modified to detect slightly curved filaments and this modification is also described here briefly. A sketch of the steps involved in the detection of F-actin filaments is shown in Figure 3.8.

3.9.1 Pre-processing

In the first step, the fluorescence images of SiR-actin labeled platelets were pre-processed by applying three filters to reduce noise and to enhance linear features.

- 1) Firstly, an isotropic Gaussian filter with a standard deviation $\sigma = 1.0$ pixel was applied to reduce the brightness variations on very short scales which were most likely caused due to the noise from the camera (see Figure 3.8A left panel).
- 2) Then an 8-neighborhood Laplacian filter was used to sharpen the local features in the images by adding a multiple (by a factor L) of the filtered images to the original images (see Figure 3.8A middle panel). A range of factors $L = 2.0$ - 4.0 were used for all the images.
- 3) After applying the Laplacian filter, the bright features of the images could sometimes appear grainy. Hence, a directed Gaussian filter ($\sigma = 5.0$ pixels) was further applied to achieve a more homogeneous brightness along the linear features (see Figure 3.8A right panel). The filter determines the Gaussian weighted mean brightness values along pixel

lines of different orientations and chooses the maximum value as the new brightness value.

3.9.2 Binarization

In the second step, the pre-processed images were binarized (Figure 3.8C) by using three image processing steps [39], briefly described below.

- 1) First, the platelet areas were roughly estimated using a global brightness 'Li' threshold [80] and the images were restricted to these areas.
- 2) The next step was to define the 'white' and 'black' pixels. For this purpose, for each pixel, the brightness of its surroundings was determined by smoothing the pre-processed images with a Gaussian filter ($\sigma = 2.0$ pixels) and this was compared to the original pre-processed images. Then, the 'white' pixels were defined as those that were brighter in the original pre-processed images than in the smoothed images, and the rest of the pixels were considered as 'black' pixels.
- 3) Lastly, to rule out white pixels due to any remaining noise, a directed Gaussian filter ($\sigma = 4.0$ pixels) was applied to the pre-processed images. However, in this case, the σ and the average of the brightness values for the different orientations were compared and if the σ was below 4.0% of the average, the pixel was switched to black.

3.9.3 Width map generation

After the pre-processing and binarization steps, all the white pixels obtained were assigned with a width to generate a 'width map' (see Figure 3.8D). The width map is an essential preliminary step for the final line (F-actin filament) detection algorithm. For assigning a width value to every white pixel, their circular neighborhoods were looked at iteratively [39]. During the iteration, the width value was increased successively until a certain condition (namely that 95% of the pixels in the neighborhood are white, as explained below) was violated. The iteration started with a width value of 1 pixel and a neighborhood diameter of 2 pixels. Then, the widths were assigned as described briefly below.

- 1) Firstly, all the white and black pixels in this neighborhood were counted and if less than 95% pixels were white, then the iteration stopped. If this was not the case, the width was increased to the current neighborhood diameter (e.g. 2 pixels in the first iteration) and then the diameter of the neighborhood was increased by 1 pixel (e.g. from 2 pixels to 3

pixels in the first iteration). This iteration was repeated until less than 95% of the pixels in the neighborhood were white.

- 2) When the iteration stopped, the final width value was given by the diameter of the last neighborhood containing at least 95% white pixels.

3.9.4 Line (filament) detection and total line length plots

In the last step, the lines (F-actin filaments) were detected by using the line sensor algorithm as described in [39]. This algorithm was modified to detect slightly curved lines starting at every white pixel as follows.

- 1) The algorithm first checked the width map in 120 different directions which were each 3° apart.
- 2) Then it calculated the mean width values of all pairs of directions, where the angle between the two directions was in the range $180^\circ \pm 3^\circ$.
- 3) Then, it chose the pair of directions with the largest mean width value and consecutively followed both these directions.
- 4) When following a direction, the algorithm switched between moving forward by 5 pixels and readjusting its direction. After every 5 pixels, the algorithm checked the width map in three different directions (shown in different shades of blue in Figure 3.8E) and again followed the direction of the largest mean width value (shown in green in Figure 3.8E), while disregarding the other two directions. In this way, for every readjustment step, it changed its direction by up to 3° , thus piecewise linearly mapping curved lines (orange lines in Figure 3.8E and F) giving the final line length values. If the line was curved by more than 3° at every 5 pixels, the algorithm did not follow it. The minimal length of lines was set to 30 - 40 pixels, depending on the size of the platelet.
- 5) If two lines joined at some point to follow the same path, one of these lines was truncated at the joining point based on the angle between the orientations of the two lines in the overlapping region. If this angle was below 30° (20° or 45° for some datasets), the shorter line (or a random line if the two lines are of the same length) was truncated.

The lengths of all lines detected in each image of the fluorescence stack were summed up and these total line lengths were Gaussian smoothed ($\sigma = 10$ images) using a self-written Python script and then plotted over time (Figure 3.8G).

A summary of all the parameters used for the pre-processing, binarization and line detection steps is shown in Appendix D.

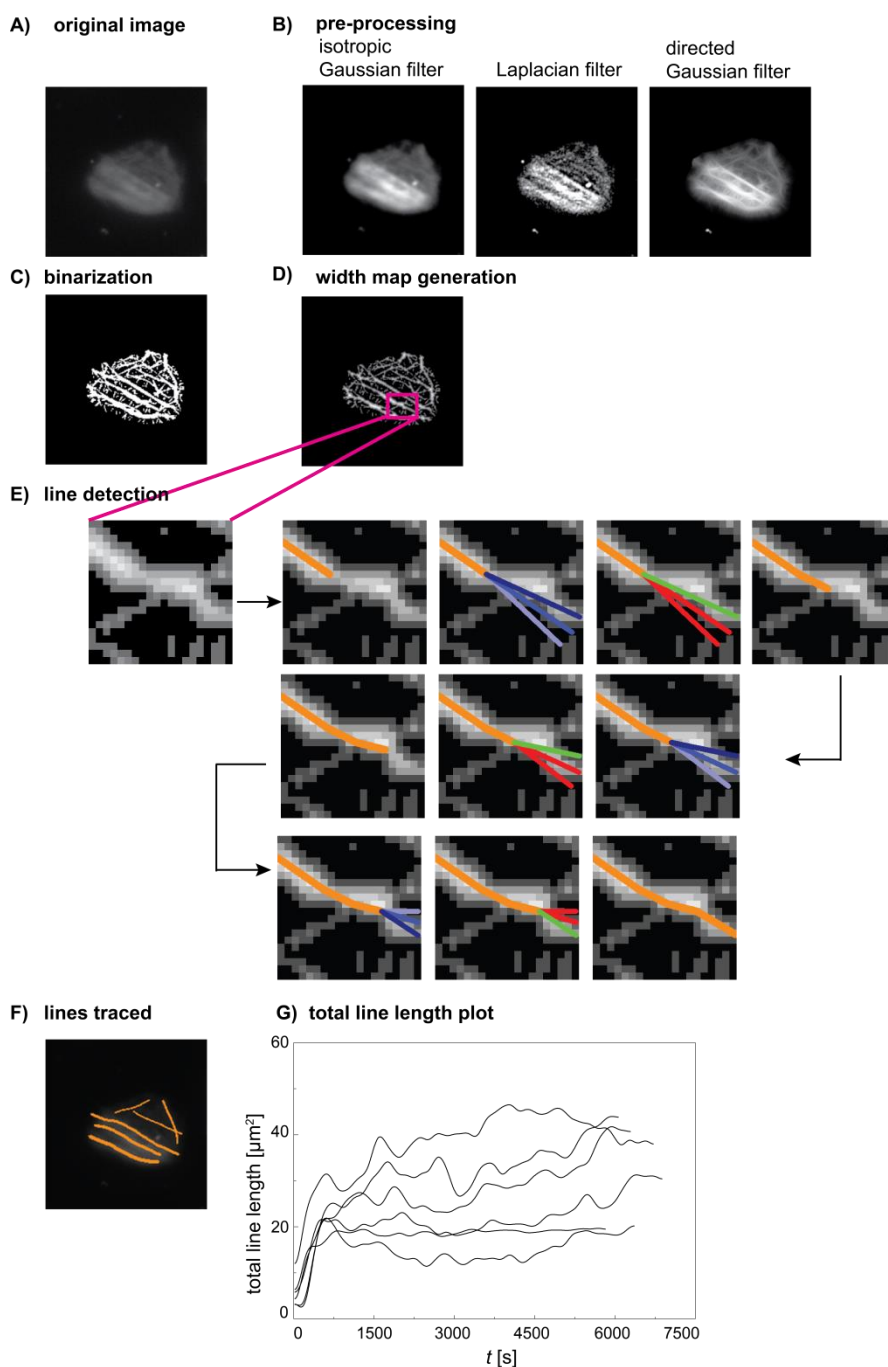


Figure 3.8: Steps involved in line (filament) detection by FS program

An exemplary fluorescence image from a stack of a SiR-actin labeled platelet is shown. The A) fluorescence images were B) preprocessed to reduce noise and to enhance linear features. C) The pre-processed images were then C) binarized and D) all the white pixels were assigned with a width to generate a 'width map' which was used (magnified) E) by the line sensor algorithm to piecewise linearly detect lines. The modified algorithm detected slightly curved lines, where it alternated between moving ahead by 5 px and then readjusted its direction. After every 5 px it checked the width map in three directions (indicated by shades of blue) and followed the direction of the largest mean width value (in green) while discarding the other two directions (in red). In this manner, the algorithm changed its direction up to 3° for every readjustment step (black arrows), thus piecewise linearly mapping curved lines (in orange), to give the final line length. F) These steps were followed for detecting all lines and G) the total line lengths were plotted over time.

3.10 Piecewise linear model fit

The platelet area $A(t)$ and total line length plots were fitted with a simple model to determine the 'turning time point' (t_1) at which the area or the F-actin stress fiber-like network growth slowed down. For that, the total line length, when the platelets had adhered but not spread, was assumed to be zero. Then, the line length increased rapidly starting at t_0 with a slope s_0 and finally at time t_1 settled into a phase where it changed only with a small slope s_1 . For the area, the time t_0 was always negative, so there was no initial phase of zero area. The model was formulated as below:

$$L(t) = \begin{cases} 0 & \text{for } t \leq t_0 \\ (t - t_0)s_0 & \text{for } t_0 < t \leq t_1 \\ (t_1 - t_0)s_0 + (t - t_1)s_1 & \text{for } t > t_1 \end{cases} \quad (1)$$

To estimate these parameters, a minimization was performed (here 'argmin' refers to minimizing a function, but not taking the minimal *value* of it but rather the *argument* minimizing the function).

$$(\hat{t}_0, \hat{t}_1, \hat{s}_0, \hat{s}_1) = \underset{t_0, t_1, s_0, s_1}{\operatorname{argmin}} \sum_{t=1}^T (X(t) - L(t))^2 \quad (2)$$

where $X(t)$ are the measured values for the platelet area/total line length and T is the number of measured time points. To estimate variances of the fitted parameters, bootstrap methods were used. For the bootstrap, a parametric model was assumed, where the data were described by the random variable

$$X(t) = L(t) + \sigma \varepsilon(t) \quad (3)$$

where $\varepsilon(t)$ is standard Gaussian white noise and σ is estimated from the fit. Thousand bootstrap samples were used. The bootstrap standard deviation for t_1 was less than a minute for all the analyzed platelets.

3.11 Spreading status counts and statistics

The effects of pharmacological agents (see section 3.4) on the spreading of SiR-actin/SiR-tubulin labeled platelets was determined by quantifying the relative numbers of spread/unspread platelets in experiments, where these platelets were treated with each of these

agents, and comparing them with the relative numbers of spread/unsread platelets in experiments, where these platelets were left untreated. For this purpose, BF images taken after the time-lapse movies (see section 3.5.2) were analyzed to quantify the number of spread and unsread platelets from the total number of adhered platelets. For each BF image, the numbers of spread and unsread platelets were manually counted. The platelets that showed complete lamellipodial spreading with circular, triangular or polygonal morphologies were considered as 'spread' whereas those that show rounded morphologies occasionally with filopodia and very small lamellipodia were considered as 'unsread'. Platelets lying on the image borders and also platelet clusters where individual platelets were hard to distinguish, were not considered for counting (see Figure 3.9).

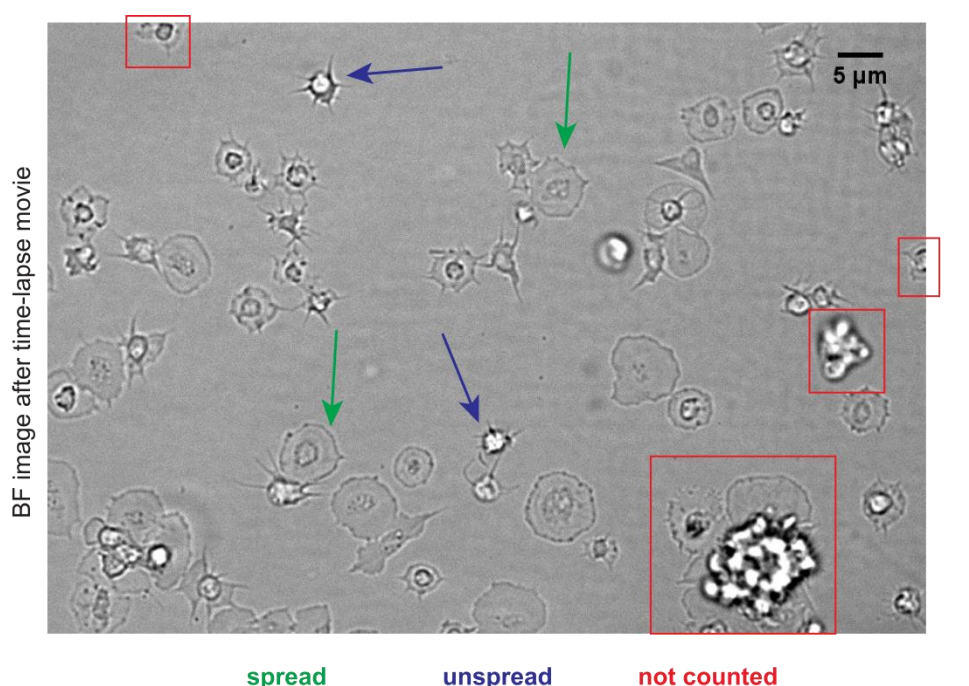


Figure 3.9: Determination of spread and unsread platelets

The effects of pharmacological agents on the spreading of SiR-actin/SiR-tubulin platelets were evaluated by quantifying the relative numbers of spread/unsread platelets after these experiments. Platelets were counted manually from the BF images taken after the time-lapse movies. Platelets showing flat circular, triangular or polygonal morphologies were considered as 'spread' (indicated by green arrows) whereas those that show rounded morphologies occasionally with some filopodia and very small lamellipodia were considered as 'unsread' (indicated by blue arrows). Platelets lying on the image borders and platelet clusters where individual platelets were not distinguishable were not counted (indicated by red boxes).

For every experimental condition, at least three images each, from at least three 'independent' datasets were analyzed (here 'independent' datasets refers to experiments performed on three different days, using platelets obtained from three different platelet concentrates). The steps involved in quantifying these counts and getting the relative numbers is described below for

one experimental condition (also see Appendix E). These same set of steps were repeated for all the experimental conditions-

1) The number of spread ($S_i = S_1, S_2, \dots, S_n$) and unspread ($U_i = U_1, U_2, \dots, U_n$) platelets from all images of all datasets were counted, where n refers to the number of datasets. The total (T_1, T_2, \dots, T_n) number of platelets for each dataset were then the sum of these two ($T_1 = S_1 + U_1, T_2 = S_2 + U_2 \dots T_n = S_n + U_n$) and the final number of platelets counted for all the datasets were, $N = T_1 + T_2 + \dots + T_n$.

2) In the second step, the percentages of spread and unspread platelets for each of the datasets were calculated ($\bar{S}_1, \bar{S}_2, \dots, \bar{S}_n$ and $\bar{U}_1, \bar{U}_2, \dots, \bar{U}_n$) and were averaged to give the final percentage of spread and unspread platelets for that experimental condition, $\bar{S} =$

$$\frac{\sum_{i=1}^n \bar{S}_i}{n} \text{ and } \bar{U} = \frac{\sum_{i=1}^n \bar{U}_i}{n}. \text{ The standard deviation was also calculated, } \sigma_{\bar{S}} = \sqrt{\frac{\sum (\bar{S}_i - \bar{S})^2}{n-1}}$$

and these values were then plotted.

Statistical analysis was performed to determine the significant difference between each condition by using an independent two-sample t -test for unequal variances with a p -value < 0.05 considered as statistically significant. The manual counts from all experiments and for all experimental conditions, and an exemplary dataset showing the statistical significance analysis by the two-sample t -test, is shown in Appendix E.

4. Results and Discussion

4.1 The cytoskeleton post-fixation

As has been discussed in the previous sections, platelets do not have a nucleus, and the usual technique for visualizing their cytoskeleton is to fix them and then stain their specific cytoskeletal components. In this chapter, the results of these post-fixation approaches done for visualizing the platelet cytoskeleton are shown, followed by a short discussion of the results with respect to the existing literature. These experiments are done to visualize the distribution and reorganization of the F-actin and to also visualize the qualitative distribution of the sites of focal adhesion (via vinculin) and force generation (via myosin), as the platelets spread. The platelets are fixed after certain time points during their spreading, and stained for their F-actin (with phalloidin) and vinculin or non-muscle myosin IIA (with specific antibodies; see section 3.3.1) and then imaged in the Cy5 and BF channels (see section 3.5.2). The post-fixation stainings of F-actin complement the live F-actin imaging in the platelets, which is discussed in details in the next chapter.

4.1.1 Distribution of F-actin only

The platelets are fixed and stained only with phalloidin at various time points of their spreading (5, 10, 15, 30, 60 and 120 minutes) to label their F-actin and the F-actin patterns formed during their spreading and imaged. Examples of five different platelets showing the most typical F-actin patterns for that particular time point are shown in Figure 4.1.

In the initial time points of spreading (5-10 minutes), the platelets extend the thin F-actin-rich filopodia forming a dendritic shape and then rapidly expand by forming the broad F-actin-rich lamellipodia that form in between or extend laterally from the filopodia (e.g. platelet 1 at 5 minutes and platelet 1 at 10 minutes in Figure 4.1). This expansion is associated with a prominent distribution of the F-actin at the cortex and central regions (indicated by the yellow arrows in Figure 4.1) of the platelets. Usually, the platelets spread completely within these 5-10 minutes and show circular, triangular or polygonal morphologies with almost no or very few filopodia. Most of the times, the intense F-actin distribution in the central regions appears

diffused, although it sometimes appears as a 'ring-like' structure (e.g. platelet 1 and platelet 4 at 5 minutes in Figure 4.1).

At the later time points of spreading (10-120 minutes), the F-actin gets reorganized into higher order, stress fiber-like structures that span across the entire length of the platelets (10-120 minutes images in Figure 4.1). These F-actin stress-fiber like structures form bundles that are commonly arranged in either ellipsoid (indicated by green arrows in Figure 4.1), triangular (indicated by cyan arrows in Figure 4.1) or circular patterns (indicated by orange arrows in Figure 4.1). The diffused F-actin distribution in the center gradually diminishes or disappears during these later time points of spreading.

The BF images of these fixed platelets are also carefully looked at and one of the most noticeable features is that the F-actin 'ring-like' structures seen in the first 5-15 minutes are associated with the platelet granules (see Figure 4.2). The F-actin 'ring-like' structures are seen prominently only when the hillock-like granules are present (indicated by yellow arrows in BF channel in Figure 4.2). As the platelets spread further (30 minutes and beyond), the granules gradually flatten out and are diminished in size (e.g. platelet 1 at 30 minutes in Figure 4.2) or no longer visible (e.g. platelet 5 at 30 minutes in Figure 4.2). Correspondingly, these F-actin 'ring-like' structures are also no longer noticeable (cyan arrows). During this time the F-actin already starts to reorganize into stress-fiber like structures (platelets 1 and 5 at 30 minutes in Figure 4.2).

Another noticeable feature is that although all the platelets at different time points show a wide distribution in their final spread sizes (areas), the platelets in the later stages of spreading i.e. around 120 minutes appear smaller in size (see Figure 4.1 and Appendix F). These platelets also often show the circular arrangement of F-actin stress fiber-like structures.

In general, during spreading, the platelets efficiently develop and rearrange their F-actin into an impressive network of stress-fiber like structures that form distinct patterns on glass.

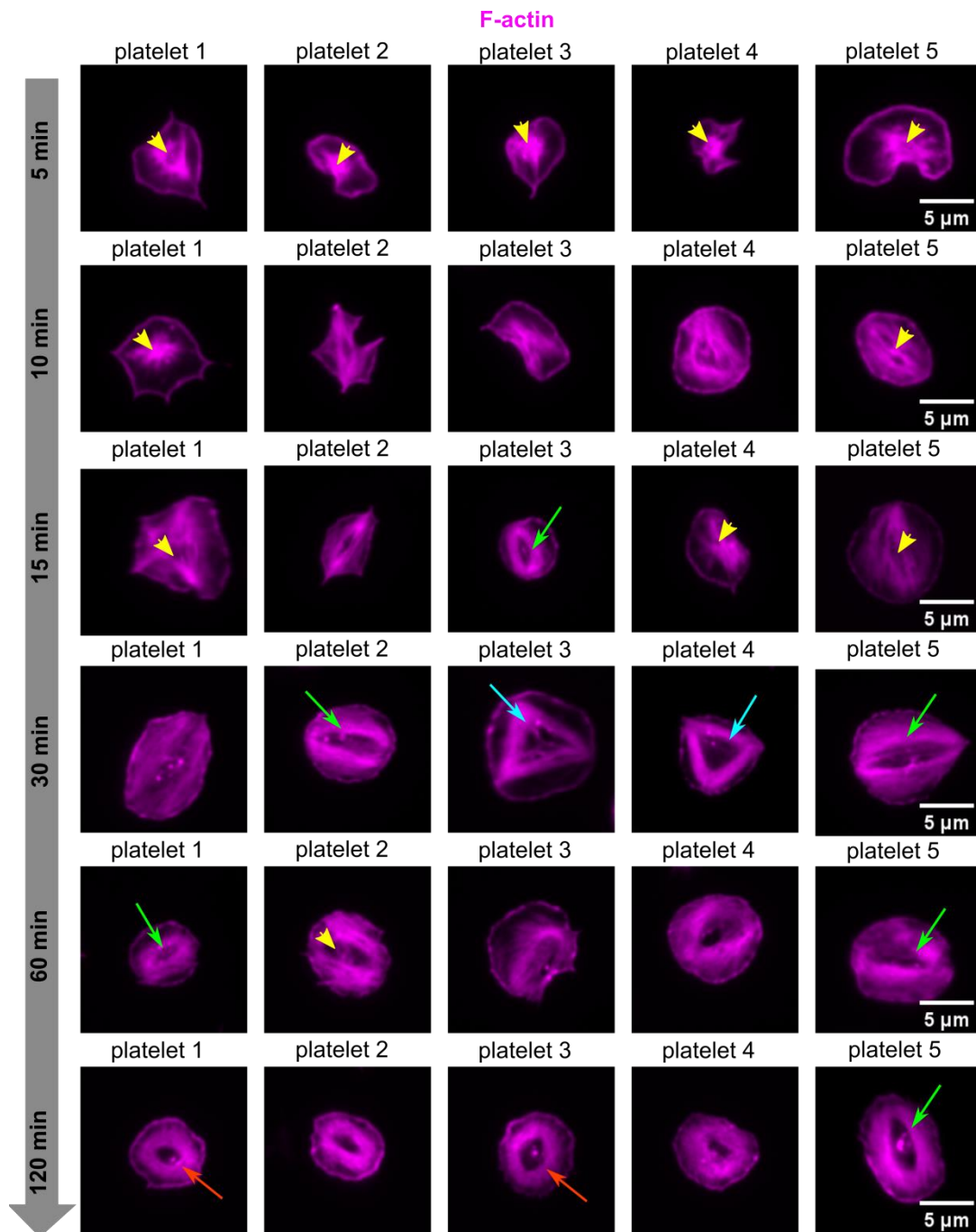


Figure 4.1: F-actin distribution and reorganization post-fixation

Epifluorescence images of platelets fixed at different time points of their spreading (5-120 minutes) and stained for their F-actin. F-actin is distributed in filopodia, lamellipodia, and predominantly in the cortex and the central regions in the form of ring-like structures (yellow arrows) in the first 5-10 minutes of spreading. The ring-like structures gradually disappear as platelets spread and further reorganize the F-actin into bundles of stress fiber-like structures that are arranged in ellipsoid (green arrows), triangular (cyan arrows) or circular (orange arrows) patterns.

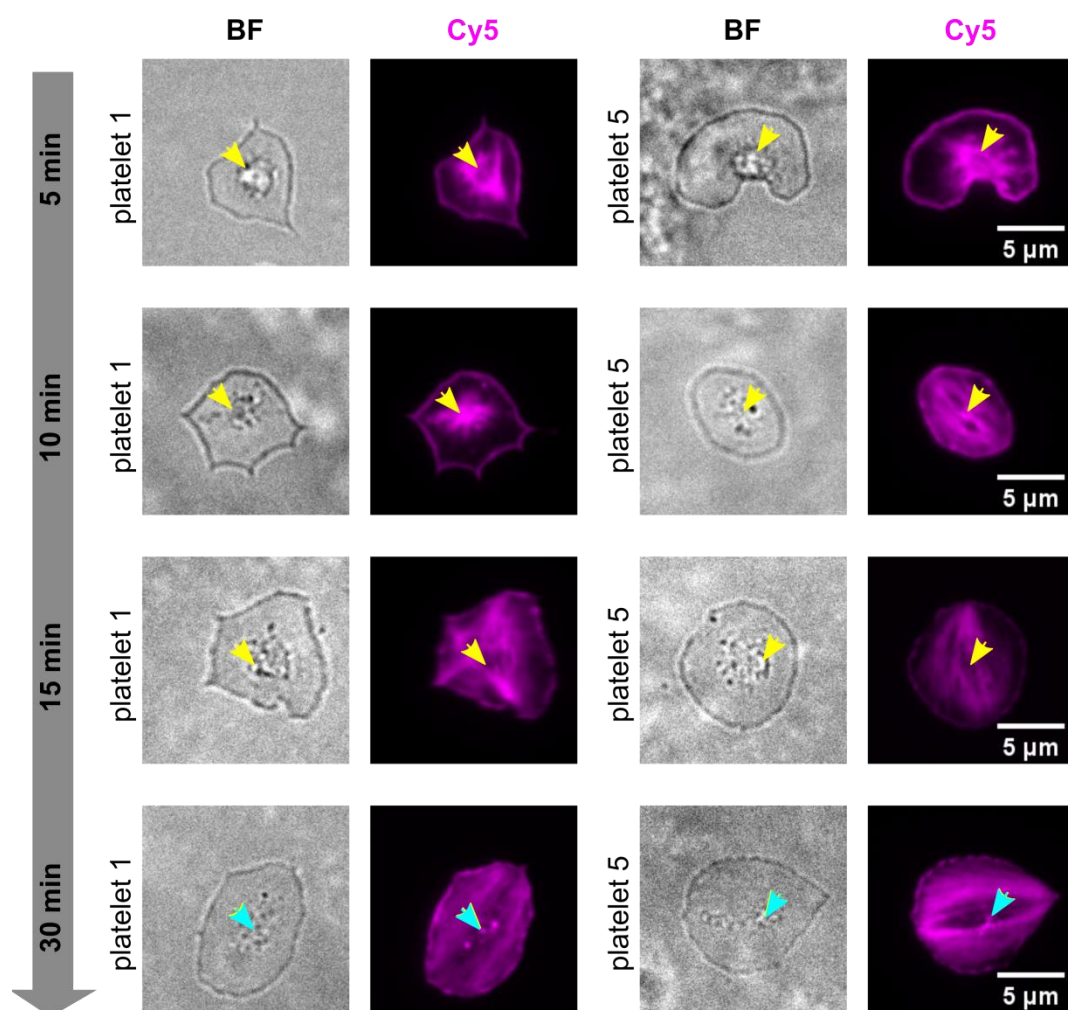


Figure 4.2: F-actin ring-like structures are associated with granules

The F-actin ring like structures formed in the first 5-15 minutes of platelet spreading (yellow arrows in Cy5 channel) seem to be associated with the hillock-like granules (yellow arrows in BF channel). As the granules flatten out during the later stages of spreading (30 minutes and beyond), the F-actin is reorganized into stress fiber-like structures and the F-actin ring like structures are almost no longer visible (cyan arrows).

4.1.2 Distribution of F-actin-vinculin or F-actin-myosin

For visualizing the distribution of vinculin or myosin with respect to F-actin, the platelets were fixed and double stained with specific antibodies and phalloidin at various time points of their spreading (5, 10, 15, 30, 60 and 120 minutes) and the qualitative distribution patterns of these proteins formed during platelet spreading is imaged. Examples of two different platelets showing the typical distribution patterns for that particular time point are shown in Figure 4.3 and Figure 4.4.

The F-actin is distributed in the filopodia and lamellipodia and later gets reorganized into the stress-fiber like structures (Cy5 channels in Figure 4.3 and Figure 4.4) in the same manner as described previously (see section 4.1.1).

In the initial stages of spreading (5-15 minutes in Figure 4.3), when the platelets have expanded via their lamellipodia, the focal adhesion protein vinculin is seen to be distributed evenly all over the cytoplasm although the staining signal is more intense at the plasma membrane and in the central region where the vinculin is arranged in a ring-like pattern (platelets 1 and 2 at 5 minutes and platelet 1 at 10 minutes in Figure 4.3). Interestingly, these vinculin ring-like patterns do not appear to coincide with the F-actin 'ring-like' structures that are described previously but rather seem to encircle the granulomere (section 4.1.1 and Figure 4.1 and Figure 4.2). A look at the BF images in the earlier spreading stages confirms this observation (platelet 1 at 10 minutes in Figure 4.5). As the platelets spread further (30 minutes and beyond), the vinculin gets distributed all over the cytoplasm but shows a predominantly higher signal at the tips of the stress fiber-like structure bundles that the platelets form (indicated by cyan arrows in Figure 4.3). At the later time points of spreading (60-120 minutes) the vinculin is associated with the circular F-actin stress fiber-like structures that the platelets form (platelet 2 at 60 minutes, platelets 1 and 2 at 120 minutes in Figure 4.3).

Over the course of the platelet spreading, the myosin distribution is comparable with that of the F-actin, except for its absence in the cortex (5-120 minutes in Figure 4.4). As the platelets spread and form filopodia and lamellipodia, the F-actin and myosin are co-distributed in these structures. Strikingly, myosin highly coincides with the F-actin 'ring-like' structures seen in the first 15 minutes of spreading (indicated by yellow arrows in platelets at 5, 10 and 15 minutes in Figure 4.4). A closer inspection of the corresponding BF images shows that these F-actin-myosin 'ring-like' structures are associated with the platelet granuloemes (platelet 1 at 10 minutes in Figure 4.5). As the platelets spread further (30-120 minutes) and reorganize into bundles of stress fiber-like structures, the myosin distribution too coincides with these bundles. During this later stage of spreading, when the granuloemes have flattened out and are no longer visible, the F-actin-myosin 'ring-like' structures too are not visible (platelet 1 at 30 minutes in Figure 4.5).

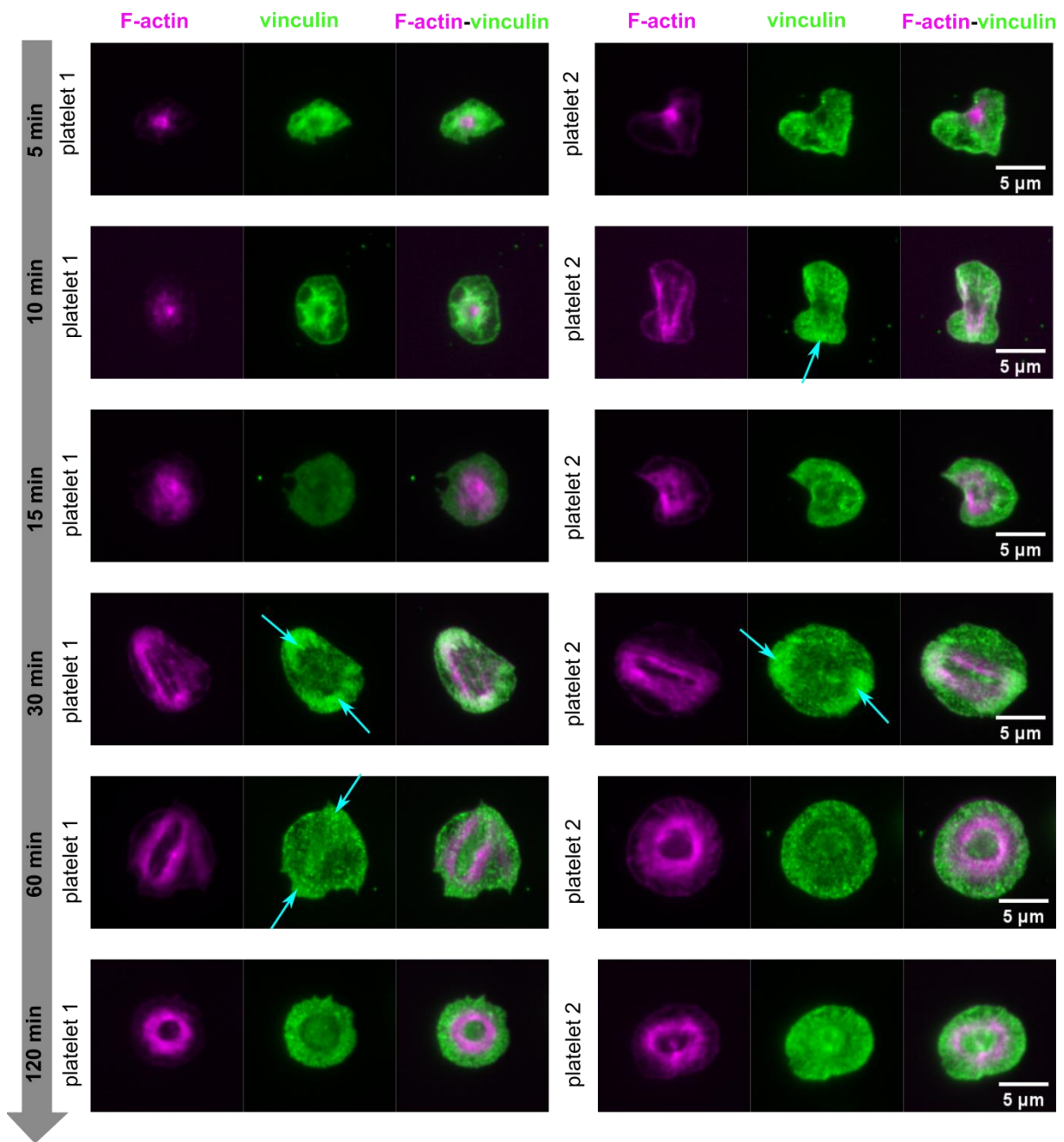


Figure 4.3: Qualitative distribution of F-actin-vinculin post-fixation

Epifluorescence images of platelets fixed at different time points of their spreading (5-120 minutes) and stained for their F-actin (Cy5) and vinculin (FITC). During the course of platelet spreading, the F-actin is seen in the filopodia, lamellipodia, cortex, and ring-like structures and gradually forms the stress-fiber like structures, whereas the vinculin is distributed all over the cytoplasm but shows a predominant distribution in the center in a ring-like pattern in the first 5-15 minutes and is later predominant at the tips of the bundles of F-actin stress fiber-like structures (indicated by cyan arrows and the white areas in the overlaid fluorescence images at time points 30, 60 and 120 minutes). All images were taken by Tim Dullweber during his Bachelor thesis.

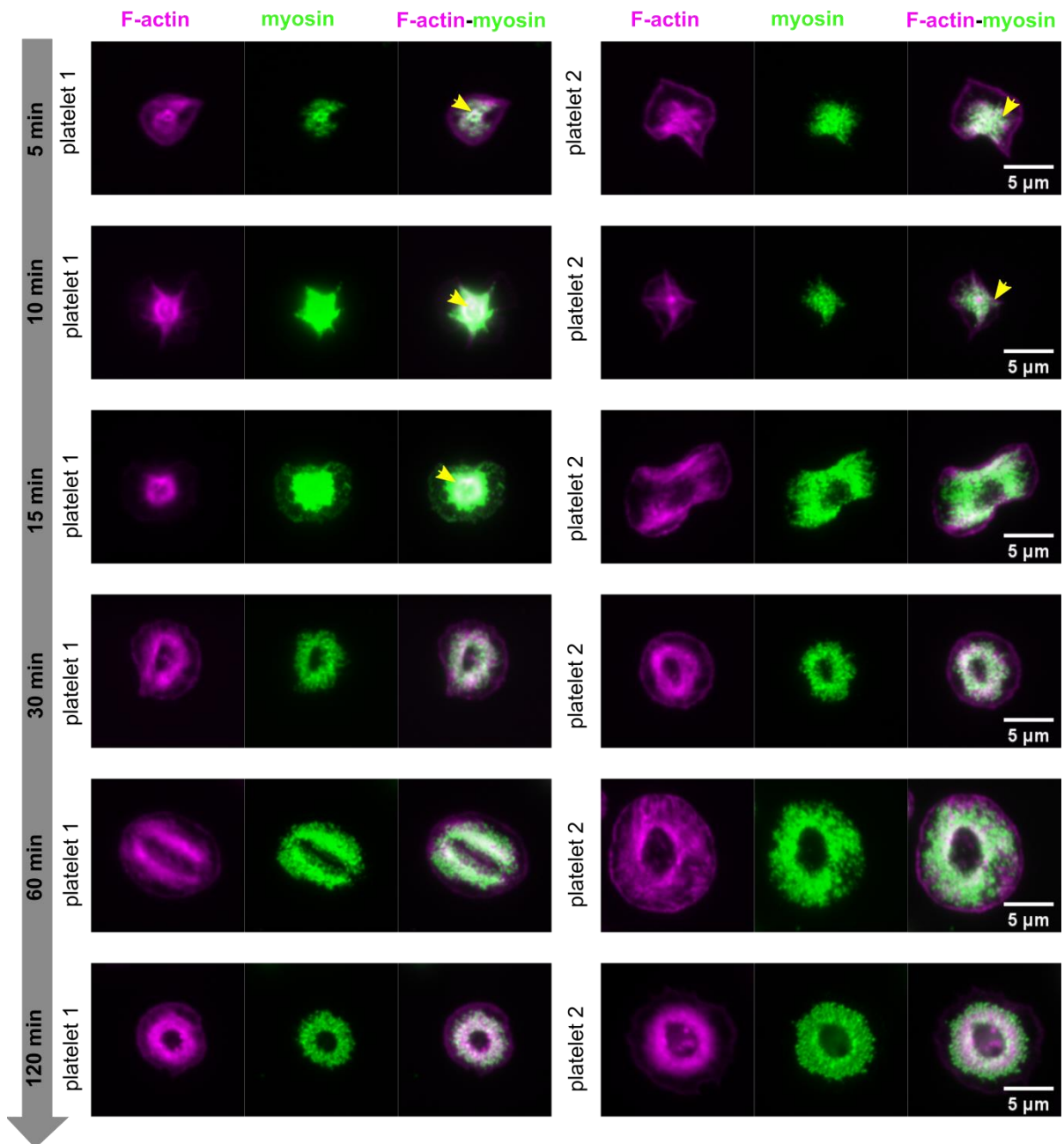


Figure 4.4: Qualitative distribution of F-actin-myosin post-fixation

Epifluorescence images of platelets fixed at different time points of their spreading (5-120 minutes) and stained for their F-actin (Cy5) and myosin (FITC). During the course of platelet spreading, the F-actin is seen in the filopodia, lamellipodia, cortex, and ring-like structures and gradually forms the stress-fiber like structures. The myosin too is associated in all of these structures with the F-actin, except in the cortex. Myosin predominantly coincides with the F-actin ring like structures seen in the first 5-15 minutes (indicated by yellow arrows) and later coincides with the bundles of F-actin stress fiber-like structures that develop at the later time points (white areas in the overlaid fluorescence images at time points 30, 60 and 120 minutes). All images were taken by Tim Dullweber during his Bachelor thesis.

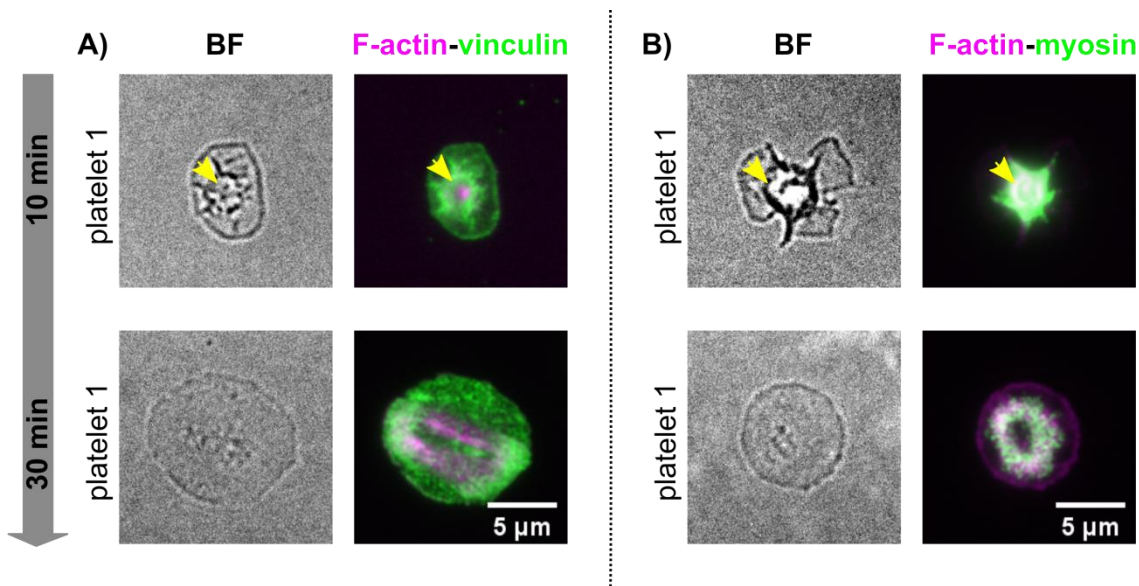


Figure 4.5: Distribution of vinculin and myosin at platelet granules

Distribution of vinculin (left panel) and myosin (right panel) in the platelet granule zone are shown with respect to F-actin during the early (top panel, 10 minutes) and later (bottom panel, 30 minutes) time points of platelet spreading. A) In the early time point, vinculin seems to encircle the granule (indicated by yellow arrow) and is not associated with the F-actin ring-like structure formed by the platelets and shows no defined association at the later time point of spreading when the granule has flattened. B) In contrast, myosin highly coincides with the F-actin ring-like structure (indicated by yellow arrow and white area in overlaid fluorescence image) in the early time point of spreading. However, there is no sign of the F-actin-myosin ring-like structure at the later time point of spreading when the granule has flattened.

In general, during platelet spreading on glass, the sites of focal adhesion (vinculin) are distributed all over the platelets with prominent distribution at their centers and at the tips of their F-actin bundles, whereas the sites of force generation (myosin) overlap with the sites of F-actin distribution, the only exception being the cortical regions.

4.1.3 Discussion of the results

Owing to their importance in the wound healing process, the cytoskeletal rearrangements in platelets have been studied in detail and since platelets do not have a nucleus, most of these studies have been performed after their chemical fixation. Numerous electron microscopy and immunofluorescence studies done on the actin cytoskeleton of fixed, glass-surface activated² platelets have shown that upon activation, platelets undergo morphological transformation from discoid to fried-egg shape. When adhered on protein-coated or non-coated glass surfaces, the platelets respond to these surfaces by extensively rearranging their F-actin

²activation refers to morphological changes occurring in platelets exposed to glass/ foreign surfaces

network into filopodia which radiate from the platelet center and contain long actin bundles, lamellipodia which consist of short orthogonally arranged actin filaments, and the stress-fiber like structures that contain parallel and/or ellipsoidal actin bundles. Further, these platelets spread into flat, polygonal or triangle shapes within 60 minutes [12, 13, 57, 99, 141, 163]. Our F-actin stainings, too, show the formation of these typical F-actin structures and also show polygonal morphologies after spreading completely within 60 minutes (Figure 4.1, Figure 4.3 and Figure 4.4).

The electron microscopy and immunofluorescence studies have also described the assembly of a circular array of F-actin filaments in the center of spreading platelets [12, 57, 57, 141]. In [12] it has been referred to as the assembly of a 'contractile ring' which is speculated to also contain myosin and is thought to first form during platelet shape change from discoid to round, when activated myosin pulls the membrane bound actin filaments into the center [141]. It has been observed that this 'contractile ring' encircles the degranulating granules and is most prominent during the first 15 minutes of platelet activation on glass [12]. It is also noted that the 'contractile ring' is easier to observe when the focal plane is slightly above the surface of the coverslip [12]. More immunofluorescence studies on platelets after adhesion have shown that these 'contractile rings' bring about the centralization of granules to the platelet granulomere zone [27]. Our single F-actin stainings, also show such 'ring-like structures' (marked by yellow arrows in Figure 4.1) and from our double F-actin-myosin stainings, it is evident that myosin is present in them (marked by yellow arrows in Figure 4.4). Also our BF images show that these 'ring-like structures' are associated with the platelet granulomeres (Figure 4.2 and Figure 4.5). All the descriptions in the above mentioned studies are consistent with our observations, thus implying that the 'ring-like structures' we see are probably the 'contractile rings'. Since we focus on the surfaces of the fibrinogen-coated coverslips, it is possible that the diffused but intensely stained central regions that we see in the early spreading stages of the platelets are the 'contractile rings' which are better distinguishable at a higher focal plane.

Immunofluorescence studies have also looked at the distribution of the focal adhesion protein, vinculin (also known as an actin binding protein) which forms FA sites by connecting the platelet α IIB β 3 integrin to the actin cytoskeletal network [94]. This connection occurs via α -actinin, which crosslinks F-actin filaments and anchors them to FA sites containing vinculin [13, 99, 114, 147]. The general observation in these studies is that in surface-activated, fully spread platelets, vinculin is present at the cell membrane and at the terminal points of F-actin bundles and serves as a connecting link between them and the ECM [99, 147]. It is speculated

in [99] that the accumulation of vinculin at the ends of F-actin bundles can occur due to their clustering which may occur when individual actin binding proteins come close to each other during stress fiber formation and augment the binding of vinculin molecules to each other. Our double F-actin-vinculin stainings, too, show that vinculin is distributed at the plasma membrane and the granulomere zone and later on at the tips of F-actin stress fiber-like structure bundles (Figure 4.3 and Figure 4.5). A recent immunofluorescence study has looked at the distribution of vinculin along with the protein Pdlim7, which is involved in facilitating dynamic interactions with the actin cytoskeleton, in platelets that spread on glass for 45 minutes [156]. Higher resolution SIM images of the distribution of these two proteins reveal that in platelets that reach the fully spread stage and form F-actin fibers, the Pdlim7 is present at the site of F-actin fibers and vinculin has a diffused distribution over the platelet surface with low distribution at the granule area. However, the line scans of fluorescence intensity reveal that although the vinculin is distributed evenly, it has higher fluorescence intensity at the cortical actin and around the F-actin fibers. The Pdlim7 and vinculin are partially co-localized and it is suggested that Pdlim7 possibly crosslinks FA-related proteins like vinculin at the sites of F-actin fibers [156]. Our vinculin distribution patterns in the platelet spreading stages where F-actin stress fiber-like structures have formed, match the description in [156]. It is also seen that during intermediate spreading stages, Pdlim7 is not present at the central granule area [156]. Since it is suggested that Pdlim7 colocalizes with vinculin, this could explain why we do not see vinculin at the granulomere. Together, all these studies imply that during platelet adhesion and early platelet spreading stages, vinculin along with other actin binding proteins serve as a scaffold and provide adhesion sites, and at later stages of spreading, when platelets form the F-actin stress fiber-like structures, these vinculin FA proteins can anchor them to the ECM. It has been suggested that vinculin reinforces the links between actin and integrins [97, 114].

Our observation that the distribution of myosin is comparable with that of the F-actin (Figure 4.5) is consistent with several other studies. Immunofluorescence and immunoelectron microscopy studies have shown that myosin associates with F-actin after platelets are activated and along with it surrounds the granulomere zone and is also present at the same sites as F-actin stress fiber-like structures that are formed later [30, 99, 147, 149].

Overall, all these immunofluorescence studies on the platelet cytoskeleton imply that during platelet spreading, the F-actin, vinculin and myosin of platelets sequentially and simultaneously undergo massive rearrangements, which enable the platelets to firmly adhere to their ECM and effectively exert their contractile forces through acto-myosin actions. These

studies also imply that these cytoskeletal components are functionally and spatially related to each other and together interact and contribute to efficiently perform platelet functions. Our post-fixation cytoskeletal stainings of these F-actin, vinculin and myosin cytoskeletal components of platelets provide an overview of how these interactions occur. The F-actin stainings in particular are useful as they provide a basis for the real-time F-actin dynamics of SiR-actin labeled platelets that are described in the next section.

4.2 Real-time F-actin dynamics

The post-fixation F-actin staining of platelets discussed in the previous chapter has given a broad overview of the F-actin reorganization that takes place in platelets as they spread. With the availability of the recently developed SiR-actin probe [86], it is now possible to visualize the F-actin dynamics in platelets in real-time. This probe is well suited for the purpose of our experiments because it specifically binds only to F-actin and after binding increases its fluorescence intensity by 100-fold [86]. So the platelets are labeled with this probe and are also treated with pharmacological agents (see sections 3.3.2 and 3.4) and their F-actin dynamics are visualized (see section 3.5.2) and quantified (see sections 3.6 and 3.9) as they spread on fibrinogen-coated glass coverslips. The platelet spreading is triggered by addition of the soluble agonist thrombin. In this chapter, the results of these SiR-actin platelet labeling experiments are shown, followed by a short discussion of the results with respect to the existing literature.

4.2.1 Direct visualization of platelet F-actin reorganization

The platelets are labeled with SiR-actin, allowed to spread on fibrinogen-coated coverslips and visualized for their F-actin in the Cy5 channel and their plasma membrane in the BF channel (as described in section 3.5.2). The time-lapse spreading snapshots of two typical SiR-actin labeled platelets imaged in both BF and Cy5 channels are shown in Figure 4.6.

As soon as the platelets adhere to fibrinogen, they start to change their shape and spread rapidly from a rounded to a flat morphology. As seen from the BF time-lapse images (BF channels in Figure 4.6A and B and earlier spreading time points for the platelet in Figure 4.6A inset), the platelets initially anchor themselves on the underlying fibrinogen-coated coverslips by extending the thin, finger-like filopodia (indicated by the magenta arrows in Figure 4.6A inset) and within a few seconds start to form the broader lamellipodia that fill up the spaces in

between these web-like filopodia or spread out laterally from the filopodia or even form directly from the edge of the platelet (indicated by the blue arrows in Figure 4.6A inset). During this period, the granules, which are noticeable as the dome-shaped structures (indicated by yellow arrow in Figure 4.6), start to move into the center and then gradually flatten out. The lamellipodia extend rapidly and the platelets appear to attend their final spread areas within minutes. The lamellipodial membranes show a membrane ruffling even after the platelets have stopped spreading. The time scale of this entire platelet spreading process, after initial contact with fibrinogen-coated glass coverslips ranges between 2-60 minutes, although in most cases very rapid spreading (2-5 minutes) is seen.

The corresponding Cy5 time-lapse images in the initial spreading time points show the formation of the F-actin-rich filopodia and lamellipodia (indicated by magenta and blue arrows in Figure 4.6). However, the fluorescence intensity is not very high. These platelets also show bright F-actin rich fluorescence spots in their centers that correspond to the granules seen in the BF channel (indicated by yellow arrows in Figure 4.6). These are presumably the contractile rings. As the platelets spread, these bright spots gradually disappear when the granules in the BF channel start to flatten out. Although the platelets finish their spreading within few minutes (as seen in the BF channel in Figure 4.6), the F-actin is seen to reorganize into higher order stress fiber-like structures for long (60-100 minutes) and there is an increase in the fluorescence intensities in the Cy5 channel during this time.

A typical Cy5 snapshot of fully spread platelets taken after the completion of a time-lapse movie is shown in Figure 4.7. All the platelets are in different spreading stages as some platelets adhere and start to spread at the very beginning or at a very early time point of the time-lapse movies, whereas other platelets adhere and spread in the middle or towards the end of the movies. However, all these spread platelets form the four typical F-actin structures - the filopodia (indicated by magenta arrows), the lamellipodia (indicated by blue arrows), the contractile ring (indicated by the yellow arrows) and the stress fiber-like structures (indicated by the green arrows). These contractile rings are seen more clearly when the focal plane is slightly changed, but otherwise appear as bright spots in the platelet centers which later dissolve or are unnoticeable as the spreading progresses. The fully spread platelets show circular, triangular or polygonal morphologies and their F-actin stress-fiber like structures are seen to form bundles that span across the entire length of the platelets with some prominent filaments arranged in triangles or ellipses. These observations are consistent with the F-actin patterns seen in the fixed-platelet time series (section 4.1.1).

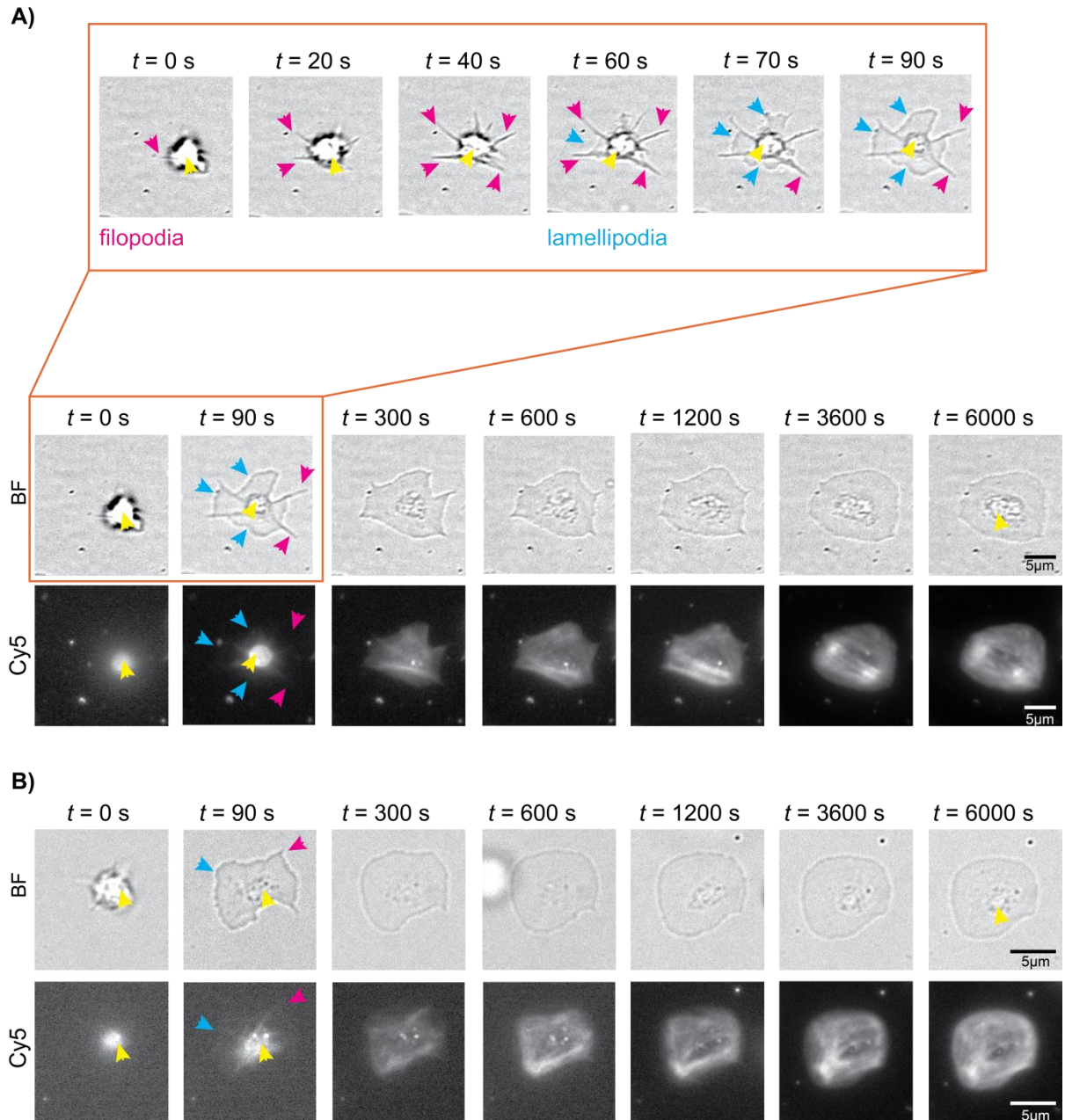


Figure 4.6: Real-time imaging of SiR-actin labeled platelet spreading

Time-lapse spreading snapshots of a two exemplary SiR-actin labeled platelets (A and B), imaged in the BF and Cy5 channels are shown. The earlier time points of spreading from 0-90 seconds, for the platelet A, imaged in the BF channel, are shown in the inset. As seen in both BF and Cy5 channels, the platelets initially anchor to the underlying fibrinogen and start to spread by extending F-actin-rich filopodia (magenta arrows) and further expand by forming the broader F-actin-rich lamellipodia (blue arrows) that form in between the filopodia or form laterally from them. At the same time the granulomer (yellow arrows) move to the platelet centers. The platelets finish spreading within few minutes, but the F-actin reorganizes into stress-fiber like structures for a longer time and there is an increase in the fluorescence intensities in the Cy5 channel over this time period.

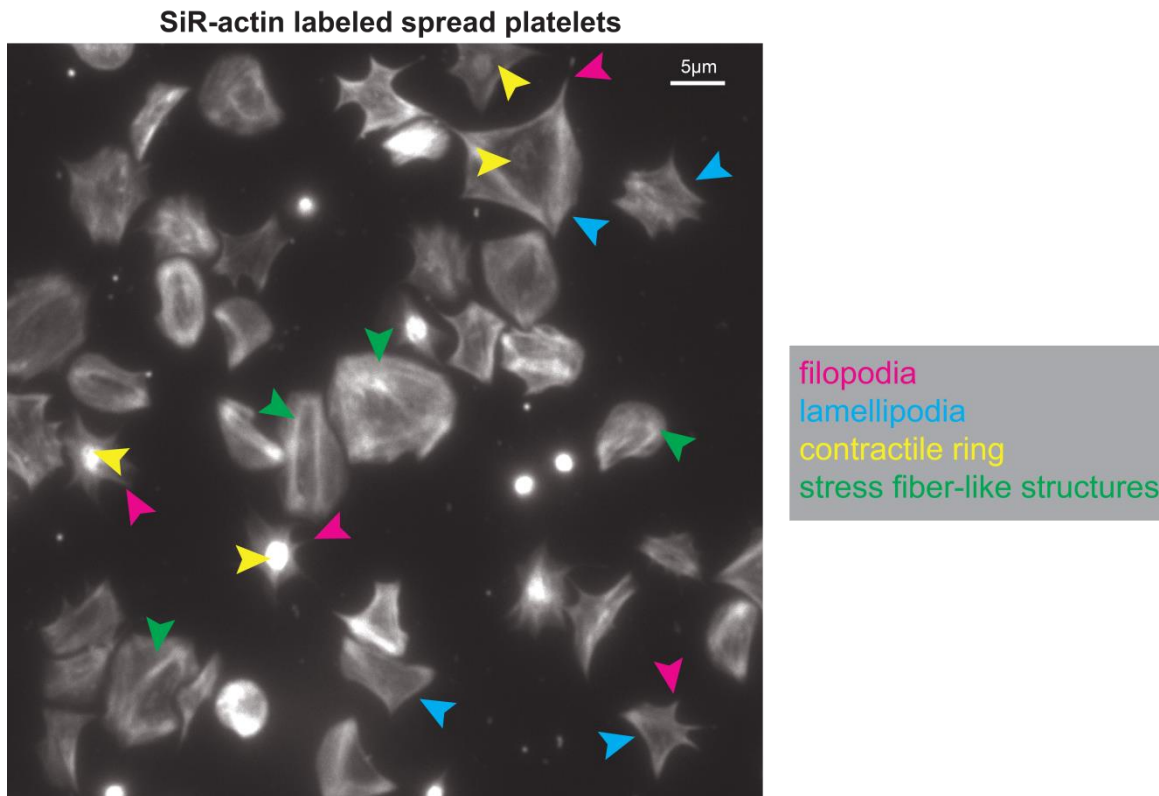


Figure 4.7: SiR-actin labeled platelets form four F-actin-rich structures while spreading

A typical snapshot of spread SiR-actin labeled platelets taken after a time-lapse movie is shown. These platelets have formed the typical F-actin structures namely the filopodia (magenta arrows), the lamellipodia (blue arrows), the contractile rings (yellow arrows) and the stress fiber-like structures. The contractile rings are seen more clearly when the focal plane is slightly changed, but otherwise appear as bright spots in the platelet centres.

4.2.2 Temporal evolution of F-actin fluorescence intensities

4.2.2.1 Quantification of F-actin fluorescence intensity increase

From the time-lapse snapshots of the SiR-actin labeled platelets, it is evident that the fluorescence intensities in the epifluorescence channel are increasing (Figure 4.6). This is most likely due to the assembly of the F-actin filaments into higher order structures. So to analyze these fluorescence intensity increases, the F-actin intensity profiles of normalized fluorescence intensities were plotted over time (as described in section 3.6.1) as the SiR-actin labeled platelets spread.

Only fully spread, single platelets that formed the stress fiber-like structures were chosen for the analysis. In the first experiments, a SiR-actin probe concentration of 2 and 6 μM was chosen for labeling the platelets and the platelets were labeled for 30 minutes without washing

off the excess probe, before starting the time-lapse experiments. The normalized F-actin intensity curves of platelets labeled with both probe concentrations are shown in Figure 4.8 (A for 6 μM and B for 2 μM concentrations). The different colors of the curves stand for group of platelets analyzed from datasets that were obtained from independent experimental days. The total number of platelets analyzed for that particular concentration is indicated by ' N '. The graph in Figure 4.8C shows the types of normalized F-actin intensities profiles typically seen for single platelets. The profiles reveal at least two but sometimes four stages - a rapid initial steep rise in the normalized fluorescence intensities, followed by a linear increase that sometimes reaches a plateau and then at times starts to decrease. These curves are all plotted starting from the first point of adhesion (the t_{zero}) of the individual platelets to fibrinogen-coated glass coverslips. Hence there are differences in the curve profiles, as not all platelets start to spread at the same time. The F-actin intensities of those platelets that start to spread early and go on spreading for 90 minutes and beyond, reach or begin to reach a plateau. These curve profiles seem to complement the stages seen in the time-lapse images of the F-actin assembly of SiR-actin labeled platelets as they spread (Figure 4.6). During the initial steep rise, rapid F-actin polymerization results in formation of the filopodia and lamellipodia by which the platelets spread fast. This is followed by the linear increase where the F-actin polymerization continues with the platelets assembling the F-actin into higher-order stress-fiber like F-actin structures (indicated by orange arrows in Figure 4.8C). For the platelets that spread longer, the intensity values saturate reaching a plateau (indicated by magenta arrows in Figure 4.8C) which may be interpreted as the cessation of F-actin assembly activity. The decrease seen in the normalized fluorescence intensities (indicated by brown arrow in Figure 4.8C) is most likely due to the bleaching of the SiR-actin probe.

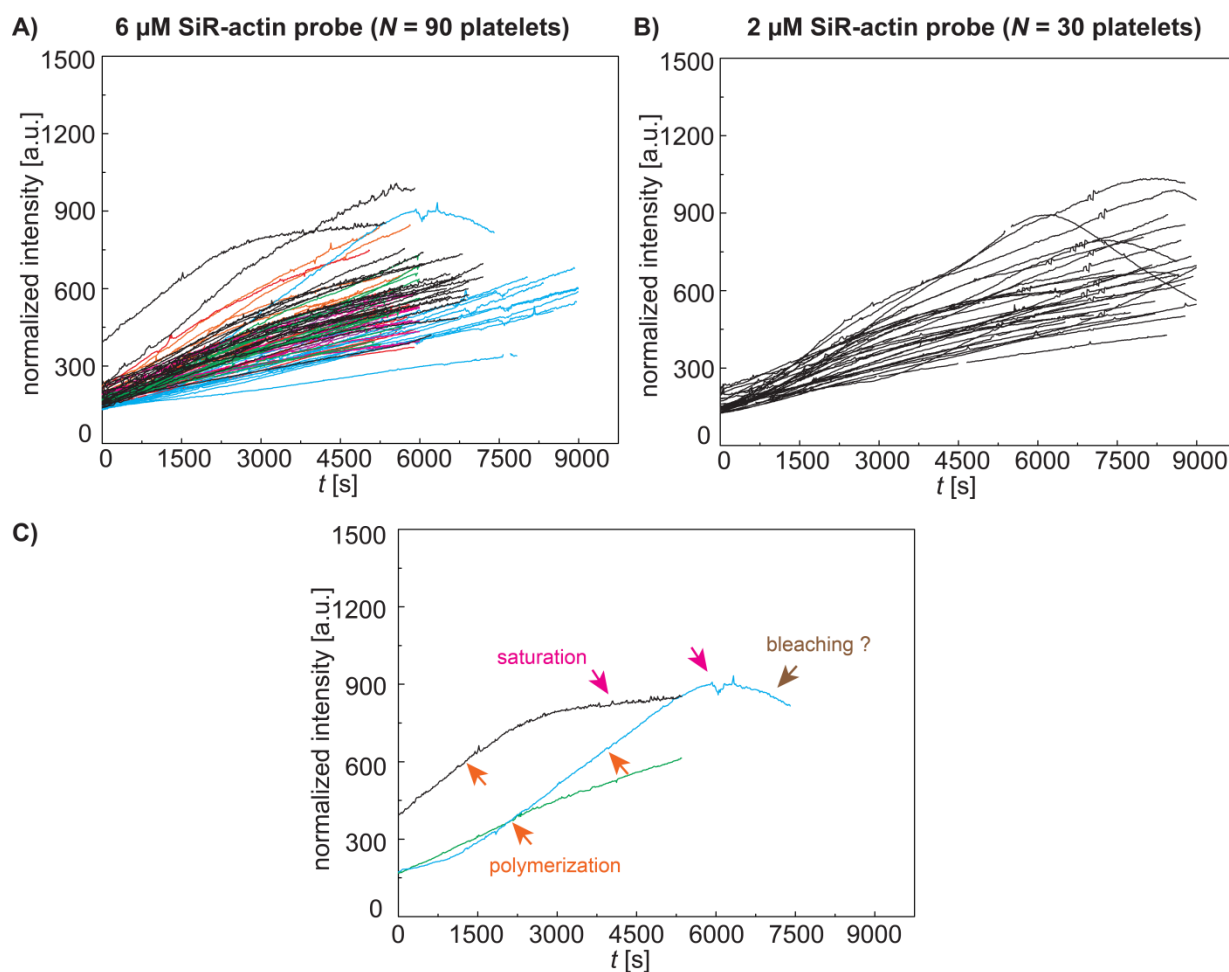


Figure 4.8: Temporal evolution of F-actin intensities of SiR-actin labeled platelets

Time lapse movies of platelets labeled with A) 6 μM and B) 2 μM of SiR-actin probe were taken and their normalized F-actin intensity curves were quantified and plotted over time. The total number of platelets analyzed is indicated by 'N' and the colors stand for group of platelets analyzed from independent datasets. C) The types of intensity profiles typically seen for single platelets are shown. Platelets labeled with both concentrations show similar intensity profiles which reveal an initial step rise followed by a linear increase indicating F-actin polymerization (orange arrows) which is then sometimes followed by a plateau (magenta arrows) which may indicate cessation of F-actin activity. The curves sometimes decrease again (brown arrow) which may indicate bleaching of the SiR-actin probe.

4.2.2.2 Characterization of the SiR-actin probe

One of the most noticeable features of the normalized F-actin fluorescence intensity profiles for the two different concentrations of SiR-actin probes is that the trend of the temporal evolution of the curves in both looks similar. So to choose a suitable concentration of the SiR-actin probe to use for labeling the platelets, some characterization tests for the probe are carried out. For that purpose, a histogram distribution (as described in section 3.6.2) of the

normalized F-actin intensity values at three different time points of platelet spreading - 5, 20 and 60 minutes (indicated by magenta, green and blue dotted lines in left panel of Figure 4.9A) is plotted (right panel Figure 4.9A and Figure 4.9B). The histograms show that the intensities at an earlier time point of spreading are clustered around a small group of values but those at later time points are more dispersed. It is observed that the trend of the intensity distribution is similar between the two different probe concentrations. So a SiR-actin probe concentration of 6 μM is used for all the experiments.

The histogram distribution enables a quick comparison of the intensity values of different experimental conditions, thus making it more comprehensive. The SiR-actin probe is characterized to find out its optimal labeling time with the platelets. The platelets are labeled for 0, 30 (as already shown Figure 4.9A) or 120 minutes before starting the time-lapse experiments and the excess probe is not washed off. These platelets are then quantified for their normalized F-actin intensities (see Appendix G) and a histogram distribution of the intensity values is plotted as before. The total number of platelets analyzed is indicated by '*N*'. The histogram distribution is compared to the intensity distribution of the 6 μM probe with 30 minutes of labeling (Figure 4.9A, C and D). Here, too, the trend of the intensity distribution is similar for the different labeling times. So a labeling time of 30 minutes before the experiments is chosen.

In all these experiments, the excess SiR-actin probe, after labeling the platelets is not washed off. So one likely reason for the rise seen in the fluorescence intensities in the F-actin intensity curves, could be due to the binding of free probe molecules still present in the surrounding buffer, to the already formed F-actin structures. To test this possibility, the excess SiR-actin probe is washed off by centrifugation of the labeled platelets and followed by their resuspension in label-free buffer. Time-lapse movies of these platelets are then taken and their normalized F-actin intensities are quantified over time (see Appendix G) and the histogram distribution of the intensity values is plotted. The total number of platelets analyzed is indicated by '*N*'. This distribution is also compared with the intensity distribution of the platelets labeled with 6 μM of the probe for 30 minutes where the excess probe is not washed off (Figure 4.9A and E). Here, too, the intensity distribution trend is similar to that of the previous histograms.

This indicates that the intensities of SiR-actin labeled spread platelets are independent of the probe concentration and the labeling times. Also, the rise in the intensities indeed comes from the probe binding to the F-actin structures that the platelets reorganize into higher order structures as they spread over time.

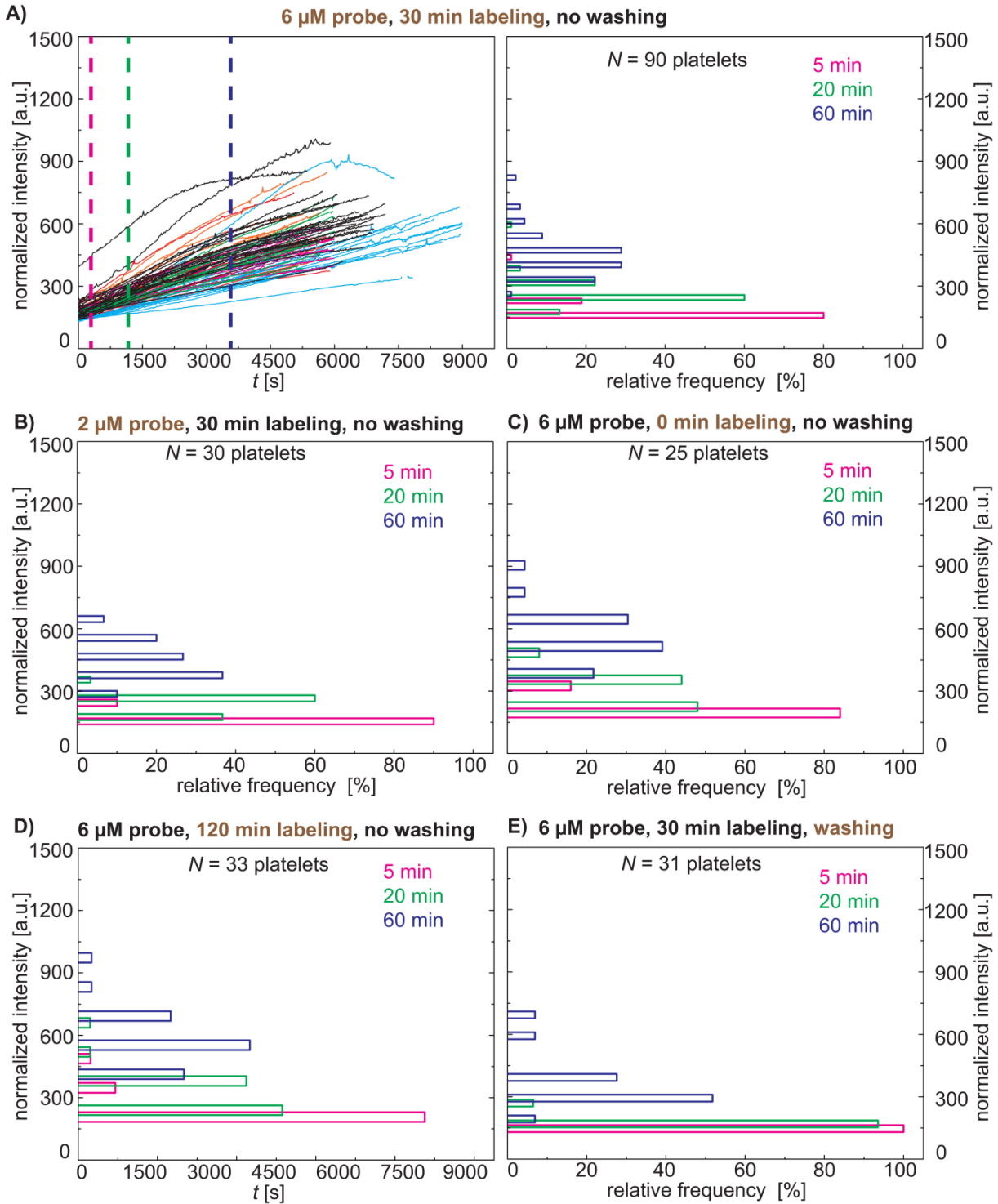


Figure 4.9: F-actin intensities are independent of probe concentration, labeling time or washing

SiR-actin probe characterization tests are carried out by varying probe concentrations (A and B), labeling times (A, C and D) and washing or not washing the excess probe (A and E) after labeling. A histogram distribution of the normalized F-actin intensity values at 5 (magenta), 20 (green) and 60 (blue) min quantified for each these tests was plotted. The histogram distribution of the F-actin intensity shows the same trend for all these tests. So finally platelets are labeled with 6 μM of the probe for 30 minutes and imaged without washing off the excess probe. (N = total number of platelets analyzed).

Hence for all the SiR-actin experiments, the platelets are labeled with 6 μM of the probe for 30 minutes and the excess probe is not washed off. In the next chapters, these parameters of the probe are designated as the 'control' parameters. At these optimal parameters, the platelets spread normally just like the untreated or only DMSO (vehicle) treated platelets (see Figure 4.10).

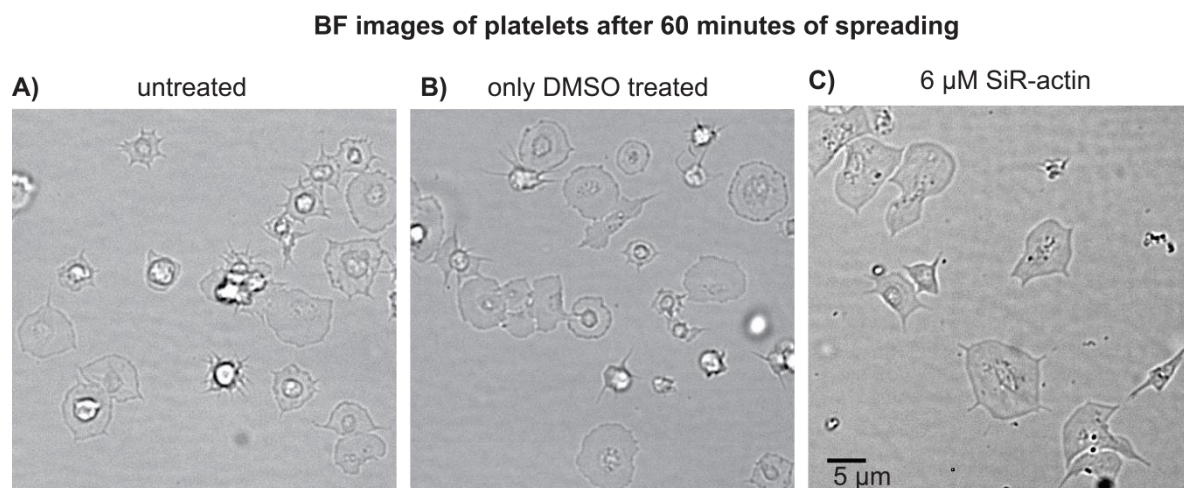


Figure 4.10: Platelets spread normally after labeling with SiR-actin probe

The BF images taken after 60 minutes of platelets spreading are shown. Platelets were left A) untreated or B) treated with the vehicle DMSO for 30 minutes or C) with 6 μM SiR-actin probe for 30 minutes. The SiR-actin probe had no deleterious effects on platelet spreading and they spread normally just like the untreated or DMSO treated platelets.

4.2.3 Multiple timescales of F-actin formation and reorganization

4.2.3.1 Platelets spread within minutes but reorganize F-actin for hours

As shown before (section 4.2.1), spreading of platelets can be visualized in real-time along with the reorganization of their F-actin into stress fiber-like structures, by labeling them with the SiR-actin probe, and imaging them in the BF and Cy5 channels. One of the most striking observations during these time-lapse movies is that the platelets seem to spread to their final areas very fast after their initial contact with fibrinogen-coated glass coverslips (see Figure 4.6 BF channel) but the F-actin structures are reorganized into higher order stress fiber-like structures for a longer time (see Figure 4.6 Cy5 channel). This is reflected in the observation that after completing their spreading, the final area of the platelets does not seem to change but their normalized fluorescence intensities still increase (Figure 4.6 and Figure 4.8).

So in order to look into this phenomenon more carefully, the temporal evolution of the platelet areas and their F-actin intensities are simultaneously quantified. For that purpose, the platelets are labeled with both, a plasma membrane dye CM green, and the SiR-actin probe and, allowed to spread while taking epifluorescence microscopy time-lapse movies. The F-actin intensity curves and areas of the spreading platelets are quantified as described before (see sections 3.6 and 3.7).

An example of the time-lapse snapshots of a platelet double stained with CM green and the SiR-actin probe is shown in Figure 4.11A. As seen in the FITC channel, the platelet spread area increases rapidly after adhesion and at some point does not change much whereas the F-actin fluorescence intensity in the Cy5 channel keeps increasing. The spread areas and normalized F-actin intensities for three platelets are plotted as shown in Figure 4.11B (the blue curves represent the platelet shown in Figure 4.11A). These plots reflect the observations from the time-lapse snapshots. After adhesion, the platelet spread areas increase rapidly and within a few minutes reach a plateau and do not change much thereafter. To determine the turning time point t_I at which the spread areas reach a plateau, the area curves are fitted with a piecewise linear model (see section 3.10). An example of this linear fit for the magenta spread area curve is shown in Figure 4.11C. From the fit, the t_I value is ~ 1 minute which shows that the platelet, after adhering spreads and finishes its spreading within a minute. On an average, it is seen that the platelets spread very fast, on the order of ~ 2 minutes. In contrast, the F-actin reorganization goes on longer as seen by the increase in the normalized fluorescence intensities, on the order of ~ 90 minutes as seen from these curves.

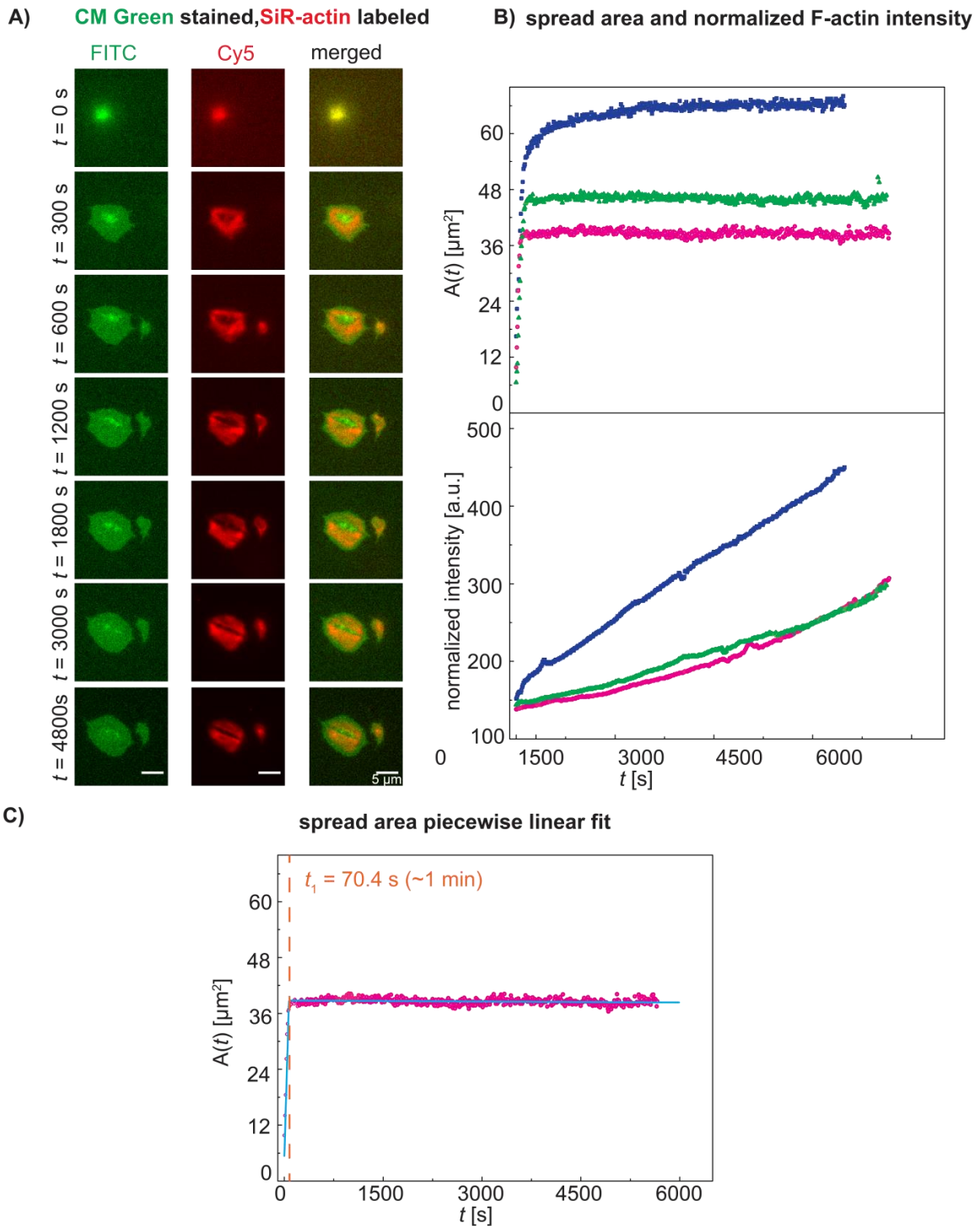


Figure 4.11: Platelets spread within minutes but reorganize F-actin for hours

A) Time-lapse snapshots of a spreading platelet labeled for both its plasma membrane by CM Green dye (FITC channel) and F-actin by SiR-actin probe (Cy5 channel) are shown. The platelet spreads rapidly and then does not change its area after a point whereas the F-actin intensity goes on increasing in the Cy5 channel. B) The spread area (top) and normalized F-actin intensity (bottom) over time of the platelet shown in A is plotted (blue curve). The other two curves (green and magenta) represent two other platelets. C) The turning time point t_1 of the spread area curves is obtained by making a linear fit to the spread area curves as shown for the magenta curve. Here the t_1 (dotted line) is ~ 1 min. On an average, after adhesion, platelets reach their final spread area within ~ 2 minutes but reorganize their F-actin until hours as seen by the increase in the normalized fluorescence intensities in B.

The reason for analyzing such few platelets for their spread areas and F-actin intensities is that the double labeling of the platelets with the two stains seems to affect their ability to reorganize the F-actin into stress fiber-like structures. Most of the platelets labeled with CM green dye and the SiR-actin probe do not form the stress fiber-like structures that are typically expected to form after platelets have spread for more than 60 minutes (see Appendix I). Also, the CM green dye internalizes relatively quickly, which makes the imaging near the end of the time-lapse movies noisy thus making the detection of the platelet areas difficult.

However these analyzes although few in number, reflect the time-lapse series observations where the platelets are seen to spread within minutes but are seen to reorganize their F-actin into stress fiber-like structures for hours.

4.2.3.2 Temporal evolution of F-actin filaments

The reorganization of the F-actin mentioned above of SiR-actin labeled platelets is further quantified by detecting individual F-actin filaments formed during this process, using the FS program [39]. Here the 'F-actin filaments' is a general term which refers to any of the F-actin higher order structures and stress fiber-like structures that the FS program can detect. In principle the FS program considers any of these detected structures as linear filaments having varying length and width.

Only single platelets that have formed the stress fiber-like structures are chosen from the time-lapse movies for the analysis. The F-actin filaments formed over time are detected and the smoothed total line (filament) lengths are plotted over time (see section 3.9) as shown in Figure 4.12A. The different colors of the length curves stand for group of platelets analyzed from datasets that were obtained from independent experimental days. The total number of platelets analyzed for that particular concentration is indicated by ' N '. The temporal evolution profiles of the total line lengths show an initial rapid rise in the first few minutes which is then followed by a slower increase that most of the times reaches a plateau. To determine the turning time point t_l at which this initial phase of rapid F-actin filament growth ends, the previously described piecewise linear fitting model (see section 3.10) is applied to these curves and an example of this fitting is shown in Figure 4.12B. Here the filled circles represent the total total line lengths and the solid line represents the Gaussian smoothed ($\sigma = 10$ images) total total line lengths. In this particular example, the t_l is ~ 12 minutes. A histogram distribution of the t_l values obtained by linear fitting of all the platelets analyzed is shown in Figure 4.12C. From these fits, on an average, it is seen that the during platelet

F-actin reorganization, the initial phase of rapid F-actin filament growth ends within ~ 9 minutes.

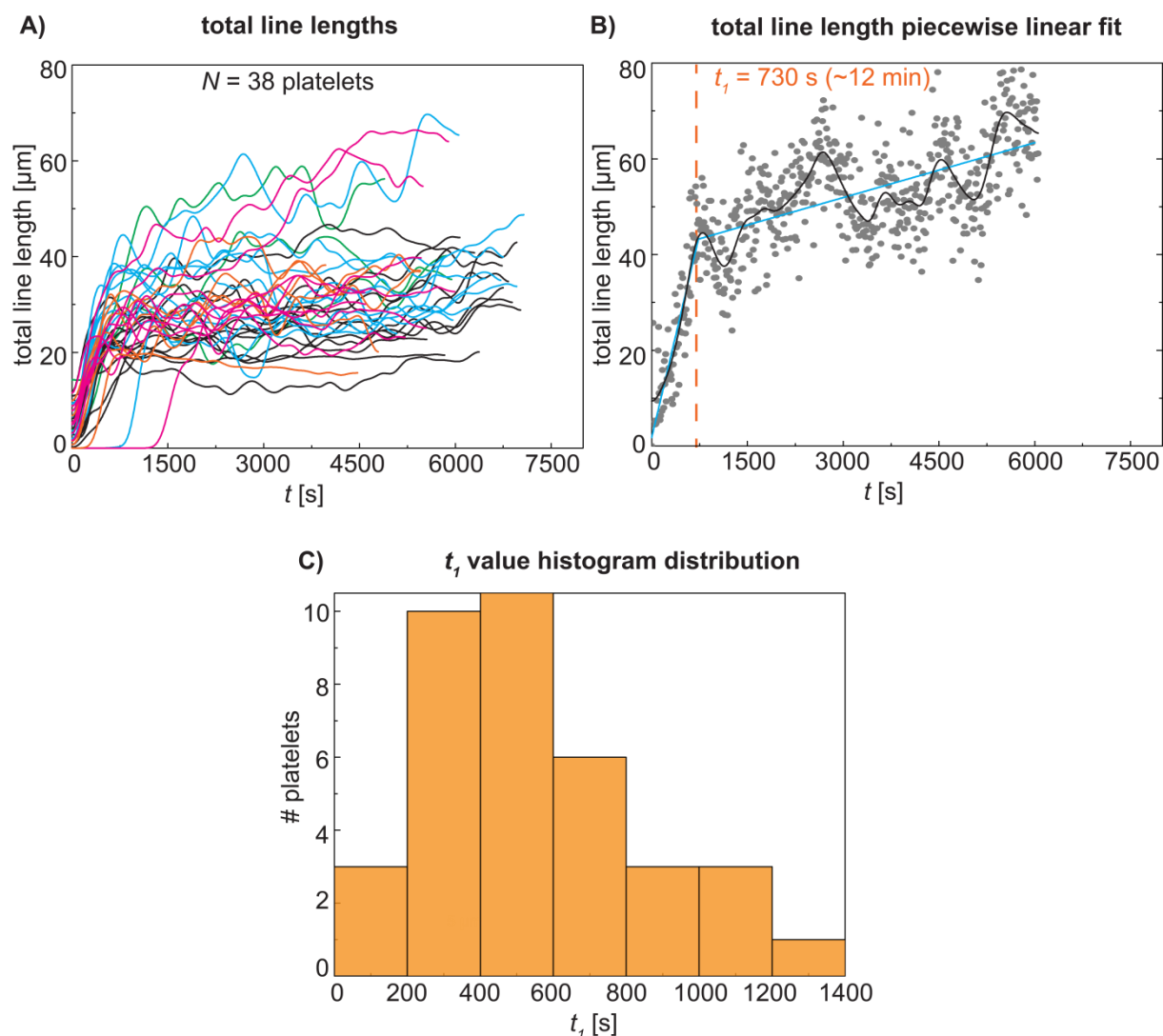


Figure 4.12: Temporal evolution of total F-actin filament lengths

A) The temporal evolution of the smoothed total line lengths detected by the FS program for individual platelets is shown. The curves show an initial rapid growth indicating the formation of major F-actin structures within minutes followed by a slow phase of F-actin network growth in hours.

B) The turning time point t_l at which this initial phase of rapid F-actin filament growth ends is determined by making a linear fit to the smoothed total line length curves as shown in this example. Here filled circles are the original total line lengths and the solid line is the smoothed total line length and the t_l (dotted line) is $\sim 12 \text{ min}$. C) Histogram distribution of t_l values ($N = 38$ platelets). On an average, the majority of the F-actin filament growth ends within ~ 9 minutes.

4.2.4 Effects of pharmacological agents on F-actin dynamics

The above results have demonstrated that it is possible to visualize and analyze the F-actin reorganization in platelets in real-time. So using the advantage of this, the temporal evolution of the effects of common pharmacological agents on platelet spreading and cytoskeletal reorganization are further investigated. The SiR-actin labeled platelets are treated with or without the pharmacological agents, the time-lapse movies are taken and the normalized F-actin intensities are quantified. These intensities are then compared to those of the control conditions (untreated 6 μM SiR-actin labeled platelets) by looking at the F-actin intensity histogram distributions. The snapshots taken after these time-lapse movies are also looked at. In all these spreading experiments, the platelet spreading is triggered by addition of thrombin. So the first immediate question that arises is what happens to the F-actin intensity distribution of the platelets that are not supplied with this agonist thrombin. The first strikingly noticeable phenomenon is that when thrombin is not supplied, only few platelets spread as compared to the control (Figure 4.13A and B). But the ones that spread show the assembly of the stress fiber-like structures, although many of them do not show smooth polygonal morphologies typically expected of normally spread platelets (see Figure 4.7) but instead show polygonal morphologies with extension of many filopodia. However, their F-actin intensities distribution trend is similar to that of the control i.e. the thrombin stimulated SiR-actin labeled platelets (Figure 4.14A right panel and B).

Next, the effects of the myosin inhibitors blebbistatin and Y-27632, which respectively inhibit the myosin II by blocking its ATPase activity or ROCK activity, are investigated. In these experiments with the myosin inhibitors, the scenarios show some change. When treated with 20 μM blebbistatin, only few platelets spread (Figure 4.13A and C). Again, the ones that spread form the stress fiber-like structures and do not differ in their F-actin intensities distribution trend as compared to that of the control platelets (Figure 4.14A right panel and C). But the treatment with 50 μM Y-27632 does not seem to reduce the number of platelets that spread. However, there is a noticeable effect on the assembly of F-actin structures. These Y-27632 treated platelets show a reduced stress-fiber like structure assembly although there is a higher localization of the F-actin at the platelet lamellipodial edges (Figure 4.13A and D). Interestingly enough, the histogram trend of the F-actin intensities distribution is similar to that of the control platelets (Figure 4.14A right panel and D).

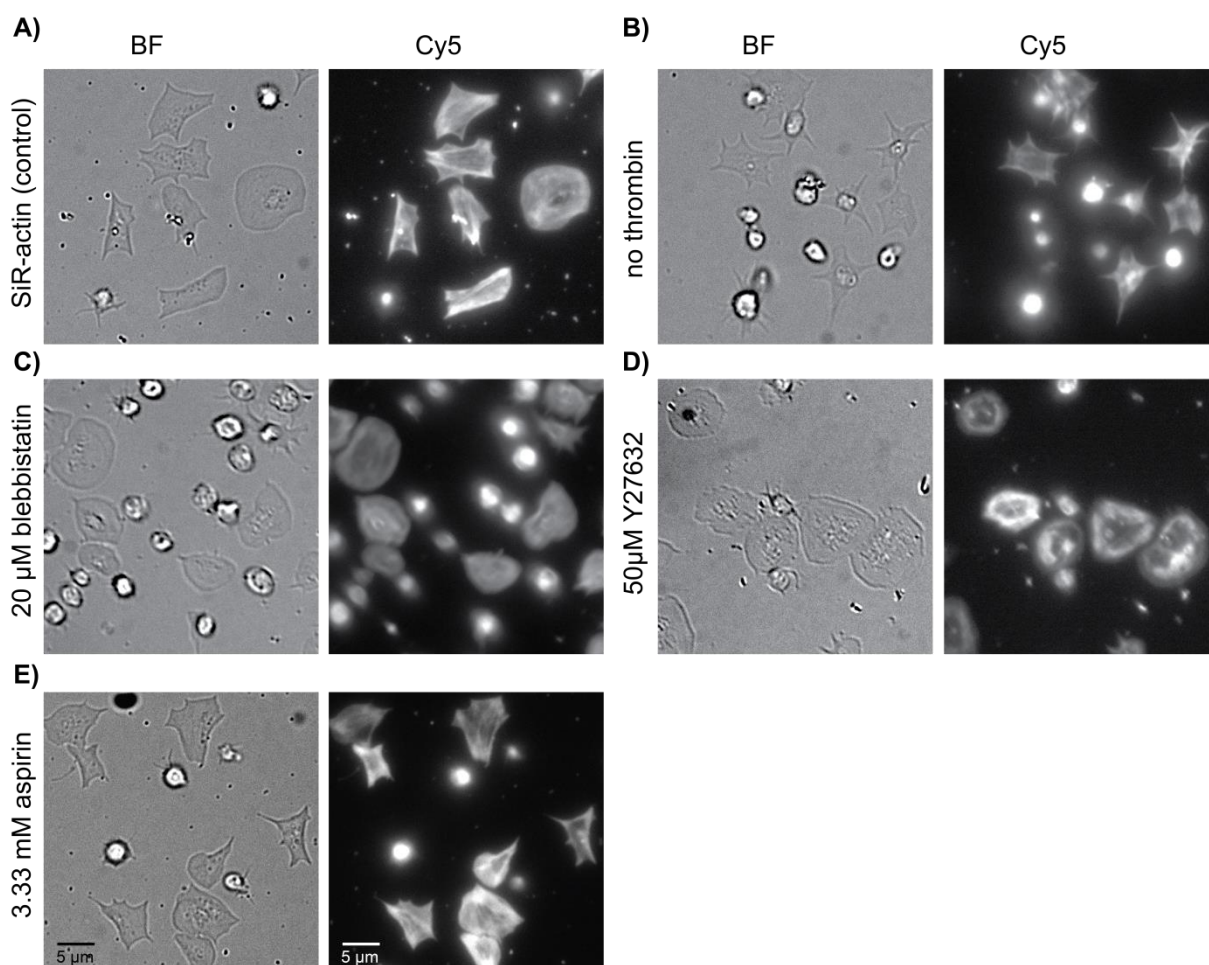


Figure 4.13: Pharmacological agents affect spread platelet numbers

BF and Cy5 time-lapse snapshots of SiR-actin labeled platelets after treatment with or A) without pharmacological agents are shown. B) Less number of platelets spread in absence of thrombin as compared to the control and show many filopodia. C) Less number of platelets spread in presence of 20 μM blebbistatin as compared to the control but those that spread show the formation of stress fiber-like structures. D) There is not much difference in the number of spread platelets as compared to the control but there is more F-actin localization at their edges in presence of 50 μM Y-27632. E) There is not much difference in the number of spread platelets in presence of 3.33 mM aspirin as compared to the control and these platelets also form the stress fiber-like structures.

Lastly, the effects of aspirin on the temporal evolution of platelet spreading and cytoskeletal reorganization are also investigated. Aspirin is a well-documented platelet aggregation inhibitor [137, 162] but its effect on single platelet spreading has not been studied in great details. Again, the platelets treated with 3.33 mM aspirin show no differences in the assembly of stress-fiber like structures (Figure 4.13A and E). For the histogram distribution, although the F-actin intensity values are slightly higher, there is no difference in the trend of the F-actin intensities distribution from that of the control platelets (Figure 4.14A right panel and E).

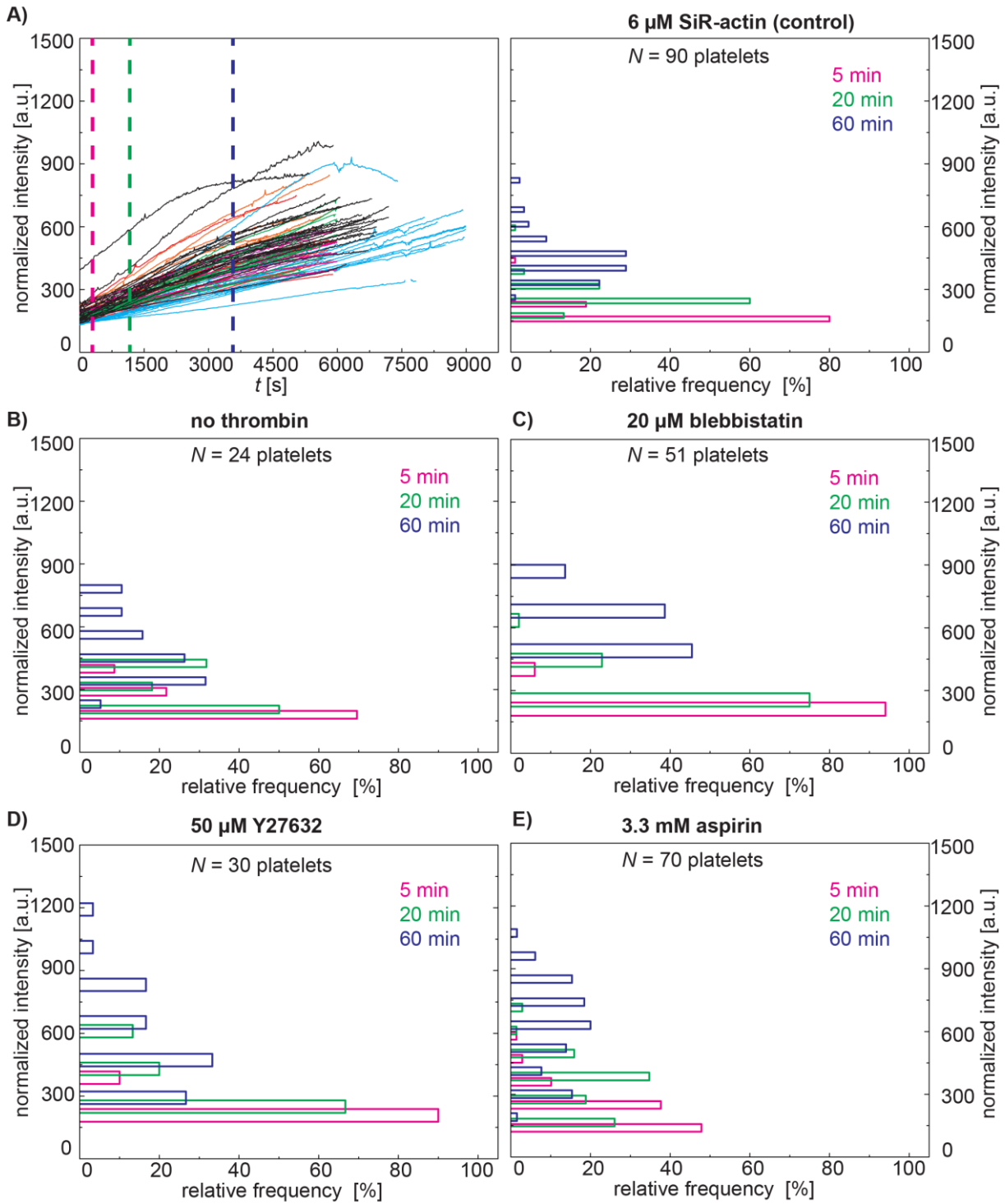


Figure 4.14: Pharmacological agents show no effect on the F-actin intensity profiles

A) The left panel shows the temporal evolution of the normalized F-actin intensities of SiR-actin labeled platelets as they spread. A-E) The right panel shows the histogram distribution of these intensity values at 5 (magenta), 20 (green) and 60 (blue) min. The histogram distribution of the F-actin intensity values at the chosen time points as compared to the control conditions in A) only SiR-actin labeled platelets show the same trend as for SiR-actin labeled platelets provided with or without the pharmacological agents- (B) with 20 μ M of the myosin II inhibitor, blebbistatin (C) with 50 μ M of the ROCK inhibitor, Y-27632 (D) without the agonist, thrombin and (E) with 3.33 mM of the platelet aggregation inhibitor, aspirin.

An important aspect to note in all these experiments is that only those platelets have been chosen to analyze that spread normally and form the stress fiber-like structures. However time-lapse imaging has showed that there is difference in the overall numbers of platelets that spread during each of these experimental conditions (as shown in Figure 4.13). So in the next step, the relative numbers of spread platelets in each of these conditions are quantified. For this purpose, the numbers of the spread and unspread platelets from the total adhered after the time-lapse BF movies are counted and compared to those numbers of the control untreated SiR-actin labeled platelets (see section 3.11).

The relative numbers quantified are shown in Figure 4.15A. The platelets that show complete lamellipodial spreading with circular, triangular or polygonal morphologies are considered as 'spread' (indicated by purple bars in Figure 4.15A) whereas those that show rounded morphologies occasionally with filopodia and very small lamellipodia are considered as 'unspread' (indicated by orange bars in Figure 4.15A). The relative numbers are also compared to the control conditions by performing a statistical analysis using a *t*-test and a *p*-value < 0.05 is considered statistically significant (Figure 4.15B). These relative numbers reflect the previous histogram intensity distribution observations. There is a significant reduction in the number of spread platelets in the absence of thrombin and in presence of blebbistatin, as compared to the control. However, this reduction is slightly larger in case of platelets not treated with thrombin. In contrast, there is no significant change in the number of spread platelets treated with Y-27632 or aspirin.

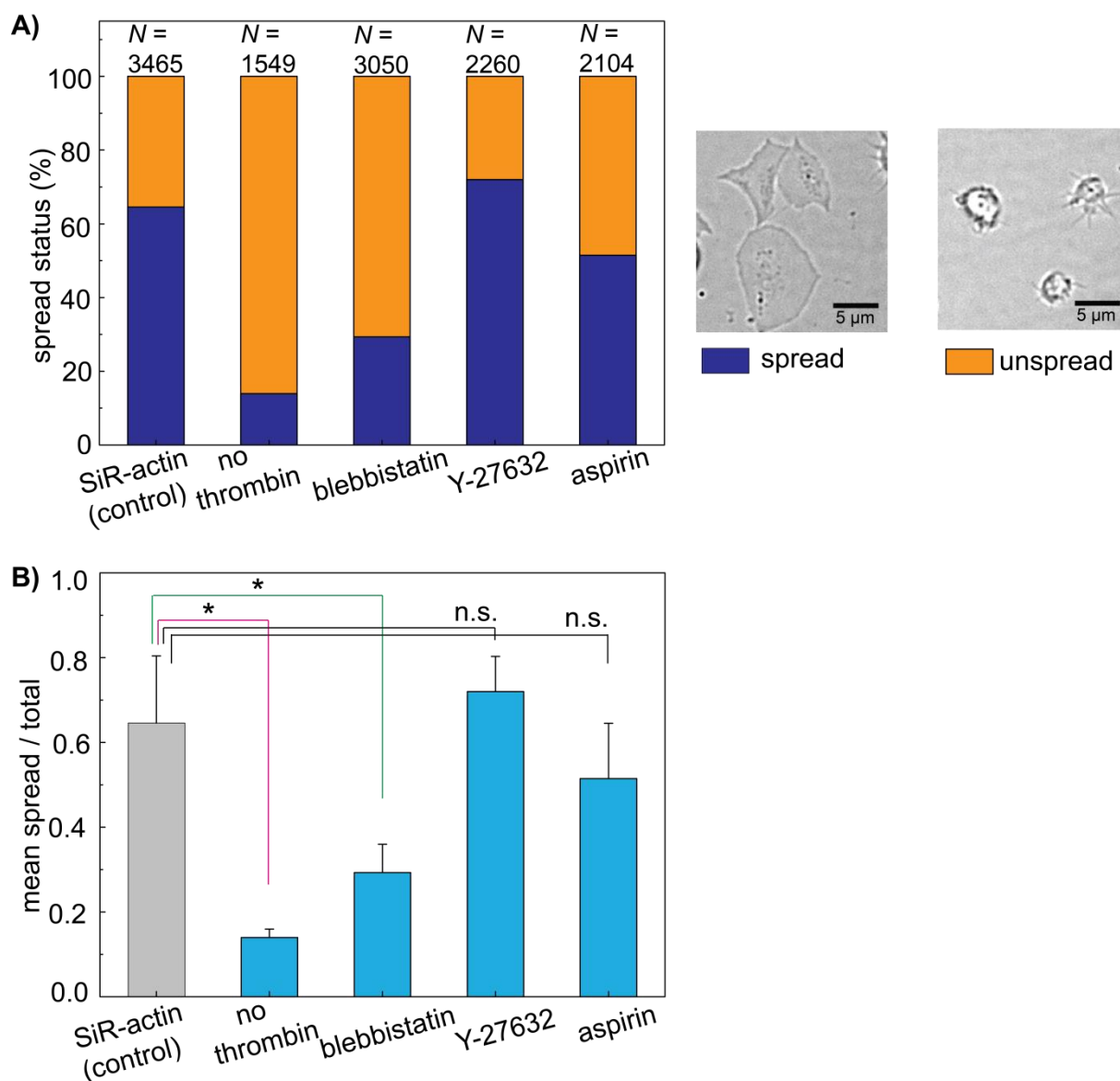


Figure 4.15: Pharmacological agents show effect on relative spread platelet numbers

A) Relative number of spread and unspread platelets and B) the average ratio of spread/ total number of adhered platelets after treatment with different pharmacological agents are shown. The error bars represent SD. As compared to the number of platelets that spread (SiR-actin control) in the presence of the agonist thrombin, significantly less number of platelets spread in its absence. Inhibition of myosin by blebbistatin but not by Y-27632 significantly affects the number of spread platelets in comparison to the control. The platelet aggregation inhibitor aspirin does not have a significant effect on platelet spreading. Data is representative of total platelets counted (indicated by 'N') from at least three independent experiments. The p -value (two sample t-test assuming unequal variance) for SiR-actin control vs. thrombin is $2.94E-05$ and for SiR-actin control vs. blebbistatin is $6.82E-04$.

4.2.5 Discussion of the results

In this chapter we have shown that it is now possible to image the F-actin reorganization of platelets as they spread in real-time. We have also shown that this platelet spreading and reorganization appear to occur on various time-scales. Lastly, we have also shown that commonly pharmacological agents that show effects on other cell types do not seem to affect the temporal F-actin dynamics during platelet spreading. However they do show effects on the relative numbers of spread platelets. In the following sections, each of these results are interpreted and discussed briefly with respect to existing literature, wherever applicable.

4.2.5.1 SiR-actin labeling is a promising tool for real-time imaging

Our real time imaging of SiR-actin labeled platelets show the sequential and simultaneous assembly of the F-actin-rich filopodia, lamellipodia, contractile rings and stress fiber-like structures in the BF and Cy5 channels (see Figure 4.6 and Figure 4.7). Many microscopy visualization studies done on membranes of spreading platelets on glass have described the assembly of first the filopodia and then lamellipodia within the first few minutes of spreading. The observation that, platelets start to spread first by forming filopodia which extend in a web-like manner and then form lamellipodia, in between these filopodia is consistent with previous optical microscopy studies of platelet spreading on glass [7]. The time-scales of the entire spreading process is also consistent with the 10-12 minutes time scale of platelet spreading seen in [7]. Besides that, we have also seen the lamellipodial ruffling activity and the movement of granules towards the center of the platelets, as described before [7, 48]. Real-time platelet spreading on glass has also been imaged by atomic force microscopy (AFM) microscopy. The authors here also show that platelets initially form filopodia and then lamellipodia and eventually flatten out. The authors also report the exocytosis of the granules which are transported towards the cortex as platelets flatten [48]. Our time-lapse BF snapshots also show the filopodia and lamellipodia formation along with the gradual flattening of the granules (Figure 4.6, BF channel). So our observations are in good agreement to the above mentioned studies. The time-scales described for the formation of platelet filopodia and lamellipodia and of the entire spreading process are also consistent with these studies.

As has been already discussed before (see section 4.1.3), numerous immunofluorescence studies on the F-actin cytoskeleton of fixed platelets have shown that platelets indeed form these filopodia, lamellipodia, contractile rings and stress fiber-like structures when spread on

glass [12, 13, 57, 99, 141, 163]. Also real-time imaging of GFP-actin in mouse platelets has shown this sequential formation of filopodia, lamellipodia and stress fiber-like structures [20]. Also the morphologies of fully spread platelets that we see closely resemble those shown in previous studies of thrombin stimulated platelet spreading on fibrinogen-coated glass coverslips [43, 105]. Our time-lapse snapshots particularly show that the F-actin-rich contractile ring is associated with the granulome and moves into the center with the movement of the granulome and disappears as the granulomes flatten (Figure 4.2 and Figure 4.6). Taking into consideration our post-fixation stainings, we have also seen that this contractile ring also has myosin along with the actin (Figure 4.4 and Figure 4.5). These observations validate the involvement of the contractile ring in the granule movement and the important degranulation event occurring in the platelets. Additionally, SEM images of platelets activated² in presence of agonists reveal the reorganization of the actin cytoskeleton by the platelets. Platelets activated² for 30 minutes and then fixed show actin filaments arranged in parallel bundles which resemble stress fibers. At time the actin filaments are also arranged in concentric masses in the cytoplasm of spread platelets or also arranged randomly in the cytoplasm [163]. Such arrangements of F-actin are also seen to be formed when SiR-actin labeled platelets spread (Figure 4.6 and Figure 4.7, Cy5 channel).

The Arp2/3 complex is one of the major regulators of actin polymerization in platelets and is responsible for formation of platelet filopodia and lamellipodia during platelet shape change [58, 82]. The authors in [82] have shown that both the Arp2/3 complex and F-actin are localized at the tips of filopodia and the edges of lamellipodia (also referred to as 'cortex') in fixed, spread platelets on glass. This would also explain our observations of a rapid spreading of platelets via their filopodia and lamellipodia.

Thus, taken together, our real-time imaging of SiR-actin labeled platelets show the formation and reorganization of these distinct filopodia, lamellipodia and stress-fiber like F-actin rich structures visualization of F-actin-rich filopodia, lamellipodia, contractile rings and stress-fiber like structure and support all the above described observations in post-fixation studies and at the same time provide the advantage of *in situ* observation of all these structures.

Each of the F-actin rich structures are thought to play important roles in the platelet function of stopping bleeding by formation of blood clots. Filopodia and lamellipodia are involved in platelet shape change. Apart from that lamellipodia spread to quickly cover open wound surfaces and filopodia recruit other platelets at the site of injury. The contractile ring is involved in platelet degranulation which is necessary for signaling the recruitment of more platelets and which eventually leads to assembly of platelet aggregates [13]. This actomyosin

²activation refers to morphological changes occurring in platelets exposed to glass/ foreign surfaces/agonists in suspension

contractile ring may also be responsible for exerting the platelet contractile forces [83, 132]. The stress-like fibers aid in contraction of the platelet aggregates eventually leading to clot retraction [12, 163]

The SiR-actin probe appears well suited to visualize all this F-actin rearrangement and reorganization in platelets. Our characterization tests have shown that the SiR-actin probe has no deleterious effect on the platelet spreading or F-actin reorganization (Figure 4.6, Figure 4.7, Figure 4.8, Figure 4.9 and Figure 4.10). The parameters used for the concentration (6 μM) and labeling time (30 minutes) and the unnecessary of washing away the excess probe are all in good agreement to those used for imaging the F-actin in human red blood cells in [86].

For all these reasons, this approach of labeling the anucleate human platelets with SiR-actin probe, to visualize the F-actin is a promising new tool to explore the complex and fascinating F-actin cytoskeletal choreography that occurs in platelets. This may help to further understand the role of the actin cytoskeleton in platelet function better.

4.2.5.2 The existence of multiple time-scales of F-actin reorganization

Our time-lapse imaging of SiR-actin labeled platelet spreading has already given us the visual perception that platelets spread rapidly once they contact the glass surface but that their F-actin gets reorganized for long (Figure 4.6). This visual perception is indeed confirmed when the platelet spread areas and their corresponding normalized F-actin intensities are quantified (Figure 4.11). The platelets do spread very fast-on the order of ~ 2 minutes but their F-actin intensities go on increasing until ~ 90 minutes. These F-actin intensity profiles are similar to the ones described before (see section 4.2.2.1) and indicate that increases in the intensities result from increase in F-actin polymerization and assembly into higher order structures which are also seen in the time-lapse snapshots (Figure 4.6). One of the possible reasons of the ability of platelets to spread so fast could be due to the structure of their OCS. The OCS of platelets has invaginations in which extra membrane is folded in. During spreading, this extra membrane rapidly extrudes out of these folds [164, 166] thus helping in achieving larger spread areas fast.

Furthermore, when we look at our plot of smoothed total line lengths of SiR-actin platelets and also carefully look at both the BF and Cy5 time-lapse movies and snapshots of these (Figure 4.12), it appears that the platelets first build up a basic, stable F-actin structural framework within the first few minutes when they spread by extending their lamellipodia, as reflected by the sharp increase in the total line lengths. After completing their spreading, this

F-actin 'framework' then remains more or less unchanged but new, smaller F-actin structures are reorganized within this 'framework' and gradually fill up entire area of the platelet to form a dense network. On an average we see that the platelets build up the majority of their F-actin filament network on the order of ~ 9 minutes. In some of these total line length plots we also see some oscillations which may correlate with a wave-like phase we see in the time-lapse movies. It is possible that this phenomenon can arise from dynamic F-actin processes occurring in the platelets. However, to elucidate the exact nature of this phenomenon warrants further research.

Overall, our findings point towards the existence of multiple time-scales of F-actin reorganization where the F-actin first assembles to form filopodia and lamellipodia enabling the platelets to spread within minutes and then assembles into higher order F-actin stress-fiber like structures enabling the platelets to reorganize the actin cytoskeleton. The authors in [30] have observed by fixed immunofluorescence stainings that, in platelets allowed to spread on glass for 20 minutes, the F-actin is cortically distributed as well as some actin aggregates are present in the platelet centers. This supports our observations where we indeed see completely spread SiR-actin labeled platelets showing F-actin rich lamellipodia within the first 20-25 minutes after adhesion, but still see a F-actin rich aggregate in the center that gradually disappears simultaneously with the formation of stress-fiber like structures (Figure 4.6).

This multi-step reorganization of the cytoskeleton seems relevant in physiological conditions where at an open site of injury the platelets must first rapidly spread via their filopodia and lamellipodia to cover the open wound surfaces and then later on form the stress fiber-like structures which will contribute to compact the blood clot by reinforcing the entire structure. Indeed, it has been shown previously that stress fiber formation is important for maintaining the integrity of platelets aggregates under flow [19].

4.2.5.3 The effects of the pharmacological agents in real-time

There are numerous studies on fixed human platelets or *in vivo* mouse models that have looked at the effects of the pharmacological agents we have used on platelet spreading and F-actin reorganization. However, the temporal evolution of these effects on the platelet F-actin dynamics has been looked at by us, for the first time, to our knowledge. In general we see that these agents have no effect on the spreading of platelets. However, the numbers of spreading platelets are certainly affected (Figure 4.13, Figure 4.14 and Figure 4.15).

To interpret all these observations, we look back into the previous studies done on the effects of these pharmacological agents on platelets. Thrombin is one of the most known potent agonists of platelet activation and activates human platelets via the GPCRs- PAR1 and PAR4 [15]. GPCRs induce integrin activation as well as promote integrin outside-in signaling which mediates cytoskeletal reorganization in platelets. Presence of thrombin thus causes the remodeling of actin in platelets via the small GTPases Cdc42, Rac1 and RhoA which respectively form the filopodia, lamellipodia and stress-fibers [11, 49, 59, 77, 81]. Moreover, platelet adhesion to immobilized fibrinogen alone results in outside-in signaling that eventually leads to spreading via actin polymerization [81, 116]. Thus by presence of both thrombin and fibrinogen, the platelet spreading is exceedingly enhanced [81]. If thrombin is absent, this would greatly reduce the ability of platelets to spread. However, presence of fibrinogen would still induce platelet spreading but not as great as together in the presence of thrombin. Our findings indeed support these views where we see less spread platelets in absence of thrombin but those that spread go on to form the stress fiber like structures (Figure 4.13B and Figure 4.14B). It has also been demonstrated that without the stimulation of PAR4, murine platelet adherence and spreading on fibrinogen is mainly filopodial [76] which could explain why we see platelets with many filopodia in absence of thrombin (Figure 4.13B and Figure 4.15). Additionally, we do not see the actin nodules that have been recently elucidated [20, 114]. Possible reasons for this could be that actin nodules form only in the initial platelet spreading stages and disappear following stress fiber formation [20]. Also their turnover rates are very fast (between 10 – 40 seconds), and it may be possible that we simply cannot resolve them with our current time-lapse frame rates [114].

Individual non-muscle myosins form bipolar filaments when MLC is phosphorylated. These filaments then bind to actin and generate forces through myosin's ATPase motor activity. Myosin phosphorylation induces platelet shape change and it occurs via two pathways- the calcium dependent Ca^{2+} /calmodulin that activates the MLCK and phosphorylates the MRLC. The second ROCK pathway is calcium independent in which the small GTPase RhoA binds to ROCK and causes MLC phosphorylation by phosphorylating and inhibiting MLC phosphatase (Figure 4.16).

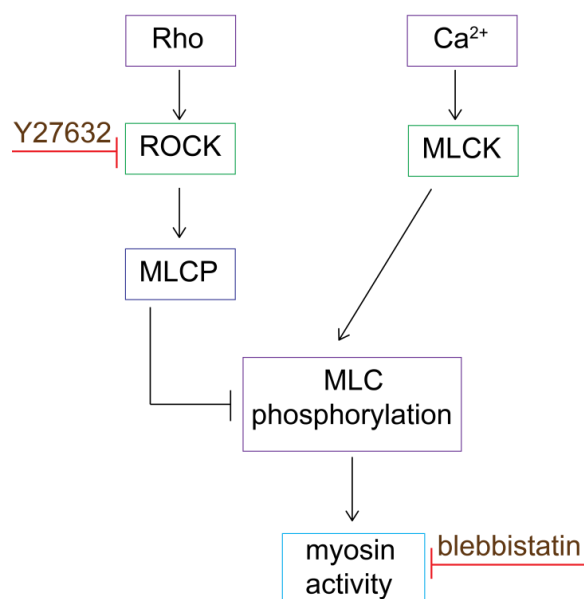


Figure 4.16: Schematic of MLC phosphorylation pathways

Myosin activity occurs by the phosphorylation of the myosin light chain (MLC). This is brought about by the biochemical regulators calcium dependent myosin light chain kinase (MLCK) and calcium independent Rho-kinase (ROCK). RhoA binds to ROCK and causes MLC phosphorylation by phosphorylating and inhibiting MLC phosphatase. Y-27632 inhibits ROCK whereas blebbistatin inhibits the ATPase activity of myosin.

Most of the platelet agonists can activate both these MLC phosphorylation pathways. Myosin II activity is also required for assembly of actin and this requires a functional MRLC kinase but does not require the myosin ATPase activity [68, 94]. Blebbistatin is known to inhibit the ATPase activity of myosin without inhibiting the MRLC kinase [144] so the formation of myosin bipolar filaments or the actin assembly is not affected. This is consistent with some recent studies where they have demonstrated that at lower concentrations of blebbistatin (10 μM) there is minimal inhibition of platelet shape change (the extension of filopodia and lamellipodia) as the actin assembly is not affected. However at higher blebbistatin concentrations (25-100 μM) the platelet shape change is inhibited in a concentration-dependent manner [68]. The authors have shown that this is due to the inhibition of Rho activation by higher concentrations of blebbistatin which affects the MRLC phosphorylation thus inhibiting platelet shape change. Our experiments reflect these observations. We use a blebbistatin concentration of 20 μM which is intermediate between those used by the authors in [68] and which may explain why there are still some platelets that change their shape and spread (Figure 4.13C and Figure 4.14C) although the overall number of spread platelets is less than that in the control (Figure 4.15) indicating that myosin II is necessary for platelet spreading.

Our results with the ROCK inhibitor Y-27632 are consistent with previous observations that inhibition of ROCK does not affect platelet spreading on fibrinogen [77]. However the authors in [19] have shown that ROCK plays a critical role in assembly of stress fibers in platelets spreading on collagen which are important for maintaining thrombus integrity. Nucleated mammalian cells are known to balance a pro-lamellipodial (mediated via Rac1) or a pro-stress fiber (mediated via Rho) state and the upregulation of one of the GTPases results in the downregulation of the other and vice versa [55]. When ROCK is inhibited, Rho is downregulated which shifts the equilibrium to a pro-lamellipodial state. This could explain our observations of a higher localization of F-actin at the platelet edges in the presence of Y-27632 and a lack of formation of proper stress fiber-like structures (Figure 4.13D). The authors in [124] have shown that platelet spreading is not affected in presence of Y-27632 which is also consistent with our observations (Figure 4.15). Overall, our results indirectly demonstrate that the MLCK pathway may play a more critical role in platelet spreading. A recent study which has shown that stiffness-mediated platelet spreading on fibrinogen is dependent on myosin activity regulated by the MLCK pathway [116] supports our speculation.

The adhesion of platelets on immobilized fibrinogen results in their activation and can cause release of secondary agonists such as thromboxane A₂ [116]. The formation of thromboxane A₂ can be blocked by aspirin as it irreversibly binds with platelet cyclooxygenase thus inhibiting the conversion of arachidonic acid to thromboxane A₂. This reaction further blocks the secretion of agents that promote platelet aggregation, a phenomenon which is well known. In a recent study done on platelet mechanosensing, the authors in [116] showed that the spreading of platelets is not mediated by the endogenous secretion of thromboxane A₂. Our studies too show that platelet spreading is not affected in presence of aspirin (Figure 4.13E, Figure 4.14E and Figure 4.15) and support the observations reported by these authors.

Taken together, our observations validate the previously reported literature studies of the effects of these pharmacological agents on platelet spreading. With our approach, it is now possible to further vary the concentrations of these pharmacological agents or even combine two or more agents and observe their effects on the F-actin dynamics of platelets as they spread. This approach may prove useful to further elucidate the role of individual cytoskeletal components in platelets.

4.3 Real-time MT dynamics

The real-time visualization and quantification of the F-actin dynamics in platelets using the SiR-actin probe has been introduced in the previous chapter. The MT dynamics in platelets can also be visualized in real-time using the SiR-tubulin probe. This probe specifically binds only to MTs and after binding increases its fluorescence intensity by 10-fold [86]. So the platelets are again labeled with this probe and their MT dynamics are visualized as they spread on fibrinogen-coated glass coverslips (see section 3.5.2) and further they are also treated with pharmacological agents (see sections 3.3.2 and 3.4) to elucidate the role of MTs in platelet spreading. The platelet spreading is triggered by addition of the soluble agonist thrombin. The concentration and labeling parameters for the SiR-tubulin probe are the same as that used for the SiR-actin probe and also in these experiments the excess probe is not washed off. In this chapter, the results of these SiR-tubulin platelet labeling experiments are shown, followed by a short discussion of the results with respect to the existing literature.

4.3.1 Imaging of MT over time

The platelets are labeled with SiR-tubulin, allowed to spread on fibrinogen-coated coverslips and visualized for their MTs in the Cy5 channel and their plasma membrane in the BF channel (as described in section 3.5.2). The time-lapse spreading snapshots of two typical SiR-tubulin labeled platelets imaged in both BF and Cy5 channels are shown in Figure 4.17.

The time-lapse snapshots in the BF channel show the earlier described features- formation of filopodia and lamellipodia, movement of the granules in the center and their gradual flattening (BF channels in Figure 4.17A and B). The platelets again are seen to spread within ~ 10 minutes after initial contact with the fibrinogen-coated coverslips.

The time-lapse snapshots in the corresponding Cy5 channels in the initial stages of platelet spreading show bright spots in the middle which corresponds to the granule of the platelets. These 'bright spots' appear as 'MT ring-like' structures which is more evident in case of unspread platelets (Figure 4.18). These 'MT ring-like' structures follow the granules towards the platelet centers as the platelets start to spread and extend filopodia and some lamellipodia. As the platelets spread completely two scenarios are observed. A commonly observed scenario is shown in Figure 4.17A. As the granules start to flatten out these round, 'MT ring-like' structures also seem to disintegrate and individual MTs appear to move outwards to the periphery of the platelets and span the entire lamellipodial membrane of the

platelet (Figure 4.17B). The platelets have almost stopped spreading at this point and only show some membrane ruffling (Figure 4.17A BF channel). After moving towards the periphery, almost immediately the individual MTs rapidly start to move back to the center of the platelets and form elongated spindle-shaped MT structures which are most obvious in this example at the last time point (Figure 4.17A Cy5 channel). In a second scenario (Figure 4.17), which is seen rarely, these round 'MT ring-like' structures do not disintegrate completely but simply elongate as they move towards the center of platelets while simultaneously showing individual MTs moving to the periphery of the already spread platelets (Figure 4.17A and B).

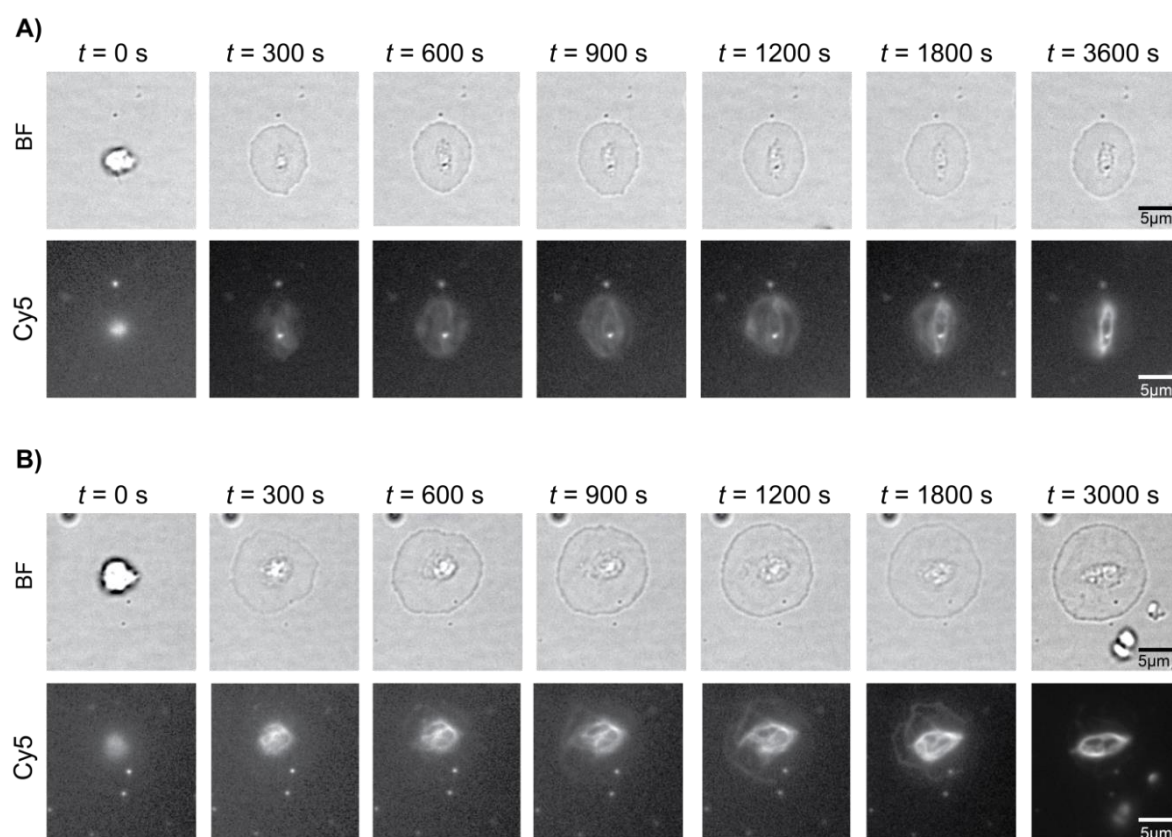


Figure 4.17: Real-time imaging of SiR-tubulin labeled platelet spreading

Time-lapse spreading snapshots of a two exemplary SiR-tubulin labeled platelets (A and B), imaged in the BF and Cy5 channels are shown. As the platelets spread and the granules start to flatten out (BF), the round MT ring (Cy5) A) either disintegrates completely and individual MTs move outwards to the periphery of the platelet and start to reassemble in a spindle-shape in the central region or (B) disintegrates partially and elongates as it moves to the center with individual MTs moving to the periphery simultaneously. The MT structures in the center follow the granules.

A particularly noticeable feature is that in the case of unspread or incompletely spread platelets (Figure 4.18) the granules do not flatten out as observed in completely spread platelets. Such platelets extend only some filopodia and lamellipodia (Figure 4.18 BF channel magenta and blue arrows). In these platelets, the round 'MT ring-like' structures do not disintegrate but instead remain intact (Figure 4.18 Cy5 channel). The fully spread platelets show polygonal morphologies and it is evident that the MTs are associated with the granule areas and follow them closely.

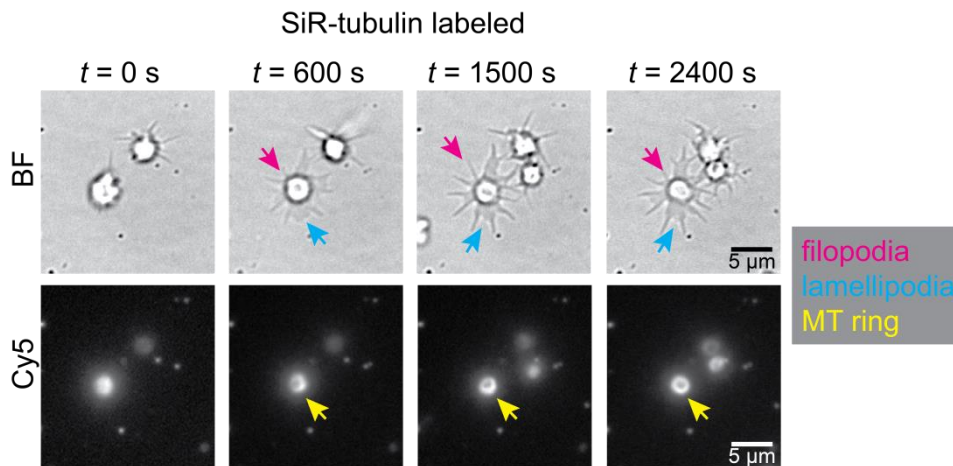


Figure 4.18: Incompletely spread and unspread platelets show intact MT rings

Time-lapse spreading snapshots of a incompletely spread and unspread SiR-tubulin labeled platelets are shown. Incompletely spread platelets extend few filopodia (magenta arrows) and lamellipodia (cyan arrows) and show intact, round MT rings in the center (yellow arrows) that correlate with the granules seen in the BF channel. Unspread platelets too show these intact, round MT rings.

4.3.2 The role of MTs and myosin in complete platelet spreading

The above results have demonstrated that it is possible to visualize and analyze the MT reorganization in platelets in real-time. So using the advantage of this, the role of myosin II and MTs during prolonged platelet spreading is further investigated by using the pharmacological agents, blebbistatin and nocodazole which inhibit myosin and depolymerize MTs respectively. The SiR-tubulin labeled platelets are treated with blebbistatin or with nocodazole or with a combination of both blebbistatin and nocodazole and the time-lapse movies are taken. After that the relative spread platelet numbers for each of these conditions are quantified as described before (see section 3.11) and compared with that of the control conditions (only SiR-tubulin labeled platelets- positive control). The relative spread platelet numbers of unlabeled, untreated and unlabeled but only DMSO (vehicle) containing platelets are also quantified as negative controls (Figure 4.19).

As seen from the BF snapshots, the platelets having only DMSO or the SiR-tubulin probe spread normally like the unlabeled, untreated platelets and show no significant difference in the relative numbers of spread platelets. The platelets treated with 5 μM nocodazole show a diffused staining of the MTs indicating MT fragmentation but still spread normally and also show no significant difference in the number of spread platelets as compared to the SiR-tubulin labeled platelets (Figure 4.19A, B and C). To ensure a complete inactivation of myosin II, a higher concentration (50 μM) of blebbistatin is used. As seen earlier (Figure 4.13 and Figure 4.15C), in presence of blebbistatin there are significantly fewer spread platelets and these numbers are even lower than those in the presence of a lower concentration of blebbistatin (Figure 4.19A, B and C). The blebbistatin-treated unspread platelets show intact, round MT rings in the Cy5 snapshots (indicated in Figure 4.19A by yellow arrows). Also, when a combination of blebbistatin and nocodazole is used, there is again significantly less number of spread platelets. The unspread platelets, too, show the intact and round MT rings which is intriguing as one would expect that presence of nocodazole would result in a diffused staining as it would depolymerize the MTs.

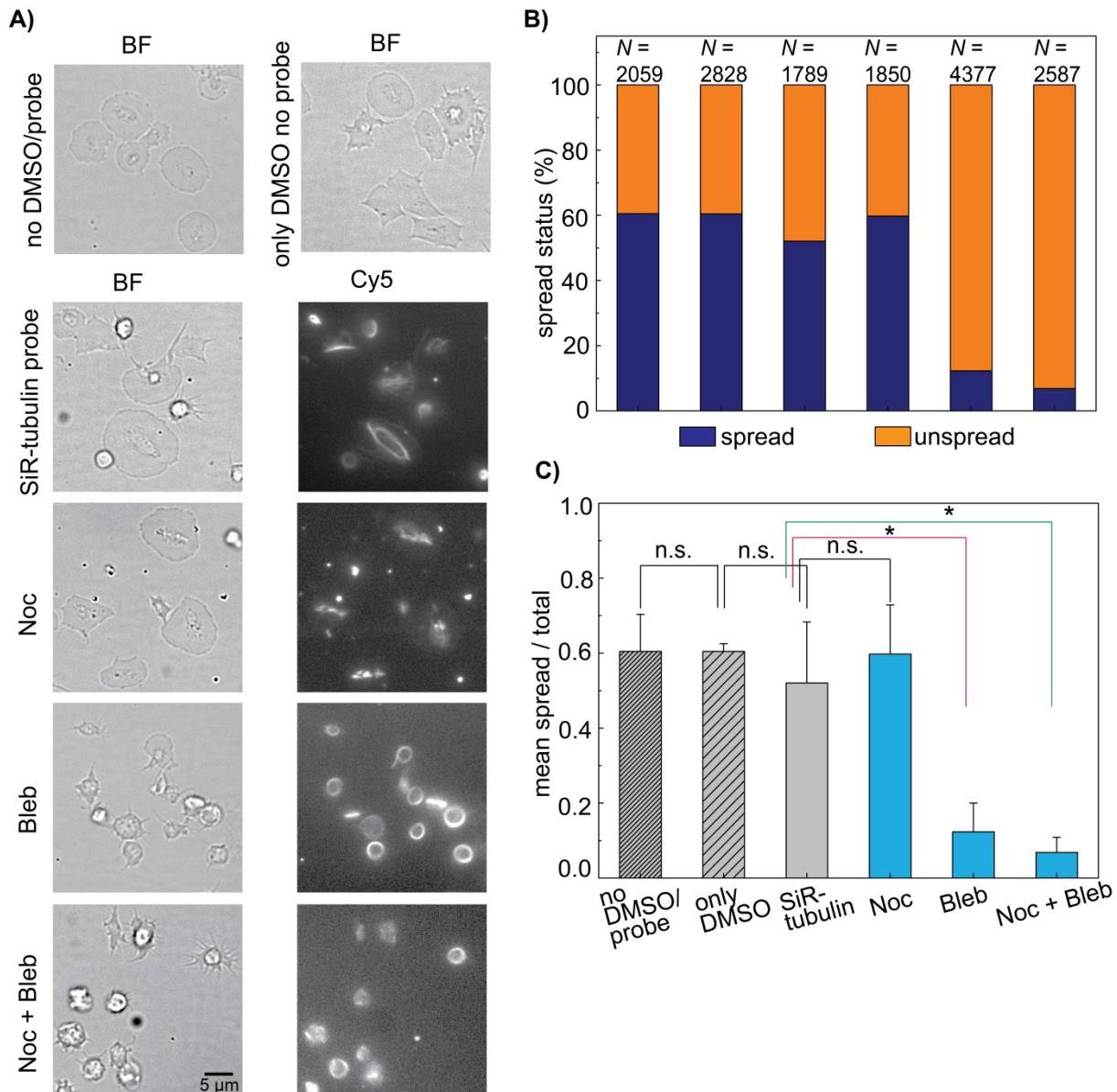


Figure 4.19: MT ring disintegration is essential for full platelet spreading and needs myosin

A) BF (top) and Cy5 snapshots of platelets that spread in the presence or absence of the pharmacological agents nocodazole and blebbistatin are shown. Platelets in Cy5 snapshots are labeled with the SiR-tubulin probe. The untreated, DMSO (vehicle) treated and SiR-tubulin treated platelets spread normally. The platelets show a diffused and fragmented MT labeling when treated with the MT depolymerizing agent nocodazole but they also spread normally. There is a difference in the spreading in presence of blebbistatin or a combination of blebbistatin and nocodazole. Most platelets do not spread which is seen by their intact MT rings. B and C) Relative number of spread platelets for the conditions shown in A) verify the observations seen in these snapshots. The disintegration of both the MTs and myosin inhibits platelet spreading highlighting the importance of MT ring disintegration an intact myosin function for complete platelet spreading. Data is representative of total platelets counted (indicated by 'N') from at least three independent experiments. The *p*-values (two sample *t*-test assuming unequal variance) for SiR-tubulin control vs. blebbistatin and for SiR-actin control vs. blebbistatin are 0.036.

4.3.3 Discussion of results

As discussed before in section 2.6.4, the MBs i.e. MT coils/rings in discoid platelets, depending on the strength of the activation stimulus, either form flat MT rings or smaller MT rings during transient or irreversible platelet activation. The platelets used in our experiments are stored for several days and there is a possibility that these platelets are either transiently or irreversibly activated² in suspension in the platelet concentrate bags [90], prior to our spreading experiments, and may have already formed the flat MT rings or the smaller MT rings. Hence, it is most likely that we see a mixture of such platelet MT rings in the platelet population. When these platelets start to spread, it is very likely that some of these MT rings undergo the coiling and compression stages as described previously [36]. However, these changes occur quickly and depend on the strength of the activation impetus [122]. In our case, we use a high concentration of the agonist thrombin, and hence it is likely that we cannot elucidate these early steps in the platelet activation. Nevertheless, we are interested in the MT dynamics during prolonged spreading and we observe that the MT rings disintegrate either partially or completely during platelet spreading, with individual MTs moving towards the periphery of platelets.

Electron microscopy studies done on platelets adhered and spread on glass for 30 minutes have observed that the MTs constrict and form rings in the platelet center that surrounds the granules. Such MT rings are also formed after treating the platelets with MT stabilizing agent taxol or after their exposure to cold temperatures during which MTs are known to disassemble [165, 167]. In one study, it is observed that in platelets that spread, the MTs after constricting in the center, appear to radiate from the platelet center towards the margin and then again move back towards the platelet centers [70, 165]. All of these studies have evaluated the platelet activation, shape change and secretion by aggregation studies using an aggregometer and have seen no changes in the responses of untreated and taxol or cold temperature treated platelets. This has led to the speculation that MTs have no apparent role in platelet functions. It is important to note that these studies have supported the single MT model in platelets where one long MT is thought to form the circumferential MB band by winding around several times, in discoid platelets. However, recent insights into the platelet MT cytoskeleton have revealed that the MB of platelets is in fact a bipolar array, comprising of both stable and dynamic MTs [108]. This discovery sheds a new light on the speculations of the electron microscopy data. It is implied that the use of strong fixatives during these studies may result in the loss of dynamic MTs [108]. Furthermore, due to the PTMs occurring

²activation refers to morphological changes occurring in platelets exposed to glass/ foreign surfaces/agonists in suspension

in MTs, there is a population of both detyrosinated/acetylated/stable and tyrosinated/deacetylated/dynamic MTs in the MB [122]. It has been shown that detyrosination levels (see section 2.4.2) of MTs increase in the presence of taxol [170]. This means that the stable MT of the MB will be further stabilized in the presence of taxol. The electron microscopy studies probably see these persistently stable MT rings in the center of activated² platelets. However, the question still remains why then the platelet shape change and aggregation responses are not affected in these electron microscopy studies. One possible explanation could be that the platelet shape change, meaning the transition to the spherical shape, and the extension of filopodia (which are needed for aggregation) are brought about by the tyrosinated/deacetylated/dynamic MTs in the bipolar MB array. It has indeed been shown that during platelet activation, tubulin is deacetylated within minutes [123]. Taking into consideration all of these recent pioneering studies [36, 108, 122, 123], in the context of the electron microscopy studies, a possible explanation is that the detyrosinated/acetylated/stable MTs in the platelet MB detach from the actomyosin cortex during platelet activation, coil and constrict into the center due to the contractile actions of the cortex and hence change to the spherical shape. At the same time, the tyrosinated/deacetylated/dynamic MTs of this MB, slide away from the MB and make space for filopodia extension which may allow further aggregation. If this explanation is correct, the observations from our experiments support it. We too see intact MT rings in the center of incompletely spread or unspread platelets (Figure 4.18). These could probably be the detyrosinated/acetylated/stable MT rings. In incompletely spread platelets, it is possible that the tyrosinated/deacetylated/dynamic MTs form the few filopodia and lamellipodia that are seen. In completely spread platelets (Figure 4.17A), where the central, round MT rings are not seen anymore, it is possible that the detyrosinated/acetylated/stable MTs break down completely as platelets spread and release their granules. Indeed, it has been demonstrated that after 5 minutes of platelet spreading on glass, there is a decrease of acetylated tubulin (i.e. stable MTs) and tubulin acetylation disappears completely after 30 - 60 minutes, when platelets reach maximal spreading [123]. Furthermore, we see that individual MTs move towards the periphery of platelets during platelet spreading. A possible explanation of these observations may come from one of the recent immunofluorescence studies on platelets, adhered, spread on glass for 20 minutes and fixed. In this study, it has been observed that β -dystroglycan, an actin and tubulin binding protein, stabilizes the MTs at the plasma membrane of spread platelets and modulates FA assembly during the platelet adhesion process. It is suggested that at the leading edge of the

²activation refers to morphological changes occurring in platelets exposed to glass/ foreign surfaces/agonists in suspension

lamellipodia, the MTs interact with F-actin filaments to form and the leading edge pushes against this MT-F-actin meshwork [28].

Our results also show that the MTs always encircle the granules implying that they are involved in granule trafficking in platelets in some manner. Immunofluorescence studies on adhered, spread and fixed platelets have shown that granular trafficking is strongly regulated by F-actin filaments and MTs during the adhesion process of platelets. It begins with centralization of the granules in the granulomere by F-actin contractile rings and the MTs then further reorganize from the granulomere to traffic the granules to the plasma membrane of platelets [27, 28]. Our time-lapse snapshots of SiR-tubulin platelets show this movement of the individual MTs towards the platelet membranes and these MTs appear to follow the granules (Figure 4.17). Furthermore, our earlier observations have already shown the existence of F-actin contractile rings (Figure 4.6 and Figure 4.7) associated with the granules. This further implies that the F-actin contractile rings are also composed of MTs, which are most likely the stable MTs. The disintegration of the MT rings as the granules flatten may indicate their role in granule release via the OCS to the platelet membrane. Additionally, the observations of individual MTs at the periphery, moving back to the center, and reassembling again (Figure 4.17) may indicate a second process of granule centralization which may point to multiple exocytosis events taking place during platelet spreading. This is however just a speculation.

Our time-lapse snapshots of incompletely spread or unspread platelets show the intact and round MT rings (Figure 4.18). Similarly the time-lapse snapshots of blebbistatin treated platelets also show intact MT rings (Figure 4.19A). This may indicate that for the platelets to initiate complete spreading and possibly also to perform exocytosis, the stable MT ring has to be somehow broken down/disintegrated. Also the action of myosin seems to play a major role in this process (Figure 4.19). This seems to be the case because, in the case of untreated platelets, the myosin II function is intact and these platelets start to spread and the MT rings are disintegrated perhaps together by the concerted action of actin and myosin which enables the platelets to spread completely, as discussed above. In nocodazole-treated platelets, the MTs are already fragmented and in concerted action with the intact myosin can disintegrate the MT ring further to allow platelets to spread completely. A recent study has indeed shown that platelet spreading is not affected in presence of nocodazole [124]. As myosin II is inhibited by blebbistatin, it is not available to disintegrate the MT rings and although few platelets show some filopodia and occasionally lamellipodia, they do not spread completely. In the case of both nocodazole and blebbistatin-treated platelets too, the myosin function is

absent and hence MT rings are seen. The fact that we see intact and round MT rings even in the presence of nocodazole could be because blebbistatin is known to stabilize MTs [146]. Myosin II plays a role when the actomyosin contraction is required for the compression of the coiled MBs during platelet activation [36].

Taken together, and based on recent studies [36, 108, 122, 123], we suggest from our data that full platelet spreading, along with granule release occurs, only when the stable MT rings that are part of the bipolar MB array of platelets, are broken. Incomplete platelet spreading which shows filopodial and lamellipodial extension may be an effect of the sliding of the dynamic MTs that are part of the bipolar MB array of platelets. Furthermore, the MTs appear to play a role in exocytosis of granules during platelet spreading. Since the exocytosis process occurs during spreading and also after completion of spreading [13], the granulomeres have to degranulate which basically occurs when they flatten out. For this degranulation process to take place it seems from our results that the stable MT ring has to somehow be broken down and in this process, the myosin II plays a major role.

5. Summary & Conclusions

Anucleate, human blood platelets play an important role in haemostasis to prevent excessive blood loss from a vascular damage. Their actin and MT cytoskeleton is especially responsible for bringing about dramatic morphological and biochemical changes in them, which enables the platelets to change their shape, secrete granular contents, aggregate, adhere, spread, and retract in a platelet haemostatic plug, to seal the vascular breach. The platelets are thus extremely important cells from a medical point of view and the study of their cytoskeletal changes is essential. Because platelets do not have a nucleus, they cannot be transfected, microinjected or manipulated in any way. This has restricted the study of their cytoskeleton with classic post chemical fixation approaches. However, with the introduction of the novel cytoskeletal probes, the SiR-actin and SiR-tubulin, it is now possible to monitor the actin and MT cytoskeleton in real-time, in cells, which are otherwise difficult to transfect [86]. These probes specifically bind to F-actin and MTs and increase their fluorescence intensity after binding. In this dissertation, we image the F-actin and MTs of platelets while they remodel during their spreading, in a time-resolved manner, by labeling them with the novel, fluorogenic, SiR-actin and SiR-tubulin probes. Furthermore, we treat these labeled platelets with pharmacological agents and image the real-time dynamics of F-actin and MT cytoskeleton in their presence, during platelet spreading.

Using the SiR-actin probe, we demonstrate the ability to directly visualize the different F-actin rich filopodia, lamellipodia, contractile ring and stress fiber-like structures that the platelets sequentially form as they spread. As the platelets form these higher order F-actin structures, the binding of the SiR-actin probe also increases, which is reflected by the increase of fluorescence intensities, which we quantify. The averaged actin intensity of single platelets over time reveals an initial step rise followed by a linear increase that gradually reaches a plateau indicating the formation and increase in the content of polymerized actin until the platelets spread completely. Next, we characterize the parameters for the SiR-actin probe and demonstrate that platelets labeled for 30 minutes, with a 6 μM concentration of SiR-actin and not washed for removal of the excess probe, spread normally. We further quantify the platelet spread areas and determine the temporal growth of their F-actin filaments using the Filament Sensor program [1], and observe that the F-actin dynamics in platelets during their spreading occurs on multiple time-scales. Upon adherence, the platelets first spread rapidly within ~ 2

minutes, build their F-actin network within ~ 9 minutes, which later reorganizes into F-actin stress fiber-like structures for hours. Additionally, we observe that the temporal spreading dynamics of platelets is not majorly affected in the presence of the myosin inhibitors, Y-27632 and blebbistatin or in the presence of the aggregation inhibitor, aspirin or in the absence of the soluble agonist, thrombin. However, these pharmacological agents show significant effects on the relative numbers of spread platelets. Furthermore, our observations indirectly demonstrate the critical role of the MLCK pathway in platelet spreading.

Using the SiR-tubulin probe, we demonstrate the ability to directly visualize the MT dynamics of platelets as they spread. Our data suggest that the stable and dynamic MTs, contained in the circumferential, bipolar MB of platelets that give them their discoid shape, could both be involved in platelet spreading. To spread completely, the platelets must break their stable MT rings and by using blebbistatin, we observe that this process requires the action of myosin II. During spreading, it is likely that the dynamic MTs slide and move towards the periphery of the platelets and reassemble again. In incompletely spread or unspread platelets, the stable MT rings are not broken down but the dynamic MTs may slide and disassemble to allow formation of some filopodia and lamellipodia. Furthermore, the MTs in platelets appear to be involved in platelet granule exocytosis and their reassembly into the platelet centers may possibly suggest the existence of multiple exocytosis events.

The SiR-actin and SiR-tubulin probes with their excellent properties of near-infrared excitation and emission, minimal cytotoxicity, photostability and high cell permeability are well suited for the purpose of our experiments. The general impression of platelets is that they are fast cells which spread very rapidly and finish their dynamics within some minutes. However, by allowing platelets to spread for a long time, we have learned that the platelet cytoskeletal dynamics occurs for hours. Together, our data indicate that the F-actin and MTs participate in the platelet shape change, adhesion, spreading and secretion and regulate these processes via their dynamic remodeling. The F-actin cytoskeleton polymerizes to form the F-actin rich filopodia and lamellipodia enabling platelet adhesion, shape change and extensive spreading. The actomyosin contractile ring together with the MTs constricts in the central region of platelets and moves the granules in the center, and the platelets continue to mature their adhesion process for long by reorganizing their F-actin to form stress fiber-like structures and bringing about dynamic ordering in their MTs. Our real-time F-actin and MT dynamics are in good agreement to the studies of the cytoskeleton in fixed platelets and indicate that both the F-actin and MT dynamics are related to each other.

Our results may reflect the dynamics that may occur *in vivo*. The multi-step remodeling of the F-actin cytoskeleton may be especially important at an open bleeding wound, where it is essential to first adhere and spread rapidly to quickly cover the open holes and then later form higher-order stress fiber-like structures, to reinforce and compact the clot. The existence of multiple exocytosis events may be favorable in a growing thrombus where the secretion of activating molecules from the granules is necessary to recruit many more platelets into the thrombus.

Taken together, our findings show a novel way to observe the *in situ* formation and reorganization of the F-actin and MT cytoskeleton of human platelets, which has hitherto been impossible, due to their lack of a nucleus. We can monitor platelet F-actin and MT dynamics in real-time and our relatively simple experimental setup provides an easy way to do this. The actin and MT cytoskeleton of human platelets is impaired during many platelet-related disorders such as Glanzmann thrombasthenia, Bernard–Soulier syndrome, myosin-heavy chain 9 (MYH9)-related disorders, congenital macrothrombocytopenia [140]. Now that we have the technique to directly visualize the cytoskeletal changes in real-time, it is desirable to use this to compare normal human platelets with platelets from patients with such disorders. This approach can provide innovative insights into platelet function and perhaps may lead to the development of novel agents that may help to alleviate these disorders. Platelets *in vivo* encounter a variety of stiffnesses in the physiological range (1-100 kPa) and also encounter structured wound surfaces [125]. Our technique to directly visualize the F-actin and MT cytoskeletal changes in real-time can help in elucidating the spreading dynamics on such surfaces. Overall using this technique will improve our understanding of the role of the platelet cytoskeleton in aiding the platelet functions, better.

Despite their functional diversity, the actin and MTs are highly conserved amongst all eukaryotes [13, 67]. By studying their dynamics in simple, anucleate cells such as the platelets, the knowledge gained about them can be extrapolated to other cells.

References

1. Filament Sensor Program (version 0.2.2e). <http://www.stochastik.math.uni-goettingen.de/index.php?id=197>
2. Abberior STAR 635. <http://www.abberior.com/shop/Labels-by-Application/Confocal-Epi-SIM/Abberior-STAR-635:8.html>
3. AHF Analysentechnik FITC/Cy5 Dualband H Filterset. https://www.ahf.de/art-FITC_Cy5_Dualband_H_Filterset;F56-200.html
4. Spirochrome Probes for Imaging SiR-Cytoskeleton kit. <http://spirochrome.com/product/cytoskeleton-kit/>
5. ThermoFisher Scientific CellMask Stains datasheet. https://tools.thermofisher.com/content/sfs/manuals/CellMask_Plasma_Membrane_Stains_PI.pdf
6. ThermoFisher Scientific Fluorescence Spectraviewer Alexa 488. <https://www.thermofisher.com/de/de/home/life-science/cell-analysis/labeling-chemistry/fluorescence-spectraviewer.html>
7. Allen RD, Zacharski LR, Widirstky ST et al. (1979) Transformation and motility of human platelets: details of the shape change and release reaction observed by optical and electron microscopy. *J Cell Biol* 83(1): 126–142
8. Andrews DA, Low PS (1999) Role of red blood cells in thrombosis. *Curr Opin Hematol* 6(2): 76–82
9. Aslan JE, Baker SM, Loren CP et al. (2013) The PAK system links Rho GTPase signaling to thrombin-mediated platelet activation. *Am J Physiol Cell Physiol* 305(5): C519-28. doi: 10.1152/ajpcell.00418.2012
10. Aslan JE, Phillips KG, Healy LD et al. (2013) Histone deacetylase 6-mediated deacetylation of alpha-tubulin coordinates cytoskeletal and signaling events during platelet activation. *Am J Physiol Cell Physiol* 305(12): C1230-9. doi: 10.1152/ajpcell.00053.2013
11. Azim AC, Barkalow K, Chou J et al. (2000) Activation of the small GTPases, rac and cdc42, after ligation of the platelet PAR-1 receptor. *Blood* 95(3): 959–964
12. Bearer EL (1995) Cytoskeletal domains in the activated platelet. *Cell Motil Cytoskeleton* 30(1): 50–66. doi: 10.1002/cm.970300107

REFERENCES

13. Bearer EL, Prakash JM, Li Z (2002) Actin dynamics in platelets. *Int Rev Cytol* 217: 137–182
14. Berry S, Dawicki DD, Agarwal KC et al. (1989) The role of microtubules in platelet secretory release. *Biochimica et Biophysica Acta (BBA) - Molecular Cell Research* 1012(1): 46–56. doi: 10.1016/0167-4889(89)90009-8
15. Brass LF (2003) Thrombin and platelet activation. *Chest* 124(3 Suppl): 18–25
16. Brewer DB (2006) Max Schultze (1865), G. Bizzozero (1882) and the discovery of the platelet. *Br J Haematol* 133(3): 251–258. doi: 10.1111/j.1365-2141.2006.06036.x
17. Burkhardt JM, Vaudel M, Gambaryan S et al. (2012) The first comprehensive and quantitative analysis of human platelet protein composition allows the comparative analysis of structural and functional pathways. *Blood* 120(15): 82. doi: 10.1182/blood-2012-04-416594
18. Bustelo XR, Sauzeau V, Berenjano IM (2007) GTP-binding proteins of the Rho/Rac family: regulation, effectors and functions in vivo. *Bioessays* 29(4): 356–370. doi: 10.1002/bies.20558
19. Calaminus SDJ, Auger JM, McCarty OJT et al. (2007) MyosinIIa contractility is required for maintenance of platelet structure during spreading on collagen and contributes to thrombus stability. *J Thromb Haemost* 5(10): 2136–2145. doi: 10.1111/j.1538-7836.2007.02696.x
20. Calaminus SDJ, Thomas S, McCarty OJT et al. (2008) Identification of a novel, actin-rich structure, the actin nodule, in the early stages of platelet spreading. *J Thromb Haemost* 6(11): 1944–1952. doi: 10.1111/j.1538-7836.2008.03141.x
21. Calderwood DA, Yan B, Pereda JM de et al. (2002) The phosphotyrosine binding-like domain of talin activates integrins. *J Biol Chem* 277(24): 21749–21758. doi: 10.1074/jbc.M111996200
22. Canny J (1986) A Computational Approach to Edge Detection. *IEEE Trans. Pattern Anal. Mach. Intell. PAMI-8(6)*: 679–698. doi: 10.1109/TPAMI.1986.4767851
23. Canobbio I, Noris P, Pecci A et al. (2005) Altered cytoskeleton organization in platelets from patients with MYH9-related disease. *J Thromb Haemost* 3(5): 1026–1035. doi: 10.1111/j.1538-7836.2005.01244.x
24. Cardo L, Thomas SG, Mazharian A et al. (2015) Accessible Synthetic Probes for Staining Actin inside Platelets and Megakaryocytes by Employing Lifeact Peptide. *Chembiochem* 16(11): 1680–1688. doi: 10.1002/cbic.201500120

REFERENCES

25. Carlier MF, Jean C, Rieger KJ et al. (1993) Modulation of the interaction between G-actin and thymosin beta 4 by the ATP/ADP ratio: possible implication in the regulation of actin dynamics. *Proc Natl Acad Sci U S A* 90(11): 5034–5038
26. Carlier M-F, Ducruix A, Pantaloni D (1999) Signalling to actin. The Cdc42-N-WASP-Arp2/3 connection. *Chemistry & Biology* 6(9): R235-R240. doi: 10.1016/S1074-5521(99)80107-0
27. Cerecedo D, Cisneros B, Mondragon R et al. (2010) Actin filaments and microtubule dual-granule transport in human adhered platelets: the role of alpha-dystrobrevins. *Br J Haematol* 149(1): 124–136. doi: 10.1111/j.1365-2141.2010.08085.x
28. Cerecedo D, Cisneros B, Suarez-Sanchez R et al. (2008) beta-Dystroglycan modulates the interplay between actin and microtubules in human-adhered platelets. *Br J Haematol* 141(4): 517–528. doi: 10.1111/j.1365-2141.2008.07048.x
29. Cerecedo D, Mondragon R, Cisneros B et al. (2006) Role of dystrophins and utrophins in platelet adhesion process. *Br J Haematol* 134(1): 83–91. doi: 10.1111/j.1365-2141.2006.06120.x
30. Cerecedo D, Stock R, Gonzalez S et al. (2002) Modification of actin, myosin and tubulin distribution during cytoplasmic granule movements associated with platelet adhesion. *Haematologica* 87(11): 1165–1176
31. Clemetson KJ (2012) Platelets and primary haemostasis. *Thromb Res* 129(3): 220–224. doi: 10.1016/j.thromres.2011.11.036
32. Clemetson KJ, Clemetson JM (2001) Platelet collagen receptors. *Thromb Haemost* 86(1): 189–197
33. Cooper B (2005) Osler's role in defining the third corpuscle, or “blood plates”. *Proc (Bayl Univ Med Cent)* 18(4): 376–378
34. Cosen-Binker LI, Kapus A (2006) Cortactin: the gray eminence of the cytoskeleton. *Physiology (Bethesda)* 21: 352–361. doi: 10.1152/physiol.00012.2006
35. Desai A, Mitchison TJ (1997) Microtubule polymerization dynamics. *Annu Rev Cell Dev Biol* 13: 83–117. doi: 10.1146/annurev.cellbio.13.1.83
36. Diagouraga B, Grichine A, Fertin A et al. (2014) Motor-driven marginal band coiling promotes cell shape change during platelet activation. *J Cell Biol* 204(2): 177–185. doi: 10.1083/jcb.201306085
37. Dmitrieff Serge , Alsina Adolfo , Mathur Aastha , Nédélec François (2016) Balance of microtubule stiffness and cortical tension determines the size of blood cells with marginal band across species. arXiv:1610.10035

REFERENCES

38. Egawa T, Hanaoka K, Koide Y et al. (2011) Development of a far-red to near-infrared fluorescence probe for calcium ion and its application to multicolor neuronal imaging. *J Am Chem Soc* 133(36): 14157–14159. doi: 10.1021/ja205809h
39. Eltzner B, Wollnik C, Gottschlich C et al. (2015) The filament sensor for near real-time detection of cytoskeletal fiber structures. *PLoS One* 10(5): e0126346. doi: 10.1371/journal.pone.0126346
40. Escolar G, Sauk J, Bravo ML et al. (1987) Immunogold staining of microtubules in resting and activated platelets. *Am J Hematol* 24(2): 177–188
41. Falet H, Hoffmeister KM, Neujahr R et al. (2002) Normal Arp2/3 complex activation in platelets lacking WASp. *Blood* 100(6): 2113–2122
42. Feghhi S, Tooley WW, Sniadecki NJ (2016) Nonmuscle Myosin IIA Regulates Platelet Contractile Forces Through Rho Kinase and Myosin Light-Chain Kinase. *J Biomech Eng* 138(10). doi: 10.1115/1.4034489
43. Feuerstein IA, Sheppard JI (1993) States in adherent platelet morphology and the processing of adsorbed protein on biomaterials. *Biomaterials* 14(2): 137–147
44. Finkenstaedt-Quinn SA, Qiu TA, Shin K et al. (2016) Super-resolution imaging for monitoring cytoskeleton dynamics. *Analyst* 141(20): 5674–5688. doi: 10.1039/c6an00731g
45. Flaumenhaft R, Dilks JR, Rozenvayn N et al. (2005) The actin cytoskeleton differentially regulates platelet alpha-granule and dense-granule secretion. *Blood* 105(10): 3879–3887. doi: 10.1182/blood-2004-04-1392
46. Fouchard J, Mitrossilis D, Asnacios A (2011) Acto-myosin based response to stiffness and rigidity sensing. *Cell Adh Migr* 5(1): 16–19. doi: 10.4161/cam.5.1.13281
47. Fox JE, Boyles JK, Reynolds CC et al. (1984) Actin filament content and organization in unstimulated platelets. *J Cell Biol* 98(6): 1985–1991
48. Fritz M, Radmacher M, Gaub HE (1994) Granula motion and membrane spreading during activation of human platelets imaged by atomic force microscopy. *Biophysical Journal* 66(5): 1328–1334. doi: 10.1016/S0006-3495(94)80963-4
49. Gao G, Chen L, Dong B et al. (2009) RhoA effector mDia1 is required for PI 3-kinase-dependent actin remodeling and spreading by thrombin in platelets. *Biochem Biophys Res Commun* 385(3): 439–444. doi: 10.1016/j.bbrc.2009.05.090
50. Goggs R, Williams CM, Mellor H et al. (2015) Platelet Rho GTPases—a focus on novel players, roles and relationships. *Biochem J* 466(3): 431–442. doi: 10.1042/BJ20141404

REFERENCES

51. Goh WI, Sudhaharan T, Lim KB et al. (2011) Rif-mDia1 interaction is involved in filopodium formation independent of Cdc42 and Rac effectors. *J Biol Chem* 286(15): 13681–13694. doi: 10.1074/jbc.M110.182683
52. Gokhin DS, Nowak RB, Khoory JA et al. (2015) Dynamic actin filaments control the mechanical behavior of the human red blood cell membrane. *Mol Biol Cell* 26(9): 1699–1710. doi: 10.1091/mbc.E14-12-1583
53. Golebiewska EM, Poole AW (2013) Secrets of platelet exocytosis - what do we really know about platelet secretion mechanisms? *Br J Haematol*. doi: 10.1111/bjh.12682
54. Hagmann J Pattern assembly and handedness in the cytoskeleton of human platelets. *Proceedings of the National Academy of Sciences* 90: 3280
55. Hall A (1998) Rho GTPases and the actin cytoskeleton. *Science* 279(5350): 509–514
56. Hartwig JH (1991) The cytoskeleton of the resting human blood platelet. Structure of the membrane skeleton and its attachment to actin filaments. *J Cell Biol* 112(3): 407–425. doi: 10.1083/jcb.112.3.407
57. Hartwig JH (1992) Mechanisms of actin rearrangements mediating platelet activation. *J Cell Biol* 118(6): 1421–1442
58. Hartwig JH (2006) The platelet: form and function. *Semin Hematol* 43(1 Suppl 1): 100. doi: 10.1053/j.seminhematol.2005.11.004
59. Hartwig JH, Bokoch GM, Carpenter CL et al. (1995) Thrombin receptor ligation and activated Rac uncap actin filament barbed ends through phosphoinositide synthesis in permeabilized human platelets. *Cell* 82(4): 643–653
60. Hartwig JH, Kung S, Kovacsovics T et al. (1996) D3 phosphoinositides and outside-in integrin signaling by glycoprotein IIb-IIIa mediate platelet actin assembly and filopodial extension induced by phorbol 12-myristate 13-acetate. *J Biol Chem* 271(51): 32986–32993
61. Holme PA, Orvim U, Hamers MJAG et al. (1997) Shear-Induced Platelet Activation and Platelet Microparticle Formation at Blood Flow Conditions as in Arteries With a Severe Stenosis. *Arterioscler Thromb Vasc Biol* 17(4): 646–653. doi: 10.1161/01.ATV.17.4.646
62. Honda S, Shirotani-Ikejima H, Tadokoro S et al. (2009) Integrin-linked kinase associated with integrin activation. *Blood* 113(21): 5304–5313. doi: 10.1182/blood-2008-07-169136
63. Italiano JE, JR, Battinelli EM (2009) Selective sorting of alpha-granule proteins. *J Thromb Haemost* 7 Suppl 1: 173–176. doi: 10.1111/j.1538-7836.2009.03387.x
64. Italiano JE, JR, Bergmeier W, Tiwari S et al. (2003) Mechanisms and implications of platelet discoid shape. *Blood* 101(12): 4789–4796. doi: 10.1182/blood-2002-11-3491

REFERENCES

65. Italiano JE, JR, Lecine P, Shivdasani RA et al. (1999) Blood platelets are assembled principally at the ends of proplatelet processes produced by differentiated megakaryocytes. *J Cell Biol* 147(6): 1299–1312
66. Janke C, Bulinski JC (2011) Post-translational regulation of the microtubule cytoskeleton: mechanisms and functions. *Nat Rev Mol Cell Biol* 12(12): 773–786. doi: 10.1038/nrm3227
67. Janke C, Chloë Bulinski J (2012) Post-translational regulation of the microtubule cytoskeleton. Mechanisms and functions. *Nat Rev Mol Cell Biol*. doi: 10.1038/nrm3310
68. Johnson GJ, Leis LA, Krumwiede MD et al. (2007) The critical role of myosin IIA in platelet internal contraction. *J Thromb Haemost* 5(7): 1516–1529. doi: 10.1111/j.1538-7836.2007.02611.x
69. Kamath S, Blann AD, Lip GY (2001) Platelet activation: assessment and quantification. *Eur Heart J* 22(17): 1561–1571. doi: 10.1053/euhj.2000.2515
70. Karlsson R, Lassing I, Hoglund AS et al. (1984) The organization of microfilaments in spreading platelets: a comparison with fibroblasts and glial cells. *J Cell Physiol* 121(1): 96–113. doi: 10.1002/jcp.1041210113
71. Katoh K, Kano Y, Amano M et al. (2001) Rho-kinase--mediated contraction of isolated stress fibers. *J Cell Biol* 153(3): 569–584
72. Kenney DM, Linck RW (1985) The cytoskeleton of unstimulated blood platelets: structure and composition of the isolated marginal microtubular band. *J Cell Sci* 78: 1–22
73. Koide Y, Urano Y, Hanaoka K et al. (2011) Development of an Si-rhodamine-based far-red to near-infrared fluorescence probe selective for hypochlorous acid and its applications for biological imaging. *J Am Chem Soc* 133(15): 5680–5682. doi: 10.1021/ja111470n
74. Koide Y, Urano Y, Hanaoka K et al. (2011) Evolution of group 14 rhodamines as platforms for near-infrared fluorescence probes utilizing photoinduced electron transfer. *ACS Chem Biol* 6(6): 600–608. doi: 10.1021/cb1002416
75. Koseoglu S, Peters CG, Fitch-Tewfik JL et al. (2015) VAMP-7 links granule exocytosis to actin reorganization during platelet activation. *Blood* 126(5): 651–660. doi: 10.1182/blood-2014-12-618744
76. Lee D, Fong KP, King MR et al. (2012) Differential dynamics of platelet contact and spreading. *Biophysical Journal* 102(3): 472–482. doi: 10.1016/j.bpj.2011.10.056
77. Leng L, Kashiwagi H, Ren XD et al. (1998) RhoA and the function of platelet integrin α IIb β 3. *Blood* 91(11): 4206–4215

REFERENCES

78. Leon C, Eckly A, Hechler B et al. (2007) Megakaryocyte-restricted MYH9 inactivation dramatically affects hemostasis while preserving platelet aggregation and secretion. *Blood* 110(9): 3183–3191. doi: 10.1182/blood-2007-03-080184
79. Lewis JC, White MS, Prater T et al. (1982) Ultrastructural analysis of platelets in nonhuman primates. III. Stereo microscopy of microtubules during platelet adhesion and the release reaction. *Exp Mol Pathol* 37(3): 370–381
80. Li CH, Tam P (1998) An iterative algorithm for minimum cross entropy thresholding. *Pattern Recognition Letters* 19(8): 771–776. doi: 10.1016/S0167-8655(98)00057-9
81. Li Z, Delaney MK, O'Brien KA et al. (2010) Signaling during platelet adhesion and activation. *Arterioscler Thromb Vasc Biol* 30(12): 2341–2349. doi: 10.1161/ATVBAHA.110.207522
82. Li Z, Kim ES, Bearer EL (2002) Arp2/3 complex is required for actin polymerization during platelet shape change. *Blood* 99(12): 4466–4474
83. Liang XM, Han SJ, Reems J-A et al. (2010) Platelet retraction force measurements using flexible post force sensors. *Lab Chip* 10(8): 991–998. doi: 10.1039/b918719g
84. Lodish HF (2016) *Molecular cell biology*, Eighth edition. W.H. Freeman-Macmillan Learning, New York
85. Loftus JC, Choate J, Albrecht RM (1984) Platelet activation and cytoskeletal reorganization: high voltage electron microscopic examination of intact and Triton-extracted whole mounts. *J Cell Biol* 98(6): 2019–2025
86. Lukinavicius G, Reymond L, D'Este E et al. (2014) Fluorogenic probes for live-cell imaging of the cytoskeleton. *Nat Methods* 11(7): 731–733. doi: 10.1038/nmeth.2972
87. Lukinavicius G, Umezawa K, Olivier N et al. (2013) A near-infrared fluorophore for live-cell super-resolution microscopy of cellular proteins. *Nat Chem* 5(2): 132–139. doi: 10.1038/nchem.1546
88. Machlus KR, Italiano JE, JR (2013) The incredible journey: From megakaryocyte development to platelet formation. *J Cell Biol* 201(6): 785–796. doi: 10.1083/jcb.201304054
89. Mattila PK, Lappalainen P (2008) Filopodia: molecular architecture and cellular functions. *Nat Rev Mol Cell Biol* 9(6): 446–454. doi: 10.1038/nrm2406
90. Maurer-Spurej E, Pfeiler G, Maurer N et al. (2001) Room temperature activates human blood platelets. *Lab Invest* 81(4): 581–592
91. May RC (2001) The Arp2/3 complex: a central regulator of the actin cytoskeleton. *Cell Mol Life Sci* 58(11): 1607–1626. doi: 10.1007/PL00000800

REFERENCES

92. McCarty OJT, Larson MK, Auger JM et al. (2005) Rac1 is essential for platelet lamellipodia formation and aggregate stability under flow. *J Biol Chem* 280(47): 39474–39484. doi: 10.1074/jbc.M504672200
93. Mellor H (2010) The role of formins in filopodia formation. *Biochim Biophys Acta* 1803(2): 191–200. doi: 10.1016/j.bbamcr.2008.12.018
94. Michelson AD (2013) Platelets, Third edition. Academic Press, Amsterdam
95. (2010) Microsoft Excel. Microsoft Office Professional Plus 2010
96. Mitrossilis D, Fouchard J, Guiroy A et al. (2009) Single-cell response to stiffness exhibits muscle-like behavior. *Proc Natl Acad Sci U S A* 106(43): 18243–18248. doi: 10.1073/pnas.0903994106
97. Mitsios JV, Prevost N, Kasirer-Friede A et al. (2010) What is vinculin needed for in platelets? *J Thromb Haemost* 8(10): 2294–2304. doi: 10.1111/j.1538-7836.2010.03998.x
98. Moore PB, Huxley HE, DeRosier DJ (1970) Three-dimensional reconstruction of F-actin, thin filaments and decorated thin filaments. *J Mol Biol* 50(2): 279–295
99. Nachmias VT, Golla R (1991) Vinculin in relation to stress fibers in spread platelets. *Cell Motil Cytoskeleton* 20(3): 190–202. doi: 10.1002/cm.970200303
100. Nakamura N, Oshiro N, Fukata Y et al. (2000) Phosphorylation of ERM proteins at filopodia induced by Cdc42. *Genes Cells* 5(7): 571–581. doi: 10.1046/j.1365-2443.2000.00348.x
101. Nejedla M, Sadi S, Sulimenko V et al. (2016) Profilin connects actin assembly with microtubule dynamics. *Mol Biol Cell* 27(15): 2381–2393. doi: 10.1091/mbc.E15-11-0799
102. Neumüller J, Ellinger A, Wagner T (2015) Transmission Electron Microscopy of Platelets FROM Apheresis and Buffy-Coat-Derived Platelet Concentrates. In: Maaz K (ed) *The Transmission Electron Microscope - Theory and Applications*. InTech
103. Nobes CD, Hall A (1995) Rho, rac, and cdc42 GTPases regulate the assembly of multimolecular focal complexes associated with actin stress fibers, lamellipodia, and filopodia. *Cell* 81(1): 53–62
104. Oakes PW, Beckham Y, Stricker J et al. (2012) Tension is required but not sufficient for focal adhesion maturation without a stress fiber template. *J Cell Biol* 196(3): 363–374. doi: 10.1083/jcb.201107042
105. Obydennyy SI, Sveshnikova AN, Ataulakhanov FI et al. (2016) Dynamics of calcium spiking, mitochondrial collapse and phosphatidylserine exposure in platelet

REFERENCES

- subpopulations during activation. *J Thromb Haemost* 14(9): 1867–1881. doi: 10.1111/jth.13395
106. Offermanns S (2006) Activation of platelet function through G protein-coupled receptors. *Circ Res* 99(12): 1293–1304. doi: 10.1161/01.RES.0000251742.71301.16
107. Painter RG, Ginsberg MH (1984) Centripetal myosin redistribution in thrombin-stimulated platelets. Relationship to platelet Factor 4 secretion. *Exp Cell Res* 155(1): 198–212
108. Patel-Hett S, Richardson JL, Schulze H et al. (2008) Visualization of microtubule growth in living platelets reveals a dynamic marginal band with multiple microtubules. *Blood* 111(9): 4605–4616. doi: 10.1182/blood-2007-10-118844
109. Patel-Hett S, Wang H, Begonja AJ et al. (2011) The spectrin-based membrane skeleton stabilizes mouse megakaryocyte membrane systems and is essential for proplatelet and platelet formation. *Blood* 118(6): 1641–1652. doi: 10.1182/blood-2011-01-330688
110. Pellegrin S, Mellor H (2007) Actin stress fibres. *J Cell Sci* 120(Pt 20): 3491–3499. doi: 10.1242/jcs.018473
111. Phillips DR, Nannizzi-Alaimo L, Prasad KS (2001) Beta3 tyrosine phosphorylation in alphaIIb beta3 (platelet membrane GP IIb-IIIa) outside-in integrin signaling. *Thromb Haemost* 86(1): 246–258
112. Pleines I, Eckly A, Elvers M et al. (2010) Multiple alterations of platelet functions dominated by increased secretion in mice lacking Cdc42 in platelets. *Blood* 115(16): 3364–3373. doi: 10.1182/blood-2009-09-242271
113. Pleines I, Hagedorn I, Gupta S et al. (2012) Megakaryocyte-specific RhoA deficiency causes macrothrombocytopenia and defective platelet activation in hemostasis and thrombosis. *Blood* 119(4): 1054–1063. doi: 10.1182/blood-2011-08-372193
114. Poulter NS, Pollitt AY, Davies A et al. (2015) Platelet actin nodules are podosome-like structures dependent on Wiskott-Aldrich syndrome protein and ARP2/3 complex. *Nat Commun* 6: 7254. doi: 10.1038/ncomms8254
115. Poulter NS, Thomas SG (2015) Cytoskeletal regulation of platelet formation: Coordination of F-actin and microtubules. *Int J Biochem Cell Biol* 66: 69–74. doi: 10.1016/j.biocel.2015.07.008
116. Qiu Y, Brown AC, Myers DR et al. (2014) Platelet mechanosensing of substrate stiffness during clot formation mediates adhesion, spreading, and activation. *Proc Natl Acad Sci U S A* 111(40): 14430–14435. doi: 10.1073/pnas.1322917111

REFERENCES

117. Rai AK, Rai A, Ramaiya AJ et al. (2013) Molecular adaptations allow dynein to generate large collective forces inside cells. *Cell* 152(1-2): 172–182. doi: 10.1016/j.cell.2012.11.044
118. Reed GL, Fitzgerald ML, Polgar J (2000) Molecular mechanisms of platelet exocytosis: insights into the "secrete" life of thrombocytes. *Blood* 96(10): 3334–3342
119. Riedl J, Crevenna AH, Kessenbrock K et al. (2008) Lifeact: a versatile marker to visualize F-actin. *Nat Methods* 5(7): 605–607. doi: 10.1038/nmeth.1220
120. Riedl J, Flynn KC, Raducanu A et al. (2010) Lifeact mice for studying F-actin dynamics. *Nat Methods* 7(3): 168–169. doi: 10.1038/nmeth0310-168
121. Robb-Smith AHT (1967) Why the Platelets were Discovered. *Br J Haematol* 13(s1): 618–637. doi: 10.1111/j.1365-2141.1967.tb00769.x
122. Sadoul K (2015) New explanations for old observations: marginal band coiling during platelet activation. *J Thromb Haemost* 13(3): 333–346. doi: 10.1111/jth.12819
123. Sadoul K, Wang J, Diagouraga B et al. (2012) HDAC6 controls the kinetics of platelet activation. *Blood* 120(20): 4215–4218. doi: 10.1182/blood-2012-05-428011
124. Sakurai Y, Fitch-Tewfik JL, Qiu Y et al. (2015) Platelet geometry sensing spatially regulates alpha-granule secretion to enable matrix self-deposition. *Blood* 126(4): 531–538. doi: 10.1182/blood-2014-11-607614
125. Sandmann R (2015) Blood Platelet Behavior on Structured Substrates. From Spreading Dynamics to Cell Morphology. Dissertation, Georg-August-Universität
126. Sandmann R, Koster S (2016) Topographic Cues Reveal Two Distinct Spreading Mechanisms in Blood Platelets. *Sci Rep* 6: 22357. doi: 10.1038/srep22357
127. Sandmann R, Köster S, Rehfeldt F Blood platelet behavior on structured substrates. From spreading dynamics to cell morphology. @Göttingen, Univ., Diss., 2015
128. Schachtner H, Calaminus SDJ, Thomas SG et al. (2013) Podosomes in adhesion, migration, mechanosensing and matrix remodeling. *Cytoskeleton (Hoboken)* 70(10): 572–589. doi: 10.1002/cm.21119
129. Schachtner H, Li A, Stevenson D et al. (2012) Tissue inducible Lifeact expression allows visualization of actin dynamics in vivo and ex vivo. *Eur J Cell Biol* 91(11-12): 923–929. doi: 10.1016/j.ejcb.2012.04.002
130. Schneider CA, Rasband WS, Eliceiri KW (2012) NIH Image to ImageJ: 25 years of image analysis. *Nat Methods* 9(7): 671–675

REFERENCES

131. Schubert P, Devine DV (2010) De novo protein synthesis in mature platelets: a consideration for transfusion medicine. *Vox Sang* 99(2): 112–122. doi: 10.1111/j.1423-0410.2010.01333.x
132. Schwarz Henriques S, Sandmann R, Strate A et al. (2012) Force field evolution during human blood platelet activation. *J Cell Sci* 125(Pt 16): 3914–3920. doi: 10.1242/jcs.108126
133. Schwertz H, Koster S, Kahr WHA et al. (2010) Anucleate platelets generate progeny. *Blood* 115(18): 3801–3809. doi: 10.1182/blood-2009-08-239558
134. Severin S, Gaits-Iacovoni F, Allart S et al. (2013) A confocal-based morphometric analysis shows a functional crosstalk between the actin filament system and microtubules in thrombin-stimulated platelets. *J Thromb Haemost* 11(1): 183–186. doi: 10.1111/jth.12053
135. Shattil SJ, Kashiwagi H, Pampori N (1998) Integrin signaling: the platelet paradigm. *Blood* 91(8): 2645–2657
136. Shcherbina A, Bretscher A, Kenney DM et al. (1999) Moesin, the major ERM protein of lymphocytes and platelets, differs from ezrin in its insensitivity to calpain. *FEBS Lett* 443(1): 31–36
137. SMITH JB, WILLIS AL (1971) Aspirin Selectively Inhibits Prostaglandin Production in Human Platelets. *Nat New Biol* 231(25): 235–237. doi: 10.1038/newbio231235a0
138. Sneddon JM (1971) Effect of mitosis inhibitors on blood platelet microtubules and aggregation. *The Journal of Physiology* 214(1): 145–158. doi: 10.1113/jphysiol.1971.sp009424
139. Sorrentino S, Studt J-D, Horev MB et al. (2016) Toward correlating structure and mechanics of platelets. *Cell Adh Migr* 10(5): 568–575. doi: 10.1080/19336918.2016.1173803
140. Sorrentino S, Studt J-D, Medalia O et al. (2015) Roll, adhere, spread and contract: structural mechanics of platelet function. *Eur J Cell Biol* 94(3-4): 129–138. doi: 10.1016/j.ejcb.2015.01.001
141. Stark F, Golla R, Nachmias VT (1991) Formation and contraction of a microfilamentous shell in saponin-permeabilized platelets. *J Cell Biol* 112(5): 903–913
142. Steiner M, Ikeda Y (1979) Quantitative assessment of polymerized and depolymerized platelet microtubules. Changes caused by aggregating agents. *J Clin Invest* 63(3): 443–448. doi: 10.1172/JCI109321

REFERENCES

143. Stenberg PE, Shuman MA, Levine SP et al. (1984) Redistribution of alpha-granules and their contents in thrombin-stimulated platelets. *J Cell Biol* 98(2): 748–760
144. Straight AF, Cheung A, Limouze J et al. (2003) Dissecting temporal and spatial control of cytokinesis with a myosin II Inhibitor. *Science* 299(5613): 1743–1747. doi: 10.1126/science.1081412
145. Subramanian R, Kapoor TM (2012) Building complexity: insights into self-organized assembly of microtubule-based architectures. *Dev Cell* 23(5): 874–885. doi: 10.1016/j.devcel.2012.10.011
146. Takesono A, Heasman SJ, Wojciak-Stothard B et al. (2010) Microtubules regulate migratory polarity through Rho/ROCK signaling in T cells. *PLoS One* 5(1): e8774. doi: 10.1371/journal.pone.0008774
147. Takubo T, Hino M, Suzuki K et al. (2009) Localization of Myosin, Actin, α -Actinin, Tropomyosin and Vinculin in Surface-Activated, Spreading Human Platelets. *Biotechnic & Histochemistry* 73(6): 310–315. doi: 10.3109/10520299809141124
148. Tanaka K, Itoh K (1998) Reorganization of stress fiber-like structures in spreading platelets during surface activation. *J Struct Biol* 124(1): 13–41. doi: 10.1006/jsbi.1998.4051
149. Tanaka K, Shibata N, Okamoto K et al. (1986) Reorganization of myosin in surface-activated spreading platelets. *J Ultrastruct Mol Struct Res* 97(1-3): 165–186
150. Tanenbaum ME, Vale RD, McKenney RJ (2013) Cytoplasmic dynein crosslinks and slides anti-parallel microtubules using its two motor domains. *Elife* 2: e00943. doi: 10.7554/eLife.00943
151. Tea Vallenius (2004) Characterization of actin stress fibers: involvement of PDZ-LIM adapter proteins and the novel Clik1 kinase. Academic Dissertation, Institute of Biomedicine, Biomedicum Helsinki
152. Thomas SG, Calaminus SDJ, Machesky LM et al. (2011) G-protein coupled and ITAM receptor regulation of the formin FHOD1 through Rho kinase in platelets. *J Thromb Haemost* 9(8): 1648–1651. doi: 10.1111/j.1538-7836.2011.04357.x
153. Thon JN, Macleod H, Begonja AJ et al. (2012) Microtubule and cortical forces determine platelet size during vascular platelet production. *Nat Commun* 3: 852. doi: 10.1038/ncomms1838
154. Thon JN, Montalvo A, Patel-Hett S et al. (2010) Cytoskeletal mechanics of proplatelet maturation and platelet release. *J Cell Biol* 191(4): 861–874. doi: 10.1083/jcb.201006102

REFERENCES

155. Tojkander S, Gateva G, Lappalainen P (2012) Actin stress fibers--assembly, dynamics and biological roles. *J Cell Sci* 125(Pt 8): 1855–1864. doi: 10.1242/jcs.098087
156. Urban AE, Quick EO, Miller KP et al. (2016) Pdlim7 Regulates Arf6-Dependent Actin Dynamics and Is Required for Platelet-Mediated Thrombosis in Mice. *PLoS One* 11(10): e0164042. doi: 10.1371/journal.pone.0164042
157. van Nispen tot Pannerden H, Haas F de, Geerts W et al. (2010) The platelet interior revisited: electron tomography reveals tubular alpha-granule subtypes. *Blood* 116(7): 1147–1156. doi: 10.1182/blood-2010-02-268680
158. Varga-Szabo D, Pleines I, Nieswandt B (2008) Cell adhesion mechanisms in platelets. *Arterioscler Thromb Vasc Biol* 28(3): 403–412. doi: 10.1161/ATVBAHA.107.150474
159. Vu TK, Hung DT, Wheaton VI et al. (1991) Molecular cloning of a functional thrombin receptor reveals a novel proteolytic mechanism of receptor activation. *Cell* 64(6): 1057–1068
160. Wagner CL, Mascelli MA, Neblock DS et al. (1996) Analysis of GPIIb/IIIa receptor number by quantification of 7E3 binding to human platelets. *Blood* 88(3): 907–914
161. Wegner A (1982) Treadmilling of actin at physiological salt concentrations. An analysis of the critical concentrations of actin filaments. *J Mol Biol* 161(4): 607–615
162. Weiss HJ, Aledort LM (1967) Impaired platelet-connective-tissue reaction in man after aspirin ingestion. *Lancet* 2(7514): 495–497
163. White JG (1987) Views of the platelet cytoskeleton at rest and at work. *Ann N Y Acad Sci* 509: 156–176
164. White JG (2005) Platelets are coverocytes, not phagocytes: uptake of bacteria involves channels of the open canalicular system. *Platelets* 16(2): 121–131. doi: 10.1080/09537100400007390
165. White JG, Burriss SM (1984) Morphometry of platelet internal contraction. *Am J Pathol* 115(3): 412–417
166. White JG, Escolar G (1993) Current concepts of platelet membrane response to surface activation. *Platelets* 4(4): 175–189. doi: 10.3109/09537109309013215
167. White JG, Rao GH (1982) Effects of a microtubule stabilizing agent on the response of platelets to vincristine. *Blood* 60(2): 474–483
168. White JG, Rao GH (1983) Influence of a microtubule stabilizing agent on platelet structural physiology. *Am J Pathol* 112(2): 207–217
169. White JG, Rao GH (1998) Microtubule coils versus the surface membrane cytoskeleton in maintenance and restoration of platelet discoid shape. *Am J Pathol* 152(2): 597–609

REFERENCES

170. Wloga D, Gaertig J (2010) Post-translational modifications of microtubules. *J Cell Sci* 123(Pt 20): 3447–3455. doi: 10.1242/jcs.063727
171. Woronowicz K, Dilks JR, Rozenvayn N et al. (2010) The platelet actin cytoskeleton associates with SNAREs and participates in alpha-granule secretion. *Biochemistry* 49(21): 4533–4542. doi: 10.1021/bi100541t
172. Wozniak MA, Modzelewska K, Kwong L et al. (2004) Focal adhesion regulation of cell behavior. *Biochim Biophys Acta* 1692(2-3): 103–119. doi: 10.1016/j.bbamcr.2004.04.007
173. Zucker-Franklin D, Grusky G (1972) The actin and myosin filaments of human and bovine blood platelets. *J Clin Invest* 51(2): 419–430. doi: 10.1172/JCI106828

Appendix

A. Recipes of buffers (sample preparation and platelet purification)

All buffers used for the experiments (refer to chapter 3, section 3.2) were prepared in ultrapure water (Milli-Q, Millipore, MA, USA).

➤ Phosphate buffered saline (PBS) from a 10X PBS stock solution

Chemicals	Final concentration (mM)
NaCl	1370
Na ₂ HPO ₄ ·12H ₂ O	43
KCl	27
KCl KH ₂ PO ₄	14

The pH was adjusted to 7.2. PBS solution was prepared by diluting the 10X stock solution 10 times. The buffer was sterilized by autoclaving before use.

➤ PIPES-saline glucose (PSG) buffer

Chemicals	Final concentration (mM)
NaCl	145
PIPES	5
Glucose	5
KCl	4
MgCl ₂ ·6H ₂ O	1
Na ₂ HPO ₄ ·12H ₂ O	0.05

The pH was adjusted to 6.8 and the buffer was sterilized by autoclaving before use.

➤ Hepes Tyrode buffer with BSA (HT-BSA)

Chemicals	Final concentration (mM)
NaCl	134
NAHCO ₃	12
HEPES	5
Glucose	5
KCl	2.9
anhydrous MgCl ₂	1
NaH ₂ PO ₄	0.34

The pH was adjusted to 7.4 and the buffer was sterilized by autoclaving before use. On the day of the platelet purification, BSA was added to HT buffer at a final concentration of 5 mg/ml.

B. Normalized F-actin intensity analysis MATLAB script

- The normalized F-actin intensities of SiR-actin labeled platelets as they spread were obtained using an in-house MATLAB script kindly provided by Gerrit Brehm (details in chapter 3, section 3.6.1). The MATLAB script used is shown below.

```
%      F-actin normalized intensity with choosing ROI
%      by Gerrit Brehm

%the mat lab function 'textprogressbar.m' has do be in the folder that the
%programm works properly.

close all
clear all

[file_name, folder_name]=uigetfile('*.tif','select *.tif Image or Stack');
                                %choose the file, *.tif file needed
if folder_name(1)==0           %If no file selected, stop
    disp('Error in StackSlider: No files chosen');
    return
end
file = [folder_name file_name];
info = imfinfo(file);
num_images = numel (info);      %number of pictures
pic=imread(file);
fac=1/num_images;              %define scaling factor
pic_gray=mat2gray(pic)*fac;     %change the picture zu gray values [0,1]
pixel=numel(pic);              %pixelnumber
I_max=0;
set(0,'RecursionLimit',num_images); %resets the counter to max possible
recursions

if ~exist([pwd, '\results'], 'dir') %creating results folder if not
existend
    mkdir([pwd, '\results'])
end
```

```

save_data = ['intensity_' file_name '.txt'];
sum_intensitaeten = fopen(save_data,'wt'); %open textfile to write in

%section for ROI

disp('choosing ROI:');
disp('*****');

textprogressbar('load data:'); %progressbar

for k = 2:num_images
    pic2=imread(file,k);
    pic2_gray=mat2gray(pic2)*fac;
    pic_gray=pic_gray+pic2_gray;
    textprogressbar(uint8(double(k/num_images)*100));
end
overlaid=im2uint16(pic_gray); %transforming the grey overlaid picture to
16bit
textprogressbar('finished');
    BW=roipoly(overlaid); %making the ROI
    bpixel = nnz(BW==0); %number of black pixel in the Mask

%summed intensities

disp('calculating intensities in ROI:');
disp('*****');

textprogressbar('progress:');

for k = 1:num_images
    I=imread(file, k); %load the actual picture
    I(~BW) = 0; %applying the mask
    av_intensity = sum(sum(I))/(pixel-bpixel); %intensity per pixel
in the frame
    I_act = max(max(I));
    if I_act >= I_max
        I_max=I_act;
    end
    fprintf(sum_intensitaeten,' %5.f %10.f %5.f\n', k, av_intensity, I_act);
%output of the data in 'intensity.txt'
    textprogressbar(uint8(double(k/num_images)*100));
end
textprogressbar('finished');
fclose(sum_intensitaeten);

%movie of intensities

disp('creating movie of intensities');
disp('*****');

textprogressbar('progress:');
for k = 1:num_images
    I=imread(file, k); %load the actual picture
    I(~BW) = 0; %applying the mask
    figure(1);
    h=figure(1);
    imagesc(I);
    set(h,'Units','normalized','Position', [0.5, 0.5, 0.4, 0.4]); % [left,
bottom, width, height][0,1];
    caxis([0,I_max]);

```

```

colorbar;
colormap(jet); %colour images
%colormap(gray); %gray images
frame=getframe(h);

imwrite(frame.cdata,fullfile('results',['movie_',file_name]),'WriteMode','append',
'Compression','none');
    textprogressbar(uint8(double(k/num_images)*100));
end
textprogressbar('finished');

[x,y,z]=textread(save_data,'%f %f %f'); %reading in the saved data x=image
number, y=mean intensity, z= max intensity
%hold on;
plot(x,y); %plotting the data frame (x) vs average intensity (y)
%plot(x,z); %plotting the data frame vs maximum intensity (z)
%hold off;
return;

```

C. Platelet contour detection and spread area calculation MATLAB scripts

- The scripts were kindly provided by Rabea Sandmann and Bernd Nöding (details in chapter 3, section 3.7). Firstly, the contours of the fluorescently stained platelet were detected by the following script that employed a Wiener filter and a *canny* edge detection algorithm.

```

% PROGRAM TO DETECT PLATELET OUTLINES BY WIENER FILTER+CANNY ALGORITHM %
% written by Rabea Sandmann%

close all
clear all

cellimagesfiltered = ['*filename.tif'];

info1 = imfinfo (cellimagesfiltered);
z1 = numel(info1); % number of images in stack as defined in info-file of image
[r1,s1]=size(cellimagesfiltered);

for i = 1:z1;
    Image = imread(cellimagesfiltered,i, 'Info', info1);
    a=[0.08,0.18];
    L = wiener2(Image,[8 8]);
    BW = edge(L,'canny',a);
    Im_filtered=zeros(r1, s1);
    h_filtered=figure(1);

imwrite(BW,['*filename_wiener*parameters*_canny*parameters*.tif'],'WriteMode',
'append','Compression','none');
end

```

- Then a second MATLAB script ran two functions as shown below.

```

%Program to binarize and then select objects above certain threshold (pixel
size) only
% Written by Bernd Noeding

allererstes=input('erstes frameNo: '); % first frame number of stack
allerletztes=input('letztes frameNo: ');% last frame number of stack
date=input('Datum eingeben (Form YYMMDD): ','s');% stack data saved in YYMMDD
format
for i= allererstes : allerletztes
runningnumber=num2str(i);
disp(['Stack Nummer', runningnumber]);
filamentnumber= runningnumber; %input('Filamentnummer eingeben (laufende
nummer): ','s');
pics= 300; %input('Number of images: ');
first_pic=1 ; %input('First image: ');

thresholding_binarizing_stack;
disp(['Ende Thresholding Stack Nummer', runningnumber]);

muellabfuhr_B;
disp(['Ende AufräumenStack Nummer', runningnumber]);

end;

```

Firstly, it re-binarized the filled platelet images stack (function shown below).

```

%Programm zur Binarisierung von Originalbilder

function [] = thresholding_binarizing_J (date, filamentnumber, pics,
first_pic)
disp('Binärbild');
clear C line

N = pics; %input('Gesamtzahl der Bilder: ');
Image_1 = first_pic; %input('Nummer des ersten Bildes: ');

for i=1:N

    Imagenr = Image_1+i-1;

    disp(['Bild Nummer ',int2str(Imagenr)]);

    filename = strcat('filelocation\filename.tif'); % Hier unbedingt den
richtigen Pfad eingeben!!!
    savename = strcat('filelocation\binary\filename-binary.tif',date, 'v',
filamentnumber, 'b.tif'); % Hier unbedingt den richtigen Pfad eingeben!!!

    im=imread(filename, Imagenr);
    bwim=im2bw(im,0.0275); %converts the indexed image X with colormap map to a
binary image: im2bw(X, map, level).
    imwrite(bwim,savename,'Compression','none', 'WriteMode', 'append');

    %clear C line
end

```

```
%clear C Endung Image* N a c d filename i pat root save* zahl zero ImErased b
```

and then removed all detected objects other than the filled platelet masks, by employing a threshold

```
%Programm zur Selektion der grüñen Objekte in Binärbildern
%Bestimmt die Konturlinien aller Objekte im Binärbild, sucht dann die
längste Konturlinie und löscht alle Objekte außer dieser grüñen
```

```
%Bilder einlesen:
```

```
function[] = muellabfuhr_B;
disp('Aufträge');
clear C line
```

```
N = 270; %input('Gesamtzahl der Bilder: ');
Image_1 = 1; % input('Nummer des ersten Bildes: ');
```

```
for i=1:N
```

```
    Imagenr = Image_1+i-1;
    disp(['Bild Nummer ',int2str(Imagenr)]);
```

```
    filename = strcat('filelocation\binary\filename.tif'); % Hier unbedingt
den richtigen Pfad eingeben!!!
    savename = strcat('filelocation\clear\filename-clear.tif'); % Hier
unbedingt den richtigen Pfad eingeben!!!
```

```
    Image = double(imread(filename, Imagenr)) + 1;
```

```
    %Konturlinien finden und grünes Objekt selektieren:
```

```
    C = contour(Image, 1); % 1 Konturebene
    S=find(C(1,.)==1.5);
    [a, b] = max(C(2,S));
    line = C(:,(S(b)+1):(S(b)+a));
    ImErased = roipoly(Image, line(1,:), line(2,:));
```

```
    imwrite(ImErased,savename,'Compression','none', 'WriteMode', 'append');
```

```
    %clear C line
```

```
end
```

```
%clear C Endung Image* N a c d filename i pat root save* zahl zero ImErased b
```

- The third MATLAB script, calculated the platelet spread area from the binarized and filled (masks) platelet images stack using the *regionprops* function-

APPENDIX

```
% PROGRAM TO CALCULATE PLATELET SPREAD AREA AFTER BINARIZATION %
% written by Rabea Sandmann%

close all
clear all

global data;
data='*filename';

zoom=0.109/1; % 1 px = 0.109 µm for the ORCA Flash 4.0 V2 digital camera

t=5; %area threshold in pixels for objects being identified as cell

binarisedcellimages = [data, '.tif'];

info3 = imfinfo (binarisedcellimages);
z3 = numel(info3); % number of images in stack as defined in info-file of
image

fileID = fopen([data, '*filename_Area.txt'], 'w'); % open a textfile
fprintf(fileID, 'image \t cell nr\t area [um^2]\t perimeter cell [u]\t maj.
axis [um]\t min. axis [um]\t lambda \t perimeter ellipse [u]\t relative
perimeter \n\n');

for i = 1:z3;
    FImage = imread(binarisedcellimages,i, 'Info', info3);

    %Calculate cell area and perimeter
    [cells nrcells]=bwlabel(FImage,4); % gives a number to every object

    for j=1:nrcells
        Cell_info
        regionprops(cells, 'Area', 'Perimeter', 'MajorAxisLength', 'MinorAxisLength');
        Area= Cell_info(j,1).Area*zoom*zoom;
        Perimeter=Cell_info(j,1).Perimeter*zoom;
        MajorAxis=Cell_info(j,1).MajorAxisLength*zoom;
        MinorAxis=Cell_info(j,1).MinorAxisLength*zoom;
        lambda=(MajorAxis/2 - MinorAxis/2)/(MajorAxis/2 + MinorAxis/2);
        Ellipseperimeter=
        pi*(MajorAxis/2
        MinorAxis/2)*(1+(3*lambda^2)/(10+(4-3*lambda^2)^(1/2)));
        relPerimeter=Perimeter/Ellipseperimeter;
        if Area>t;
            fprintf(fileID, '%g \t%g \t%g \t%g \t%g \t%g \t%g \t%g
            \t%g\n', [i;j;Area;Perimeter;MajorAxis;MinorAxis;lambda;Ellipseperimeter;re
            lPerimeter]);
        end
    end
end
end
```

D. Parameters used for Filament Sensor program

- A summarized list of the values of the parameters used to detect the F-actin filaments of SiR-actin labeled platelets by the FS program (details in chapter 3, section 3.9). The modified version of the FS program can be accessed here [1].

Parameters	Values used
Pre-processing	
isotropic Gaussian filter, $\sigma =$	1.0
8-neighborhood Laplacian filter	2.0 - 4.0
directed Gaussian filter, $\sigma =$	5.0
Binarization	
global brightness Li threshold	25
adaptive means Gaussian filter, $\sigma =$	2.0
directed Gaussian filter, $\sigma =$	4.0
Width map generation	
black pixel tolerance	5.0%
Line (F-actin filament) detection	
distance between direction changes	5.0 pixels
Size of direction steps	3.0°
minimal line length (depending on platelet size)	30 – 40 pixels
minimal line crossing angle	20°, 30° (most used), 45°

APPENDIX

E. Relative numbers of spread/unsread platelets and statistical analysis by *t*-test.

➤ The relative numbers of spread and unsread, SiR-actin labeled platelets counted for all experimental conditions (details in chapter 3, section 3.4 and section 3.11) are given below-

condition	datasets date	spread $S_i = S_{i1} + S_{i2..} + S_{in}$	unsread $U_i = U_{i1} + U_{i2..} + U_{in}$	total $T_i = S_i + U_i$	spread(%) \bar{S}_i	unsread(%) \bar{U}_i	spread/total S_i/T_i	final counted $N = T_{i1} + T_{i2..} + T_{in}$
SiR-actin only								
S_i/U_{i1}	61015	345	243	588	58.7	41.3	0.587	3465
S_i/U_{i2}	121015	452	197	649	69.6	30.4	0.696	
S_i/U_{i3}	211015	211	116	327	64.5	35.5	0.645	
S_i/U_{i4}	301015	86	27	113	76.1	23.9	0.761	
S_i/U_{i5}	41115	267	33	300	89.0	11.0	0.890	
S_i/U_{i6}	100216	278	145	423	65.7	34.3	0.657	
S_i/U_{i7}	80716	342	238	580	59.0	41.0	0.590	
S_i/U_{i8}	120716	165	320	485	34.0	66.0	0.340	
average (\bar{S}, \bar{U})					64.6	35.4	0.646	
std dev (σ)							0.158	
no thrombin								
S_i/U_{i1}	61015	113	845	958	11.8	88.2	0.118	1549
S_i/U_{i2}	80716	49	296	345	14.2	85.8	0.142	
S_i/U_{i3}	120716	39	207	246	15.9	84.1	0.159	
average (\bar{S}, \bar{U})					14.0	86.0	0.140	
std dev (σ)							0.020	
20µM blebbistatin								
S_i/U_{i1}	121015	270	976	1246	21.7	78.3	0.217	3050
S_i/U_{i2}	211015	455	951	1406	32.4	67.6	0.324	
S_i/U_{i3}	80716	135	263	398	33.9	66.1	0.339	
average (\bar{S}, \bar{U})					29.3	70.7	0.293	
std dev (σ)							0.067	
50µM Y27632								
S_i/U_{i1}	301015	958	514	1472	65.1	34.9	0.651	2260
S_i/U_{i2}	41115	535	124	659	81.2	18.8	0.812	
S_i/U_{i3}	80716	90	39	129	69.8	30.2	0.698	
average (\bar{S}, \bar{U})					72.0	28.0	0.720	
std dev (σ)							0.083	
3.33mM aspirin								
S_i/U_{i1}	100216	460	339	799	57.6	42.4	0.576	2104
S_i/U_{i2}	310516	369	243	612	60.3	39.7	0.603	
S_i/U_{i3}	80716	253	440	693	36.5	63.5	0.365	
average (\bar{S}, \bar{U})					51.5	48.5	0.515	
std dev (σ)							0.130	

➤ The relative numbers of spread and unsread, SiR-tubulin labeled platelets counted for all experimental conditions (details in chapter 3, sections 3.4 and 3.11) are given below-

condition	datasets date	spread $S_i = S_{i1} + S_{i2..} + S_{in}$	unsread $U_i = U_{i1} + U_{i2..} + U_{in}$	total $T_i = S_i + U_i$	spread(%) \bar{S}_i	unsread(%) \bar{U}_i	spread/total S_i/T_i	final counted $N = T_{i1} + T_{i2..} + T_{in}$
no dms0/no probe								
S_i/U_{i1}	310516	891	404	1295	68.8	31.2	0.688	2059
S_i/U_{i2}	80716	329	193	522	63.0	37.0	0.630	
S_i/U_{i3}	120716	120	122	242	49.6	50.4	0.496	
average (\bar{S}, \bar{U})					60.5	39.5	0.605	
std dev (σ)							0.099	
only dms0/no probe								
S_i/U_{i1}	310516	901	616	1517	59.4	40.6	0.594	2828
S_i/U_{i2}	80716	414	286	700	59.1	40.9	0.591	
S_i/U_{i3}	120716	384	227	611	62.8	37.2	0.628	
average (\bar{S}, \bar{U})					60.5	39.5	0.605	
std dev (σ)							0.021	
only SiR-tubulin								
S_i/U_{i1}	270416	280	538	818	34.2	65.8	0.342	1789
S_i/U_{i2}	80716	292	149	441	66.2	33.8	0.662	
S_i/U_{i3}	120716	295	235	530	55.7	44.3	0.557	
average (\bar{S}, \bar{U})					52.0	48.0	0.520	
std dev (σ)							0.163	
5µM nocodazole								
S_i/U_{i1}	270416	163	208	371	43.9	56.1	0.439	1850
S_i/U_{i2}	310516	502	170	672	74.7	25.3	0.747	
S_i/U_{i3}	80716	250	201	451	55.4	44.6	0.554	
S_i/U_{i4}	120716	231	125	356	64.9	35.1	0.649	
average (\bar{S}, \bar{U})					59.7	40.3	0.597	
std dev (σ)							0.131	
50µM blebbistatin								
S_i/U_{i1}	270416	74	1318	1392	5.3	94.7	0.053	4377
S_i/U_{i2}	310516	120	1716	1836	6.5	93.5	0.065	
S_i/U_{i3}	80716	115	423	538	21.4	78.6	0.214	
S_i/U_{i4}	120716	98	513	611	16.0	84.0	0.160	
average (\bar{S}, \bar{U})					12.3	87.7	0.123	
std dev (σ)							0.077	
5µM noc+50µM bleb								
S_i/U_{i1}	270416	37	1071	1108	3.3	96.7	0.033	2587
S_i/U_{i2}	310516	52	657	709	7.3	92.7	0.073	
S_i/U_{i3}	80716	45	320	365	12.3	87.7	0.123	
S_i/U_{i4}	120716	18	387	405	4.4	95.6	0.044	
average (\bar{S}, \bar{U})					6.9	93.1	0.069	
std dev (σ)							0.040	

APPENDIX

- A *t*-test was done to statistically compare untreated and pharmacological agent treated platelets. A *p*-value < 0.05 was considered statistically significant and the test was carried out in OriginPro 8.5. Two examples of the independent two-sample *t*-test for unequal variances are shown below. In the first example, the *t*-test shows that there is no significant difference in the spreading between only DMSO treated but non-labeled platelets and only SiR-tubulin labeled platelets-

Two sample *t* Test (08/18/16 20:24:25)

Notes

Input Data

Descriptive Statistics

	N	Mean	SD	SEM
1	3	0.60461	0.0207	0.01195
2	3	0.52034	0.16297	0.09409
Difference		0.08427		

N= number of datasets
only DMSO/no SiR-tubulin probe
only SiR-tubulin probe

t-Test Statistics

	t Statistic	DF	Prob> t
Equal Variance Assumed	0.88847	4	0.42449
Equal Variance NOT Assumed	0.88847	2.06455	0.46549

Null Hypothesis: mean1-mean2 = 0
 Alternative Hypothesis: mean1-mean2 <> 0
 At the 0.05 level, the difference of the population means is NOT significantly different with the test difference(0)

In the second example, the *t*-test shows that there is a significant difference in the spreading between only SiR-tubulin labeled platelets and SiR-tubulin labeled platelets, treated with blebbistatin-

Two sample *t* Test (07/21/16 20:48:06)

Notes

Input Data

Descriptive Statistics

	N	Mean	SD	SEM
1	3	0.52034	0.16297	0.09409
2	4	0.12317	0.0771	0.03855
Difference		0.39718		

N= number of datasets
only SiR-tubulin probe
SiR-tubulin + blebbistatin

t-Test Statistics

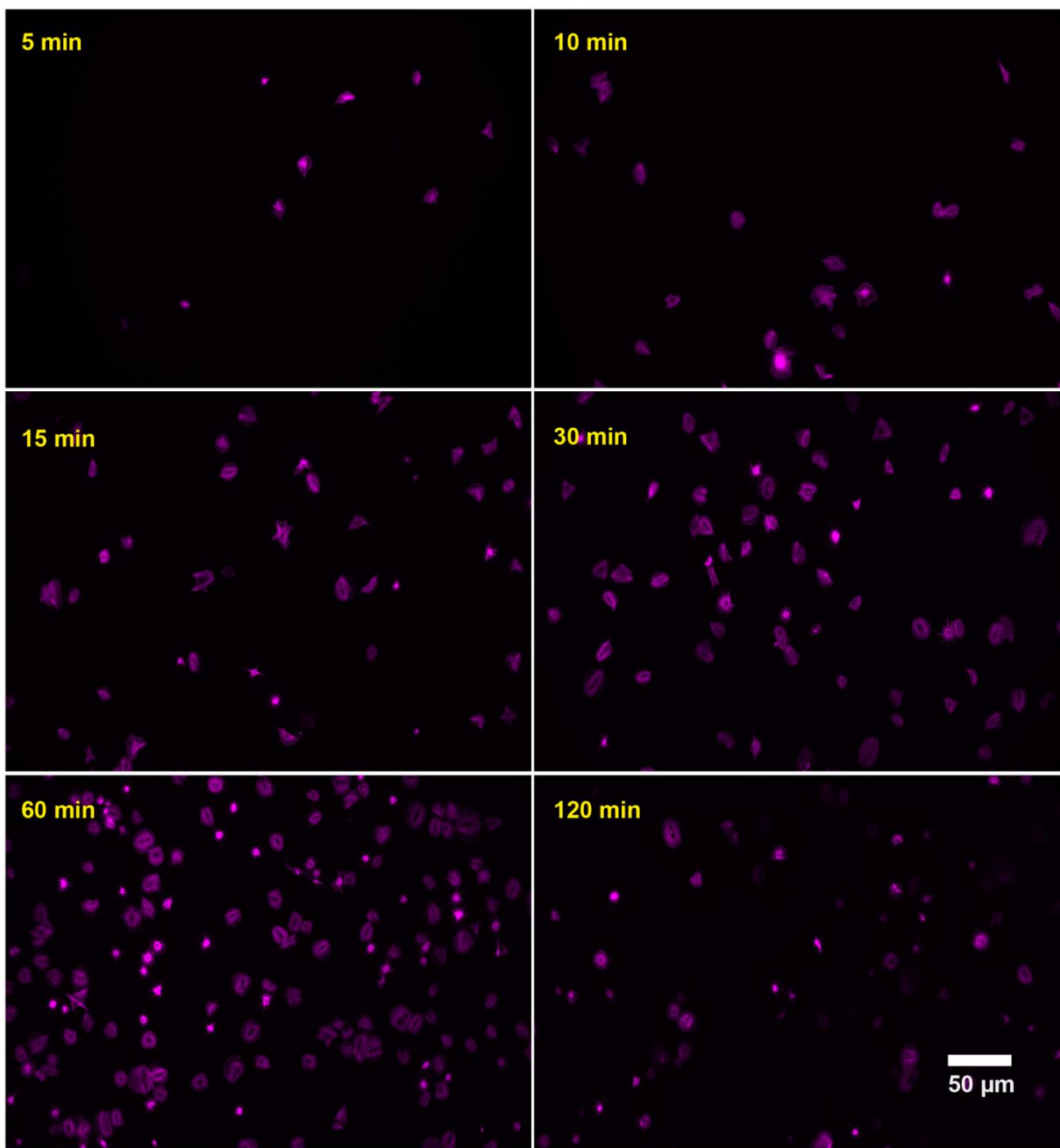
	t Statistic	DF	Prob> t
Equal Variance Assumed	4.36541	5	0.00725
Equal Variance NOT Assumed	3.90606	2.67755	0.0365

Null Hypothesis: mean1-mean2 = 0
 Alternative Hypothesis: mean1-mean2 <> 0
 At the 0.05 level, the difference of the population means is significantly different with the test difference(0)

F. Representative images of fixed-platelet cytoskeleton time series

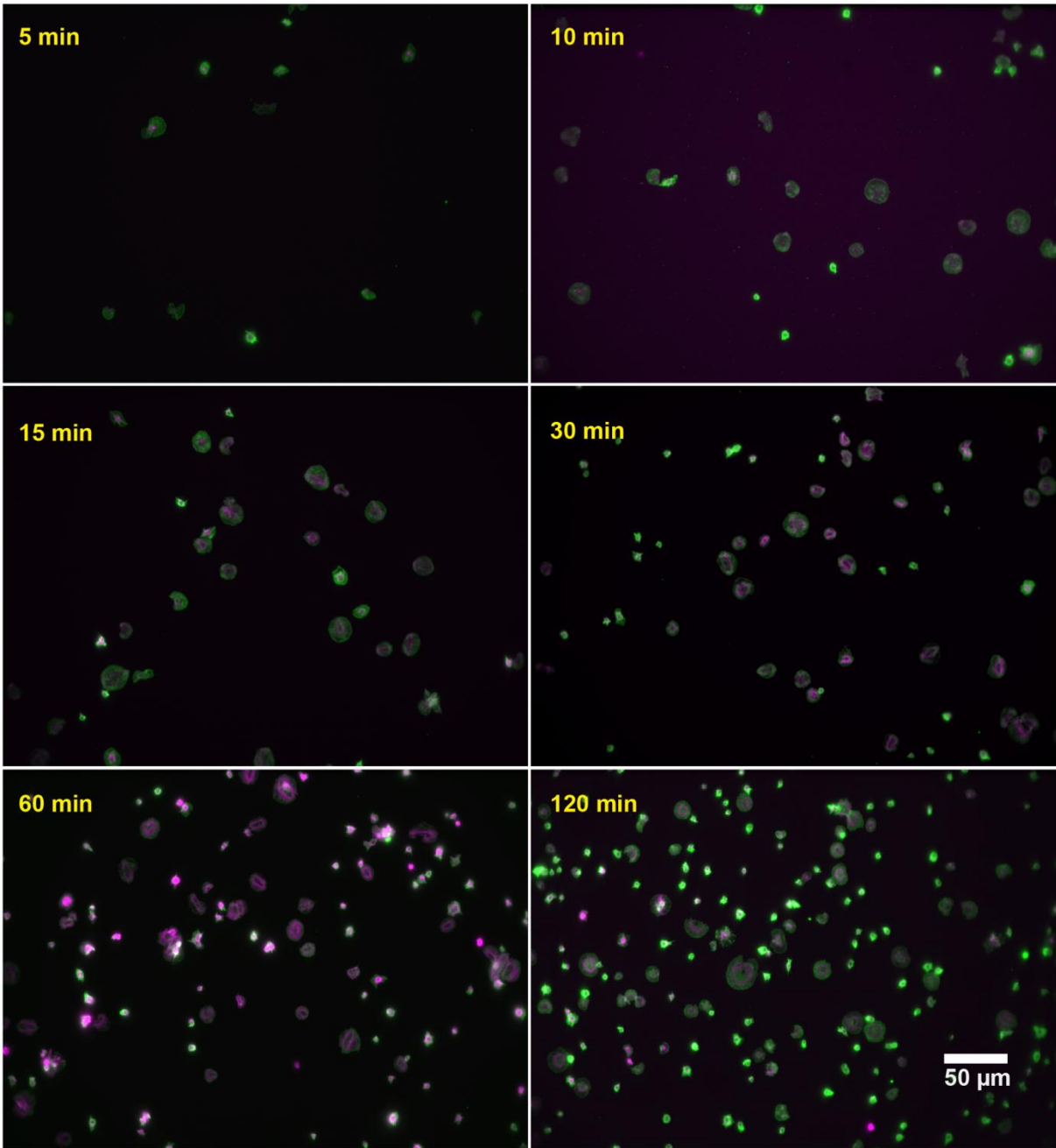
The images were kindly taken by Tim Dullweber during his Bachelor thesis done under my supervision.

- Representative images for each time point of the fixed-platelet time series for the single F-actin and double F-actin-vinculin and F-actin-myosin are shown below (details in chapter 4). An increase in the number of adhered platelets with time was generally observed. The platelet sizes (spread areas) were also observed to increase with time. However, the platelet sizes after two hours were smaller, possibly because the platelets had retracted.

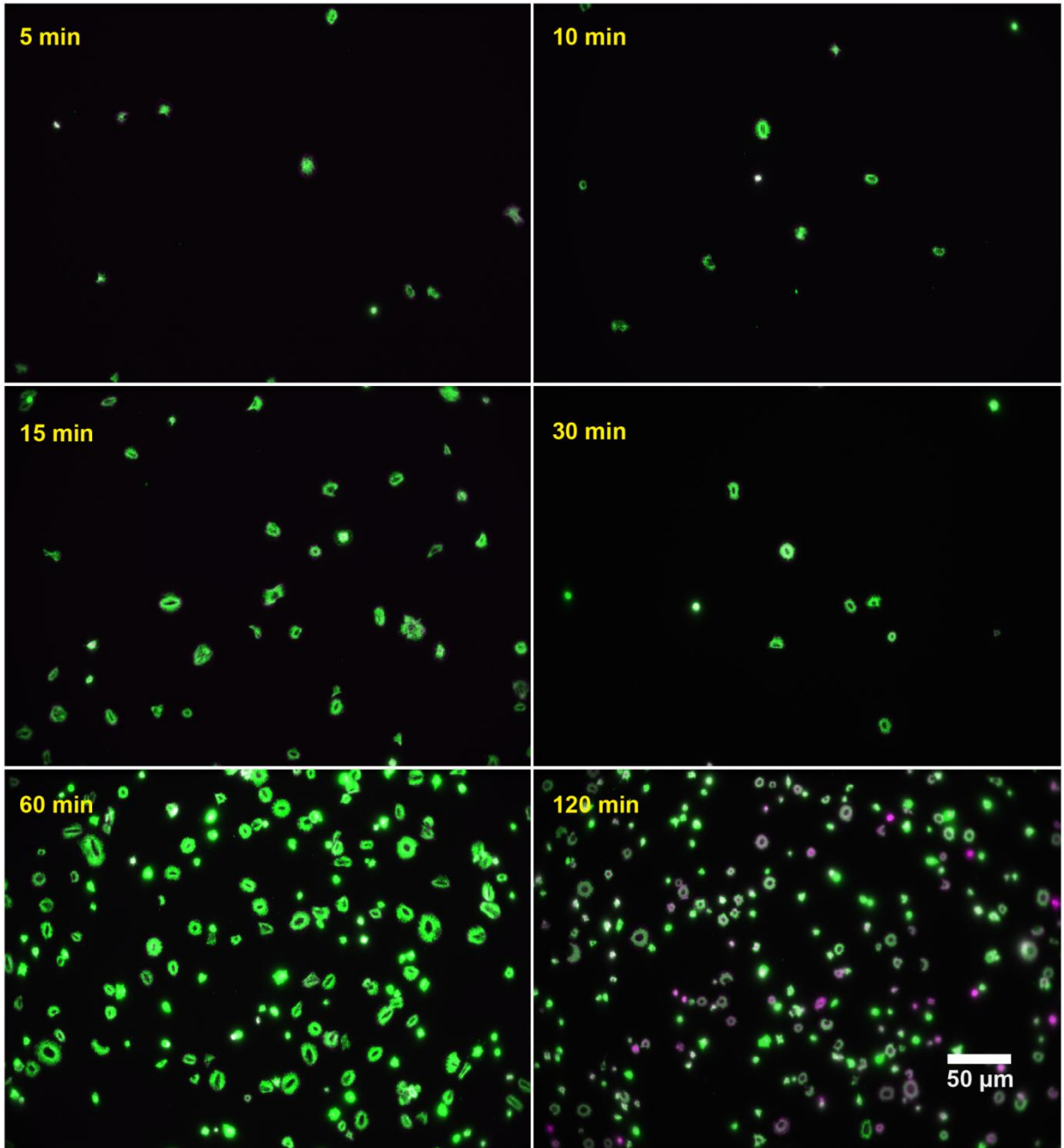
F-actin

APPENDIX

F-actin-vinculin

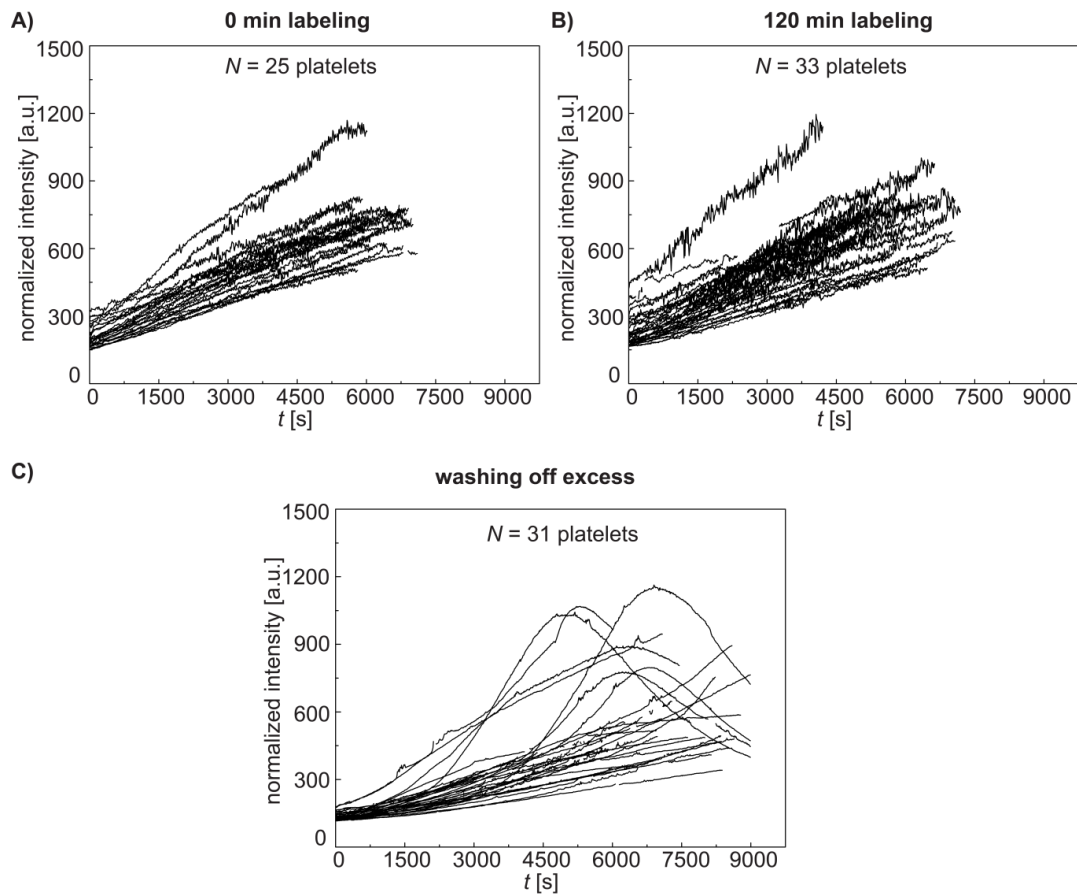


F-actin-myosin



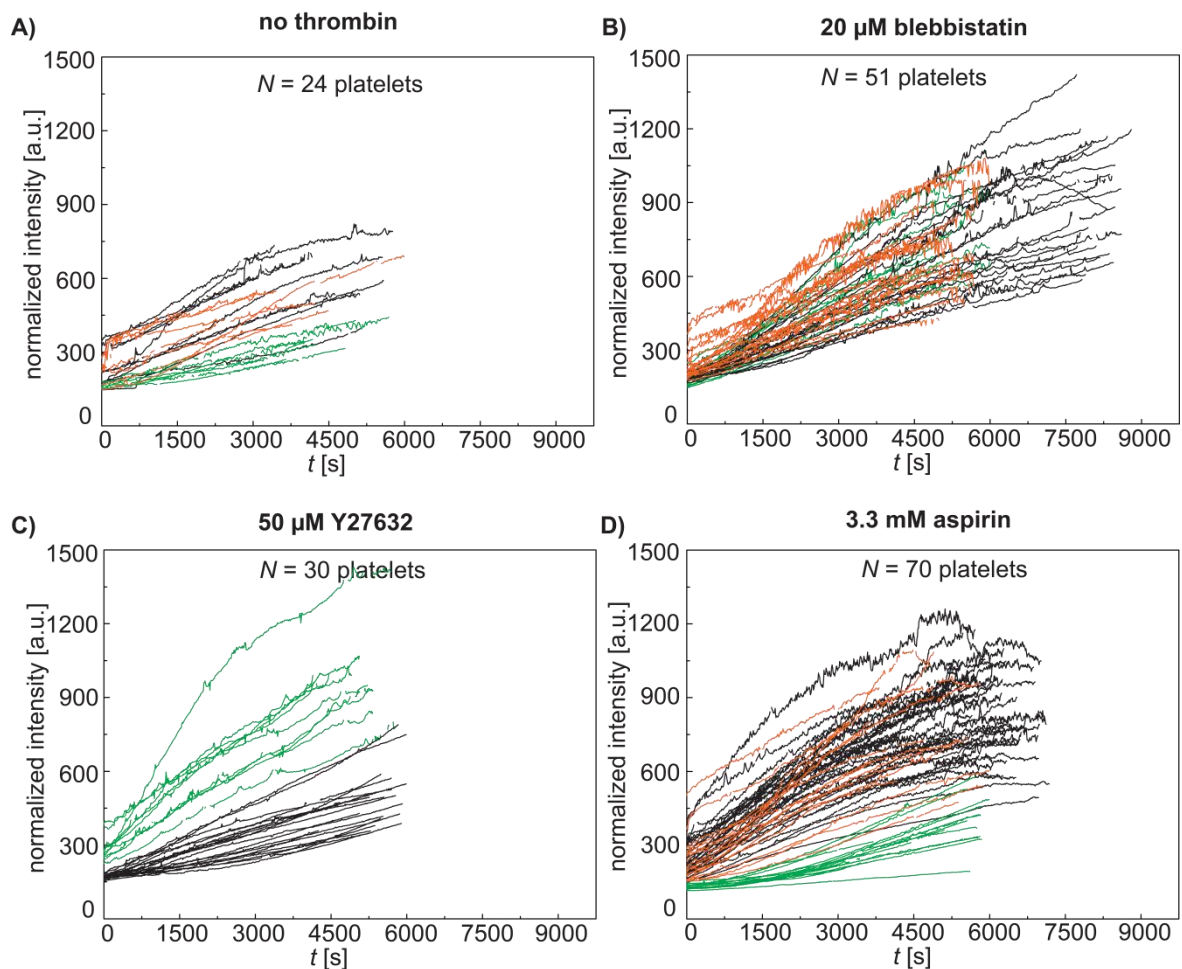
G. SiR-actin probe characterization and spreading tests

- The normalized F-actin fluorescence intensities of platelets that were quantified after labeling them with SiR-actin immediately (0 min labeling), or after 120 minutes, and when the excess SiR-actin probe was washed off, are shown below (details in chapter 4.2, section 4.2.2). Here the ' N ' refers to the number of platelets analyzed from one single experimental dataset. The intensity profiles are similar to those of the 6 and 2 μM SiR-actin probes (Figure 4.8).



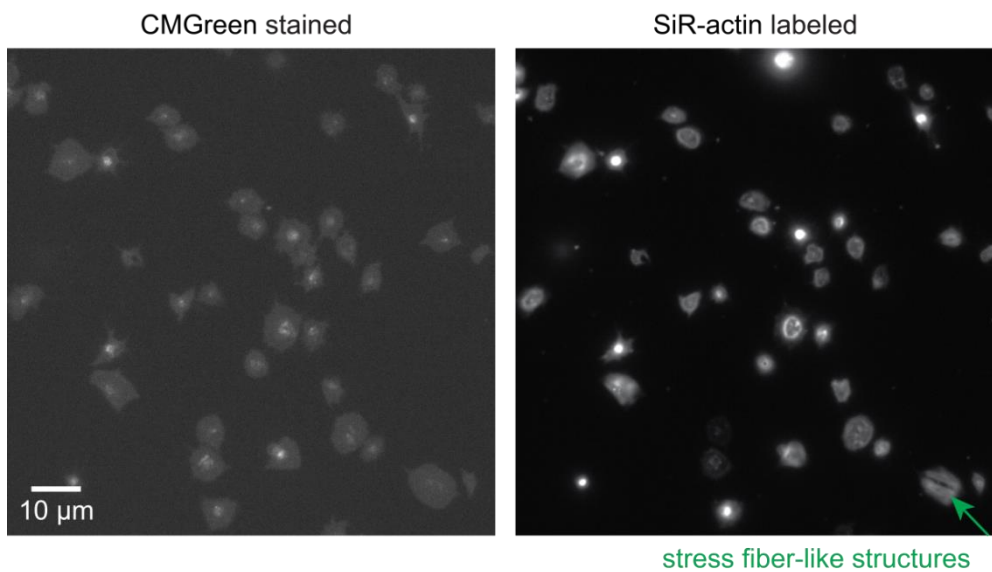
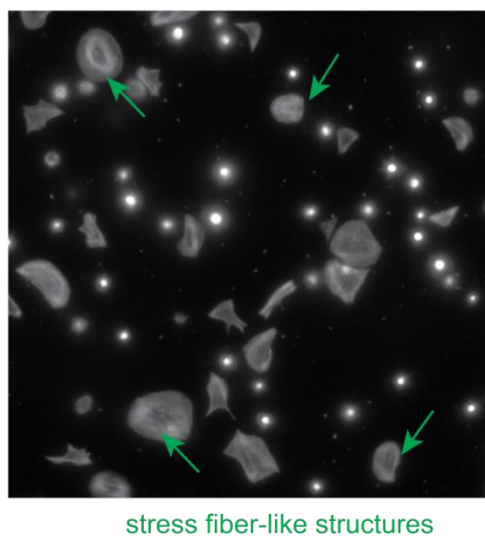
H. Normalized F-actin intensity profiles of platelets treated with pharmacological agents are similar to those of control conditions

- The normalized F-actin fluorescence intensities of platelets that were quantified after not adding thrombin, treating them with 20 μM blebbistatin; treating them with 50 μM Y-27632 and treating them with 3.3 mM aspirin during their spreading (details in chapter 4.2, section 4.2.4). Here the 'N' refers to the total number of platelets analyzed from multiple (each dataset represented by black, green or orange curves) experimental datasets. The intensity profiles are similar to those of the control conditions (Figure 4.8 and Figure 4.14). This indicates that those platelets that spread do so normally and the pharmacological agents have no effect on them.



I. F-actin morphologies of CMGreen and SiR-actin double labeled are different than only single SiR-actin labeled platelets

- The platelets labeled with both CMGreen dye and the SiR-actin probe did not reorganize the F-actin into stress fiber-like structures that are typically formed by only SiR-actin labeled platelets (details in chapter 4.2, section 4.2.3.1). Shown below are representative images of the double labeled (CMGreen + SiR-actin) and single labeled (SiR-actin) platelets. The double labeled platelets rarely formed the stress-fiber like structures (green arrows) which indicated that the labeling with two stains was proving detrimental to the normal spreading of the platelets.

Double labeled (CMGreen + SiR-actin) platelets after 100 minutes of spreading**Single labeled (SiR-actin) platelets after 100 minutes of spreading**

List of Abbreviations and Symbols

ADF	Actin depolymerizing factor
ADP	Adenosine diphosphate
AFM	Atomic force microscopy
Arp2/3	Actin-related proteins ARP2 and ARP3
ATP	Adenosine triphosphate
BF	Bright-field
BSA	Bovine serum albumin
DAG	Diacylglycerol
DMSO	Dimethyl sulfoxide
dSTORM	Direct Stochastic optical reconstruction microscopy
DTS	Dense tubular system of platelets
ECM	Extracellular matrix
F-actin	Filamentous actin
FA(s)	Focal adhesions
FS	Filament sensor
G-actin	Globular (monomeric) actin
GDP	Guanosine-5'-diphosphate
GFP	Green fluorescent protein
GPCR(s)	G-protein-coupled receptor(s)
GTP	Guanosine-5'-triphosphate
HDAC6	Histone deacetylase 6 (for deacetylation associated with dynamic MTs)
HSCs	Hematopoietic stem cells
HT-BSA	Hepes-Tyrode BSA
IMS	Invaginated membrane system
IP ₃	Inositol-1,4,5-triphosphate
LVHR-SEM	Low-voltage, high-resolution scanning electron microscopy
MAPs	Microtubule associated proteins
MB	(circumferential) Marginal band
MK(s)	Megakaryocyte(s)

ABREVIATIONS & SYMBOLS

MLC	Myosin light chain
MLCK	Myosin light chain kinase
MRLC	Myosin regulatory light chain
MT(s)	Microtubule(s)
MTOC	Microtubule organizing center
MT ring/coil	Microtubule circumferential marginal band
Myosin(II)	Refers to non-muscle myosin II expressed in platelets
NA	Numerical aperture
OCS	Open canalicular system of platelets
PAR(s)	Protease activated receptor(s) (for thrombin)
PBS	Phosphate buffered saline
PGE ₁	Prostaglandin E ₁
PGI ₂	Prostaglandin I ₂
PIP ₂	phosphatidylinositol-4,5-biphosphate
PKC	Protein kinase C
PLC ₂	Phospholipase C ₂
PSG	PIPES Saline Glucose
PTM(s)	Post translational modification(s)
RBCs	Red blood cells
ROCK	Rho-associated protein kinase
ROI	Region of interest
RF	Radio frequency
RT	Room temperature
SEM	Scanning electron microscopy
SIM	Structured illumination microscopy
SiR	Silicon-rhodamine
Src	Proto-oncogene tyrosine protein kinase
STED	Stimulated Emission Depletion
Syk	Spleen tyrosine kinase
TIRF	Total internal reflection fluorescence
TP	Thromboxane A ₂ receptor
TTL	Tubulin tyrosine ligase (for tyrosination associated with dynamic MTs)
TAT1	Tubulin acetyltransferase (for acetylation associated with stable MTs)
TXA ₂	Thromboxane A ₂

ABBREVIATIONS & SYMBOLS

VASP	Vasoactive-stimulated phosphoprotein
WASp	Wiskott-Aldrich syndrome protein
C_c	Critical concentration
k_{on}	Rate of ATP-G-actin addition
k_{off}	Rate of ADP-G-actin loss
t_{zero}	First time point of platelet adhesion
A	Platelet spread area
h	Histogram bin width
I	Normalized fluorescence intensity
N	Final number of platelets analyzed/counted per experimental condition
σ	Standard deviation
t_l	Turning time point

Acknowledgements

This is one of my most favorite parts of the dissertation because I get to jog down the memory lane and think about all the wonderful memories I have shared with the people involved in my doctoral journey! Through these words, I take the opportunity to express my deep gratitude to each and every one of them!

My foremost gratitude goes to my thesis supervisor **Prof. Dr. Sarah Köster**.

Thank you Sarah for believing in my capabilities and always encouraging me when my morale was down! I have learned so much from your expertise! From fruitful discussions about the project to training to think in a scientific way and right down to acquiring the nuances of technical writing, I have learnt it all from you!

I am extremely grateful to **Prof. Dr. Erwin Neher** for reviewing this thesis and being my second thesis committee supervisor.

Thank you for your nice suggestions during the thesis committee meetings and all the helpful discussions over these years. It has been an immense honor to have you as my supervisor, Professor!

I want to express my deep gratitude to **Prof. Dr. Ivo Feußner**, **Prof. Dr. Jörg Großhans**, **Prof. Dr. Kai Tittmann** and **Prof. Dr. Stefan Jakobs** for kindly obliging to be the part of my examination committee.

I thank the **SFB 937** for funding the research project. I am grateful to **Prof. Dr. Dieter Heineke** and **Dr. Jonas Barth** for ensuring my smooth admission to the GAUSS Grund Biology Program and for advising and helping me with all the administrative details.

I thank the **University of Göttingen Klinikum** for providing us with the platelet concentrates. I also thank **Dr. Tobias Legler**, **Dr. Joachim Riggert** and **Dr. Alexander Strate** for helpful discussions and all the **Klinikum staff** for their friendly nature.

I am very grateful to **Dr. Assaf Zemel** from the Institute of Dental Sciences and Fritz Haber Center for Molecular Dynamics, Hebrew University of Jerusalem, Israel for many invaluable and friendly discussions about my work.

I thank **Dr. Benjamin Eltzner** from the Institute of Mathematical Stochastics, Göttingen for providing us the Filament Sensor program, for analyzing the actin data, for help with writing the relevant part of the thesis and for always patiently answering all the data analysis and

ACKNOWLEDGEMENTS

technical questions. I thank **Dr. Rabea Sandmann**, **Dr. Bernd Nöding** and **Gerrit Brehm** from the Köster Group for providing the MATLAB scripts for data analysis.

Special thanks to **Prof. Dr. Stefan Hell** and his group at the Max Planck Institute for Biophysical Chemistry- **Dr. Fabian Göttfert** and **Dr. Elisa D'Este** for introducing us to these novel cytoskeletal probes and for the helpful discussions related to the project.

I express my gratitude to **Prof. Tim Salditt** for the nice conversations and to the IRP secretaries **Kerstin Pluschke**, **Sabine Balder** and **Michaela Ständer** for being very friendly, taking care of all the administrative formalities and always ensuring that there were never any delays!

My heart-felt thanks to our IRP systems administrator **Jan Goeman** for always helping me promptly with any issues with my computer and the server! I also thank **Jochen Herbst** for helping with all the technical stuff. I thank the members from Olympus GmbH, **Dr. Ines Höfer** and **Thomas Wenninger** for help with the microscope technicalities.

I am thankful to each and every one in my wonderful **AG Köster group**, for providing a great work environment and for all the fruitful, scientific help and suggestions.

Susanne Bauch, thank you for providing all the technical help. It has been wonderful knowing you and I hope you will visit me in India someday! Thanks to my all girls platelet crew **Sarah Schwarz G.Henriques**, **Rabea Sandmann**, **Jana Hanke** and **Christiane Ranke** for all the helpful platelet discussions and for our nice chats about everything under the sun! It has been fun knowing and working with you! Kudos to girl-power! I am immensely grateful to **Eleonora Perego** and **Andrew Wittmeier** for encouraging me in my difficult days and for always keeping me in good spirits during the most stressful times. I will really miss our coffee breaks together, our fun outings, and the deep discussions about everything other than the scientific life! I am so glad to have found such dear friends in you both! Thank you **Viktor Schroeder** for being such a good friend and for always helping me to clear my plate off the famous Nord Mensa food! Thank you **Daniel Schmitz** and **Clément Hemmonot** for all the awesome times! I am so glad I found such great friends in you! **Tim Dullweber** thanks for the amazing hard work you put in during your internship and your bachelor thesis! It was a tedious project and I am so grateful for your dedication, enthusiasm and your positive attitude during these times! It was a lot of fun to work with you! **Gerrit Brehm** a big thank you for all your help. You have been everything a person could ask for in an office mate. A wonderful friend, patient listener, problem-solver, German translator! Thanks for always keeping me in good spirits! Thanks **Chiara Cassini**, **Manuela Denz**, **Oliva Saldanha**, **Rita Graceffa**, and **Johanna Block** for making my time in the group memorable! I also thank all the **former**

ACKNOWLEDGEMENTS

group members and all the **IRP members** for being so helpful and for providing a good working environment.

I thank my close friends, **Mithila Vaidya, Rashmi Yadav, Abhay Yadav, Gitanjali Jain,** and **Gaurav Jain** who are like my family away from home, for being there for me always!

Thank you **Narain Karedla** for being such a great friend, for checking in on me and being so supportive during the stressful times! I thank my friends and fellow researchers, **Siddharth Ghosh, Olaf Schulz** and **Meenakshi Prabhune** for all the good times!

I also thank all my **family** and **friends** back home in Pune, India, USA for sending me all their blessings and love from so far away.

Special thanks to my mother-in-law **Mrs. Sunita Giri** (Aai) and my brother-in-law **Dhawal Giri** for their love, support, encouragement.

I take this opportunity to thank my best friend and husband, **Dr. Chaitanya Giri**.

Thank you Chaitanya for your support, for your willing ear when I discussed my work with you and most importantly for being there for me in all the trying times! I look forward to joining you soon and begin a new chapter in our life together!

Lastly, I am deeply thankful to my loving parents **Dr. Kishore Paknikar (Baba)** and **Dr. Mrs. Savita Paknikar (Aai)**.

Thank you for making me the person that I am today. Thank you for exposing me to all sorts of new opportunities while I was growing up, for always being there to hear and discuss all my scientific work or otherwise and to give me valuable advice! While I can go on for several pages about the profound impact you both have had on my life, I will just as easily sum it up in one sentence- I couldn't have asked for better parents!

To you both Aai-Baba, I dedicate this dissertation!

ACKNOWLEDGEMENTS

Curriculum Vitae

PERSONAL INFORMATION

Name: Aishwarya Kishore Paknikar
Birthdate: 9th December, 1987
Email address: aishwarya.paknikar@gmail.com

EDUCATION AND RESEARCH EXPERIENCE

June 2012-present	Doctor of Philosophy (Ph.D) in Biology Institute for X-Ray Physics, Georg-August-Universität Göttingen, Göttingen, Germany PhD Thesis: Cytoskeletal reorganization in human blood platelets during spreading Supervisors: Prof. Dr. Sarah Köster and Prof. Dr. Erwin Neher
October 2008-July 2011	Master of Science (M.Sc.) in Biochemistry and Molecular Biology University of Bremen and Max Planck Institute for Marine Microbiology, Bremen, Germany Master Thesis: Anaerobic degradation of cyclic alkanes by nitrate-reducing enrichment cultures Supervisors: Dr. Florin Musat, PD Dr. Jens Harder and Prof. Dr. Friedrich Widdel Project proposal: Investigating phosphate uptake in <i>Rhodospirillum rubrum</i> Lab rotation 1: Strategies to identify the exon 1 of the putative lamin LIII gene of <i>Ornithorhynchus anatinus</i> (platypus) Supervisor: Prof. Dr. Reimer Stick

Lab rotation 2:	Physiological investigations of a nitrate-reducing enrichment culture using cyclohexane as the sole carbon source and optimization of a method for the measurement of iron
Supervisors:	Prof. Dr. Friedrich Widdel and Dr. Florin Musat

July 2005- June 2008	Bachelor of Science (B.Sc.) in Microbiology Abasaheb Garware College, University of Pune, Pune, India
-------------------------	--

Vocational subjects:	Chemistry and Industrial Microbiology
----------------------	---------------------------------------

SKILLS

Laboratory	Wide-field and confocal microscopy Gas chromatography, Basic cell biology, microbiology, immunohistochemistry, molecular biology and chemistry techniques
Computer and Software	Windows, MAC OS X MS Office Adobe Illustrator, Photoshop, Indesign, Inkscape OriginPro, MATLAB
Soft skills	Scientific writing, team work, networking

ACADEMIC MERITS

2008- 2009	1st rank in M.Sc. entrance examination in Dietetics	Interdisciplinary School of Health Sciences, University of Pune, India
2008- 2009	1st rank in M.Sc. entrance examination in Public Health	Interdisciplinary School of Health Sciences, University of Pune, India
2008- 2009	2nd rank in M.Sc. entrance examination in Health Sciences	Interdisciplinary School of Health Sciences, University of Pune, India

PUBLICATIONS

Nisenholz N, **Paknikar A**, Köster S, Zemel A. (2016) Contribution of myosin II activity to cell spreading dynamics. *Soft Matter* 12(2): 500-507. Doi: 10.1039/C5SM01733E

Paknikar A, Eltzner B, Brehm G, Köster S. (2017) Direct characterization of cytoskeletal reorganization during blood platelet spreading (*manuscript in preparation*)

POSTERS AT CONFERENCES

Physics of Cancer, Soft Matter Physics Division, University of Leipzig	in Leipzig, November, 2012
Deutsche Physikalische Gesellschaft (DPG), Spring Meeting	in Regensburg, March, 2013
Cell Physics, Universität des Saarlandes	in Saarbrücken, September, 2014
Deutsche Physikalische Gesellschaft (DPG), Spring Meeting	in Berlin, March, 2015
Physics of Cells and Tissues, European Molecular Biology Laboratory (EMBL)	in Heidelberg, October, 2015
Deutsche Physikalische Gesellschaft (DPG), Spring Meeting	in Regensburg, March, 2016